

IMPACT FACTOR
10.057

#1 NUCLEAR MEDICINE,
MOLECULAR IMAGING AND
MOLECULAR RADIOTHERAPY
JOURNAL

JNM

The Journal of Nuclear Medicine

Radiopharmaceutical Dosimetry for Cancer Therapy: From Theory to Practice

Guest Editors: Richard L. Wahl, MD and John Sunderland, PhD

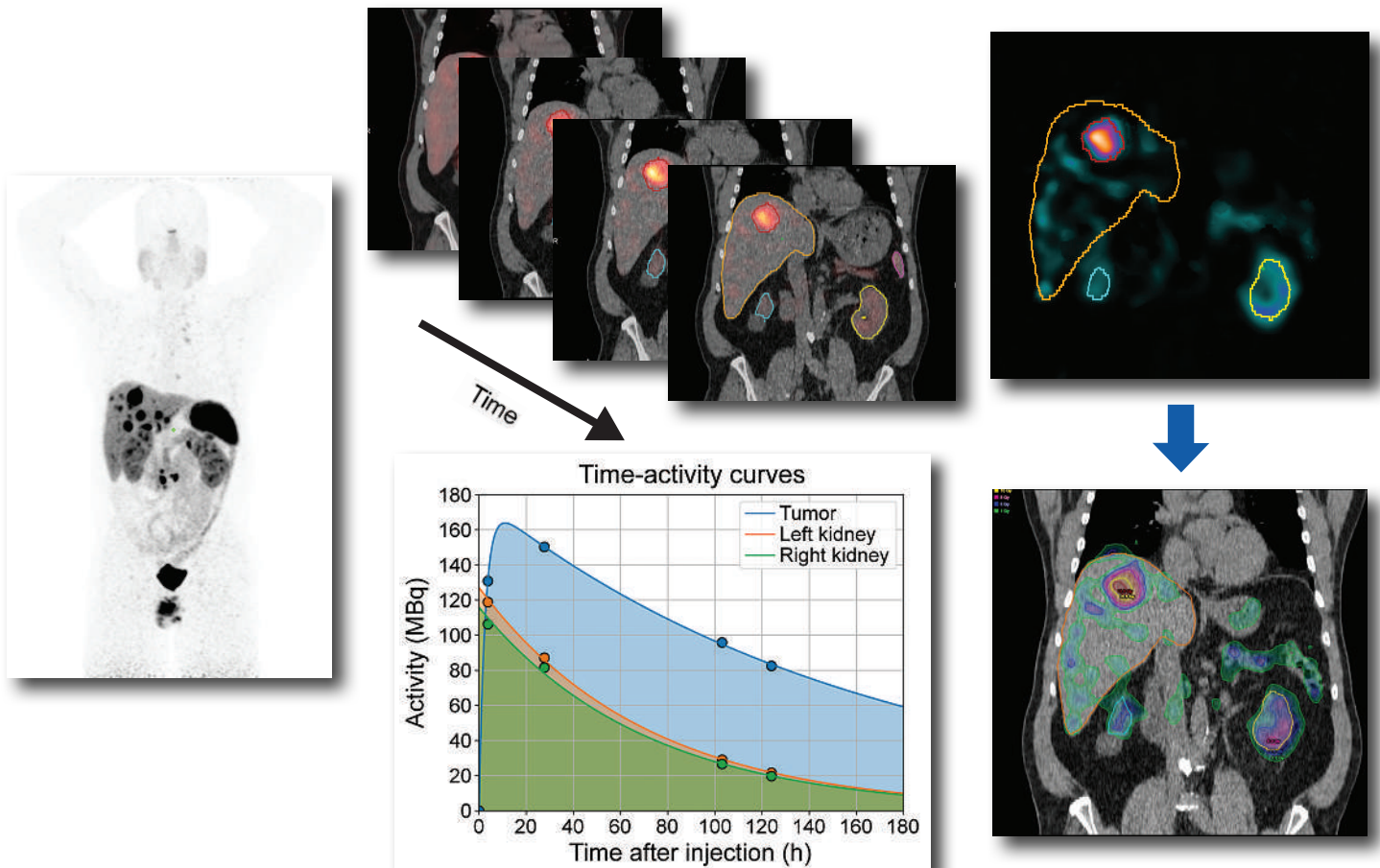
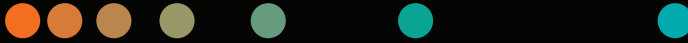
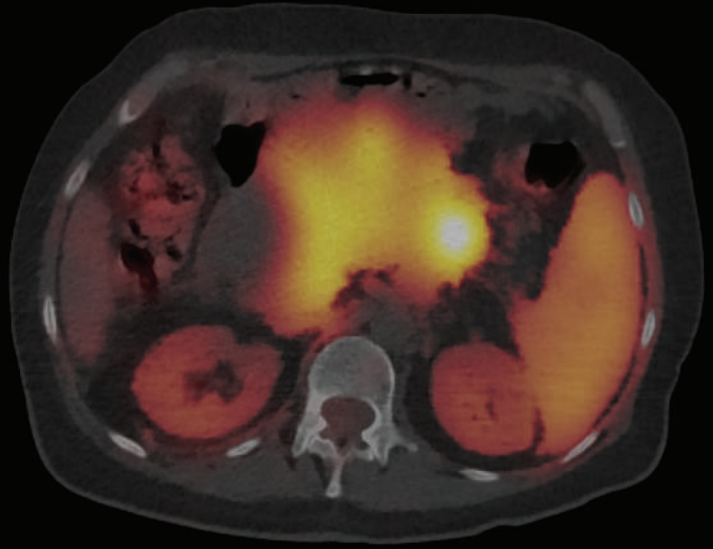


Illustration of steps in patient-specific dosimetry including pretherapy PET, quantitative SPECT at 4 time points with segmentation, integration of time-activity curves to form the time-integrated activity image, and the resulting dose map.

Expanding your theranostics program?

Give your patients the level of precision care they need and the personalized treatment they deserve with comprehensive PET/CT and SPECT/CT theranostic solutions from Siemens Healthineers.



Proven molecular imaging solutions across the entire continuum of theranostic care.



High spatial resolution and the fastest time of flight¹ in PET/CT for small lesion detection.

Improve therapy planning and deliver highly targeted therapy at the right dose and at the right time.



Precise and reproducible SPECT/CT quantification to within 5%² accuracy for low, medium, and high energy isotopes.

Optimize therapy monitoring and individualize future therapy planning based on your patient's unique needs and treatment response.

Learn more at [siemens-healthineers.com/mi](https://www.siemens-healthineers.com/mi)

¹ Based on competitive literature available at time of publication. Data on file.

² Accuracy of Bq/ml quantification measured per NEMA NU1-2018 using a uniform cylinder phantom. Calibration method: NIST-traceable source.

See NET imaging in a different light

The high **accuracy** and **accessibility** of Detectnet enable timely neuroendocrine tumor (NET) detection, diagnosis, and treatment planning¹

INCLUDED IN NCCN CLINICAL PRACTICE GUIDELINES IN ONCOLOGY (NCCN GUIDELINES®)

Effective 4/14/2021, included in the NCCN Guidelines® version 1.2021 for the evaluation of NETs.²

ACCURACY

- In a phase 3 study, Detectnet had over 98% accuracy, 100% sensitivity, and 96.8% specificity to confirm or exclude presence of disease^{1*}

ACCESS

- 12.7-hour half-life of Cu 64 facilitates an **unrestricted number of doses** and allows **flexible scheduling** for you and your patients^{1,3,4}

Visit Detectnet.com to learn more.

INDICATIONS

Detectnet is indicated for use with positron emission tomography (PET) for localization of somatostatin receptor positive neuroendocrine tumors (NETs) in adult patients.

IMPORTANT RISK INFORMATION

WARNINGS AND PRECAUTIONS

Risk for Image Misinterpretation: The uptake of copper Cu 64 dotatate reflects the level of somatostatin receptor density in NETs, however, uptake can also be seen in a variety of other tumors that also express somatostatin receptors. Increased uptake might also be seen in other non-cancerous pathologic conditions that express somatostatin receptors including thyroid disease or in subacute inflammation, or might occur as a normal physiologic variant (e.g. uncinatate process of the pancreas).

A negative scan after the administration of Detectnet in patients who do not have a history of NET disease does not rule out disease.

Please see Brief Summary of Prescribing Information on the following page.

***Study design¹:** An open-label, single-dose, single-arm, single-center prospective study to evaluate the sensitivity and specificity of Detectnet PET/computed tomography (CT) imaging in 63 subjects (42 with known or suspected NETs and 21 healthy volunteers) against an independent reader's standard of truth (SOT) for each subject. PET/CT scans were taken ~60 minutes after a single IV dose of 148 MBq ± 10% of Detectnet.

A limitation was 3 mistaken SOT determinations, but these were revised. The SOT reads for 3 subjects were incorrectly recorded as NET-positive instead of NET-negative. Because the objective of the study was to assess the performance of the PET/CT scan and not the SOT, the corrected values are shown.

References: 1. Delpassand ES, Ranganathan D, Wagh N, et al. *J Nucl Med.* 2020. doi:10.2967/jnumed.119.236091. 2. Referenced with permission from the NCCN Clinical Practice Guidelines in Oncology (NCCN Guidelines®) for Neuroendocrine and Adrenal Tumors V.1.2021. © National Comprehensive Cancer Network, Inc. 2021. All rights reserved. Accessed April 15, 2021. To view the most recent and complete version of the guideline, go online to NCCN.org. 3. Pfeifer A, Knigge U, Mortensen J, et al. *J Nucl Med.* 2012;53(8):1207-1215. 4. Detectnet. Package insert. Curium US LLC; September 2020.

CURIUM™

© 2021 Curium US LLC. Detectnet™ and Curium™ are trademarks of a Curium company.
CD0103 0721



Detectnet™
(copper Cu 64 dotatate injection)

Scan to learn more
about Detectnet
and place an order.



Detectnet™ (copper Cu 64 dotatate injection), for intravenous use

BRIEF SUMMARY OF FULL PRESCRIBING INFORMATION

(For complete details, please see full Prescribing Information available at www.curiumpharma.com)

INDICATIONS AND USAGE

Detectnet is a radioactive diagnostic agent indicated for use with positron emission tomography (PET) for localization of somatostatin receptor positive neuroendocrine tumors (NETs) in adult patients.

CONTRAINDICATIONS

None.

WARNINGS AND PRECAUTIONS

Radiation Risk: Diagnostic radiopharmaceuticals, including Detectnet, contribute to a patient's overall long-term cumulative radiation exposure. Long-term cumulative radiation exposure is associated with an increased risk of cancer. Ensure safe handling and preparation procedures to protect patients and health care workers from unintentional radiation exposure. Advise patients to hydrate before and after administration and to void frequently after administration [see *Dosage and Administration (2.1, 2.3) in the full Prescribing Information*].

Risk for Image Misinterpretation: The uptake of copper Cu 64 dotatate reflects the level of somatostatin receptor density in NETs, however, uptake can also be seen in a variety of other tumors that also express somatostatin receptors. Increased uptake might also be seen in other non-cancerous pathologic conditions that express somatostatin receptors including thyroid disease or in subacute inflammation, or might occur as a normal physiologic variant (e.g. uncinate process of the pancreas) [see *Dosage and Administration (2.5) in the full Prescribing Information*].

A negative scan after the administration of Detectnet in patients who do not have a history of NET disease does not rule out disease [see *Clinical Studies (14) in the full Prescribing Information*].

ADVERSE REACTIONS

Clinical Trials Experience: Because clinical trials are conducted under widely varying conditions, adverse reaction rates observed in the clinical trials of a drug cannot be directly compared to rates in the clinical trials of another drug and may not reflect the rates observed in practice.

In safety and efficacy trials, 71 subjects received a single dose of Detectnet. Of these 71 subjects, 21 were healthy volunteers and the remainder were patients with known or suspected NET.

The following adverse reactions occurred at a rate of < 2%:

- *Gastrointestinal Disorders:* nausea, vomiting
- *Vascular Disorders:* flushing

In published clinical experience, 126 patients with known history of NET received a single dose of copper Cu 64 dotatate injection. Four patients were reported to have experienced nausea immediately after injection.

DRUG INTERACTIONS

Somatostatin Analogs: Non-radioactive somatostatin analogs and copper Cu 64 dotatate competitively bind to somatostatin receptors (SSTR2). Image patients just prior to dosing with somatostatin analogs. For patients on long-acting somatostatin analogs,

a wash-out period of 28 days is recommended prior to imaging. For patients on short-acting somatostatin analogs, a washout period of 2 days is recommended prior to imaging [see *Dosage and Administration (2.3) in the full Prescribing Information*].

USE IN SPECIFIC POPULATIONS

Pregnancy

Risk Summary

All radiopharmaceuticals, including Detectnet, have the potential to cause fetal harm depending on the fetal stage of development and the magnitude of the radiation dose. Advise a pregnant woman of the potential risks of fetal exposure to radiation from administration of Detectnet.

There are no data on Detectnet use in pregnant women to evaluate for a drug-associated risk of major birth defects, miscarriage, or adverse maternal or fetal outcomes. No animal reproduction studies have been conducted with copper Cu 64 dotatate injection.

The estimated background risk of major birth defects and miscarriage for the indicated population is unknown. All pregnancies have a background risk of birth defects, loss, or other adverse outcomes. In the U.S. general population, the estimated background risk of major birth defects and miscarriage in clinically recognized pregnancies is 2% to 4% and 15% to 20%, respectively.

Lactation

Risk Summary

There are no data on the presence of copper Cu 64 dotatate in human milk, the effect on the breastfed infant, or the effect on milk production. Lactation studies have not been conducted in animals.

Advise a lactating woman to interrupt breastfeeding for 12 hours after Detectnet administration in order to minimize radiation exposure to a breastfed infant.

Pediatric use: The safety and effectiveness of Detectnet have not been established in pediatric patients.

Geriatric use: Clinical studies of Detectnet did not include sufficient numbers of subjects aged 65 and over to determine whether they respond differently from younger subjects. Other reported clinical experience has not identified differences in responses between the elderly and younger patients. In general, dose selection for an elderly patient should be cautious, usually starting at the low end of the dosing range, reflecting the greater frequency of decreased hepatic, renal, or cardiac function, and of concomitant disease or other drug therapy.

OVERDOSAGE

In the event of a radiation overdose, the absorbed dose to the patient should be reduced where possible by increasing the elimination of the radionuclide from the body by reinforced hydration and frequent bladder voiding. A diuretic might also be considered. If possible, estimation of the radioactive dose given to the patient should be performed.

This Brief Summary is based on Detectnet Full Prescribing Information Revised: 9/2020

Manufactured, Packed and Distributed by: Curium US LLC, 2703 Wagner Place, Maryland Heights, MO 63043

© 2020 Curium US LLC. Detectnet™ and Curium™ are trademarks of a Curium company.

CD0041 0920a

The Official Publication of **SNMMI**

Publications Committee

TODD E. PETERSON, PhD, FSNMMI
Chair

CAROLYN ANDERSON, PhD, FSNMMI
PAIGE B. BENNETT, MD
JOYITA DUTTA, PhD
MICHAEL M. GRAHAM, PhD, MD, FSNMMI
HOSSEIN JADVAR, MD, PhD, FACNM,
FSNMMI
STEVEN M. LARSON, MD, FACNM
HEINRICH R. SCHELBERT, MD, PhD, FSNMMI
HEIKO SCHÖDER, MD, MBA
DAVID M. SCHUSTER, MD
JESSICA WILLIAMS, CNMT, RT(N),
FSNMMI-TS
HARVEY A. ZIESSMAN, MD, FSNMMI

Ex officio

JOHANNES CZERNIN, MD
KATHY S. THOMAS, MHA, CNMT,
PET, FSNMMI-TS
HENRY F. VANBROCKLIN, PhD, FSNMMI
RICHARD L. WAHL, MD, FACNM

Associate Director of Communications

SUSAN ALEXANDER

Senior Copyeditor

SUSAN NATH

Senior Publications & Marketing Service Manager

STEVEN KLEIN

Editorial Production Manager

PAULETTE MCGEE

Editorial Project Manager

MARK SUMIMOTO

Director of Communications

REBECCA MAXEY

CEO

VIRGINIA PAPPAS

MISSION STATEMENT: *The Journal of Nuclear Medicine* advances the knowledge and practice of molecular imaging and therapy and nuclear medicine to improve patient care through publication of original basic science and clinical research.

JNM (ISSN 0161-5505 [print]; ISSN 2159-662X [online]) is published monthly by SNMMI, 1850 Samuel Morse Drive, Reston, VA 20190-5316. Periodicals postage is paid at Herndon, VA, and additional mailing offices. Postmaster, send address changes to *The Journal of Nuclear Medicine*, 1850 Samuel Morse Drive, Reston, VA 20190-5316. The costs of publication of all nonsolicited articles in *JNM* were defrayed in part by the payment of page charges. Therefore, and solely to indicate this fact, these articles are hereby designated "advertisements" in accordance with 18 USC section 1734.

DISCLOSURE OF COMMERCIAL INTEREST: Johannes Czernin, MD, editor-in-chief of *The Journal of Nuclear Medicine*, has indicated that he is a founder of Sofie Biosciences and holds equity in the company and in intellectual property invented by him, patented by the University of California, and licensed to Sofie Biosciences. He is also a founder and board member of Trethera Therapeutics and holds equity in the company and in intellectual property invented by him, patented by the University of California, and licensed to Triangle. He also serves on the medical advisory board of Actinium Pharmaceuticals and on the scientific advisory boards of POINT Biopharma, RayzeBio, and Jubilant Pharma and is a consultant for Amgen. No other potential conflicts of interest were reported. Manuscripts submitted to *JNM* with potential conflicts are handled by a guest editor.

EDITORIAL COMMUNICATIONS should be sent to: Editor-in-Chief, Johannes Czernin, MD, *JNM* Office, SNMMI, 1850 Samuel Morse Drive, Reston, VA 20190-5316. Phone: (703) 326-1185; Fax: (703) 708-9018. To submit a manuscript, go to <https://submit-jnm.snmjournals.org>.

BUSINESS COMMUNICATIONS concerning permission requests should be sent to the publisher, SNMMI, 1850 Samuel Morse Drive, Reston, VA 20190-5316; (703) 708-9000; home page address: jnm.snmjournals.org. Subscription requests and address changes should be sent to Membership Department, SNMMI at the address above. Notify the Society of change of address and telephone number at least 30 days before date of issue by sending both the old and new addresses. Claims for copies lost in the mail are allowed within 90 days of the date of issue. Claims are not allowed for issues lost as a result of insufficient notice of change of address. For information on advertising, contact Team SNMMI (Kevin Dunn, Rich Devanna, and Charlie Meitner; (201) 767-4170; fax: (201) 767-8065; TeamSNMMI@cunnesso.com). Advertisements are subject to editorial approval and are restricted to products or services pertinent to nuclear medicine. Closing date is the first of the month preceding the date of issue.

INDIVIDUAL SUBSCRIPTION RATES for the 2021 calendar year are \$574 within the United States and Canada; \$617 elsewhere. Make checks payable to the SNMMI. CPC IPM Sales Agreement No. 1415158. Sales of individual back copies from 1999 through the current issue are available for \$60 at <http://www.snmgi.org/subscribe> (subscriptions@snmgi.org; fax: (703) 667-5134). Individual articles are available for sale online at <http://jnm.snmjournals.org>.

COPYRIGHT © 2021 by the Society of Nuclear Medicine and Molecular Imaging. All rights reserved. No part of this work may be reproduced or translated without permission from the copyright owner. Individuals with inquiries regarding permission requests, please visit <http://jnm.snmjournals.org/site/misc/permission.xhtml>. Because the copyright on articles published in *The Journal of Nuclear Medicine* is held by the Society, each author of accepted manuscripts must sign a statement transferring copyright (available for downloading at <http://jnm.snmjournals.org/site/misc/ifafora.xhtml>). See Information for Authors for further explanation (available for downloading at <http://www.snmjournals.org/site/misc/ifafora.xhtml>).

The ideas and opinions expressed in *JNM* do not necessarily reflect those of the SNMMI or the Editors of *JNM* unless so stated. Publication of an advertisement or other product mentioned in *JNM* should not be construed as an endorsement of the product or the manufacturer's claims. Readers are encouraged to contact the manufacturer with any questions about the features or limitations of the products mentioned. The SNMMI does not assume any responsibility for any injury or damage to persons or property arising from or related to any use of the material contained in this journal. The reader is advised to check the appropriate medical literature and the product information currently provided by the manufacturer of each drug to be administered to verify the dosage, the method and duration of administration, and contraindications.



Practical Dosimetry Achieved

Not all dosimetry solutions are the same.

Nuclear Medicine requires automation to enable clinical dosimetry without adding time to the workflow.

MIM SurePlan™ MRT

Advancing Molecular Radiotherapy

Calculating patient-specific dose doesn't have to add significant time to your workflow. MIM SurePlan MRT provides a single solution for effective dosimetry, organ and tumor segmentation, deformable registration, and communication tools that help reduce clinical effort.



AI Segmentation*

Utilize artificial intelligence to automate organ segmentation, which greatly reduces time and is a key to making dosimetry practical.

**AI segmentation may not be available in all countries. Contact MIM Software for more information.*



Quantitative SPECT Reconstruction

Generate quantitative images for measuring dose — no new cameras or additional software required. SPECTRA Quant® is included, which provides vendor-neutral quantitative SPECT reconstruction.



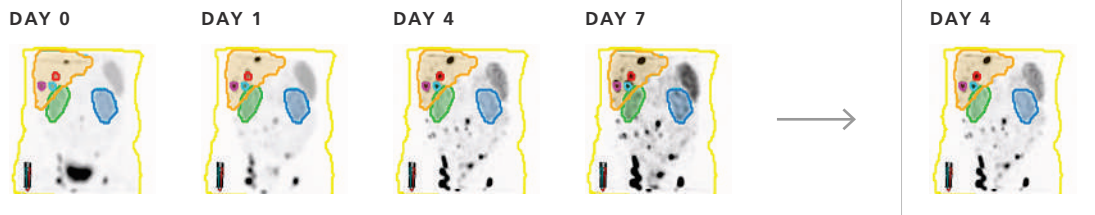
Multi-Tracer Theranostics Support

Support for multiple Molecular Radiotherapy tracers, such as Lu-177 dotatate, I-131 mIBG, [I-131] NAI for thyroid, and more.



Single Timepoint Dosimetry

Accurately estimate the absorbed dose with only a single SPECT/CT, further reducing the requirements needed to perform dosimetry.



MIM SurePlan MRT supports both multiple timepoint and single timepoint dosimetry.



Scan the QR code or visit <https://go.mimsoftware.com/JNM> to schedule a demo or learn more.

MIM Software Inc. • 25800 Science Park Drive – Suite 180, Cleveland, Ohio 44122 • 866-421-2536
© 2021 MIM Software Inc. • All Rights Reserved • Details subject to change • TD1104 – 11 Nov 2021

1S Radiopharmaceutical Dosimetry for Cancer

Therapy: From Theory to Practice

Richard L. Wahl and John Sunderland

Wahl and Sunderland introduce this special *JNM* supplement designed as a snapshot in time addressing both the rapid progress and challenges in applying patient-specific radiation dosimetry to guide radiopharmaceutical therapies.

3S Dosimetry for Radiopharmaceutical Therapy: Current Practices and Commercial Resources

Jacek Capala, Stephen A. Graves, Aaron Scott, George Sgouros, Sara St. James, Pat Zanzonico, and Brian E. Zimmerman

Capala and colleagues provide an overview of the state of the art of patient-specific dosimetry for radiopharmaceutical therapy, including current methods and commercially available software and other resources.

12S Tumor Response to Radiopharmaceutical Therapies: The Knowns and the Unknowns

George Sgouros, Yuni K. Dewaraja, Freddy Escorcia, Stephen A. Graves, Thomas A. Hope, Amir Iravani, Neeta Pandit-Taskar, Babak Saboury, Sara St. James, and Pat B. Zanzonico

Sgouros and colleagues elucidate factors affecting the absorbed dose-versus-response relationship for radiopharmaceutical agents, including inflammation- or immune-mediated effects, theranostic imaging, radiobiology, differences in dosimetry methods, pharmacokinetic differences, and tumor hypoxia.

23S Normal-Tissue Tolerance to Radiopharmaceutical Therapies, the Knowns and the Unknowns

Richard L. Wahl, George Sgouros, Amir Iravani, Heather Jacene, Daniel Pryma, Babak Saboury, Jacek Capala, and Stephen A. Graves

Wahl and colleagues look at the knowns and unknowns of dose-toxicity relationships in radiopharmaceutical therapies, including irradiation mechanisms, specific pharmacokinetics, secondary malignancies and side effects, and gaps in understanding, with key recommendations for the future.

36S An International Study of Factors Affecting Variability of Dosimetry Calculations, Part 1: Design and Early Results of the SNMMI Dosimetry Challenge

Carlos Uribe, Avery Peterson, Benjamin Van, Roberto Fedrigo, Jake Carlson, John Sunderland, Eric Frey, and Yuni K. Dewaraja

Uribe and colleagues detail initial results from a ^{177}Lu dosimetry challenge designed to collect data from the global nuclear

medicine community to identify, understand, and quantitatively characterize the consequences of sources of variability in dosimetry.

48S Reimbursement Approaches for Radiopharmaceutical Dosimetry: Current Status and Future Opportunities

Stephen A. Graves, Alexandru Bageac, James R. Crowley, and Denise A.M. Merlino

Graves and colleagues from the SNMMI Molecular Imaging Dosimetry Task Force review rationales and workflows for radiopharmaceutical therapy dosimetry, as well as current and suggested future strategies for reimbursement for dosimetry-related clinical activities.

60S Dosimetry in Clinical Radiopharmaceutical Therapy of Cancer: Practicality Versus Perfection in Current Practice

Neeta Pandit-Taskar, Amir Iravani, Dan Lee, Heather Jacene, Dan Pryma, Thomas Hope, Babak Saboury, Jacek Capala, and Richard L. Wahl

Pandit-Taskar and colleagues review dosimetric approaches in radiopharmaceutical therapy and clinical trials, including the extent of dosimetry use, pros and cons of dosimetry-based versus fixed activity, and limiting factors in current clinical practice.

73S Dosimetry for Radiopharmaceutical Therapy: The European Perspective

Michael Lassmann, Uta Eberlein, Jonathan Gear, Mark Konijnenberg, and Jolanta Kunikowska

Lassmann and colleagues summarize recent efforts in Europe targeting standardization of quantitative imaging and dosimetry and the results of several European research projects on practices regarding radiopharmaceutical therapies.

GUEST EDITORS

Richard L. Wahl, MD
Mallinckrodt Institute of Radiology
St. Louis, Missouri

John Sunderland, PhD
University of Iowa
Iowa City, Iowa

Editor-in-Chief
Johannes Czernin, MD
David Geffen School of Medicine at UCLA
Los Angeles, California

Opinions expressed in the contributions to this supplement are solely those of the authors and do not necessarily reflect those of *The Journal of Nuclear Medicine* or the Society of Nuclear Medicine and Molecular Imaging. The journal, however, invites and welcomes different opinions in order to initiate and stimulate discussion.

EDITOR-IN-CHIEF

Johannes Czernin, MD
University of California at Los Angeles
Los Angeles, California

IMMEDIATE PAST EDITOR

Dominique Delbeke, MD, PhD
Vanderbilt University Medical Center
Nashville, Tennessee

NEWSLINE EDITOR

Harvey A. Ziessman, MD
Takoma Park, Maryland

ASSOCIATE EDITORS, CONTINUING EDUCATION

Heiko Schöder, MD
Memorial Sloan Kettering Cancer Center
New York, New York
H. William Strauss, MD
Memorial Sloan Kettering Cancer Center
New York, New York

ASSOCIATE EDITORS

Ramsey Derek Badawi, PhD
UC Davis Medical Center
Sacramento, California
Henryk Barthel, MD, PhD
Leipzig University
Leipzig, Germany
Frank M. Bengel, MD
Hannover Medical School
Hannover, Germany
Lisa Bodei, MD, PhD
Memorial Sloan Kettering Cancer Center
New York, New York
Irene Buvat, PhD
Université Paris Sud
Orsay, France
Jérémie Calais, MD
University of California at Los Angeles
Los Angeles, California
Marcelo F. Di Carli, MD
Brigham and Women's Hospital
Boston, Massachusetts
Alexander E. Drzezga
University Hospital of Cologne
Cologne, Germany
Jan Grimm, MD, PhD
Memorial Sloan Kettering Cancer Center
New York, New York
Ken Herrmann, MD, MBA
Universitätsklinikum Essen
Essen, Germany
Lale Kostakoglu, MD, MPH
University of Virginia Health System
Charlottesville, Virginia
Jason S. Lewis, PhD
Memorial Sloan Kettering Cancer Center
New York, New York
David A. Mankoff, MD, PhD
University of Pennsylvania
Philadelphia, Pennsylvania
Wolfgang Weber, MD
Technical University of Munich
München, Germany

SERIES EDITOR, FOCUS ON MI

Carolyn J. Anderson, PhD
University of Missouri
Columbia, Missouri

SERIES EDITOR, HOT TOPICS

Heinrich R. Schelbert, MD, PhD
University of California at Los Angeles
Los Angeles, California

CONSULTING EDITORS

Nancy Knight, PhD
University of Maryland School of Medicine
Baltimore, Maryland
Barry A. Siegel, MD
Mallinckrodt Institute of Radiology
St. Louis, Missouri
Arnold M. Strashun, MD
SUNY Downstate Medical Center
Scarsdale, New York

ASSOCIATE EDITORS (INTERNATIONAL)

Gerald Antoch, MD
Dusseldorf, Germany

Richard P. Baum, MD, PhD

Bad Berka, Germany
Ambros J. Beer, MD
Ulm, Germany
Francois Benard, MD
Vancouver, Canada
Thomas Beyer, PhD
Vienna, Austria
Andreas K. Buck, MD
Würzburg, Germany
Ignasi Carrió, MD
Barcelona, Spain
June-Key Chung, MD
Seoul, Korea
Stefano Fanti, MD
Bologna, Italy
Markus Hacker, MD
Wien, Austria
Rodney J. Hicks, MD
Melbourne, Australia
Michael S. Hofman, MBBS
Melbourne, Australia
Ora Israel, MD
Haifa, Israel
Andreas Kjaer, MD, PhD, DMSc
Copenhagen, Denmark
Adriaan A. Lammertsma, PhD
Amsterdam, The Netherlands
Michael Lassman, PhD
Würzburg, Germany
Helmut R. Mäcke, PhD
Freiburg, Germany
Wim J.G. Oyen, MD, PhD
Milan, Italy
John O. Prior, MD, PhD
Lausanne, Switzerland
Osman Ratib, MD, PhD
Geneva, Switzerland
Mike Satheke, MChB, MMed, PhD
Pretoria, South Africa
Markus Schwaiger, MD
München, Germany
Andrew M. Scott, MD
Heidelberg, Australia
Nagara Tamaki, MD, PhD
Kyoto, Japan
Jia-He Tian, PhD
Beijing, China
Mei Tian, MD, PhD
Hangzhou, China
Hans-Jürgen Wester, PhD
Garching, Germany

EDITORIAL CONSULTANTS

Martin S. Allen-Auerbach, MD
Los Angeles, California
Magnus Dahlbom, PhD
Los Angeles, California
Andrew Quon, MD
Los Angeles, California
Christiaan Schiepers, MD, PhD
Los Angeles, California
Daniel H. Silverman, MD, PhD
Los Angeles, California
Roger Slavik, PhD
Winterthur, Switzerland

EDITORIAL BOARD

Diane S. Abou, PhD
St. Louis, Missouri
Valentina Ambrosini, MD, PhD
Bologna, Italy
Norbert Avril, MD
Cleveland, Ohio
Shadfar Bahri
Los Angeles, California
Jacques Barbet, PhD
Saint-Herbalin, France
Bradley Jay Beattie, PhD
New York, New York
Matthias Richard Benz, MD
Los Angeles, California
Pradeep Bhambhani, MD
Birmingham, Alabama
Angelika Bischof-Delaloye, MD
Lausanne, Switzerland

Christina Bluemel, MD

Würzburg, Germany
Ronald Boellaard, PhD
Groningen, The Netherlands
Nicolaas Bohnen, MD
Ann Arbor, Michigan
Wesley E. Bolch, PhD
Gainesville, Florida
Elias H. Botvinick, MD
San Francisco, California
Winfried Brenner, MD, PhD
Berlin, Germany
Richard C. Brunken, MD
Cleveland, Ohio
Ralph Buchert, PhD
Hamburg, Germany
Alfred Buck, MD
Menzingen, Switzerland
Denis B. Buxton, PhD
Bethesda, Maryland
Weibo Cai, PhD
Madison, Wisconsin
Federico Caobelli, MD
Basel, Switzerland
Giuseppe Carlucci, PhD
Los Angeles, California
Richard E. Carson, PhD
New Haven, Connecticut
Paolo Castellucci, MD
Bologna, Italy
Francesco Ceci, MD, PhD
Turin, Italy
Juliano J. Cerci
Curitiba, Brazil
Delphine Chen, MD
Seattle, Washington
Xiaoyuan Chen, PhD
Singapore
Simon R. Cherry
Davis, California
Arturo Chiti, MD
Rozzano, Italy
Peter M. Clark, PhD
Los Angeles, California
Christian Cohade, MD
Montreal, Canada
Ekaterina (Kate) Dadachova, PhD
Saskatoon, Canada
Issa J. Dahabreh, MD
Boston, Massachusetts
Heike Elisabeth Daldrop-Link, MD, PhD
Stanford, California
Farrokh Dehdashti, MD
St. Louis, Missouri
Robert C. Delgado-Bolton, MD, PhD
Logroño, Spain
Thorsten Derlin, MD
Hannover, Germany
Elisabeth G.E. de Vries, PhD
Groningen, The Netherlands
David W. Dick, PhD
Iowa City, Iowa
Vasken Dilisizian, MD
Baltimore, Maryland
Sharmila Dorbala, MBBS
Lexington, Massachusetts
Jacob Dubroff, MD, PhD
Philadelphia, Pennsylvania
Janet F. Eary, MD
Bethesda, Maryland
W. Barry Edwards, PhD
Columbia, Missouri
Matthias Eiber, MD
Munich, Germany
David Eidelberg, MD
Manhasset, New York
Georges El Fakhri, PhD
Boston, Massachusetts
Peter J. Ell, MD
London, United Kingdom
Keigo Endo, MD
Nantan, Japan
Einat Even-Sapir, MD, PhD
Tel Aviv, Israel
Frederic H. Fahey, DSc
Boston, Massachusetts

Developing next-generation radiopharmaceuticals for precision oncology.

Fusion Pharmaceuticals is a clinical-stage oncology company focused on developing next-generation radiopharmaceuticals as precision medicines. Fusion is currently opening trial sites and recruiting patients for its Phase 1 clinical studies of FPI-1434 targeting IGF-1R, and FPI-1966 targeting FGFR3, in patients with solid tumors.

www.fusionpharma.com

info@fusionpharma.com



EDITORIAL BOARD, continued

Melpomeni Fani, PhD, MSc
Basel, Switzerland
Wolfgang Peter Fendler, MD
Essen, Germany
James W. Fletcher, MD
Indianapolis, Indiana
Amy M. Fowler, MD, PhD
Madison, Wisconsin
Kirk A. Frey, MD, PhD
Ann Arbor, Michigan
Andrei Gafita
Los Angeles, California
Victor H. Gerbaudo, PhD, MSHCA
Boston, Massachusetts
Frederik L. Giesel, MD, PhD, MBA
Düsseldorf, Germany
Serge Goldman, MD, PhD
Brussels, Belgium
Stanley J. Goldsmith, MD
New York, New York
Martin Gotthardt, MD, PhD
Nijmegen, The Netherlands
Michael Graham, MD, PhD
Iowa City, Iowa
David Groheux, MD, PhD
Paris, France
Uwe A. Haberkorn, MD
Heidelberg, Germany
Mathieu Hatt, PhD, HDR
Brest, France
Wolf-Dieter Heiss, MD
Cologne, Germany
Karl Herholz, MD
Manchester, United Kingdom
Thomas F. Heston, MD
Las Vegas, Nevada
John M. Hoffman, MD
Salt Lake City, Utah
Carl K. Hoh, MD
San Diego, California
Jason P. Holland, DPhil
Zurich, Switzerland
Thomas A. Hope, MD
San Francisco, California
Roland Hustinx, MD, PhD
Liege, Belgium
Andrei H. Iagaru, MD
Stanford, California
Masanori Ichise, MD
Chiba, Japan
Heather A. Jacene, MD
Boston, Massachusetts
Hossein Jadvar, MD, PhD, MPH, MBA
Los Angeles, California
Francois Jamar, MD, PhD
Brussels, Belgium
Jae Min Jeong, PhD
Seoul, Korea
John A. Katzenellenbogen, PhD
Urbana, Illinois
Kimberly A. Kelly, PhD
Charlottesville, Virginia
Laura M. Kenny, MD, PhD
London, United Kingdom
Fabian Kiessling, MD
Aachen, Germany
E. Edmund Kim, MD, MS
Orange, California
Francoise Kraeber-Bodéré, MD, PhD
Nantes, France
Clemens Kratochwil, MD
Heidelberg, Germany
Kenneth A. Krohn, PhD
Portland, Oregon
Brenda F. Kurland, PhD
Pittsburgh, Pennsylvania
Constantin Lapa, MD
Augsburg, Germany
Suzanne E. Lapi, PhD
Birmingham, Alabama
Steven M. Larson, MD
New York, New York
Dong Soo Lee, MD, PhD
Seoul, Korea
Jeffrey Leyton, PhD
Sherbrooke, Canada
Hannah M. Linden, MD
Seattle, Washington
Martin A. Lodge, PhD
Baltimore, Maryland

Egesta Lopci, MD, PhD
Milan, Italy
Katharina Lücknerath, PhD
Los Angeles, California
Susanne Lütje, MD, PhD
Bonn, Germany
Umar Mahmood, MD, PhD
Boston, Massachusetts
H. Charles Manning, PhD
Nashville, Tennessee
Giuliano Mariani, MD
Pisa, Italy
Chester A. Mathis, PhD
Pittsburgh, Pennsylvania
Alan H. Maurer, MD
Philadelphia, Pennsylvania
Jonathan McConathy, MD, PhD
Birmingham, Alabama
Alexander J.B. McEwan, MD
Edmonton, Canada
Yusuf Menda, MD
Iowa City, Iowa
Philipp T. Meyer, MD, PhD
Freiburg, Germany
Matthias Miederer, MD
Mainz, Germany
Erik Mittra, MD, PhD
Portland, Oregon
Christine E. Mona, PhD
Los Angeles, California
Dae Hyuk Moon, MD
Seoul, Korea
Jennifer Murphy, PhD
Los Angeles, California
Helen Nadel, MD, FRCPC
Stanford, California
Matthias Nahrendorf, MD, PhD
Boston, Massachusetts
Yuji Nakamoto, MD, PhD
Kyoto, Japan
David A. Nathanson, PhD
Los Angeles, California
Sridhar Nimmagadda, PhD
Baltimore, Maryland
Egbert U. Nitzsche, MD
Aarau, Switzerland
Medhat M. Osman, MD, PhD
Saint Louis, Missouri
Christopher J. Palestro, MD
New Hyde Park, New York
Miguel Hernandez Pampaloni, MD, PhD
San Francisco, California
Neeta Pandit-Taskar, MD
New York, New York
Michael E. Phelps, PhD
Los Angeles, California
Gerold Porenta, MD, PhD
Vienna, Austria
Sophie Poty, PhD
Montpellier, France
Edwin (Chuck) Pratt, PhD, MS Eng
New York, New York
Daniel A. Pryma, MD
Philadelphia, Pennsylvania
Valery Radchenko, PhD
Vancouver, Canada
Caius G. Radu, MD
Los Angeles, California
Isabel Rauscher, MD
Munich, Germany
Nick S. Reed, MBBS
Glasgow, United Kingdom
Mark Rijpkema, PhD
Nijmegen, The Netherlands
Steven P. Rowe, MD, PhD
Baltimore, Maryland
Mehran Sadeghi, MD
West Haven, Connecticut
Orazio Schillaci, MD
Rome, Italy
Charles Ross Schmidlein, PhD
New York, New York
David M. Schuster, MD
Atlanta, Georgia
Travis Shaffer, PhD
Stanford, California
Sai Kiran Sharma, PhD
New York, New York
Anthony F. Shields, MD, PhD
Detroit, Michigan

Barry L. Shulkin, MD, MBA
Memphis, Tennessee
Yu Shyr, PhD
Nashville, Tennessee
Albert J. Sinusas, MD
New Haven, Connecticut
Riener H.J.A. Slart, MD, PhD
Groningen, The Netherlands
Piotr Slomka, PhD, FACC
Los Angeles, California
Ida Sonni, MD
Los Angeles, California
Michael G. Stabin, PhD
Richland, Washington
Lisa J. States, MD
Philadelphia, Pennsylvania
Sven-Erik Strand, PhD
Lund, Sweden
Rathan M. Subramaniam, MD, PhD, MPH
Dunedin, New Zealand
John Sunderland, PhD
Iowa City, Iowa
Suleman Surti, PhD
Philadelphia, Pennsylvania
Julie Sutcliffe, PhD
Sacramento, California
Laura H. Tang, MD, PhD
New York, New York
Ukihide Tateishi, MD, PhD
Tokyo, Japan
James T. Thackeray, PhD
Hannover, Germany
Mathew L. Thakur, PhD
Philadelphia, Pennsylvania
Alexander Thiel, MD
Montreal, Canada
Daniel L.J. Thorek, PhD
St. Louis, Missouri
David W. Townsend, PhD
Singapore
Timothy Turkington, PhD
Durham, North Carolina
Gary A. Ulaner, MD, PhD
Irvine, California
David Ulmert, MD, PhD
Los Angeles, California
Christopher H. van Dyck, MD
New Haven, Connecticut
Douglas Van Nostrand, MD
Washington, District of Columbia
Patrick Veit-Haibach, MD
Toronto, Canada
Nerissa Viola-Villegas, PhD
Detroit, Michigan
John R. Votaw, PhD
Atlanta, Georgia
Richard L. Wahl, MD
St. Louis, Missouri
Anne Marie Wallace, MD
La Jolla, California
Martin A. Walter, MD
Geneva, Switzerland
Rudolf A. Werner, MD
Wuerzburg, Germany
Andreas G. Wibmer, MD
New York, New York
Anna M. Wu, PhD
Duarte, California
Randy Yeh, MD
New York, New York
Hyewon (Helen) Youn, PhD
Seoul, Korea
Pat B. Zanzonico, PhD
New York, New York
Brian M. Zeglis, PhD
New York, New York
Robert Zeiser, MD
Freiburg, Germany
Hong Zhang, MD, PhD
Hangzhou, China
Hongming Zhuang, MD, PhD
Philadelphia, Pennsylvania
Sibylle I. Ziegler, PhD
Munich, Germany
ASSISTANT TO THE EDITOR
Joshua N. Wachtel
Los Angeles, California



Global Imaging CRO

Complete Radiopharmaceutical Therapy & Theranostics Services

**Radiochemistry | Preclinical | Phase 0-IV
Imaging Core Lab | Dosimetry | Advanced Analytics & AI**

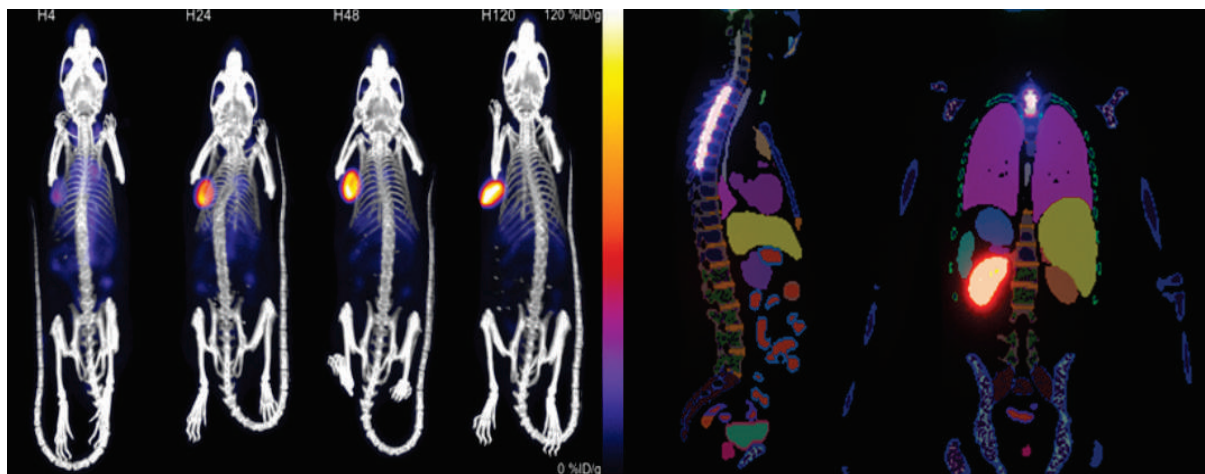


Image Sources: Left - Preclinical evaluation of an $^{111}\text{In}/^{225}\text{Ac}$ theranostic targeting transformed MUC1 for triple negative breast cancer (Vanessa J Kelly et al. Theranostics 2020). Right - Three-Dimensional Dosimetry for Radiation Safety Estimates from Intrathecal Administration (Hesterman et al. JNM 2017).

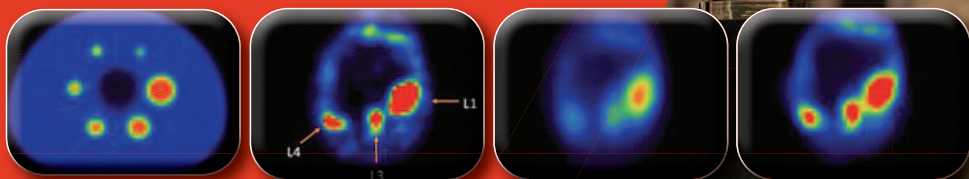
Streamlined Development, Evaluation and Clinical Translation of Radiopharmaceuticals

Operational Excellence | Scientific & Regulatory Expertise

+1 617-904-2100
info@invicro.com
www.invicro.com
f t in

Download
Radiopharmaceutical Therapy
Informational Guide





Explore the Latest Innovations and Clinical Applications in Radiopharmaceutical Therapy

Register now to attend the **SNMMI 2022 Therapeutics Conference**, taking place **March 10-12** in **New Orleans, LA**.

As an attendee, you'll have the opportunity to connect directly with an esteemed group of experts and learn more about the latest innovations and clinical applications in radiopharmaceutical therapy.

Topics include:

- Operational Issues
- Radiation Safety and Research
- MIBG
- Dosimetry
- Lymphoma/Leukemia
- Neuroendocrine Cancer
- Prostate Cancer
- Thyroid
- Future Strategies for Radiopharmaceutical Therapy

Join us in New Orleans, reconnect with colleagues, and be part of the discussion on the future of personalized medicine. Register early. Space is limited.



Learn more and register today!
www.snmmi.org/TC2022

Early-bird Deadline: January 20, 2022



Dosimetry Made Simple

Rapid provides comprehensive expert services and software solutions related to quantitative imaging and dosimetry, in support of pre-clinical and clinical studies needed for regulatory approval and for the effective and safe clinical implementation of radiopharmaceutical therapies.

Rapid provides a full range of services including imaging and dosimetry analysis of human & pre-clinical data.

- ▶ Support for imaging trial design such as determining the number of measurement time points as well as their intervals and image acquisition settings.
- ▶ Description of phantom studies to assure accuracy and the development of imaging manuals, including detailed standard operating procedures.
- ▶ Centralized vendor-agnostic quantitative SPECT reconstruction for a wide range of radionuclides (Tc-99m, I-123, I-131, Lu-177 and In-111), including hard-to-image radionuclides such as Ra-223, Ac-225, Th-227, Y-90, and Pb-212.
- ▶ Unique expertise on alpha-emitter imaging and dosimetry, including accounting for daughter distributions.



**DEDICATED EXPERT
FULL-TIME STAFF**



**PROFESSIONAL
EXPERIENCE**



**REAL-TIME PROCESS
TO START CALCULATION**

First product 3D-RD-S to launch in Quarter 1 of 2022

3D-RD-S is a web-based application used to perform radiopharmaceutical dosimetry based on the MIRD S-value methodology. 3D-RD-S is used to calculate the absorbed dose and related radiobiological quantities that translate absorbed doses into likely biological response.

Rapid brings more than 80 years of experience in the fields of nuclear medicine, quantitative imaging, and dosimetry to help solve imaging and dosimetry challenges.

(443) 524-7396 | info@rapiddosimetry.com | rapiddosimetry.com

Learn More:



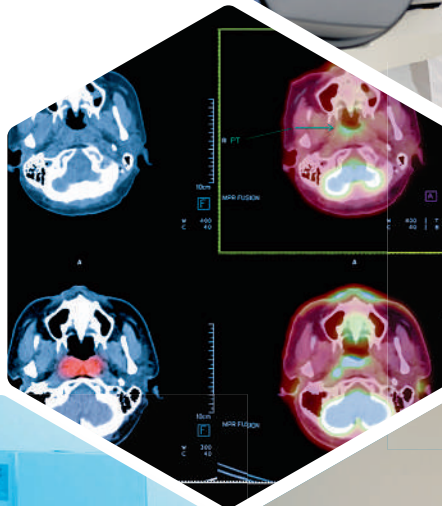


MIRION
TECHNOLOGIES

RADIATION SAFETY, EXPERTISE AND INNOVATION

Powered by an unstoppable drive for discovery. Backed by 60+ years of radiation measurement, innovation, and science expertise. Mirion's trusted family of brands and industry-leading products and services are helping to advance human health around the world.

- *Nuclear Medicine Devices*
- *Radiation Shielding and Accessories*



Driving Innovation, Together:



CAPINTEC, INC.
Part of Mirion Technologies



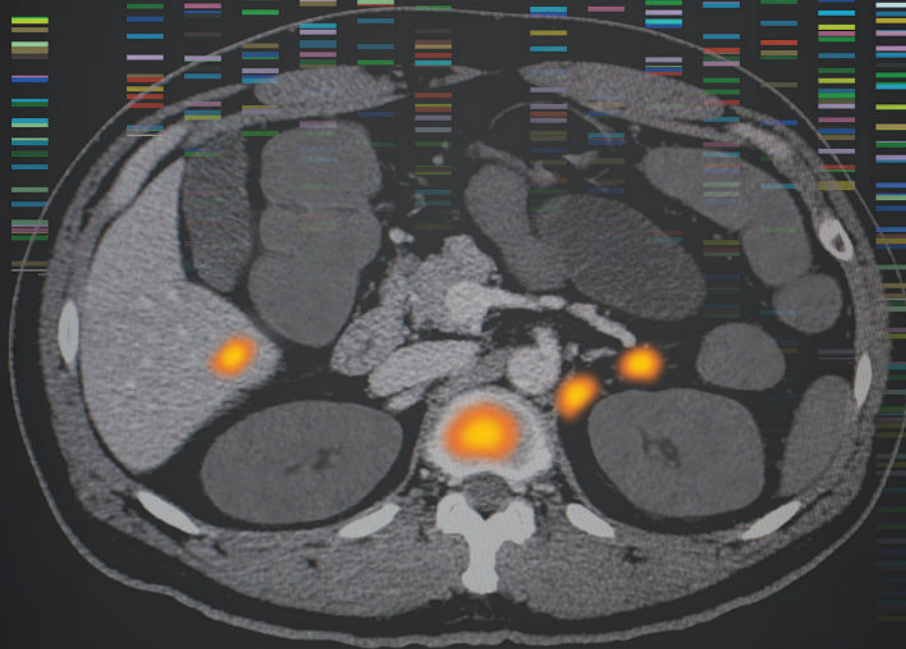
BIODEX
Part of Mirion Technologies

Visit capintec.com to learn how we can support your unique requirements.

Mirion, the Mirion logo, and other trade names of Mirion products listed herein are registered trademarks or trademarks of Mirion Technologies, Inc. or its affiliates in the United States and other countries.

FOR YOUR PATIENTS WITH ADVANCED PROSTATE CANCER

HOW CAN PHENOTYPIC BIOMARKERS INCREASE THE USE OF PRECISION MEDICINE IN ADVANCED PROSTATE CANCER?



Phenotypic precision medicine facilitates clinical decision making based on observable characteristics, or phenotypes.¹⁻³

PSMA PET imaging is a noninvasive diagnostic that can detect phenotypic biomarkers, such as PSMA, which may simplify your approach to precision medicine.¹⁻⁷

Learn more at www.PhenotypicPrecisionMedicine.com.

PET, positron emission tomography; PSMA, prostate-specific membrane antigen.

References

1. Hofman MS et al. *Lancet*. 2020;395(10231):1208-1216.
2. Müller J et al. *Eur J Nucl Med Mol Imaging*. 2019;46(4):889-900.
3. Calais J et al. *J Nucl Med*. 2018;59(3):434-441.
4. Rowe SP et al. *J Nucl Med*. 2015;56(7):1003-1010.
5. Osborne JR et al. *J Urol*. 2014;191(5):1439-1445.
6. Sant GR et al. *NPJ Precis Oncol*. 2017;1(1):21.
7. Kratochwil C et al. *J Nucl Med*. 2016;57:1170-1176.

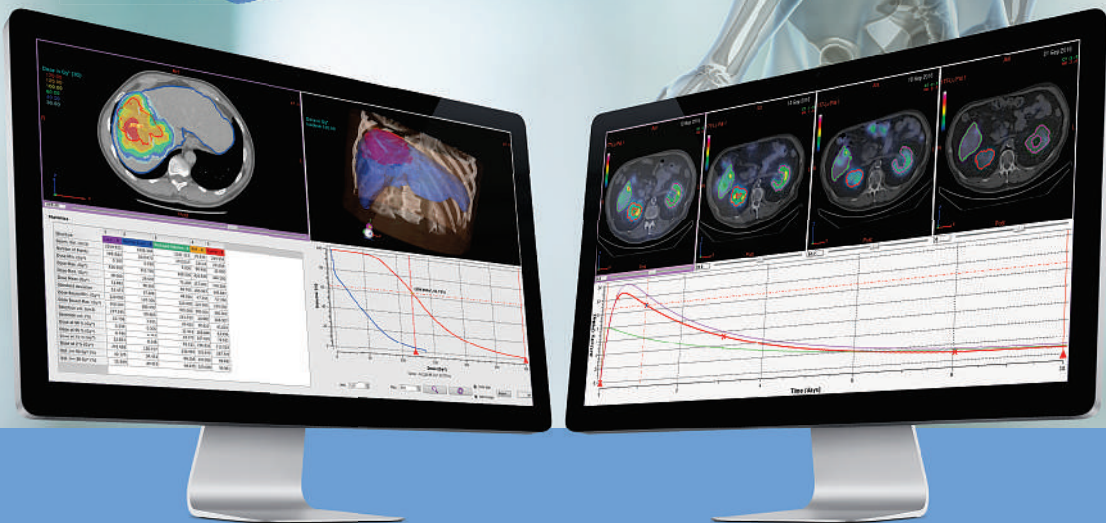
© 2020 Advanced Accelerator Applications | All Rights Reserved
November 2020 | PSM-1237214





PLANET[®] Software

Patient-Specific Dosimetry for Radiopharmaceutical Therapy



Integrated Dosimetry Workflow

Patient diagnostics,
Treatment planning,
In vivo dose control,
Disease follow-up

Multi-radionuclide Platform

Pre-Post 3D dosimetry
for ⁹⁰Yttrium-SIRT,
¹⁷⁷Lutetium & ¹³¹Iodine*
based therapies,
DVH analysis

Innovative Imaging Features

AI-based auto contouring
assistance*,
Texture analysis for
Radiomics studies

DOSI  soft

PLANET[®] Suite is developed by DOSIsoft SA in France.
Technical specifications are subject to change without notice.
The product or certain features may or may not be available for clinical use in any particular country.
Please contact your local representative for more information.
*Ongoing clinical validation, not for clinical use.



THE CONVERSATION CANCER DOESN'T WANT YOU TO HAVE.

Join an expert roundtable to discuss the benefits of advanced RPT dosimetry with Dr. Richard Wahl, Dr. Homer Macapinlac and Dr. Stephen Graves. While cancer may not want to hear about personalized dosimetry, it's a conversation you don't want to miss.



Roundtable: *Exploring the Benefits of Advanced Dosimetric Methods*
Join online February 23rd • Register at personalized-rpt.com

Hosted by
VOXIMETRY

The most powerful words you'll ever hear.

“Thank You.”

With your contribution, our profession can continue efforts leading to critical advances in cancer treatments and care.

The **Value Initiative Transformative Leadership Campaign** is the cornerstone for making these efforts a reality for patients of all ages.

The world needs more “thank you’s.”

Help improve the life of a patient. Lend your support today.

Make Your Tax-Deductible
Donation by December 31

www.snmmi.org/TransformativeLeadership

SNMMI is a 501 (c)(3) tax id 36-2496678. Your donation is tax deductible as per current IRS regulations. Please remember SNMMI in your estate plans.

SNMMI Value Initiative
MI
SOCIETY OF NUCLEAR MEDICINE & MOLECULAR IMAGING

Radiopharmaceutical Dosimetry for Cancer Therapy: From Theory to Practice

Richard L. Wahl¹ and John Sunderland²

¹Mallinckrodt Institute of Radiology, St. Louis, Missouri; and ²University of Iowa, Iowa City, Iowa

This supplement to *The Journal of Nuclear Medicine* includes 7 articles that address several of the critical facets of the current state of radiation dosimetry in radiopharmaceutical therapy. This supplement is designed to be a snapshot in time that attempts to address both the rapid progress and the challenges in applying patient-specific radiation dosimetry to guide radiopharmaceutical therapies. Six of the articles were generated by the Society of Nuclear Medicine and Molecular Imaging (SNMMI) Dosimetry Task Force led by Drs. Pat Zanzonico and George Sgouros, under the umbrella of the SNMMI's Research and Discovery Domain. As the perspective of the articles herein are largely based on practices in North America, an additional article is an invited perspective from Europe on the European approach to applying imaging-based dosimetry.

Looking back in time, ¹³¹I has long been used for thyroid cancer therapies but normally has a sufficiently high therapeutic index that dosimetry is not required, though it is feasible. The first radiopharmaceutical therapy of cancer requiring dosimetry in the Food and Drug Administration (FDA) label was ¹³¹I tositumomab, which was known commercially as Bexxar (*I*). The therapeutic regimen showed that it was feasible to generate a dosimetry-based dosing scheme for individual patients that could be widely disseminated. However, some viewed the dosimetry as too difficult (3 whole-body scans), and others felt the drug was too expensive. Long-term follow-up of randomized trials with the drug show significantly greater progression-free survival (PFS) than with standard therapies; nonetheless, the therapy was a commercial failure. Nearly 3 decades later, are we ready to revisit patient-specific dosimetry to drive radiopharmaceutical therapies?

Fueled by FDA approval of ¹⁷⁷Lu-DOTATATE in 2018, and the promising published results of the ¹⁷⁷Lu-PSMA-617 phase 3 VISION trial earlier this year (2,3), the nuclear medicine community is experiencing an unprecedented and palpable optimism for the future of the profession. In the wake of these developments, a slew of theranostic radiopharmaceuticals aimed at a variety of molecular targets and diseases are now rapidly entering early clinical trials, representing promise for downstream growth in the field. In parallel with these clinical developments, technologic and commercial advances in quantitative SPECT imaging, and development of sophisticated commercial internal radiation dosimetry software, are creating an environment whereby the vision of

accurate, reproducible personalized radiation dosimetry may be possible in the routine clinical practice of radiopharmaceutical therapy.

However, just because we can does not necessarily mean we should. This supplement begins to address whether radiopharmaceutical therapy is best performed as radioactive chemotherapy, for which the patient receives a standard dose that is determined from typical phase I–II dose escalation studies, and the toxicity profile from a given treatment is used to determine if subsequent administered activity levels should be adjusted upward or downward. This approach represents the “patient as the dosimeter” paradigm, with demonstration of physiologic toxicity as the readout of greatest relevance. However, because treatment decisions must be made promptly, this approach is difficult to use if toxicities are expected to be late in onset, potentially leading to underdosing of patients to avoid late toxicities. This supplement also addresses whether prospective imaging before a given treatment (or after, to verify dose delivery) can be used to guide patient-specific administered activity levels, which adjust for patient pharmacokinetics and which, in principle, would be expected to have greater efficacy and lower toxicity than a “one-dose-fits-all” approach.

It is clear that our radiotherapeutic armamentarium, current and future, contains a continuum of therapeutic indices. ¹³¹I therapy has historically had such a high therapeutic index that quantitative dosimetry would likely be a pointless exercise, resulting in little to no clinical benefit. ¹⁷⁷Lu-DOTATATE and ¹⁷⁷Lu-PSMA-617 both generate substantial survival benefit without patient-specific dosimetry—but how much better clinical performance might be achieved with dosimetry-guided optimization? And for new agents under current study, the therapeutic indices may be low enough that using patient-specific dosimetry is requisite to either qualify patients for the therapeutic radiopharmaceutical, or to titrate the therapeutic through image guidance. Clearly there are numerous questions still to both ask and answer.

Thus, we are currently facing the question “To D or not to D?” (where D = dosimetry) in no patients, selected patients, or all patients. We are probably not yet ready to answer this question, as it will require randomized trials to determine if dosimetry does, indeed, improve outcomes. On first principles, and based on decades-long experience with external-beam radiation therapy, it would seem that the ability to adjust dosing to a patient's specific pharmacokinetics and dosimetry would be more efficacious than giving repeated safe doses, which likely will result in underdosing the majority of patients. We cannot imagine giving external-beam therapy without dosimetry guidance. Will this eventually be the case for radiopharmaceutical therapies? And mission critical

Received Oct. 28, 2021.
For correspondence or reprints, contact Richard L. Wahl (rwahl@wustl.edu).
COPYRIGHT © 2021 by the Society of Nuclear Medicine and Molecular Imaging.
DOI: 10.2967/jnumed.121.263273

questions still remain, some scientific and some economic. What are the accuracies, variability, and reproducibility of our current dosimetry methodologies? (Short answer, we have substantial room for improvement.) What commercial tools are available? What is the outlook for reimbursement of dosimetry-related procedures? Under what circumstance does performing dosimetry have positive clinical impact?

The 7 articles in this supplement make a first-blush attempt to address these issues based on current information.

The first article, “Dosimetry for Radiopharmaceutical Therapy: Current Practices and Commercial Resources,” summarizes the current quantitative paradigms for dosimetry calculations and provides detailed and up-to-date descriptions of currently available resources to perform dosimetry, including approved and evolving commercial software and standard radiation sources (4).

The second article, “Tumor Response to Radiopharmaceutical Therapies: The Knowns and the Unknowns,” attempts to elucidate our current understanding (and lack thereof) of the subtle complexities underlying biologic responses of tissues to radiation. These include such topics as immune-mediated effects, radiobiologic mechanisms, tumor hypoxia, and dose rate effects (5).

Addressed in the third article, “Normal-Tissue Tolerance to Radiopharmaceutical Therapies, the Knowns and the Unknowns,” is the critical topic of radiation-induced organ toxicities—the primary limiting factor in our dosing paradigm. This article reviews much of our current knowledge base, mostly derived from the high-dose-rate external-beam radiation therapy literature, which has potentially limited applicability to our low-dose-rate radiopharmaceutical therapy. The article clearly describes the significant *lack* of scientific organ radiation toxicity data for low-dose-rate treatments, for which cellular repair can play a significant role, and points out opportunities for careful future studies (6).

“An International Study of Factors Affecting Variability of Dosimetry Calculations, Part 1: Design and Early Results of the SNMMI Dosimetry Challenge,” the fourth article, primarily describes the methodology associated with an international crowd-sourced project attempting to quantify variabilities associated with discrete steps in the dosimetry workflow (7). Multisite variability projects have precedent in both the imaging and the therapy space (8,9) but have not broken down individual steps as in the current challenge. In this progressive dosimetry calculation exercise, sites all over the world were provided identical multi-time-point DICOM SPECT/CT image data from 2 patients who underwent administration of ¹⁷⁷Lu-DOTATATE and were asked to report stepwise dosimetric calculations. This article reports very early results (the challenge is still in progress) and demographics of respondents. Early data show there is considerable room for improvement in the consistency of dose estimation.

The fifth article, “Reimbursement Approaches for Radiopharmaceutical Dosimetry: Current Status and Future Opportunities,” is perhaps the most pragmatic of the articles in this special edition and consists largely of a description of the various steps in the dosimetry workflow, and more importantly, current CPT codes that are likely appropriate to the various steps (10).

The current state of dosimetry (or lack thereof) in clinical practice today—largely in the United States but not exclusively—associated with approved radiopharmaceutical therapy agents is described in the sixth article. “Dosimetry in Clinical Radiopharmaceutical

Therapy of Cancer: Practicality Versus Perfection in Current Practice” discusses challenges associated with implementing dosimetry in the clinical space and limitations in available data currently supporting the use of dosimetry in standard clinical practice (11).

Finally, the seventh article, “Dosimetry for Radiopharmaceutical Therapy: The European Perspective,” describes the European approach to dosimetry in clinical practice. In many ways the European nuclear medicine community has much more rapidly adopted the concept and practice of quantitative image-based dosimetry than the United States. This article describes the European dosimetry practice and details relevant position papers by the European Association of Nuclear Medicine (12).

Taken together, these articles provide a current state-of-the-art understanding of the many elements of radiopharmaceutical therapy, highlighting the practical, the optimal, the knowns, and the unknowns, and provide valuable insights regarding commercial resources and billing approaches for dosimetry. The variability studies are of particular interest as they tell us that there are many opportunities to reduce variance and produce more uniform dosimetry.

We are hopeful these articles will provide a useful starting point and review for sites considering implementing dosimetry in their clinical practice or research operations. There is great interest and opportunity. The time to hesitate is through—there is much to do.

REFERENCES

1. Shadman M, Li H, Rimsza L, et al. Continued excellent outcomes in previously untreated patients with follicular lymphoma after treatment with CHOP plus rituximab or CHOP plus ¹³¹I-tositumomab: long-term follow-up of phase III randomized study SWOG-S0016. *J Clin Oncol*. 2018;36:697.
2. Strosberg J, El-Haddad G, Wolin E, et al.; for the NETTER-1 Trial investigators. Phase 3 trial of ¹⁷⁷Lu-DOTATATE for midgut neuroendocrine tumors. *N Engl J Med*. 2017;376:125–135.
3. Sartor O, de Bono J, Chi, KN, et al. Lutetium-177-PSMA-617 for metastatic castration-resistant prostate cancer. *N Engl J Med*. 2021;385:1091–1103.
4. Capala J, Graves S, Scott A, et al. Dosimetry for radiopharmaceutical therapy: current practices and commercial resources. *J Nucl Med*. 2021;62(suppl 3):3S–11S.
5. Sgouros G, Dewaraja YK, Escorcía F, et al. Tumor response to radiopharmaceutical therapies: the knowns and the unknowns. *J Nucl Med*. 2021;62(suppl 3):12S–22S.
6. Wahl R, Sgouros G, Iravani A, et al. Normal-tissue tolerance to radiopharmaceutical therapies, the knowns and the unknowns. *J Nucl Med*. 2021;62(suppl 3):23S–35S.
7. Uribe C, Peterson A, Van B, et al. An international study of factors affecting variability of dosimetry calculations, part 1: design and early results of the SNMMI dosimetry challenge. *J Nucl Med*. 2021;62(suppl 3):36S–47S.
8. O JH, Jacene H, Luber B, Wang H, et al. Quantitation of cancer treatment response by ¹⁸F-FDG PET/CT: multicenter assessment of measurement variability. *J Nucl Med*. 2017;58:1429–1434.
9. Mora-Ramirez E, Santoro L, Cassol E, et al. Comparison of commercial dosimetric software platforms in patients treated with ¹⁷⁷Lu-DOTATATE for peptide receptor radionuclide therapy. *Med Phys*. 2020;47:4602–4615.
10. Graves SA, Bageac A, Crowley JR, Merlino DAM. Reimbursement approaches for radiopharmaceutical dosimetry: current status and future opportunities. *J Nucl Med*. 2021;62(suppl 3):48S–59S.
11. Pandit-Taskar N, Iravani A, Lee D, et al. Dosimetry in clinical radiopharmaceutical therapy of cancer: practicality versus perfection in current practice. *J Nucl Med*. 2021;62(suppl 3):60S–72S.
12. Lassmann M, Eberlein U, Gear J, Konijnenberg M, Kunikowska J. Dosimetry for radiopharmaceutical therapy: The European perspective. *J Nucl Med*. 2021;62(suppl 3):73S–79S.

Dosimetry for Radiopharmaceutical Therapy: Current Practices and Commercial Resources

Jacek Capala¹, Stephen A. Graves², Aaron Scott³, George Sgouros³, Sara St. James⁴, Pat Zanzonico⁵, and Brian E. Zimmerman⁶

¹National Cancer Institute, Bethesda, Maryland; ²University of Iowa, Iowa City, Iowa; ³Johns Hopkins University, Baltimore, Maryland; ⁴University of California, San Francisco, California; ⁵Memorial Sloan Kettering Cancer Center, New York, New York; and ⁶National Institute of Standards and Technology, Gaithersburg, Maryland

With the ongoing dramatic growth of radiopharmaceutical therapy, research and development in internal radiation dosimetry continue to advance both at academic medical centers and in industry. The basic paradigm for patient-specific dosimetry includes administration of a pretreatment tracer activity of the therapeutic radiopharmaceutical; measurement of its time-dependent biodistribution; definition of the pertinent anatomy; integration of the measured time-activity data to derive source-region time-integrated activities; calculation of the tumor, organ-at-risk, and/or whole-body absorbed doses; and prescription of the therapeutic administered activity. This paper provides an overview of the state of the art of patient-specific dosimetry for radiopharmaceutical therapy, including current methods and commercially available software and other resources.

Key Words: dosimetry; radiopharmaceutical therapy; SPECT

J Nucl Med 2021; 62:3S–11S
DOI: 10.2967/jnumed.121.262749

In parallel with the ongoing, dramatic growth in molecularly targeted radiopharmaceutical therapies (RPTs), there is intense interest in the development of individualized radiation dosimetry for such therapies. This paper reviews the state of the art of patient-specific dosimetry, including current methods and commercially available software and other resources.

DOSE PRESCRIPTION ALGORITHMS

Historically, 3 dose (i.e., administered activity)-prescription algorithms for RPT have been used (1,2): fixed administered activity—all patients receive the same administered dose; maximum tolerated dose (MTD)—patients receive an individualized administered activity projected to deliver the maximum tolerated absorbed dose to the therapy-limiting normal tissue; and prescribed tumor-absorbed dose—patients receive an individualized administered activity projected to deliver a specified therapeutic absorbed dose to the tumor or target tissue. The fixed-administered-activity approach does not require any kinetic or other patient measurements but is at the risk of either exceeding the MTD or treating at well below the MTD of individual patients. (In some countries, however, patient-specific dosimetry is required by regulations

even for RPTs using fixed administered activities.) The patient-specific-MTD and prescribed-tumor-dose approaches typically require a series of pretherapy measurements to derive the administered activity to deliver either the MTD or the prescribed tumor-absorbed dose.

PARADIGM FOR PATIENT-SPECIFIC DOSIMETRY

The basic paradigm for patient-specific dosimetry for RPT is as follows: administration of a pretreatment tracer activity of the therapeutic radiopharmaceutical; measurement of the radiopharmaceutical's time-dependent biodistribution and clearance; definition of the pertinent anatomy by CT or MRI; integration of the measured time-activity data to derive source-region time-integrated activities (TIAs); calculation of the tumor, organ-at-risk, or whole-body absorbed dose coefficients (i.e., the absorbed doses per unit administered activity); and prescription of the therapeutic administered activity to deliver the MTD or the prescribed tumor-absorbed dose.

Important refinements of the foregoing paradigm are incorporation of voxel-level dosimetry to derive the 3-dimensional (3D) dose distributions and mathematic modeling of the biologic impact of the spatial and the temporal nonuniformity of the doses, with adjustment for the latter requiring calculation of and integration of dose rates.

MEASUREMENT OF TIME-ACTIVITY DATA

Planar Imaging

A widely used approach to determining source-region activities is conjugate-view γ -camera imaging (3,4). Anterior and posterior conjugate-view whole-body scans are acquired. The geometric mean of the aligned scans is then calculated, and the net (i.e., background-subtracted) count rates in regions of interest (ROIs) corresponding to tumors, normal organs, and, possibly, the whole body are determined. Assuming a known uniform linear attenuation coefficient μ through the full thickness T of the patient, a first-order attenuation correction may be applied by multiplying the net counts by $e^{\mu(T/2)}$. Alternatively, a transmission image through the patient of a uniform source of activity (such as a commercially available ⁵⁷Co flood source) may be used to derive a measured attenuation correction, with appropriate adjustment (if applicable) of the energy-related difference in attenuation between the γ -rays emitted by the flood source and those emitted by the radionuclide administered to the patient (5). A transmission image through the patient with a ⁵⁷Co flood source can also be used to measure the thickness of the patient (6). The attenuation-corrected

Received Jun. 30, 2021; revision accepted Oct. 22, 2021.
For correspondence or reprints, contact Pat Zanzonico
(zanzonip@mskcc.org).

COPYRIGHT © 2021 by the Society of Nuclear Medicine and Molecular Imaging.

source-region ROI count rates are converted to activities using a measured system calibration factor (e.g., cps/MBq) and then to activities per unit of administered activity. The conjugate-view method works reasonably well for normal-organ dosimetry but is generally less accurate for tumor dosimetry unless incorporated into a hybrid-imaging approach.

SPECT and SPECT/CT

The count rate per voxel in reconstructed SPECT image sets is proportional to the activity concentration, subject to the corrections for collimator–detector response (7,8), scatter (e.g., using the triple-energy window method (5,7,9,10)), attenuation (based on CT imaging (7)), and partial-volume averaging (based on CT-derived source-region dimensions and phantom study–derived recovery coefficients (11,12)). The corrected count rate per voxel is divided by the system calibration factor [(cps/voxel)/(kBq/mL)] to yield the activity concentration.

Hybrid SPECT–Planar Imaging

A practical alternative to serial whole-body SPECT is hybrid SPECT–planar imaging, in which both SPECT and planar scans are acquired at a single time point and only the more rapid planar scans are acquired at the remaining time points (Fig. 1) (7). The multiple planar scans provide the shapes of the time–activity curves, and the single SPECT study provides the (more reliable) activity estimate in the respective source regions at the time point of the SPECT study. The one time point at which both SPECT and planar scans are acquired thus provides a scaling factor to convert the source-region counts in each of the multiple planar scans to activity.

Single-Time-Point Imaging

For radiopharmaceuticals for which the kinetics are well characterized and exhibit little variability among patients, population-averaged normal-organ time–activity curves may be scaled by the respective image-derived, patient-specific organ activities measured at an appropriate single time point to derive individualized time–activity curves and TIAs (13). The reliability of this approach requires validation, however, and the variable biology among tumors makes it unlikely to be translatable to lesion dosimetry.

PET and PET/CT

Quantitative PET remains more routine than quantitative SPECT. With rare exceptions (14), positron-emitting radionuclides have not been used in RPT. Among other reasons, a surrogate PET radionuclide and the therapeutic radionuclide must be

reasonably well matched in terms of physical half-life so that serial PET scans can be performed over a sufficiently long total time frame to yield reliable estimates of the time–activity data, and that is often not the case for commonly used positron emitters. For example, ^{68}Ga -DOTATATE (NETSPOT; Advanced Accelerator Applications) (^{68}Ga physical half-life, 67.7 m) is far too short-lived to estimate tumor and normal-organ activities of ^{177}Lu -DOTATATE (LUTATHERA; Advanced Accelerator Applications) (^{177}Lu physical half-life, 6.65 d) out to several days or longer after administration, as required for ^{177}Lu -DOTATATE dosimetry. On the other hand, surrogates of therapeutic radiopharmaceuticals labeled with positron-emitting ^{124}I (physical half-life, 4.18 d) can provide reasonable estimates of the time–activity curve for radiopharmaceuticals labeled with ^{131}I (physical half-life, 8.04 d) (15).

Ancillary Measurements

Blood and Bone Marrow Activity. The hematopoietic marrow is highly radiosensitive and often the dose-limiting normal tissue in RPT, particularly for radiolabeled antibodies and peptides. Quantitation of marrow activity is particularly challenging, however, as it is a widely distributed and cannot be directly sampled except by biopsy. Practical approaches are based on counting of blood samples and estimates of the marrow extracellular fluid fraction (16,17) or on scintigraphic imaging of vertebral marrow (18,19).

Whole-Body Activity. Whole-body activity may be measured by an adaptation of the conjugate-view method, with the patient undergoing a conjugate-view whole-body scan (or probe-based counting) shortly after the radiopharmaceutical administration (i.e., at time $t \approx 0$) but before the patient’s first postadministration void or bowel movement. The net geometric-mean whole-body count rate at each subsequent time point is normalized to the zero-time (i.e., 100%) value to yield the whole-body percentage of the administered activity.

CALCULATION OF TIAS

The TIA (in h), $\tilde{A}(r_S)$, is the total number of radioactive decays in source region r_S ; the TIA coefficient (in h/MBq), $\tilde{a}(r_S)$, is the total number of decays per unit of administered activity in source region r_S (20). There are 3 basic approaches to the calculation of cumulated activities: curve fitting (often fit to exponential functions) and analytic integration; numeric integration (i.e., the trapezoidal rule), often assuming elimination by physical decay after the last measurement or by extrapolating the clearance rate deduced from the last 2 measured time points; and compartmental modeling (21). A compartmental model is a mathematic representation—a system of linked differential equations—of the exchange of a radiopharmaceutical among compartments in the body. Many compartmental-modeling programs are available, and some provide estimates of TIAs. An advantage of compartmental modeling is its ability to yield TIAs in source regions that cannot be radioassayed directly (regions such as the cell surface or the cell nucleus).

MIRD pamphlet 16 (5) provides guidance on choosing suitable time points and the number of samples for adequately defining a source region time–activity curve and TIA.

DEFINITION OF PATIENT-SPECIFIC ANATOMY

The most reliable approach to defining patient anatomy is either CT or MRI. Multimodality SPECT/CT scanners expedite the registration of scintigraphic and anatomic image sets (22). Tumor and

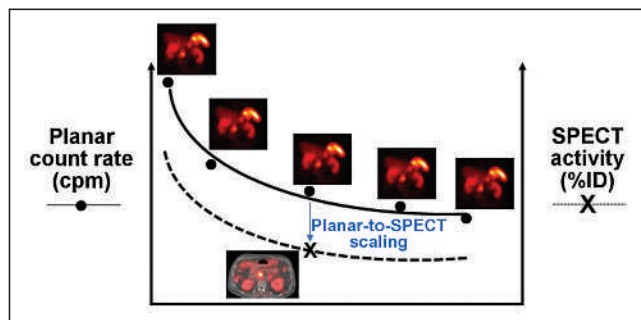


FIGURE 1. Hybrid SPECT–planar imaging approach to measurement of radiopharmaceutical kinetics.

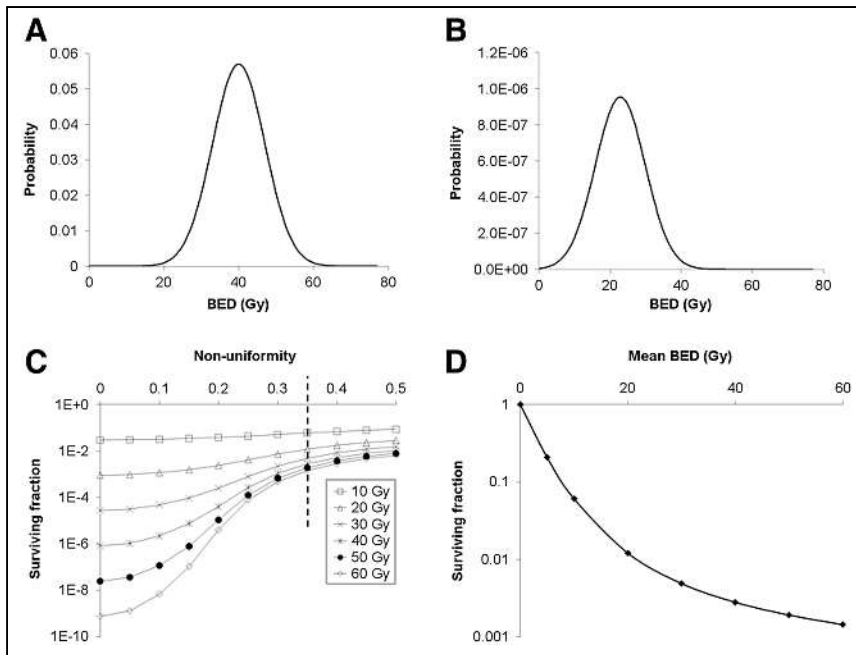


FIGURE 2. Effect of dose nonuniformity on tumor response. (A) Hypothetical nonuniform dose to tumor cell population represented by normal distribution with average of 40 Gy, SD of 7 Gy, and fractional SD of 7 Gy/40 Gy = 0.175. (B) Overall tumor cell survival fraction as function of dose nonuniformity expressed as fractional SD of average dose from 0 (i.e., uniform dose) to 0.5 and of average tumor dose from 10 Gy (highest curve) to 60 Gy (lowest curve). Tumor cell survival is greater as dose nonuniformity increases. (C) Tumor cell survival probability for dose distribution in A, assuming monoexponential tumor cell survival curve with mean lethal dose D_0 of 2.85 Gy (i.e., $\alpha = 0.35/\text{Gy}$). Overall tumor cell survival fraction is area under curve. (D) Dose–response for dose nonuniformity (i.e., fractional SD) of 0.35, corresponding to points intersecting dotted vertical line, is concave upward. (Adapted from reference (57).)

organ volumes of interest (VOIs) may be defined by manual segmentation or by various thresholding, seed-growing, and other automated techniques, now widely available and increasingly accurate.

CALCULATION OF ABSORBED DOSES

The ultimate objective of dosimetry is the determination of organ or tumor absorbed doses, since biologic effects will be better predicted by absorbed dose than by administered activity. There are 3 basic approaches to the calculation of absorbed dose: the dose factor (S value)–based calculation, dose-point kernel convolution, and Monte Carlo (MC) radiation transport simulation.

Organ-Level Dosimetry

One of the most widely used approaches at the organ level is the MIRD schema (20,21). Several personal computer–compatible versions of the MIRD formalism have been developed, including MIRDOSE (23), OLINDA/EXM (24), IDAC Dose (25), and MIRDcalc. Adaptations of the MIRD formalism have been incorporated into various commercially available software packages.

In the MIRD formalism (20,21), the mean absorbed dose to a target region r_T equals the summation over all source regions r_S of the products of 2 terms—the TIA in source region r_S , $A(r_S)$, and the radionuclide S value for the source-region–target-region pair, $S(r_T \leftarrow r_S)$ (26). By modeling tumors as spheres, the MIRD formalism may be adapted to tumor self-irradiation (i.e., for $r_T = r_S$) dosimetry using tabulated values of sphere self-irradiation absorbed fractions.

Voxel-Level Dosimetry

Voxel-level dosimetry is addressable by dose-point kernel convolution, MC algorithms, or voxel S values. A dose-point kernel represents the radial distance–dependent absorbed dose about a point source of radiation in an infinite homogeneous (typically, water-equivalent) medium (27). The development of faster computer processors, the availability of more plentiful memory, porting of MC packages to parallel computing architectures, and other technical developments (e.g., approximation techniques) have made computationally onerous MC methods, considered the most accurate approach to voxel-level dosimetry, increasingly practical. The MIRD formalism has been extended to arbitrary macroscopic activity distributions in 3 dimensions for calculation of the dose distribution using voxel S values (28).

Cell-Level Dosimetry

The differential delivery to and uptake among and within cells of administered radiopharmaceuticals make it difficult to predict the radiation response of cell populations to radiopharmaceuticals based solely on the mean absorbed dose. A web-based applet, MIRDcell, has been developed that adapts the MIRD formalism to cellular and subcellular dosimetry (29). This applet models the dose to the cellular and subcellular compartments (i.e., the cell membrane, cytoplasm, and nucleus) for both isolated cells and clusters of cells using cellular S values (30,31) and mathematically models the responses of labeled and unlabeled cells as a function of the fraction of cells labeled.

BIOEFFECTS MODELING

The absorbed dose is not the only dosimetric factor impacting biologic outcomes of RPT. Other relevant factors include radiosensitivity and the spatial and temporal distributions of absorbed dose. Attempts have thus been made to model the biologic effects of radiation. Such bioeffects modeling is particularly relevant to RPT, as its clinical effects are impacted by the low and time-varying dose rates and the nonuniform dose distributions within associated targeted tissues.

Dose-dependent cell survival is often described by the target theory–based linear quadratic (LQ) model (32,33):

$$\text{SF} = e^{-(\alpha D + \beta D^2)} \quad \text{Eq. 1}$$

where SF is the surviving fraction, D is the absorbed dose (in Gy), α is the linear sensitivity coefficient (in Gy^{-1}), and β is the quadratic sensitivity coefficient (in Gy^{-2}). Important modifiers of the biologic response to radiation include the dose rate and the dose distribution. Both are particularly important for RPT, given the low, time-varying dose rates and spatially nonuniform dose distributions, especially in tumors, associated with such therapy. The various dose metrics and associated parameters for bioeffects modeling of RPT are summarized in Table 1.

TABLE 1
 Bioeffects Modeling of RPT: Dose Metrics and Related Parameters (19)

Parameter	Definition or description
Lea–Catcheside time factor (46)	<p>Radiation delivered at high dose rate is more biologically damaging than same dose delivered at low dose rate as a result of cells' ability to repair sublethal damage over duration of irradiation. Modifying effect of repair has been modeled with Lea–Catcheside time factor,</p> $G(T) = \frac{2}{D^2} \cdot \int_0^T \dot{D}(t) dt \int_0^t \dot{D}(w) \cdot e^{-\mu(t-w)} dw,$ <p>where D is total absorbed dose; \dot{D} is dose rate; μ is repair rate, assuming that probability of repair event decreases exponentially as function of time; w is time of first single-strand DNA break; t is time of second break; and T is duration of irradiation. For protracted irradiations such as those encountered in RPT, surviving fraction thus becomes $SF = e^{-(\alpha D + G(T)\beta D^2)}$.</p>
Biologically effective dose (47–49)	<p>Variation in biologic response to same absorbed dose delivered at different dose rates or different numbers of fractions has led to concept of biologically effective dose (BED) (or extrapolated tolerance dose, ETD), the absorbed dose required to cause biologic effect if dose were delivered in infinitely small doses per fraction or, equivalently, at very low dose rates: $SF = e^{-\alpha BED} = e^{-(\alpha D + G(T)\beta D^2)}$ and therefore $BED = D \left(1 + \frac{G(T)}{\alpha/\beta} \cdot D \right)$.</p>
Equieffective dose (50,51)	<p>Equieffective dose (EQDX in Gy) is a quantity that, like BED, is intended to account for differences in fractionation or dose rate; X in this notation refers to reference value of absorbed dose (Gy) per fraction d. It has been recommended that nomenclature for equieffective dose include α/β ratio as well as reference to X: $EQDX_{\alpha/\beta} = D \cdot \frac{\alpha/\beta + d}{\alpha/\beta + X}$. Newer notation for equieffective dose is thus $EQDX_{\alpha/\beta}$, with recommended standard of $EQD2_{\alpha/\beta}$, where 2 refers to reference 2-Gy daily fraction. BED is equivalent to $EQD0$ (52) and is thus particularly relevant to RPT. Low, continuous dose rates delivered by radiopharmaceuticals require modification of this equation to incorporate Lea–Catcheside time factor $G(T = \infty)$ (53–55): $EDQX_{\alpha/\beta} = D \cdot \frac{(\alpha/\beta + G(\infty) \cdot D)}{(\alpha/\beta + X)}$.</p>
Equivalent uniform dose (56–58)	<p>Tumor therapeutic response and normal-tissue toxicity may not correlate with average absorbed doses even when based on individualized biodistribution and kinetic data because of spatial nonuniformity of dose (Fig. 2 (57)). A quantity has therefore been developed, equivalent uniform dose (EUD), that provides a single value weighted to account for surviving fraction of tumor cells, given spatial distribution of absorbed dose within tumor volume. For any dose distribution, corresponding EUD is absorbed dose (Gy), which, when distributed uniformly across target volume comprised of N voxels, achieves same survival fraction among clonogenic cells:</p> $SF = e^{-\alpha EUD - \beta EUD^2} = \frac{\sum_{i=1}^N e^{-\alpha D_i - \beta D_i^2}}{N} \text{ or } EUD = \frac{1}{2\beta} \left(-\alpha + \sqrt{\alpha^2 - 4\beta \cdot \ln \left(\frac{\sum_{i=1}^N e^{-\alpha D_i - \beta D_i^2}}{N} \right)} \right).$
Equivalent uniform biologically effective dose (56–58)	<p>EUD has been formulated as equivalent uniform biologic effective dose, EUBED), as first described by O'Donoghue (57). It is often expressed using only linear component of linear-quadratic model: $e^{-\alpha EUBED} = \frac{\sum_{i=1}^N e^{-\alpha BED_i}}{N}$. Solving for EUBED yields $-\frac{1}{\alpha} \ln \left(\frac{\sum_{i=1}^N e^{-\alpha BED_i}}{N} \right)$.</p>

Several studies have shown a better response correlation with these metrics than with the average tumor-absorbed dose (34–37).

UNCERTAINTIES IN DOSE ESTIMATION

Sources of uncertainty in radiopharmaceutical dosimetry include assay of the administered activity, determination of organ and tumor volumes or masses (often the greatest contributor to uncertainty), measurement of time-dependent source-region activities, calculation of source-region TIAs, and translation of TIAs and anatomic data to absorbed dose. Assuming they are independent of each other, the respective fractional uncertainties of these quantities can be summed in quadrature to yield the overall uncertainty of the absorbed dose. In a clinical example (38), ⁹⁰Y-DOTATATE radiopeptide therapy in combination with ¹¹¹In-DOTATATE imaging of neuroendocrine cancer, the overall uncertainties in the estimated mean absorbed doses to at-risk normal organs (kidney,

spleen, and liver), large (>100-cm³) lesions, and small (~10-cm³) lesions were 10%, 15%, and 40%, respectively, providing some insight into the range of uncertainties one may expect in best-practice radiopharmaceutical dosimetry.

COMMERCIAL RESOURCES

The following 2 subsections describe currently marketed commercial products relevant to radiopharmaceutical dosimetry, based on material provided by the respective vendors. We note as a disclaimer that certain commercial equipment, instruments, and materials are identified in this paper solely to promote understanding. Such identification does not imply recommendation by the Society of Nuclear Medicine and Molecular Imaging or the National Institute of Standards and Technology (NIST), nor does it imply that the products identified are necessarily the best available for the purpose cited.

Standard Sources

Traceability to national agencies of standard, or reference, sources is critical in RPT dosimetry for accurate measurement of activities administered to patients and accurate calibration of imaging systems (based on the image-derived count rate of a known activity) for the measurement of time–activity data in patients. Errors in the measured administered activity or calibration activity will be propagated through the dosimetry workflow and result in systematic underestimation or overestimation of the resulting patient tissue activities and doses (as high as 20% (39)). Dose calibrators (also known as activity meters) are ionization chambers with a variable charge, or current, response that depends on the type, flux, and energy of the emitted radiations among different radionuclides. Traceable standards of precisely known activities are thus required by dose calibrator manufacturers and, in some cases, end users to derive radionuclide- and geometry-specific factors for converting measured charge (or current) to activity and are thus essential in ensuring that the correct radiopharmaceutical activity is being administered to the patient or added to a calibration phantom. Traceable standards are important in multicenter clinical trials to ensure consistency in activity- and dose-dependent results among the participating centers, particularly for radionuclides that are pure β -particle emitters (such as ^{90}Y), for which assays must be based on measurement of the associated bremsstrahlung spectrum, or which have complex decay schemes (including ^{177}Lu and many α -particle emitters and their progeny) with multiple x- and γ -ray emissions.

NIST. NIST is responsible for developing and disseminating standards for radioactivity measurements in the United States. NIST has established national standards for every radionuclide currently used in Food and Drug Administration (FDA)–approved radiopharmaceuticals. Work was recently completed on a standard for ^{223}Ra , and NIST plans to develop standards for such emerging radionuclides as ^{67}Cu and ^{89}Zr and the α -particle emitters ^{212}Pb , ^{227}Th , and ^{225}Ac .

The mission of the NIST Radioactivity Measurement Assurance Program is to enable radiopharmacies, isotope producers, and radiopharmaceutical manufacturers to establish and maintain traceability through direct comparisons of calibrated solutions between the participants and NIST. The comparison can be done either through the distribution of NIST-calibrated solutions distributed as blind samples or by the submission of a measured solution by the participant to NIST, which then assays that solution. Traceability is established by comparing the participant's result with the NIST-determined value. More recently, NIST calibration of phantoms (typically large solid cylindrical sources containing ^{68}Ge , ^{133}Ba , and ^{75}Se as surrogates for ^{18}F , ^{131}I , and ^{177}Lu , respectively) allows the direct calibration of SPECT and PET scanners and provides a means of comparing imaging results across multiple clinical sites.

Eckert and Ziegler Isotope Products. Eckert and Ziegler Isotope Products holds an International Organization for Standardization 17025:2017 accreditation for its Valencia Calibration Laboratory through the German accreditation service Deutsche Akkreditierungsstelle GmbH. This accreditation ensures that it maintains not only measurement capabilities for NIST traceability but also the necessary quality management system compliant with good measurement practices globally. Sealed-source configurations include line- and point-source arrays; custom-sized 2-dimensional and 3D phantoms; and vials, tubes, and syringes. Any fillable phantom can be converted to a long-lived sealed source with the desired nuclide in water-equivalent epoxy with NIST traceability. In

addition, Eckert and Ziegler Isotope Products has a patented process for manufacturing phantoms with lesions embedded directly in a “warm” background with no nonradioactive encapsulation of the lesions. Lesions can be fabricated in various shapes and sizes (including anthropomorphic shapes). Eckert and Ziegler Isotope Products has the capability to calibrate solutions of longer-lived radiopharmaceuticals such as ^{177}Lu , ^{111}In , and ^{131}I or other radionuclides with physical half-lives of 2 d or longer. Calibration of shorter-lived nuclides may also be possible, depending on customer location and shipment time constraints. A wide range of sealed sources and solutions for reference and calibration for over 80 nuclides and multinuclide combinations are available.

Sanders Medical Products. Sanders Medical Products manufactures a complete line of NIST-traceable ^{68}Ge cylindrical uniform phantoms (activity, $\leq 370\text{ MBq}$ [10 mCi] $\pm 3\%$; ^{68}Ge radionuclidic purity, 99.8%). The phantoms use a high-density polyethylene thermoplastic polymer shell with a uniform cast polymer matrix of ^{68}Ge . The units are checked by high-resolution PET/CT scanning before release. Sanders also produces positron-emitter calibration standards composed of uniform solid suspensions of ^{68}Ge encased and sealed in plastic bottles for use with PET scanners, dose calibrators, and survey meters.

Dosimetry Software

By design, the following compilation of dosimetry software is limited to packages that are commercially available and therefore readily obtainable by the user community. Of course, many academic investigators have developed software packages with comparable functionality.

QDOSE. QDOSE (ABX-CRO) is a stand-alone software suite for internal dosimetry using serial nuclear medicine and anatomic DICOM images of diagnostic or therapeutic radionuclides, including ^{90}Y -microsphere selective internal radiation therapy (SIRT). QDOSE supports calculations using planar imaging, including attenuation and background corrections, tomographic imaging, and hybrid imaging. Planar images can be calibrated using a system calibration factor based on a reference vial (as for PET and SPECT) or total-body activity. QDOSE provides automatic (rigid and deformable) and manual registration of serial planar or tomographic images and multiple options for drawing planar-image ROIs and tomographic VOIs and for manual, semiautomatic, and automatic organ segmentation. Time–activity curves are generated and can be fit to exponential functions and integrated to yield TIAs, with accounting for the total-body or remainder-of-body activity. TIAs can also be calculated using the trapezoidal approach. Time–activity curves and TIAs (e.g., red-marrow data based on blood sampling) derived outside QDOSE can be imported. QDOSE uses the IDAC-Dose program (25) (which includes 27 commonly used radionuclides) to calculate the mean normal-organ absorbed doses as the sum of the self-dose and cross-organ absorbed doses based on the Cristy–Eckerman stylized phantoms (40). For more patient-specific dose results, the standard organ masses can be edited or calculated from the 3D segmented organs. Absorbed-dose distributions may also be calculated by convolution of voxel S values with the voxel TIAs in segmented source regions, yielding dose–volume histograms (DVHs) and patient-specific dose distribution images. The mean absorbed doses and dose distributions to tumor-simulating spheres may also be calculated.

The results of IDAC Dose, version 1.0, mean organ dose calculations were compared with those of OLINDA/EXM, version 1.

Version 2.1 of IDAC Dose was validated against version 1.0. This validation was used for the certification according to Directive 93/42/EEC (Medical Device Directive). QDOSE is CE (Conformite Europeenne)-approved for clinical use within the European Union and for use as a research device outside the European Union.

PLANET Dose. PLANET Dose (DOSIsoft), for 3D RPT dosimetry, is FDA-approved for ^{90}Y -microsphere SIRT and CE-marked for other isotopes (^{90}Y , ^{177}Lu , ^{131}I [pending]) or workflows. Images (DICOM-compatible) from CT, MRI, planar γ -cameras, SPECT, and PET are supported as input, with correction for partial-volume averaging available. Rigid or deformable registration of multiple image sets and of VOIs can be performed manually or semiautomatically (based on user-selected anatomic fiducial markers). Time-activity curves can be integrated by the trapezoidal method or fit to affine or to exponential functions and integrated analytically. 3D voxel-based doses are calculated using voxel S values, with tissue mass-density corrections available. Target-region dosimetry results are reported in color-wash or isodose-contour displays and as DVHs. PLANET Dose has been validated against MC simulations and OLINDA/EXM.

GE Dosimetry Toolkit and Q.Thera AI. The GE Dosimetry Toolkit (GE Healthcare) is an application to define and report patient organ volumes and time-activity curves and to calculate the organ TIAs and mean absorbed doses on the basis of serial whole-body planar scans, serial SPECT/CT scans, or hybrid imaging. Specific dosimetry applications include ^{131}I -iodide thyroid cancer therapy, ^{90}Y -SIRT, and ^{177}Lu therapies. There are 4 steps in the GE Dosimetry Toolkit SPECT workflow: SPECT/CT image reconstruction, with detection of patient motion and correction for attenuation, scatter, and collimator-detector blurring; registration of serial scans to one common reference image with semiautomatic (seed-growing) or manual tools; segmentation of the target organs and generation of VOIs; and calculation of volumes, activities, and TIAs. A standard-activity syringe can be included in the field of view to measure system sensitivity for each scan. The measured time-activity curves are fit to exponential functions. All outputs are provided as Microsoft Excel files or in an OLINDA/EXM-compatible format.

Q.Thera AI is a technology in development by GE Healthcare; it is not currently FDA-approved. Automatic registration and segmentation of organs and lesions (and calculation of the percentage injected dose for each source region) are performed. The resulting time-activity curves are fit to exponential functions and integrated either analytically or by the trapezoidal method. Organ-absorbed doses are calculated for the user-entered radionuclide, model (newborn to adults), source-region TIAs, and, optionally, volumes. If the total-body mass only is altered, the reference-phantom organ masses remain the same, but if the user selects the option to normalize by patient body mass, the total body and all the internal organs will be scaled accordingly. Self-irradiation absorbed doses for unit-density spheres (1–1,000 g in mass) are also calculated.

Hermes Medical Solutions. Hermes Medical Solutions markets a suite of dosimetry tools, including scanner-independent quantitative SPECT reconstruction (HybridRecon of DICOM-compatible SPECT/CT data); SIRT planning and verification (HermesSIRT); OLINDA, version 2.2; and voxel-level dosimetry. The HybridRecon SPECT reconstruction currently handles ^{67}Ga , ^{123}I , ^{131}I , ^{111}In , ^{81}Kr , ^{177}Lu , $^{99\text{m}}\text{Tc}$, ^{201}Tl , ^{166}Ho , ^{90}Y , and ^{133}Ba . With Hermes SIRT, the planning tumor volume, lean body mass, or partition models can be used to calculate the individual-patient dose on the basis of a $^{99\text{m}}\text{Tc}$ -macroaggregated albumen scan. The user is

guided through alignment, segmentation, and normalization of serial images and curve fitting of the organ time-activity curves and TIAs as input to OLINDA, version 2.2. The Hermes Medical Solutions voxel-level dosimetry product uses a fast MC algorithm to simulate an activity distribution from serial SPECT or PET images plus CT scans to calculate a dose map. Organ mean and maximum absorbed doses and DVHs are reported.

MIM Software. MIM Software dosimetry includes quantitative ordered-subsets expectation maximization SPECT image reconstruction (SPECTRA Quant) with CT-derived attenuation correction, energy window-based scatter correction and resolution recovery, organ and tumor segmentation (using an FDA-approved artificial-intelligence autosegmentation platform), and absorbed-dose calculations. SPECTRA Quant has been tested for quantitative accuracy, and corrections have been developed for several radionuclides. For a simulated ^{177}Lu test with the SIMIND MC code, an 85% recovery was found for a 32-mm-diameter sphere with a 10:1 activity concentration ratio between the sphere and background. Local rigid registrations among SPECT images are performed using only the information in and around each segmented region, and these are then merged to generate a composite aligned SPECT image, with validation against manual registration (agreement within 1% of TIAs for both organ and tumors). For β -emitters such as ^{90}Y , MIM Software supports dosimetry using either local deposition or voxel S-value kernel convolution and can be performed on either bremsstrahlung SPECT or PET images. For γ -ray emitters such as ^{177}Lu and ^{131}I , voxel S-value kernel convolution with CT-based density correction is available, and dosimetry can be performed using multiple SPECT/CT scans, a hybrid approach, or a single SPECT/CT scan. For dosimetry with multiple SPECT/CT scans and hybrid SPECT/planar scanning, TIAs are calculated using either trapezoidal integration with exponential terms for extrapolation or one of several exponential models. With serial SPECT/CT scans, these can be applied on an organ-level or a voxel-level basis. With hybrid SPECT/planar scanning, integration is based on the planar-image activities, with scaling based on the SPECT-derived activity. Planar image corrections for scatter, attenuation, and background are available. MIM Software is also developing 2 methods of single-time-point dosimetry for ^{177}Lu DOTATATE: the Hänscheid approach (which assumes an exponential time-activity curve) (41,42) and the a priori information approach (which relies on a patient-specific time-activity curve measured by serial SPECT/CT scans of a prior therapy cycle).

PMOD. PMOD (PMOD Technologies) supports an automated workflow of preprocessing steps to derive dosimetry input data from a set of sequential image acquisitions, using its PBAS tool and the PKIN kinetic modeling tool. The first task is to combine these images into a dynamic series using PMOD's Merge tool. Organ VOIs are defined by isocontouring, manual or semiautomatic outlining, or use of a matched anatomic dataset. Using a drop-down list, each VOI can be assigned to an organ in a particular reference phantom. Each organ VOI's activity concentration is then transferred to PKIN, PMOD's kinetic modeling tool, as a time-activity curve. These curves may be time-shifted to account for acquisitions with multiple bed positions and integrated to yield TIAs by rectangular or trapezoidal integration followed by isotope decay, fitting of the declining portion to exponential functions and analytic integration, or a combination of both. The resulting TIAs may be directly imported into an OLINDA/EXM case file or an IDAC, version 2.1, file.

Rapid. Rapid offers quantitative imaging and dosimetry consulting and analysis services and the software required for implementation. The specific services include analysis and dosimetry of preclinical data, support for imaging trial design (i.e., determining the number and temporal spacing of the image acquisitions and their settings, describing and analyzing phantom studies for site qualification and calibration, developing imaging manuals and procedures, and performing centralized vendor-agnostic quantitative SPECT reconstruction), and standard phantom and patient-specific 3D dosimetry calculations.

Based on the open-source 3D Slicer package, RPTDose generates MC-derived 3D dose distribution maps and radiobiologic dosimetric parameters for a radiopharmaceutical. RPTDose incorporates 2 software packages (IRL and 3D-RD) that were originally developed and validated at the Johns Hopkins University and have been licensed by Rapid. IRL (Iterative Reconstruction Library) is a vendor-neutral software package for quantitative ordered-subsets expectation maximization reconstruction of SPECT images, with compensation for attenuation (based on CT-derived attenuation maps), scatter (using the effective source scatter estimation method with approximations for nonuniform attenuators and multiple scatters), and collimator–detector response (estimated by MC simulation of point sources at various distances from the collimator face and propagation of photons in the collimator and detector). IRL has been validated for a number of radionuclides (including ^{90}Y , $^{99\text{m}}\text{Tc}$, ^{111}In , ^{123}I , ^{131}I , ^{201}Tl , ^{223}Ra , and ^{227}Th) on the basis of data from physical phantom studies and MC-simulated projection data. The second software package, 3D-RD, performs patient-specific absorbed dose calculations using electron γ -shower MC simulations based on CT-derived 3D density maps and the quantitative SPECT-derived activity distributions at multiple time points. The dose rates for each VOI are fit using nonlinear least-squares fitting to model functions, and the absorbed doses are then calculated as the area under the dose-rate curve from 0 to infinity.

Rapid has also developed and validated a web-based, multiuser reference-phantom, organ-level MIRD-style dosimetry software tool, 3D-RD-S, currently in the final stages of development for a 510k application for FDA clearance. 3D-RD-S uses International Commission on Radiological Protection publication 89 phantoms (43), publication 107 radionuclide decay data (44), and publication 133 specific absorbed fractions (72 source and 43 target regions (45)). 3D-RD-S also supports calculation of tumor self-dose for spheric tumors with 5 compositions and 10 diameters from 0.2 to 12 cm. The code supports dose calculation for a radionuclide and all its radioactive progeny, allowing the user to assume that the daughters have the same distribution as the parent or a distribution that is scaled to that of the parent or independent of it. Rapid is also developing a software package to perform quantitative SPECT reconstruction of difficult-to-image therapeutic radionuclides, including α -particle emitters, yielding output directly importable into 3D-RD-S.

Simplicit90Y. Simplicit90Y (Mirada Medical) is a software package developed for personalized ^{90}Y -SIRT planning, incorporating multimodality images with a variety of rigid and deformable registration tools. It also includes calculation of dosimetry parameters with multicompartment, voxelwise techniques and pre- and posttreatment dosimetry. The application does not perform SPECT or PET image reconstruction but rather uses DICOM-formatted reconstructed tomographic image data. Simplicit90Y generates MIRD-schema phantom-based, organ-level absorbed-dose distributions (e.g., displayed as isodose contours) and DVHs based on the assumptions of complete physical decay in situ and local dose deposition.

RapidSphere Dosimetry Navigator and RapidSphere Tradeoff Explorer Navigator. The RapidSphere Dosimetry Navigator (Varian Medical Systems) is a software tool for ^{90}Y -microsphere dosimetry. Conversion of the posttherapy SPECT/CT or PET/CT reconstructed image set is used to create an RTDose object representing the delivered dose (Gy). The user next defines the patient's external body and lung contours or selects predefined contours to be used in the dosimetry calculation for the local deposition model. The local deposition model assumes that count levels are proportional to the injected activity of ^{90}Y . β -particles released within a voxel are absorbed locally, and ^{90}Y is eliminated by physical decay only. In the event that the entire lungs are not included in the RTDose object, the independently evaluated lung shunt fraction is entered by the user. The user also specifies structure-specific tissue densities and structures for DVH analysis during the exploration step. The RapidSphere Dosimetry Navigator, an interactive tool intended to be used retrospectively to assess how various parameters impact the ^{90}Y -microsphere dose distribution, generates DVHs and isodose contours.

Voximetry Torch. Voximetry markets a software package called Torch, which incorporates an automated or manual dosimetry workflow. Torch is configured to use the parallel-processing capabilities of graphics-processing units to handle the successive steps of image registration, contour propagation, kinetic modeling, and radiation transport. A key component of this workflow is the software's proprietary graphics-processing-unit-accelerated MC algorithm. Torch can be operated either in an automated click-and-go fashion or in a manual advanced mode. The first step is DICOM import of CT and PET or SPECT datasets for each time point. Currently, Torch does not perform SPECT calibration, so the user must input a calibration (e.g., cps/MBq) factor. Next, the user imports either a DICOM structure image set or ROI index files for at least one imaging time point. For multiple-time-point dosimetry, the user is required to import a set of ROIs for the first time point from external software. For subsequent time points, Torch will propagate the contours across time points using proprietary graphics-processing-unit-accelerated deformable registration algorithms, or users can import their own ROIs for these additional time points.

To calculate TIAs, Torch uses the Akaike information criterion to find the function that best fits the time–activity curves; the Akaike information criterion is an estimator of prediction error and therefore of the relative quality of statistical models for a given dataset. The user can accept the result, choose from other fitting functions, or manually adjust the parameters of the selected function. Trapezoidal integration followed by physical decay after the final time point may also be selected.

Next, a modified version of the MC code dose-planning method, optimized to operate on graphics processing units, is applied. Electron transport is done using the condensed history method, in which large energy transfers are accounted for in an analog manner and small energy transfers are accounted for by the continuous slowing-down approximation. After each step, the angular distribution of electrons is determined using step size-independent multiple-scattering theory. Photons are transported using a standard analog approach accounting for photoelectric absorption, Compton scattering, and, when applicable, pair production

Lastly, the radiation transport distribution is evaluated using DVHs and dose statistics. It is possible to generate a dosimetry report structured to meet the requirements for complex dosimetry billing codes in the United States. In addition, dose volumes can

be exported in either DICOM-RT or raw format to be visualized in another software package—for example, for possible combination with external-beam radiotherapy.

Torch has been benchmarked and validated using both computational and physical phantoms. The dose calculation algorithm in Torch has been benchmarked against the GEANT4 MC code, using voxel S-value kernels in water and using patient datasets for multiple isotopes, including ^{90}Y , ^{177}Lu , ^{131}I , and ^{223}Ra . In addition, Torch has also been benchmarked using data provided by the OpenDose collaboration, which averages the results of 4 MC codes (electron γ -shower++ 2018, GATE 7.2, GATE 8.1, and GEANT4 10.5). Reference S values have been calculated for the International Commission on Radiological Protection adult male and female standard phantoms (43) for both monoenergetic sources and various isotopes, with better than $\pm 5\%$ agreement for all source-region–target-region combinations. Voximetry has also partnered with the University of Wisconsin Accredited Dosimetry Calibration Laboratory to design and acquire physical measurements to evaluate the accuracy of Torch. In measurements to date, excellent agreement has been observed between Torch-calculated and radiochromic film–measured ^{90}Y depth-dose distributions in solid water.

DISCLOSURE

George Sgouros is a founding official of Rapid, the manufacturer of one of the dosimetry software products described in the paper. Brian Zimmerman is currently the Leader of the Radioactivity Group at NIST, and products and services offered by NIST are also described. Jacek Capala is a program director at the Clinical Radiation Oncology Branch in the Radiation Research Program of the National Cancer Institute and oversees a portfolio of research grants in the field of targeted radiopharmaceuticals therapy and its combination with other treatment modalities. Pat Zanzonico is a coinventor of intellectual property licensed to Y-mAbs Therapeutics and a paid consultant to Novartis. The opinions expressed in this publication are the author(s)' own and do not reflect the view of the National Institutes of Health, the Department of Health and Human Services, or the United States government. No other potential conflict of interest relevant to this article was reported.

REFERENCES

- Zanzonico PB, Brill AB, Becker DV. Radiation dosimetry. In: Wagner H, Szabo Z, Buchanan, J, eds. *Principles of Nuclear Medicine*. 2nd ed. W.B. Saunders; 1995:106–134.
- Zanzonico PB. Internal radionuclide radiation dosimetry: a review of basic concepts and recent developments. *J Nucl Med*. 2000;41:297–308.
- Fleming JS. A technique for the absolute measurement of activity using a gamma camera and computer. *Phys Med Biol*. 1979;24:176–180.
- Thomas SR, Maxon HR, Kereiakes JG. In vivo quantitation of lesion radioactivity using external counting methods. *Med Phys*. 1976;03:253–255.
- Siegel JA, Thomas SR, Stubbs JB, et al. MIRD pamphlet no. 16: techniques for quantitative radiopharmaceutical biodistribution data acquisition and analysis for use in human radiation dose estimates. *J Nucl Med*. 1999;40(suppl):37S–61S.
- Minarik D, Sjogreen K, Ljungberg M. A new method to obtain transmission images for planar whole-body activity quantification. *Cancer Biother Radiopharm*. 2005;20:72–76.
- Dewaraja YK, Frey EC, Sgouros G, et al. MIRD pamphlet no. 23: quantitative SPECT for patient-specific 3-dimensional dosimetry in internal radionuclide therapy. *J Nucl Med*. 2012;53:1310–1325.
- Metz CE, Atkins FB, Beck RN. The geometric transfer function component for scintillation camera collimators with straight parallel holes. *Phys Med Biol*. 1980; 25:1059–1070.
- Quantitative Nuclear Medicine Imaging: Concepts, Requirements and Methods*. International Atomic Energy Agency; 2014.
- Ljungberg M. Quantitative SPECT imaging. In: Khalil MM, ed. *Basic Sciences of Nuclear Medicine*. Springer-Verlag; 2011:285–309.
- Frey EC, Humm JL, Ljungberg M. Accuracy and precision of radioactivity quantification in nuclear medicine images. *Semin Nucl Med*. 2012;42:208–218.
- Hoffman EJ, Huang SC, Phelps ME. Quantitation in positron emission computed tomography: 1. Effect of object size. *J Comput Assist Tomogr*. 1979;3: 299–308.
- Madsen MT, Menda Y, O'Dorisio TM, et al. Technical note: single time point dose estimate for exponential clearance. *Med Phys*. 2018;45:2318–2324.
- Souweidane MM, Kramer K, Pandit-Taskar N, et al. Convection-enhanced delivery for diffuse intrinsic pontine glioma: a single-centre, dose-escalation, phase I trial. *Lancet Oncol*. 2018;19:1040–1050.
- Bockisch A. Matched pairs for radionuclide-based imaging and therapy. *Eur J Nucl Med Mol Imaging*. 2011;38(suppl 1):S1–S3.
- Sgouros G. Bone marrow dosimetry for radioimmunotherapy: theoretical considerations. *J Nucl Med*. 1993;34:689–694.
- Siegel JA, Pawlyk DA, Lee RE, et al. Tumor, red marrow, and organ dosimetry for ^{131}I -labeled anti-carcinoembryonic antigen monoclonal antibody. *Cancer Res*. 1990;50(suppl):1039s–1042s.
- Ferrer L, Malek E, Bodet-Milin C, et al. Comparisons of dosimetric approaches for fractionated radioimmunotherapy of non-Hodgkin lymphoma. *Q J Nucl Med Mol Imaging*. 2012;56:529–537.
- Siegel JA, Lee RE, Pawlyk DA, et al. Sacral scintigraphy for bone marrow dosimetry in radioimmunotherapy. *Int J Rad Appl Instrum B*. 1989;16:553–559.
- Bolch WE, Eckerman KF, Sgouros G, et al. MIRD pamphlet no. 21: a generalized schema for radiopharmaceutical dosimetry—standardization of nomenclature. *J Nucl Med*. 2009;50:477–484.
- MIRD Committee. *MIRD Primer 2020: A Complete Guide to Radiopharmaceutical Dosimetry*. Society of Nuclear Medicine and Molecular Imaging. In press.
- Dewaraja YK, Wilderman SJ, Koral KF, et al. Use of integrated SPECT/CT imaging for tumor dosimetry in I-131 radioimmunotherapy: a pilot patient study. *Cancer Biother Radiopharm*. 2009;24:417–426.
- Stabin MG. MIRDose: personal computer software for internal dose assessment in nuclear medicine. *J Nucl Med*. 1996;37:538–546.
- Stabin MG, Sparks RB, Crowe E. OLINDA/EXM: the second-generation personal computer software for internal dose assessment in nuclear medicine. *J Nucl Med*. 2005;46:1023–1027.
- Andersson M, Johansson L, Eckerman K, et al. IDAC-Dose 2.1, an internal dosimetry program for diagnostic nuclear medicine based on the ICRP adult reference voxel phantoms. *EJNMMI Res*. 2017;7:88.
- Snyder WS, Ford MR, Warner GG, Watson SB. *MIRD Pamphlet No. 11: "S," Absorbed Dose per Unit Cumulated Activity for Selected Radionuclides and Organs*. Society of Nuclear Medicine and Molecular Imaging; 1975.
- Graves SA, Flynn RT, Hyer DE. Dose point kernels for 2,174 radionuclides. *Med Phys*. 2019;46:5284–5293.
- Bolch WE, Bouchet LG, Robertson JS, et al. MIRD pamphlet no. 17: the dosimetry of nonuniform activity distributions—radionuclide S values at the voxel level. *J Nucl Med*. 1999;40(suppl):11S–36S.
- Vaziri B, Wu H, Dhawan AP, et al. MIRD pamphlet no. 25: MIRDcell V2.0 software tool for dosimetric analysis of biologic response of multicellular populations. *J Nucl Med*. 2014;55:1557–1564.
- Goddu SM, Howell RW, Bouchet LG, Bolch WE, Rao DV. *MIRD Cellular S Values*. Society of Nuclear Medicine and Molecular Imaging; 1997.
- Goddu SM, Howell RW, Rao DV. Cellular dosimetry: absorbed fractions for monoenergetic electron and alpha particle sources and S-values for radionuclides uniformly distributed in different cell compartments. *J Nucl Med*. 1994;35: 303–316.
- Bodgi L, Canet A, Pujo-Menjouet L, et al. Mathematical models of radiation action on living cells: from the target theory to the modern approaches—a historical and critical review. *J Theor Biol*. 2016;394:93–101.
- Lea D. *Actions of Radiations in Living Cells*. Cambridge University Press; 1946.
- Amro H, Wilderman SJ, Dewaraja YK, et al. Methodology to incorporate biologically effective dose and equivalent uniform dose in patient-specific 3-dimensional dosimetry for non-Hodgkin lymphoma patients targeted with ^{131}I -tositumomab therapy. *J Nucl Med*. 2010;51:654–659.
- Dewaraja YK, Schipper MJ, Roberson PL, et al. ^{131}I -tositumomab radioimmunotherapy: initial tumor dose-response results using 3-dimensional dosimetry including radiobiologic modeling. *J Nucl Med*. 2010;51:1155–1162.
- Hobbs RF, Wahl RL, Frey EC, et al. Radiobiologic optimization of combination radiopharmaceutical therapy applied to myeloablative treatment of non-Hodgkin lymphoma. *J Nucl Med*. 2013;54:1535–1542.

37. Kutcher GJ, Burman C. Calculation of complication probability factors for non-uniform normal tissue irradiation: the effective volume method. *Int J Radiat Oncol Biol Phys.* 1989;16:1623–1630.
38. Gear JI, Cox MG, Gustafsson J, et al. EANM practical guidance on uncertainty analysis for molecular radiotherapy absorbed dose calculations. *Eur J Nucl Med Mol Imaging.* 2018;45:2456–2474.
39. Bailey DL, Hofman MS, Forwood NJ, et al. Accuracy of dose calibrators for ^{68}Ga PET imaging: unexpected findings in a multicenter clinical pretrial assessment. *J Nucl Med.* 2018;59:636–638.
40. Cristy M, Eckerman KF. *Specific Absorbed Fractions of Energy at Various Ages from Internal Photon Sources.* Oak Ridge National Laboratory; 1987.
41. Hänscheid H, Lapa C, Buck AK, et al. Absorbed dose estimates from a single measurement one to three days after the administration of ^{177}Lu -DOTATATE/-TOC. *Nuklearmedizin.* 2017;56:219–224.
42. Hänscheid H, Lapa C, Buck AK, et al. Dose mapping after endoradiotherapy with ^{177}Lu -DOTATATE/DOTATOC by a single measurement after 4 days. *J Nucl Med.* 2018;59:75–81.
43. ICRP publication 89: basic anatomical and physiological data for use in radiation protection—reference values. *Ann ICRP.* 2002;32:1–277.
44. Eckerman K, Endo A. ICRP publication 107: nuclear decay data for dosimetric calculations. *Ann ICRP.* 2008;38:7–96.
45. Bolch WE, Jokisch D, Zankl M, et al. ICRP publication 133: the ICRP computational framework for internal dose assessment for reference adults: specific absorbed fractions. *Ann ICRP.* 2016;45:5–73.
46. Lea DE, Catcheside D. The mechanism of the induction by radiation of chromosome aberrations in *Tradescantia*. *J Genet.* 1942;44:216–245.
47. Barendsen GW. Dose fractionation, dose rate and iso-effect relationships for normal tissue responses. *Int J Radiat Oncol Biol Phys.* 1982;8:1981–1997.
48. Dale RG. Dose-rate effects in targeted radiotherapy. *Phys Med Biol.* 1996;41:1871–1884.
49. Fowler JF. Radiobiological aspects of low dose rates in radioimmunotherapy. *Int J Radiat Oncol Biol Phys.* 1990;18:1261–1269.
50. Bentzen SM, Dorr W, Gahbauer R, et al. Bioeffect modeling and equieffective dose concepts in radiation oncology: terminology, quantities and units. *Radiother Oncol.* 2012;105:266–268.
51. Withers HR, Thames HD Jr, Peters LJ. A new isoeffect curve for change in dose per fraction. *Radiother Oncol.* 1983;1:187–191.
52. Hobbs RF, Howell RW, Song H, et al. Redefining relative biological effectiveness in the context of the EQDX formalism: implications for alpha-particle emitter therapy. *Radiat Res.* 2014;181:90–98.
53. Barone R, Borson-Chazot F, Valkema R, et al. Patient-specific dosimetry in predicting renal toxicity with ^{90}Y -DOTATOC: relevance of kidney volume and dose rate in finding a dose-effect relationship. *J Nucl Med.* 2005;46(suppl 1):99S–106S.
54. Hobbs RF, McNutt T, Baechler S, et al. A treatment planning method for sequentially combining radiopharmaceutical therapy and external radiation therapy. *Int J Radiat Oncol Biol Phys.* 2011;80:1256–1262.
55. Konijnenberg MW. Is the renal dosimetry for [^{90}Y -DOTA0, Tyr3]octreotide accurate enough to predict thresholds for individual patients? *Cancer Biother Radiopharm.* 2003;18:619–625.
56. Niemierko A. Reporting and analyzing dose distributions: a concept of equivalent uniform dose. *Med Phys.* 1997;24:103–110.
57. O'Donoghue JA. Implications of nonuniform tumor doses for radioimmunotherapy. *J Nucl Med.* 1999;40:1337–1341.
58. Prideaux AR, Song H, Hobbs RF, et al. Three-dimensional radiobiologic dosimetry: application of radiobiologic modeling to patient-specific 3-dimensional imaging-based internal dosimetry. *J Nucl Med.* 2007;48:1008–1016.

Tumor Response to Radiopharmaceutical Therapies: The Knowns and the Unknowns

George Sgouros¹, Yuni K. Dewaraja², Freddy Escorcia³, Stephen A. Graves⁴, Thomas A. Hope⁵, Amir Irvani⁶, Neeta Pandit-Taskar⁷, Babak Saboury⁸, Sara St. James⁵, and Pat B. Zanzonico⁹

¹Department of Radiology, Johns Hopkins University, Baltimore, Maryland; ²Department of Radiology, University of Michigan, Ann Arbor, Michigan; ³Molecular Imaging Branch, Radiation Oncology Branch, National Cancer Institute, Bethesda, Maryland; ⁴Department of Radiology, University of Iowa, Iowa City, Iowa; ⁵Department of Radiology and Biomedical Imaging, University of California, San Francisco, California; ⁶Malinckrodt Institute of Radiology, Washington University, St. Louis, Missouri; ⁷Department of Radiology, Memorial Sloan Kettering Cancer Center, New York, New York; ⁸Radiology and Imaging Sciences, National Institutes of Health, Bethesda, Maryland; and ⁹Department of Medical Physics, Memorial Sloan Kettering Cancer Center, New York, New York

Radiopharmaceutical therapy (RPT) is defined as the delivery of radioactive atoms to tumor-associated targets. In RPT, imaging is built into the mode of treatment since the radionuclides used in RPT often emit photons or can be imaged using a surrogate. Such imaging may be used to estimate tumor-absorbed dose. We examine and try to elucidate those factors that impact the absorbed dose–versus–response relationship for RPT agents. These include the role of inflammation- or immune-mediated effects, the significance of theranostic imaging, radiobiology, differences in dosimetry methods, pharmacokinetic differences across patients, and the impact of tumor hypoxia on response to RPT.

Key Words: radiopharmaceuticals; dosimetry; imaging; radionuclide therapy; radiopharmaceutical therapy; theranostics

J Nucl Med 2021; 62:12S–22S

DOI: 10.2967/jnumed.121.262750

Treatment for almost all patients with metastatic cancer is a balance between preventing or mitigating cancer progression and managing often severe, treatment-induced toxicity. One way to achieve this balance is to modulate delivery of treatment. Typically, a treatment course of cytotoxic drugs is administered over multiple cycles, spanning weeks to months. A treatment cycle is defined as drug administration followed by a rest period to recover from treatment toxicity. If, after the initial treatment course, disease progresses, oncologists offer subsequent lines of cytotoxic drugs, usually with diminishing therapeutic benefit for the patient and significant toxicity. It is unsurprising, then, that we have devoted substantial resources to developing new cancer drugs. The failure rate of cancer medication from first-in-humans trial to Food and Drug Administration approval is 97% (1). These trials are largely dominated by targeted agents. Among the factors contributing to this high failure rate is the misunderstanding of mechanism of action; remarkably, the observed therapeutic effect of many targeted investigational biologic agents is through off-target effects (2). Efforts to push the limit on patient treatment with these

agents has shifted the balance to conclude that stable disease, as measured by axial CT of an index lesion, is a desirable goal despite significant toxicities. The result, then, is a treatment paradigm focused largely on managing toxicity. Treatment toxicity cannot be predicted for an individual patient. To manage potential toxicity, treatment is protracted and typically delivered in cycles over several weeks to months. The interval between cycles allows an assessment of toxicity in each patient and dose adjustment for the subsequent cycle to avert treatment-induced morbidity. This empiric approach to individual-patient therapy has been adopted as the mainstay for the management of cancer patients and is appropriate for a treatment modality that is untargeted or cannot quantify tumor–versus–normal-tissue targeting. Radiopharmaceutical therapy (RPT) is defined by the delivery of radioactive atoms to tumor-associated targets. Cell killing is achieved by delivering ionizing radiation, a treatment modality that has been used for almost 100 years and whose mechanism of action (i.e., induction of DNA damage) is well understood and potentially less sensitive to compensatory cell-signaling networks that are activated when perturbed by small-molecule inhibitors, for example. This long history and understanding make it possible to focus on characterizing the interplay between immune-mediated or tumor microenvironmental effects and overall tumor or normal-organ response. In external-beam radiotherapy (EBRT), significant improvements in efficacy without increasing toxicity arose with the adoption of image-guided radiotherapy (3). In RPT, imaging is built into the mode of treatment since the radionuclides used in RPT often emit photons. Photon emissions may be imaged by nuclear medicine modalities (e.g., SPECT or PET) to assess the distribution of the RPT in each patient. RPT agents that exclusively emit β -particle radiation (e.g., ⁹⁰Y), which were once thought not to be imageable, have been imaged by SPECT via Bremsstrahlung photon emissions (associated with high-energy β -particle photon radiation emitted during particle deceleration) and by PET (using the very low positron yield of ⁹⁰Y) and are used for treatment verification (4–6). Efforts to image and quantify the distribution of α -particle-emitting RPT are ongoing (7,8). Alternatively, a theranostic approach may be adopted wherein a radiotracer is used to demonstrate that the patient's tumor sites express the RPT target adequately. Such imaging information may be used for dosimetry-driven treatment planning (9–14) and patient selection (the process by which the absorbed dose to tumors or normal tissues is

Received Jul. 26, 2021; revision accepted Oct. 18, 2021.
For correspondence and reprints, contact George Sgouros (gsouros@jhmi.edu).
COPYRIGHT © 2021 by the Society of Nuclear Medicine and Molecular Imaging.

considered in selecting the most appropriate RPT treatment for a given patient or population of patients).

The evidence demonstrating that patient outcomes are improved (or predicted) when dosimetry is included in RPT delivery continues to accumulate (15–22). Notably, quality of life (23) can be better with RPT agents than with conventional treatment modalities (24–29).

Despite these key distinctions, RPT is currently being delivered using traditional paradigms that are driven by managing toxicity rather than fully leveraging the modality's unique features that make it more than just radioactive chemotherapy. In this work, we focus on tumor response to RPT. We start with a review of current knowledge (the knowns) and then identify those areas that require further research (the unknowns). Such a review is particularly appropriate for RPT since many RPT patients are undertreated and it is imperative that we leverage the unique quantitative tools available for RPTs to yield precision dosing that can improve the therapeutic index for patients with late-stage cancers.

TECHNICAL FACTORS IMPACTING TUMOR-ABSORBED DOSE VERSUS RESPONSE IN RPT

The 4 pillars of the paired diagnostic and therapeutic radiopharmaceuticals are personalized treatment planning, accurate verification of treatment delivery, adaptive treatment optimization, and treatment response evaluation. This aim is achieved through better patient selection by molecular imaging phenotyping (stratification), radiopharmaceutical dose optimization by predictive dosimetry (capability for predicting target engagement at disease sites and off-target toxicities), posttreatment absorbed dose deposition mapping by imaging and dosimetry, and augmentation of therapeutic targeting by adjunct therapies (locoregional such as EBRT or systemic such as additional RPT or adjuvant chemotherapy). These inherent features of RPTs represent opportunities for molecular imaging to broaden the understanding of tumor biology beyond morphologic imaging and pave the way for personalized and precision medicine. The dominant technical factors impacting tumor-absorbed dose versus response in RPT include the accuracy of quantitative imaging, the region delineation process, and uncertainties in the overall dosimetry procedure chain (30,31).

The importance of the verification of target expression by whole-body imaging as a patient-selection criterion for RPT was established in neuroendocrine tumors (NETs) by Kwekkeboom et al. (32). In that study, high tumor uptake, assessed qualitatively by pretreatment planar ¹¹¹In-pentetreotide (OctreoScan; Mallinckrodt, Inc.), was one of the independent predictive markers of a favorable treatment outcome after peptide receptor radionuclide therapy (PRRT). Increasing use of PET tracers, with the inherent quantitative ability of PET imaging, has allowed reliable and reproducible measurement of biologic target expression, which in turn has demonstrated the predictive ability of pretreatment molecular imaging in NETs and prostate cancer (33,34). Violet et al. has demonstrated a positive correlation between lesion SUV on pretreatment ⁶⁸Ga-prostate-specific membrane antigen (PSMA) PET/CT and absorbed dose (estimated by posttreatment ¹⁷⁷Lu-PSMA SPECT/CT) that resulted in a biochemical (prostate-specific antigen) response (34). The short half-life of the most commonly used radiotracers, such as ⁶⁸Ga or ¹⁸F, or the uncertain in vivo stability of the longer-half-life radiopharmaceutical has been the main limitation in deriving a meaningful pretreatment dosimetry assessment (35). However, longer-half-life radiotracers such as ¹²⁴I have

made it possible to perform pretreatment (PET-based) dosimetry and, in RPT of thyroid cancer, has been used to confirm successful restoration of NaI symporters after targeting of the driver mutations in radioiodine-refractory thyroid cancer, thereby allowing radioiodine therapy of otherwise non-iodine-avid lesions (36,37). New imaging modalities, such as total-body PET (38), and advances in SPECT instrumentation (39,40) will likely further enhance the utility of pre- and posttherapy imaging in RPT and increase the ability to image the RPT agent itself. In addition, new advances in radiochemistry using longer-half-life radiolabels such as ⁶⁴Cu (12.7 h) and ⁸⁹Zr (78.4 h) bound to stable bioconjugates, in vivo, have demonstrated the feasibility of imaging the biologic targets beyond 24 h with PET, further facilitating the pretreatment dosimetry for personalized RPT (41–43).

Tumor heterogeneity and tissue-sampling uncertainties are known limitations of increasingly biomarker-driven treatments in precision oncology (44). These limitations have become apparent by the observation that even in highly selected patient populations (e.g., basket trials) (45), the response rates in patients with a targetable alteration in their tumors was less than 10% (46). Molecular imaging provides a whole-body assessment of the biologic target expression and also its intra- and interlesional nonuniformity. This is of particular interest given the short pathlength (millimeters for β -particles and submillimeter for α -particles) of radiation particles used in RPTs, leading to nonuniform absorbed dose distributions. The prognostic significance of intralesional and interlesional somatostatin receptor expression on pretreatment somatostatin receptor PET in patients undergoing PRRT, and PSMA expression in those undergoing PSMA RPT, has underscored the fundamental role of molecular imaging in therapeutic decisions (47–49). The combination of different radiotracers enables a comprehensive assessment of various target expressions and molecular imaging-derived tumoral heterogeneity, with significant implications for the feasibility and choice of RPTs (50). Screening patients with dual-tracer imaging, including somatostatin receptor and ¹⁸F-FDG PET in NETs or PSMA and ¹⁸F-FDG and ¹⁸F-NF PET in prostate cancer, has significant implications for patient selection for RPT. These implications include guiding selection of biopsy sites, measuring the disease burden of different phenotypes, and eventually providing prognostications (51–56). Molecular imaging has become an integral component of RPT in guiding therapeutic decisions based on imaging phenotype, optimizing RPTs through prospective dosimetry, and avoiding possibly futile therapeutic interventions.

BASIC BIOLOGY FACTORS IMPACTING TUMOR-ABSORBED DOSE VERSUS RESPONSE IN RPT

Although the variability in response to RPT may depend on the RPT itself and the tumor type, the variability is just as likely derived from inpatient or interpatient variability in tumor size and tumor location (such as bone vs. soft tissue). The microenvironment of the lesion and the tissue within which the lesion is located play a critical role. For example, skeletal metastases of thyroid cancer generally require higher administered activities of radioiodine than do soft-tissue lesions (57,58). Vascular supply to the tumor is critical for ensuring optimal delivery of the RPT to the lesion. Large, solid tumors have necrotic cores as they outgrow the vascular supply, which is mostly limited to the periphery of the tumor. Larger tumors therefore will have limited specific targeting related to receptor or target binding while requiring more

of the cross-fire effect for radiation to kill tumor cells located distal from blood vessels. For this reason, combination therapy using radionuclides with short- and long-range emissions or tumors with a mixed vascular supply is consistent with radiobiologic principles. Clinical trial data are needed to confirm that it is a suitable strategy to improve tumor-absorbed dose distribution and response. Certain tumors are inherently more vascular, such as renal and lung cancers and melanoma. Neovascular targeting agents can be combined with RPT to better treat tumors by enhancing their radiosensitivity (59). Combinations of tyrosine kinase inhibitors with girentuximab have been used for renal carcinoma (60) and have potential to be used with RPT to enhance efficacy (61). Bevacizumab targets the neovasculature and is also thought to normalize the vasculature, and although RPT delivery in areas of normal vasculature may be retained or enhanced, overall tumor vasculature may be decreased, leading to lower targeted delivery (62). Radiolabeled bevacizumab has been used to target vascular endothelial growth factor-expressing tumors, but data on combination therapy with RPT are lacking (63–65).

The tumor microenvironment plays a key role in regulating radiation response, in addition to regulating cancer growth and progression. Tumors comprise the cellular component and stroma, which includes the extracellular matrix, vascular cells, fibroblasts, and leukocytes, among others. Cancer-associated fibroblasts are known to play a role in radiation resistance mediated via secretion of various signal factors leading to contact-mediated signaling or potentiating prosurvival signal pathways (66,67). In addition, these factors may promote stem cell generation and cause immune modulatory effects (68). Besides, secretory factors such as growth factors, cytokines, and chemokines in the extracellular matrix also lead to complex interactions with cellular components. Cancer-associated fibroblasts regulate adaptive and innate immune cell-mediated effector functions, including CD8-positive T-cell anergy, release of transforming growth factor- β and vascular endothelial growth factor cytokines, and expression of programmed death-ligand 1 (69). The overall response to radiation therefore depends on this complex interaction between the cellular and extracellular environments (70). Radiation leads primarily to cellular DNA damage. However, it is known that radiation effects can be noted on distant sites or areas that are outside the radiation field, known as abscopal effects. These are thought to be a result of radiation-induced immunogenic cell death and induction of subsequent cancer neoantigen-specific immune responses (71,72). Radiation-related abscopal effects are enhanced when used in combination with checkpoint inhibitors (73). CD8-positive cells play a key role in immune modulation, and the presence of CD8-positive T cells is an important prognostic marker. Given this radiation–host immune system interplay, several studies are examining combination EBRT and immune-oncology treatments, though results from randomized trials have been negative to date (74,75), suggesting we still have much to learn. Studies using RPT and immune-oncology have been initiated (NCT03805594, NCT04261855, NCT03658447).

The inherent radiation sensitivity of the tumor is one of the prime factors that impacts response to radiation. Breast cancer, neuroblastoma, lymphoma, head and neck tumors, and lung tumors are generally radiosensitive. Although not fully understood, the intrinsic radiation sensitivity of a tumor is impacted primarily by the activity of DNA repair pathways. Tumors vary considerably in radiosensitivity, which, in turn, is affected by several factors related to DNA damage and repair, apoptosis, and

cellular proliferation. Oncogenes and tumor suppressor genes considerably influence the radiosensitivity. Defects in DNA damage repair and DNA repair signaling mechanisms such as the cell-cycle checkpoint determine radiosensitivity. Several candidate genes associated with deletion or loss of function are implicated in affecting the radiosensitivity of cells. Examples are BRCA1, BRCA2, ATM, ATR, DNA-PK, POLE, mismatch repair deficiencies, and p53. Tumors harboring such mutations may show altered radiosensitivity. Hypoxia in the tumor microenvironment is also a key factor in radiosensitivity. It increases radioresistance, making hypoxic tumors resistant to radiation therapy (76). However, the effect of hypoxia specifically on RPT has not been studied. Although the radiosensitivity is more widely characterized for radiation therapy, RPTs are currently limited to only a few tumor types. Inherent interpatient differences in RPT are likely to be more pronounced, as related to pharmacokinetic factors not operative in EBRT, including the clearance and targeting kinetics of the RPT. The differences in hematologic toxicities provide an example: whereas bone-targeting agents may be expected to cause increased toxicity with greater tumor burden ($^{223}\text{RaCl}_2$, PSMA targeting osseous disease, ^{131}I -metaiodobenzylguanidine in neuroblastoma), toxicity may also be related to target expression on hematologic cells (e.g., ^{177}Lu -DOTATATE). The impact of genetic factors (i.e., genes involved in DNA damage repair) versus physiologic factors (pharmacokinetics) on tumor-absorbed dose versus response in RPT has not yet been elucidated. Genomic and proteomic analyses and their correlation with RPT tumor response are ongoing (77,78).

ABSORBED DOSE VERSUS TUMOR RESPONSE IN EBRT

Since RPT is fundamentally a radiation delivery modality, knowledge of tumor-absorbed dose versus response in EBRT is a useful starting point for evaluating absorbed dose versus tumor response in RPT. The traditional approach to radiation delivery in EBRT has been to deliver the total dose in daily 2-Gy fractions. Fractionation in radiotherapy is based on the observation that cells making up nonproliferating normal organs repair radiation-induced DNA damage more quickly than do most cancer cells. In radiobiologic terms, late-responding tissues (e.g., normal tissues) with a typical α/β of less than 4.5 Gy are less susceptible to fractionated radiation delivery than are most cancer cells (typical α/β , >10 Gy) (α and β are parameters of the linear-quadratic model widely used to describe response to radiation [the linear quadratic model is reviewed in a number of publications, such as the MIRD Primer and International Commission on Radiation Units and Measurements report 96 (79,80)]). This approach is important when radiation targeting is suboptimal, delivering substantial radiation to normal tissues during tumor targeting. The reduction in normal-organ radiation exposure with advanced techniques has led to hypofractionation protocols—total dose delivered in fewer fractions, with each fraction greater than 2 Gy.

The response of tumors to a particular absorbed dose delivered by EBRT depends on a host of factors, including tumor histology and stage, tumor volume, fraction of tumor volume irradiated, and fractionation schedule applied. Tumor response itself is reported as locoregional (e.g., tumor volume change, absence of recurrence if given adjuvantly) or global (e.g., reduction in imaging or serum markers or, most importantly for patients, improvement in quality of life or overall survival). Accordingly, Table 1 provides the typical range of doses used in radiation oncology for different cancers.

In the selected cases for which response is provided, it is a substantial simplification of the actual anticipated response. In several cases, the absorbed dose is expressed as the biologically effective dose or as the 2-Gy equivalent dose. Both formalisms are intended to account for differences in how the total prescribed tumor-absorbed dose is fractionated. The former yields the absorbed dose to achieve a particular biologic effect if it were delivered in infinitesimally small dose fractions. The latter yields biologic effects seen with a traditional 2-Gy/fraction delivery of radiotherapy. Normal-organ dose limits are described in another paper (81) included in this supplement to *The Journal of Nuclear Medicine*.

Table 1 lists typical prescribed radiation doses for different cancer types. Consistent with genomic-based approaches to introducing precision medicine to medical oncology, genomic analysis of individual-patient tumor samples has been explored to assess tumor radiosensitivity in radiotherapy patients, with the intent of using this information to adjust the prescribed dose (82). Although promising, prospective evaluations of such approaches are needed.

CANCER CELL RESPONSE BY CATEGORY

Beyond the specific cancer types listed in Table 1, it is possible to broadly categorize tumors by tumor target and compartment. These broad categories and corresponding tumor characteristics are listed below.

Liquid Tumors (Leukemias, Lymphomas)

Liquid tumors exist within the intravascular, lymphatic, and marrow space and are generally rapidly accessible to intravenously administered RPT. They are radiosensitive because of a short cell-doubling time, tend to be clonal, and often harbor genomic lesions, increasing their susceptibility to DNA damage. These cancers are treatable with RPT absorbed doses in the range of 5–15 Gy (83).

Solid Tumors

Perhaps the most relevant tumor characteristic for RPT is the variable vascularity of, and absence of lymphatic drainage from, solid malignancies (84–86). The interstitial pressure associated with these characteristics impedes uniform penetration of

systemically administered RPT. The reduced vasculature and reduced nutrient supply lead to hypoxia and induction of hypoxia-related signaling pathways. Cancer cells with elevated hypoxia-inducible factors are more aggressive, are less sensitive to therapy, and exhibit a greater propensity for metastatic dissemination. These factors give rise to highly nonuniform intratumoral dose distributions from most RPT agents. Tumor-volume-averaged absorbed dose estimates for response to different RPT agents range from 40 to 200 Gy. In addition to all the biologic variables, this large range in absorbed doses needed for a response may also reflect the impact of absorbed dose nonuniformities. Efforts to account for this possibility using the equivalent uniform dose (EUD) formalism have been developed; however, continued rigorous evaluation of its applicability is warranted (87–89).

Metastatically Disseminated Cancer Cells

Metastatically disseminated cancer cells are the cell population perhaps most relevant for RPT. Distant metastases to bone and other viscera typically occur via hematogenous spread. It is thought that RPT may be most effective for low-volume metastases. However, given the known radiosensitivity to leukocytes, the risk of marrow toxicity is real and warrants caution.

RPT TUMOR DOSE-RESPONSE EXPERIENCE

At the most basic level, response to RPT is impacted by 2 factors: the intrinsic radiation sensitivity of the tumor, and the absorbed dose to the tumor. Although not fully understood, the intrinsic radiosensitivity of a tumor cell is impacted primarily by doubling time and ability to address genomic lesions caused by ionizing radiation. The dose to the tumor is dependent on the target expression, the residence time of the RPT once it binds to the target, and the physical properties of the radiopharmaceutical (e.g., isotope half-life and emission characteristics).

Establishing the tumor-absorbed dose-versus-response relationship in RPT has yet to be prioritized. In addition to the scarcity of studies acquiring multiple-time-point imaging data for dosimetry, tumor dosimetry is associated with the added challenge of segmentation. Although fully automatic or semiautomatic tools based

TABLE 1
Summary of Tumor-Absorbed Dose vs. Response from EBRT

Cancer	Prescribed tumor dose/fraction number	Comments	Reference
Breast	40 or 43.5 Gy/15	2.67–2.9 Gy/fraction	118,119
Prostate	76–82 Gy/38–41; 64.6 Gy/19; 60 Gy/20	2, 3.4, or 3 Gy/fraction	120,121
Head and neck cancers	70 Gy/35	2 Gy/fraction	122
Hepatocellular carcinoma	66 Gy/10	Proton therapy, 109-Gy biologically effective dose ($\alpha/\beta = 10$ Gy)	123
Lung (stage I, non-small cell lung carcinoma)	54 Gy/3	Stereotactic body radiotherapy, 18 Gy/fraction	124
Lymphoma	30 Gy	Median, 30 Gy (overall range, 24–52 Gy)	125
Oligometastatic disease	30–60 Gy/3–8; 16 Gy/1, 24 Gy/1 to CNS metastases	1–3 vs. 4–5 metastases	126

CNS = central nervous system.

TABLE 2

Studies Reporting on Tumor-Absorbed Dose vs. Response in Microsphere Radioembolization of Hepatic Malignancies

Study	<i>n</i>	Disease	Lesion size (cm)	Device	Imaging	Endpoint	Threshold mean dose (Gy)
Garin (92,127,128)	36, 71, 71	HCC	7.1 ± 3.3	⁹⁰ Y glass	^{99m} Tc-MAA SPECT	PFS, EASL	205
Mazzaferro (129)	52	HCC		⁹⁰ Y glass	^{99m} Tc-MAA SPECT	EASL (PR + CR)	500
Chiesa (130)	52	HCC	4.9 (1.8–10.3)	⁹⁰ Y glass	^{99m} Tc-MAA SPECT	EASL (PR + CR) 50% TCP	390
Chan (131)	35	HCC	7.3 (3.0–17.9)	⁹⁰ Y glass	⁹⁰ Y PET/CT	mRECIST (PR + CR)	200
Ho (132)	62	HCC		⁹⁰ Y glass	^{99m} Tc-MAA SPECT/CT	¹⁸ F-FDG, ¹¹ C PET res. > 50%	170
Kappadath (110)	34	HCC	4.1 (2.6–12.3)	⁹⁰ Y glass	⁹⁰ Y SPECT/CT	mRECIST 50% TCP	160
Dewaraja (111)	28	HCC and metastases	2.7 (1.6–11.7)	⁹⁰ Y glass	⁹⁰ Y PET/CT	mRECIST 50% TCP	290
Lau (133)	18	HCC	NA	⁹⁰ Y resin	^{99m} Tc-MAA planar	CT volume + AFP	120
Strigari (134)	73	HCC	5.8 (1.6–15.6)	⁹⁰ Y resin	⁹⁰ Y SPECT	50% TCP (PR + CR)	150
Flamen (135)	8	Colorectal	781 mL (95% CI, 332–1,230)	⁹⁰ Y resin	^{99m} Tc-MAA SPECT	¹⁸ F-FDG PET res. > 50%	46
Song (136)	23	HCC and metastases	467 mL (5–1,400)	⁹⁰ Y resin	⁹⁰ Y PET/CT	PFS, RECIST	200
Chansanti (97)	15	NET	3.9 (±2.3)	⁹⁰ Y resin	^{99m} Tc-MAA SPECT/CT	mRECIST (PR + CR)	191
Allimant (137)	38	HCC	5 (2.8–11.4)	⁹⁰ Y resin	⁹⁰ Y PET/CT	PFS, mRECIST	Area under DVH > 61 Gy
Hermann (138) (SARAH trial)	121	HCC	152 cm (IQR, 46.4–399.5)	⁹⁰ Y resin	^{99m} Tc-MAA SPECT/CT	RECIST	100

HCC = hepatocellular carcinoma; MAA = macroaggregated albumin; PFS = progression-free survival; EASL = European Association for the Study of the Liver; PR = partial response; CR = complete response; res. = response; TCP = tumor control probability measure of tumor control (typically a radiobiologically derived parameter based on linear quadratic model that accounts for nonuniformity in absorbed dose within tumor and effect this has on likelihood of tumor control; can also be obtained using statistical data-driven models [MIRD Primer and International Commission on Radiation Units and Measurements report 96]); AFP = α -fetoprotein; NA = not applicable; DVH = dose-volume histogram; IQR = interquartile range.

Data in parentheses are ranges.

on thresholding, atlas libraries, and—more recently—machine learning are available for organ segmentation, accurate tumor segmentation typically requires a radiologist either to perform the task manually or to refine outlines from emission imaging thresholding or gradient-based tools. Furthermore, standardized tumor dosimetry can be more challenging than organ dosimetry because imaging-related factors such as PET and SPECT resolution, reconstruction parameters, and partial-volume correction methods have a substantially increased impact on objects with small volumes relative to the system resolution. The criteria and timing used for response assessment will impact the tumor-absorbed dose-versus-outcome relationships. Although morphologic response on CT or MRI using criteria such as RECIST has traditionally been used to assess tumor response in dose-response studies, use of metabolic response based on PET SUV or biochemical response (e.g., chromogranin A levels for NETs or prostate-

specific antigen levels for prostate cancer) has also been reported. In some cases, implementation of proposed tumor-specific radiologic response criteria has been attempted, such as the European Association for the Study of the Liver criteria for hepatocellular carcinoma (90).

Most studies reporting a statistically significant association between absorbed dose and tumor response have been on ⁹⁰Y microsphere radioembolic therapy of hepatic malignancies (Table 2). The most extensive of these evaluations has been performed by the group of Garin et al., using ^{99m}Tc-macroaggregated albumin SPECT/CT-based estimates as a surrogate for ⁹⁰Y (91). In their initial studies, they demonstrated that the overall survival was significantly higher at 6 mo after treatment in patients who received a mean tumor-absorbed dose of at least 205 Gy than in those who received less than 205 Gy (18 mo vs. 9 mo; *P* = 0.032) (92)—a finding that was independently validated in a prospective

TABLE 3
Studies Reporting Tumor Dose–Response Relationship in Other RPTs

Study	Disease	Therapy	n	Lesion size	Dosimetry method	Endpoint	Threshold
Maxon (139)	Thyroid cancer metastases	¹³¹ I radioiodine	76		Planar conjugate views	Response on ¹³¹ I planar scans	80 Gy for metastases; 300 Gy for remnants
Wierls (140)	Thyroid cancer remnants and metastases	¹³¹ I radioiodine	47	>0.15 cm ³	¹²⁴ I PET + OLINDA sphere model	CR on ¹³¹ I SPECT or ¹²⁴ I PET	40 Gy for metastases; 90 Gy for remnants
Pauwels (102)	NET	⁹⁰ Y-DOTATOC PRRT	13	NA	⁸⁶ Y-DOTATOC PET + MIRDOSE sphere model	Volume shrinkage > 30% on CT	~150 Gy for >30% shrinkage
Ilan (103)	NET	¹⁷⁷ Lu-DOTATATE PRRT	24 (24 tumors)	>2.2 cm	SPECT/CT + OLINDA sphere model	RECIST best response > 30%	~150 Gy
Matthay (141)	Neuroblastoma	¹³¹ I-metaiodobenzylguanidine	27		Planar conjugate view + MIRDOSE	Volume shrinkage > 50% on CT	70 Gy
Dewaraja (16)	Non-Hodgkin lymphoma	¹³¹ I-radioimmunotherapy	39 (130 tumors)	Median, 20 cm ³	Multi-SPECT/CT + Monte Carlo	Progression-free survival	200 cGy

CR = complete response.

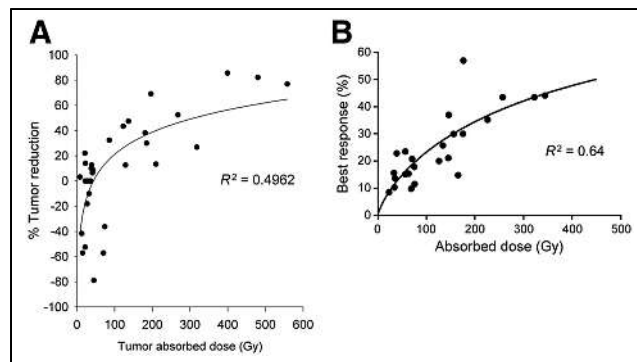


FIGURE 1. Tumor dose–response relationship in PRRT for 13 patients treated with ⁹⁰Y-DOTATOC (A) and 24 patients treated with ¹⁷⁷Lu-DOTA-TATE (B). (Adapted from Pauwels et al. (102) and Ilan et al. (103).)

study with 85 patients (91). Their findings were subsequently used to design the DOSISPHERE-01 trial, a prospective clinical trial to compare response and survival in patients receiving a personalized tumor dosimetry–guided treatment to deliver more than 205 Gy to the index lesion, compared with those receiving the standard treatment protocol for ⁹⁰Y glass microspheres. Recently published results from this trial show that personalized dosimetry significantly improved the objective response rate (71% vs. 36%; $P = 0.0074$) and survival (median 27 mo vs. 11 mo; $P = 0.0096$) over radioembolization using a standard dosimetry approach (92). Literature reports on non–hepatocellular carcinoma intrahepatic radioembolization targets—colorectal metastases, NET metastases, cholangiocarcinoma, and metastatic melanoma—also demonstrate statistically significant dose–response relationships, but with differing response thresholds (22,93–100).

A recent study on ¹⁷⁷Lu-PSMA radioligand therapy in low-volume hormone-sensitive metastatic prostate cancer patients reported a statistically significant correlation between absorbed dose to the index lesion and treatment response, defined as a prostate-specific antigen drop of more than 50% (101).

In radioiodine therapy, PRRT, and radioimmunotherapy, there have been a few studies investigating tumor dose–response relationships (Table 3). For PRRT, these data have been summarized in a recent review article (17). For NETs, the dose–response curve published in 2005 by Pauwels et al. (102) for ⁹⁰Y-DOTATOC therapy is remarkably similar to the results published by Ilan et al. (103) a decade later for ¹⁷⁷Lu-DOTATATE (Fig. 1). As the figure shows, in both cases, a 30% tumor shrinkage was achieved at approximately a 150-Gy mean absorbed dose to the tumor (over multiple cycles). Unlike the study by Ilan et al. for pancreatic NETs, a similar dose–response study on small intestinal NETs by the same group failed to demonstrate a statistically significant relationship (104). They reported mean tumor-absorbed doses of 51–487 Gy (median, 140 Gy) that showed no association with tumor reduction or biochemical response. Because of the very high radiosensitivity of lymphomas, reported absorbed doses to achieve a response in non-Hodgkin lymphoma treated with radioimmunotherapy have been about 100-fold lower than in NETs treated with PRRT. Tumor-absorbed doses reported by Sgouros et al. for a study of ¹³¹I-tositumomab RPT in non-Hodgkin lymphoma were in the range of 37–1,760 cGy (median, 300 cGy) (105). In a study of 39 patients (130 tumors) treated with ¹³¹I-tositumomab RPT, Dewaraja et al. reported longer progression-free

TABLE 4
List of Unknowns

No.	Description
1	How does inflammation- or immune-mediated effects influence dose-vs.-response relationship?
2	Does negative theranostic imaging preclude patient benefit from RPT?
3	What are radiobiologic parameter values for RPT? Do those from EBRT apply?
4	Do genomic approaches to assessing individual patient or tumor radiosensitivity (e.g., genomic-adjusted radiation dose) apply to RPT?
5	To what extent do differences in dosimetry methods vs. other factors (radiosensitivity, patient population) explain variability in dose vs. response?
6	How do immunooncologic agents such as immune checkpoint inhibitors impact RPT?
7	How do patient-specific differences (kinetics, size and distribution of lesions, overall tumor burden) impact tumor response to RPT? Can these differences be accounted for by calculating tumor-absorbed dose?
8	How does hypoxia affect response to RPT?
9	What is best formalism or approach for relating RPT to EBRT dose response ?

survival in patients receiving mean tumor-absorbed doses greater than 200 cGy than in those receiving 200 cGy or less (median progression-free survival, 13.6 vs. 1.9 mo for the 2 dose groups; $P < 0.0001$) (16). The tumor-absorbed doses in this study ranged from 94 to 711 cGy (median, 275 cGy), with 62% of patients classified as responders and 46% as complete responders. In a study of 16 patients with non-Hodgkin lymphoma treated with ¹⁷⁷Lu-lilotomab satetraxetan, the reported absorbed doses were of the same order of magnitude as reported in the studies by Dewaraja et al. and Sgouros et al. for ¹³¹I-tositumomab RPT, ranging from 35 to 859 cGy (median, 330 cGy) (106). Although most patients demonstrated a metabolic response on ¹⁸F-FDG PET, there was no overall correlation between tumor-absorbed dose and response assessed on the basis of either PET or CT measurements. This diversity of dose–response data may reflect the importance of standardizing dosimetry methods and performing rigorous trials that incorporate dosimetry to help evaluate variability in absorbed dose versus tumor response more definitively.

The importance of radiobiologic dosimetry in accounting for the effects of dose-rate and spatial nonuniformity in absorbed dose is evident when comparing the threshold tumor-absorbed doses for achieving a response reported in clinical studies with resin microspheres versus glass microspheres (Table 2). In hepatocellular carcinoma, the reported mean tumor-absorbed dose thresholds for glass are generally in the range of 200–400 Gy, whereas for resin this value is in the range 100–150 Gy. This difference has been attributed to the differences in the uniformity of microsphere distribution on a microscopic scale—uniformity that varies with the number of injected particles per gigabecquerel (107). However, this difference is difficult to resolve with PET or SPECT imaging capabilities. The higher specific activity of glass than of resin microspheres leads to a less uniform dose deposition and, hence, a lower biologic effect per gray. d’Abadie et al. (108) have attempted to use the tumor EUD to reconcile the approximately 2-fold difference in efficacy per gray between resin and glass microspheres reported in clinical studies. For hepatocellular carcinoma treated with glass microspheres, Chiesa et al. reported that responding versus nonresponding lesions were well separated regardless of the dose metric used, but the equivalent uniform biologically effective dose gave significantly better separation than

what was achieved with mean absorbed dose (AUC, 0.87 vs. 0.80) (109). Two other studies used logistical regression models for describing dose–response data for ⁹⁰Y glass microspheres showed a strong association between dose metrics and the probability of response regardless of whether mean absorbed dose or radiobiologic dose metrics were used. Although the statistical models used in these studies have no radiobiologic basis, they use a variable function to approximate the sigmoidal response function potentially caused by tumor variations in radiosensitivity, clonogen number, experimental uncertainty, and other factors (110,111). In RPT, Roberson et al. expanded their tumor radiobiologic model for non-Hodgkin lymphoma to include the effect of the cold antibody (unlabeled tositumomab) that is coadministered with both the tracer and the therapy administration of ¹³¹I-labeled tositumomab (16,112). Facilitated by access to multiple-time-point SPECT/CT imaging, they demonstrated substantial lesion shrinkage during the 7 d of imaging after the tracer and therapy administration; this shrinkage was attributed to the therapeutic effect of the cold antibody and the high radiosensitivity of lymphomas. The use of EUD for dose–response correlations using early response as the outcome resulted in an improvement over the use of mean absorbed dose. However, regarding progression-free survival, both mean tumor-absorbed dose and EUD showed a similar statistically significant association (16). Image-derived EUDs are constrained by the resolution of the SPECT or PET system. Although image-derived EUD may be valuable for tumor regions that broadly exhibit variable uptake (e.g., necrotic zones), accounting for millimeter-scale patterns of retention that could drive some degree of differential radioresistance among patients is not possible unless supplemented with a priori knowledge of the expected distribution (e.g., as may be obtained from preclinical studies).

SUMMARY AND TABLE OF UNKNOWNNS

The biologic characteristics of radiation have been extensively characterized, both in vitro and in vivo, and numerous factors are known to impact biologic response. These include total absorbed dose, dose rate, timing of sequential doses of radiation, spatial uniformity in the absorbed dose, tissue type, radiation type, and chemical factors such as tissue oxygen saturation. Dose and

treatment fractionation in particular have been tools of radiation oncology to help increase the therapeutic ratio—that is, by increasing tumor control probability relative to normal-tissue complication probability. Despite the limitations associated with extrapolating from controlled experiments (e.g., clonogenic cell survival assays) to heterogeneous patient populations, mathematic models describing these relationships, such as the linear quadratic model, have been highly influential in radiation therapy practice patterns.

Conventional (~2 Gy per fraction) EBRT practice has benefited from landmark publications, including the Emami paper (113) and the QUANTEC (Quantitative Analysis of Normal Tissue Effects in the Clinic) papers (114,115). These publications—written on the basis of available data or, when data were lacking, expert opinion—have guided the field of radiation oncology toward standardization of how normal-tissue doses affect measurable adverse events, such as fibrosis or neuropathy. As the practice of radiation oncology has evolved since 2010, hypofractionation (in which high doses of radiation are delivered in fewer fractions) has become a routine part of clinical care. As such, additional guidelines regarding normal-tissue dose tolerances have been developed, such as the HyTEC (High Dose per Fraction, Hypofractionated Treatment Effects in the Clinic) project (116). No comprehensive or authoritative resource currently exists regarding tumor control probability as a function of EBRT dose and treatment schedule. Rather than deriving the ideal treatment schedule from fundamental radiobiologic models and preclinical studies, current treatment patterns are often a reflection of historic norms, through which safety and efficacy are supported by existing data. With the exception of palliative therapy and the small subset of cases in which local control is close to 100% at moderate dose levels, historic prescribing patterns reflect a dose level that typically does not exceed normal-tissue tolerances. The intent with this approach is to maximize the therapeutic ratio in a typical patient. Radiobiologic modeling via the concept of biologically effective dose and equivalent dose in 2 Gy per fraction is often used clinically for extrapolation from conventional fractionation to other treatment schedules that are isoeffective but have reduced toxicity, isotoxic but have increased efficacy, or some combination of the two. To the extent that it has been developed, the radiobiology of low-dose-rate brachytherapy may be more relevant to RPT tumor response for a given total tumor-absorbed dose. Incorporating novel approaches, such as Decipher or genomic-adjusted radiation dose, may improve classic models by incorporating genomic data from patients (82,117). Table 4 summarizes the list of unknowns.

CONCLUSION

Within the context of RPT, direct adoption of guidelines and tumor control probability models developed for the field of EBRT may be impractical; however, the history of external-beam dosimetry refinement and optimization of treatment plans may guide similar advances with RPT. At a given average tumor-absorbed dose, RPT may lead to very different biologic effects from those of EBRT because of a reduced dose rate, a much greater nonuniformity in the spatial absorbed dose distribution at the microscopic level, differing relative biological effectiveness (via α -emitting RPTs), or differences in the total treatment time. Increased DNA repair during low-dose-rate therapy, as well as repair and proliferation between treatments, is generally expected to increase organ dose tolerance and thresholds for tumor control. As with

conventional radiation therapy, though, it is critical that we combine expert opinion with clinical experience whereby the absorbed dose to tumors and healthy structures is well estimated within conventional treatment paradigms, and radiobiologic models are subsequently used to refine treatment practice. Such efforts can help standardize the treatment of patients with RPT and improve the therapeutic index on a patient-specific basis. Importantly, we need well-designed prospective clinical trials to validate the hypothesis that, like external radiotherapy, absorbed doses to tumors and organs relate to tumor control and toxicity, respectively. Admittedly, arriving at a standardized model to test and implement is challenging, but the potential benefit is well worth the effort.

DISCLOSURE

George Sgouros is a founder of, and holds equity in, Rapid. He serves as a member of Rapid's Board of Directors. This arrangement has been reviewed and approved by the Johns Hopkins University in accordance with its conflict-of-interest policies. Yuni Dewaraja is a consultant for MIM Software and has a grant from Varian. Thomas Hope is a consultant for Curium and Rayze Bio, has a grant from Clovis Oncology, and is on the advisory board of Blue Earth Diagnostics and Ipsen. He is also a participant on a AAA/Novartis clinical trial. The opinions expressed in this publication are the author(s)' own and do not reflect the view of the National Institutes of Health, the Department of Health and Human Services, or the United States government. No other potential conflict of interest relevant to this article was reported.

REFERENCES

1. Wong CH, Siah KW, Lo AW. Estimation of clinical trial success rates and related parameters. *Biostatistics*. 2019;20:273–286.
2. Lin A, Giuliano CJ, Palladino A, et al. Off-target toxicity is a common mechanism of action of cancer drugs undergoing clinical trials. *Sci Transl Med*. 2019; 11:eaaw8412.
3. Muirhead R. Image-guided radiotherapy: the unsung hero of radiotherapy development. *Clin Oncol (R Coll Radiol)*. 2020;32:789–791.
4. Dewaraja YK, Chun SY, Srinivasa RN, et al. Improved quantitative Y-90 bremsstrahlung SPECT/CT reconstruction with Monte Carlo scatter modeling. *Med Phys*. 2017;44:6364–6376.
5. Elschot M, Lam M, van den Bosch M, Viergever MA, de Jong H. Quantitative Monte Carlo-based Y-90 SPECT reconstruction. *J Nucl Med*. 2013;54: 1557–1563.
6. Tafti BA, Padia SA. Dosimetry of Y-90 microspheres utilizing Tc-99m SPECT and Y-90 PET. *Semin Nucl Med*. 2019;49:211–217.
7. Ghaly M, Sgouros G, Frey E. Quantitative dual isotope SPECT imaging of the alpha-emitters Th-227 and Ra-223 [abstract]. *J Nucl Med*. 2019;60(suppl):41.
8. He B, Frey E, Sgouros G, Ghaly M, Tworowska I, Delpassand E. Development and Validation of Methods for Quantitative In Vivo SPECT of Pb-212 [abstract]. *J Med Imaging Radiat Sci*. 2019;50(suppl):S33.
9. Song H, He B, Prideaux A, et al. Lung dosimetry for radioiodine treatment planning in the case of diffuse lung metastases. *J Nucl Med*. 2006;47:1985–1994.
10. O'Donoghue JA, Baidoo N, Deland D, Welt S, Divgi CR, Sgouros G. Hematologic toxicity in radioimmunotherapy: dose-response relationships for I-131 labeled antibody therapy. *Cancer Biother Radiopharm*. 2002;17:435–443.
11. Sgouros G, Kolbert KS. The three-dimensional internal dosimetry software package, 3D-ID. In: Zaidi H, Sgouros G, eds. *Therapeutic Applications of Monte Carlo Calculations in Nuclear Medicine*. Institute of Physics; 2002:249–261.
12. Munn EF, Kolbert KS, Sheikh A, et al. Patient-specific PET-based 3D-dosimetry: retrospective analysis for I-131 thyroid cancer therapy [abstract]. *J Nucl Med*. 2002;43(suppl):86P.
13. Sgouros G, Stabin M, Erdi Y, et al. Red marrow dosimetry for radiolabeled antibodies that bind to marrow, bone, or blood components. *Med Phys*. 2000;27: 2150–2164.
14. Sgouros G, Barest G, Thekkumthala J, et al. Treatment planning for internal radionuclide therapy: three-dimensional dosimetry for nonuniformly distributed radionuclides. *J Nucl Med*. 1990;31:1884–1891.

15. Violet J, Jackson P, Ferdinandus J, et al. Dosimetry of Lu-177-PSMA-617 in metastatic castration-resistant prostate cancer: correlations between pretherapeutic imaging and whole-body tumor dosimetry with treatment outcomes. *J Nucl Med*. 2019;60:517–523.
16. Dewaraja YK, Schipper MJ, Shen J, et al. Tumor-absorbed dose predicts progression-free survival following ¹³¹I-tositumomab radioimmunotherapy. *J Nucl Med*. 2014;55:1047–1053.
17. Cremonesi M, Ferrari ME, Bodei L, et al. Correlation of dose with toxicity and tumour response to Y-90- and Lu-177-PRRT provides the basis for optimization through individualized treatment planning. *Eur J Nucl Med Mol Imaging*. 2018;45:2426–2441.
18. Sandström M, Garske-Roman U, Granberg D, et al. Individualized dosimetry of kidney and bone marrow in patients undergoing Lu-177-DOTA-octreotate treatment. *J Nucl Med*. 2013;54:33–41.
19. Stokke C, Gabina PM, Solny P, et al. Dosimetry-based treatment planning for molecular radiotherapy: a summary of the 2017 report from the Internal Dosimetry Task Force. *EJNMMI Phys*. 2017;4:27.
20. Sundlöv A, Sjogreen-Gleisner K, Svensson J, et al. Individualised Lu-177-DOTATATE treatment of neuroendocrine tumours based on kidney dosimetry. *Eur J Nucl Med Mol Imaging*. 2017;44:1480–1489.
21. Vilgrain V, Pereira H, Assenat E, et al. Efficacy and safety of selective internal radiotherapy with yttrium-90 resin microspheres compared with sorafenib in locally advanced and inoperable hepatocellular carcinoma (SARAH): an open-label randomised controlled phase 3 trial. *Lancet Oncol*. 2017;18:1624–1636.
22. Bastiaannet R, van Roekel C, Smits MLJ, et al. First evidence for a dose-response relationship in patients treated with Ho-166 radioembolization: a prospective study. *J Nucl Med*. 2020;61:608–612.
23. Basch E. Toward patient-centered drug development in oncology. *N Engl J Med*. 2013;369:397–400.
24. Hofman MS, Violet J, Hicks RJ, et al. [¹⁷⁷Lu]-PSMA-617 radionuclide treatment in patients with metastatic castration-resistant prostate cancer (LuPSMA trial): a single-centre, single-arm, phase 2 study. *Lancet Oncol*. 2018;19:825–833.
25. Strosberg J, Wolin E, Chasen B, et al. Health-related quality of life in patients with progressive midgut neuroendocrine tumors treated with ¹⁷⁷Lu-dotatate in the phase III NETTER-1 trial. *J Clin Oncol*. 2018;36:2578–2584.
26. Georgakopoulos A, Liotsou T, Chatziioannou SN. Quality of life in patients with neuroendocrine gastroenteropancreatic tumors treated with peptide receptor radionuclide therapy [abstract]. *Eur J Nucl Med Mol Imaging*. 2017;44(suppl):S691.
27. Brans B, Lambert B, De Beule E, et al. Quality of life assessment in radionuclide therapy: a feasibility study of the EORTC QLQ-C30 questionnaire in palliative I-131-lipiodol therapy. *Eur J Nucl Med Mol Imaging*. 2002;29:1374–1379.
28. Sgouros G, Goldenberg DM. Radiopharmaceutical therapy in the era of precision medicine. *Eur J Cancer*. 2014;50:2360–2363.
29. Hofman MS, Emmett L, Sandhu S, et al. Lu-177 Lu-PSMA-617 versus cabazitaxel in patients with metastatic castration-resistant prostate cancer (TheraP): a randomised, open-label, phase 2 trial. *Lancet*. 2021;397:797–804.
30. Ljungberg M, Gleisner KS. 3-D image-based dosimetry in radionuclide therapy. *IEEE Trans Radiat Plasma Med Sci*. 2018;2:527–540.
31. Li T, Ao ECI, Lambert B, Brans B, Vandenberghe S, Mok GSP. Quantitative imaging for targeted radionuclide therapy dosimetry: technical review. *Theranostics*. 2017;7:4551–4565.
32. Kwekkeboom DJ, de Herder WW, Kam BL, et al. Treatment with the radiolabeled somatostatin analog [¹⁷⁷Lu-DOTA⁰, Tyr³]octreotate: toxicity, efficacy, and survival. *J Clin Oncol*. 2008;26:2124–2130.
33. Kratochwil C, Stefanova M, Mavriopoulou E, et al. SUV of [⁶⁸Ga]DOTATOC-PET/CT predicts response probability of PRRT in neuroendocrine tumors. *Mol Imaging Biol*. 2015;17:313–318.
34. Violet J, Jackson P, Ferdinandus J, et al. Dosimetry of ¹⁷⁷Lu-PSMA-617 in metastatic castration-resistant prostate cancer: correlations between pretherapeutic imaging and whole-body tumor dosimetry with treatment outcomes. *J Nucl Med*. 2019;60:517–523.
35. Pfeifer A, Knigge U, Mortensen J, et al. Clinical PET of neuroendocrine tumors using ⁶⁴Cu-DOTATATE: first-in-humans study. *J Nucl Med*. 2012;53:1207–1215.
36. Sgouros G, Hobbs RF, Atkins FB, Van Nostrand D, Ladenson PW, Wahl RL. Three-dimensional radiobiological dosimetry (3D-RD) with ¹²⁴I PET for ¹³¹I therapy of thyroid cancer. *Eur J Nucl Med Mol Imaging*. 2011;38(suppl 1):S41–S47.
37. Ho AL, Grewal RK, Leboeuf R, et al. Selumetinib-enhanced radioiodine uptake in advanced thyroid cancer. *N Engl J Med*. 2013;368:623–632.
38. Spencer BA, Berg E, Schmall JP, et al. Performance evaluation of the uEXPLORER total-body PET/CT scanner based on NEMA NU 2-2018 with additional tests to characterize PET scanners with a long axial field of view. *J Nucl Med*. 2021;62:861–870.
39. Zannoni EM, Wilson MD, Bolz K, et al. Development of a multi-detector readout circuitry for ultrahigh energy resolution single-photon imaging applications. *Nucl Instrum Methods Phys Res A*. 2020;981:164531.
40. Cai L, Li N, Meng LJ. A prototype adaptive SPECT system with self-optimized angular sampling. *2011 IEEE Nuclear Science Symposium and Medical Imaging Conference (NSS/MIC)*. IEEE; 2011:4402–4406.
41. Hicks RJ, Jackson P, Kong G, et al. ⁶⁴Cu-SARTATE PET imaging of patients with neuroendocrine tumors demonstrates high tumor uptake and retention, potentially allowing prospective dosimetry for peptide receptor radionuclide therapy. *J Nucl Med*. 2019;60:777–785.
42. Lee CH, Lim I, Woo SK, et al. The feasibility of ⁶⁴Cu-PSMA I&T PET for prostate cancer. *Cancer Biother Radiopharm*. January 12, 2021 [Epub ahead of print].
43. Zia NA, Cullinane C, Van Zuylen JK, et al. A bivalent inhibitor of prostate specific membrane antigen radiolabeled with copper-64 with high tumor uptake and retention. *Angew Chem Int Ed Engl*. 2019;58:14991–14994.
44. Ileana Dumbava E, Meric-Bernstam F, Yap TA. Challenges with biomarkers in cancer drug discovery and development. *Expert Opin Drug Discov*. 2018;13:685–690.
45. Murciano-Goroff YR, Drilon A, Stadler ZK. The NCI-MATCH: a national, collaborative precision oncology trial for diverse tumor histologies. *Cancer Cell*. 2021;39:22–24.
46. Prasad V, Fojo T, Brada M. Precision oncology: origins, optimism, and potential. *Lancet Oncol*. 2016;17:e81–e86.
47. Graf J, Pape UF, Jann H, et al. Prognostic significance of somatostatin receptor heterogeneity in progressive neuroendocrine tumor treated with Lu-177 DOTA-TOC or Lu-177 DOTATATE. *Eur J Nucl Med Mol Imaging*. 2020;47:881–894.
48. Werner RA, Lapa C, Ilhan H, et al. Survival prediction in patients undergoing radionuclide therapy based on intratumoral somatostatin-receptor heterogeneity. *Oncotarget*. 2017;8:7039–7049.
49. Seifert R, Seitzer K, Herrmann K, et al. Analysis of PSMA expression and outcome in patients with advanced prostate cancer receiving ¹⁷⁷Lu-PSMA-617 radioligand therapy. *Theranostics*. 2020;10:7812–7820.
50. Irvani A, Mitchell C, Akhurst T, Sandhu S, Hofman MS, Hicks RJ. Molecular imaging of neuroendocrine differentiation of prostate cancer: a case series. *Clin Genitourin Cancer*. 2021;19:e200–e205.
51. Zidan L, Irvani A, Kong G, Akhurst T, Michael M, Hicks RJ. Theranostic implications of molecular imaging phenotype of well-differentiated pulmonary carcinoma based on ⁶⁸Ga-DOTATATE PET/CT and ¹⁸F-FDG PET/CT. *Eur J Nucl Med Mol Imaging*. 2021;48:204–216.
52. Thang SP, Violet J, Sandhu S, et al. Poor outcomes for patients with metastatic castration-resistant prostate cancer with low prostate-specific membrane antigen (PSMA) expression deemed ineligible for ¹⁷⁷Lu-labelled PSMA radioligand therapy. *Eur Urol Oncol*. 2019;2:670–676.
53. Ferdinandus J, Violet J, Sandhu S, et al. Prognostic biomarkers in men with metastatic castration-resistant prostate cancer receiving [¹⁷⁷Lu]-PSMA-617. *Eur J Nucl Med Mol Imaging*. 2020;47:2322–2327.
54. Phelps TE, Roy J, Green MV, et al. Sodium fluoride-18 and radium-223 dichloride uptake colocalize in osteoblastic mouse xenograft tumors. *Cancer Biother Radiopharm*. 2021;36:133–142.
55. Uprimny C, Sviridenka A, Fritz J, et al. Comparison of Ga-68 Ga-PSMA-11 PET/CT with F-18 NaF PET/CT in the evaluation of bone metastases in metastatic prostate cancer patients prior to radionuclide therapy. *Eur J Nucl Med Mol Imaging*. 2018;45:1873–1883.
56. Harmon SA, Bergvall E, Mena E, et al. A prospective comparison of F-18-sodium fluoride PET/CT and PSMA-targeted F-18-DCFBC PET/CT in metastatic prostate cancer. *J Nucl Med*. 2018;59:1665–1671.
57. Haugen BR, Alexander EK, Bible KC, et al. 2015 American Thyroid Association management guidelines for adult patients with thyroid nodules and differentiated thyroid cancer: the American Thyroid Association guidelines task force on thyroid nodules and differentiated thyroid cancer. *Thyroid*. 2016;26:1–133.
58. Tuttle RM, Leboeuf R, Robbins RJ, et al. Empiric radioactive iodine dosing regimens frequently exceed maximum tolerated activity levels in elderly patients with thyroid cancer. *J Nucl Med*. 2006;47:1587–1591.
59. Ue N, Takano-Kasuya M, Kitamura N, et al. The anti-angiogenic agent lenvatinib induces tumor vessel normalization and enhances radiosensitivity in hepatocellular tumors. *Med Oncol*. 2021;38:60.
60. Oosterwijk-Wakka JC, de Weijert MCA, Franssen GM, et al. Successful combination of sunitinib and girentuximab in two renal cell carcinoma animal models: a rationale for combination treatment of patients with advanced RCC. *Neoplasia*. 2015;17:215–224.
61. Muselaers CHJ, Boers-Sonderen MJ, van Oostenbrugge TJ, et al. Phase 2 study of lutetium 177-labeled anti-carbonic anhydrase IX monoclonal antibody girentuximab in patients with advanced renal cell carcinoma. *Eur Urol*. 2016;69:767–770.

62. Pastuskovas CV, Mundo EE, Williams SP, et al. Effects of Anti-VEGF on pharmacokinetics, biodistribution, and tumor penetration of trastuzumab in a preclinical breast cancer model. *Mol Cancer Ther.* 2012;11:752–762.
63. Camacho X, Calzada V, Fernandez M, et al. Lu-177-DOTA-bevacizumab: radioimmunotherapy agent for melanoma. *Curr Radiopharm.* 2017;10:21–28.
64. Kameswaran M, Pandey U, Gamre N, Vimalnath KV, Sarma HD, Dash A. Evaluation of Lu-177-CHX-A'-DTPA-bevacizumab as a radioimmunotherapy agent targeting VEGF expressing cancers. *Appl Radiat Isot.* 2016;114:196–201.
65. Kameswaran M, Sarma HD, Dash A. Preclinical evaluation of I-131-bevacizumab: a prospective agent for radioimmunotherapy in VEGF expressing cancers. *Appl Radiat Isot.* 2017;123:109–113.
66. Wang Z, Tang Y, Tan YN, Wei QC, Yu W. Cancer-associated fibroblasts in radiotherapy: challenges and new opportunities. *Cell Commun Signal.* 2019;17:47.
67. Pereira PMR, Edwards KJ, Mandleywala K, et al. iNOS regulates the therapeutic response of pancreatic cancer cells to radiotherapy. *Cancer Res.* 2020;80:1681–1692.
68. Jarosz-Biej M, Smolarczyk R, Cichon T, Kulach N. Tumor microenvironment as a “game changer” in cancer radiotherapy. *Int J Mol Sci.* 2019;20:3212.
69. Jiang H, Hegde S, DeNardo DG. Tumor-associated fibrosis as a regulator of tumor immunity and response to immunotherapy. *Cancer Immunol Immunother.* 2017;66:1037–1048.
70. Arnold KM, Flynn NJ, Raben A, et al. The impact of radiation on the tumor microenvironment: effect of dose and fractionation schedules. *Cancer Growth Metastasis.* 2018;11:1179064418761639.
71. Riaz N, Morris L, Havel JJ, Makarov V, Desrichard A, Chan TA. The role of neoantigens in response to immune checkpoint blockade. *Int Immunol.* 2016;28:411–419.
72. Demaria S, Formenti SC. The abscopal effect 67 years later: from a side story to center stage. *Br J Radiol.* 2020;93:20200042.
73. Dewan MZ, Galloway AE, Kawashima N, et al. Fractionated but not single-dose radiotherapy induces an immune-mediated abscopal effect when combined with anti-CTLA-4 antibody. *Clin Cancer Res.* 2009;15:5379–5388.
74. McBride S, Sherman E, Tsai CJ, et al. Randomized phase II trial of nivolumab with stereotactic body radiotherapy versus nivolumab alone in metastatic head and neck squamous cell carcinoma. *J Clin Oncol.* 2021;39:30–37.
75. Theelen WS, Peulen HMU, Lalezari F, et al. Effect of pembrolizumab after stereotactic body radiotherapy vs pembrolizumab alone on tumor response in patients with advanced non-small cell lung cancer: results of the PEMBRO-RT phase 2 randomized clinical trial. *JAMA Oncol.* 2019;5:1276–1282.
76. Tachibana I, Hosono M, Inada M, et al. Tumor hypoxia detected by ¹⁸F-misonidazole (F-MISO) PET/CT as a prediction of initial tumor response of radiation therapy (RT) [abstract]. *Int J Radiat Oncol Biol Phys.* 2015;93(suppl):S105.
77. Yard BD, Gopal P, Bannik K, Siemeister G, Hagemann UB, Abazeed ME. Cellular and genetic determinants of the sensitivity of cancer to alpha-particle irradiation. *Cancer Res.* 2019;79:5640–5651.
78. Sgouros G. α -particle-emitter radiopharmaceutical therapy: resistance is futile. *Cancer Res.* 2019;79:5479–5481.
79. Bartlett RM, Bolch WE, Brill AB, et al. *MIRD Primer 2020: A Complete Guide to Radiopharmaceutical Dosimetry.* Prepared by the MIRD Committee of the Society of Nuclear Medicine and Molecular Imaging (SNMMI). Reston, VA: SNMMI. In press.
80. Sgouros G, Bolch WE, Chiti A, et al. *Dosimetry-Guided Radiopharmaceutical Therapy.* ICRU report no. 96. Bethesda, MD: International Commission on Radiation Units & Measurements (ICRU). In press.
81. Wahl R, Sgouros G, Irvani A, et al. Normal-tissue tolerance to radiopharmaceutical therapies, the knowns and the unknowns. *J Nucl Med.* 2021;62(suppl 3):23S–35S.
82. Scott JG, Berglund A, Schell MJ, et al. A genome-based model for adjusting radiotherapy dose (GARD): a retrospective, cohort-based study. *Lancet Oncol.* 2017;18:202–211.
83. Jurcic JG. Targeted alpha-particle therapy for hematologic malignancies. *Semin Nucl Med.* 2020;50:152–161.
84. Baxter LT, Yuan F, Jain RK. Pharmacokinetic analysis of the perivascular distribution of bifunctional antibodies and haptens: comparison with experimental data. *Cancer Res.* 1992;52:5838–5844.
85. Baxter LT, Jain RK. Transport of fluid and macromolecules in tumors. IV. A microscopic analysis of the perivascular distribution. *Microvasc Res.* 1991;41:252–272.
86. Jain RK, Baxter LT. Mechanisms of heterogeneous distribution of monoclonal antibodies and other macromolecules in tumors: significance of elevated interstitial pressure. *Cancer Res.* 1988;48:7022–7032.
87. Prideaux AR, Song H, Hobbs RF, et al. Three-dimensional radiobiologic dosimetry: application of radiobiologic modeling to patient-specific 3-dimensional imaging-based internal dosimetry. *J Nucl Med.* 2007;48:1008–1016.
88. Amro H, Wilderman SJ, Dewaraja YK, Roberson PL. Methodology to incorporate biologically effective dose and equivalent uniform dose in patient-specific 3-dimensional dosimetry for non-Hodgkin lymphoma patients targeted with ¹³¹I-tositumomab therapy. *J Nucl Med.* 2010;51:654–659.
89. Dewaraja YK, Schipper MJ, Roberson PL, et al. ¹³¹I-tositumomab radioimmunotherapy: initial tumor dose-response results using 3-dimensional dosimetry including radiobiologic modeling. *J Nucl Med.* 2010;51:1155–1162.
90. EASL-EORTC clinical practice guidelines: management of hepatocellular carcinoma. *J Hepatol.* 2012;56:908–943.
91. Garin E, Palard X, Rolland Y. Personalised dosimetry in radioembolisation for HCC: impact on clinical outcome and on trial design. *Cancers (Basel).* 2020;12:1557.
92. Garin E, Tselikas L, Guiu B, et al. Personalised versus standard dosimetry approach of selective internal radiation therapy in patients with locally advanced hepatocellular carcinoma (DOSISPHERE-01): a randomised, multicentre, open-label phase 2 trial. *Lancet Gastroenterol Hepatol.* 2021;6:17–29.
93. Eaton BR, Kim HS, Schreibmann E, et al. Quantitative dosimetry for yttrium-90 radioisotope therapy: tumor dose predicts fluorodeoxyglucose positron emission tomography response in hepatic metastatic melanoma. *J Vasc Interv Radiol.* 2014;25:288–295.
94. van den Hoven AF, Rosenbaum C, Elias SG, et al. Insights into the dose-response relationship of radioembolization with resin Y-90-microspheres: a prospective cohort study in patients with colorectal cancer liver metastases. *J Nucl Med.* 2016;57:1014–1019.
95. Lam MG, Goris ML, Iagaru AH, Mitra ES, Louie JD, Sze DY. Prognostic utility of Y-90 radioembolization dosimetry based on fusion Tc-99m-macroaggregated albumin-Tc-99m-sulfur colloid SPECT. *J Nucl Med.* 2013;54:2055–2061.
96. Zuckerman DA, Kennard RF, Roy A, Parikh PJ, Weiner AA. Outcomes and toxicity following yttrium-90 radioembolization for hepatic metastases from neuroendocrine tumors: a single-institution experience. *J Gastrointest Oncol.* 2019;10:118–127.
97. Chansanti O, Jahangiri Y, Matsui Y, et al. Tumor dose response in yttrium-90 resin microsphere embolization for neuroendocrine liver metastases: a tumor-specific analysis with dose estimation using SPECT-CT. *J Vasc Interv Radiol.* 2017;28:1528–1535.
98. Kao YH, Steinberg JD, Tay YS, et al. Post-radioembolization yttrium-90 PET/CT: part 2—dose-response and tumor predictive dosimetry for resin microspheres. *EJNMMI Res.* 2013;3:57.
99. Demirelli S, Erkilic M, Oner AO, et al. Evaluation of factors affecting tumor response and survival in patients with primary and metastatic liver cancer treated with microspheres. *Nucl Med Commun.* 2015;36:340–349.
100. Fowler KJ, Maughan NM, Laforest R, et al. PET/MRI of hepatic ⁹⁰Y microsphere deposition determines individual tumor response. *Cardiovasc Intervent Radiol.* 2016;39:855–864.
101. Peters SMB, Prive BM, de Bakker M, et al. Intra-therapeutic dosimetry of [Lu-177]Lu-PSMA-617 in low-volume hormone-sensitive metastatic prostate cancer patients and correlation with treatment outcome. *Eur J Nucl Med Mol Imaging.* July 4, 2021 [Epub ahead of print].
102. Pauwels S, Barone R, Walrand S, et al. Practical dosimetry of peptide receptor radionuclide therapy with ⁹⁰Y-labeled somatostatin analogs. *J Nucl Med.* 2005;46(suppl):92S–98S.
103. Ilan E, Sandstrom M, Wassberg C, et al. Dose response of pancreatic neuroendocrine tumors treated with peptide receptor radionuclide therapy using Lu-177-DOTATATE. *J Nucl Med.* 2015;56:177–182.
104. Jahn U, Ilan E, Sandstrom M, Garske-Roman U, Lubberink M, Sundin A. Lu-177-DOTATATE peptide receptor radionuclide therapy: dose response in small intestinal neuroendocrine tumors. *Neuroendocrinology.* 2020;110:662–670.
105. Sgouros G, Squeri S, Ballangrud AM, et al. Patient-specific, 3-dimensional dosimetry in non-Hodgkin's lymphoma patients treated with ¹³¹I-anti-B1 antibody: assessment of tumor dose-response. *J Nucl Med.* 2003;44:260–268.
106. Løndalen A, Blakkisrud J, Revheim ME, et al. FDG PET/CT parameters and correlations with tumor-absorbed doses in a phase I trial of Lu-177-lilotomab satetaxetan for treatment of relapsed non-Hodgkin lymphoma. *Eur J Nucl Med Mol Imaging.* 2021;48:1902–1914.
107. Cremonesi M, Chiesa C, Strigari L, et al. Radioembolization of hepatic lesions from a radiobiology and dosimetric perspective. *Front Oncol.* 2014;4:210.
108. d'Abadie P, Hesse M, Jamar F, Lhommel R, Walrand S. Y-90 TOF-PET based EUD reunifies patient survival prediction in resin and glass microspheres radioembolization of HCC tumours. *Phys Med Biol.* 2018;63:245010.
109. Chiesa C, Mira M, Maccauro M, et al. A dosimetric treatment planning strategy in radioembolization of hepatocarcinoma with ⁹⁰Y glass microspheres. *Q J Nucl Med Mol Imaging.* 2012;56:503–508.
110. Kappadath SC, Mikell J, Balagopal A, Baladandayuthapani V, Kaseb A, Mahvash A. Hepatocellular carcinoma tumor dose response after Y-90-radioembolization with glass microspheres using Y-90-SPECT/CT-based voxel dosimetry. *Int J Radiat Oncol Biol Phys.* 2018;102:451–461.

111. Dewaraja YK, Devasia T, Kaza RK, et al. Prediction of tumor control in ⁹⁰Y radioembolization by logit models with PET/CT-based dose metrics. *J Nucl Med*. 2020;61:104–111.
112. Roberson PL, Amro H, Wilderman SJ, et al. Bio-effect model applied to I-131 radioimmunotherapy of refractory non-Hodgkin's lymphoma. *Eur J Nucl Med Mol Imaging*. 2011;38:874–883.
113. Emami B, Lyman J, Brown A, et al. Tolerance of normal tissue to therapeutic irradiation. *Int J Radiat Oncol Biol Phys*. 1991;21:109–122.
114. Bentzen SM, Constine LS, Deasy JO, et al. Quantitative analyses of normal tissue effects in the clinic (QUANTEC): an introduction to the scientific issues. *Int J Radiat Oncol Biol Phys*. 2010;76(suppl):S3–S9.
115. Deasy JO, Bentzen SM, Jackson A, et al. Improving normal tissue complication probability models: the need to adopt a “data-pooling” culture. *Int J Radiat Oncol Biol Phys*. 2010;76(suppl):S151–S154.
116. Grimm J, Marks LB, Jackson A, Kavanagh BD, Xue J, Yorke E. High dose per fraction, hypofractionated treatment effects in the clinic (HyTEC): an overview. *Int J Radiat Oncol Biol Phys*. 2021;110:1–10.
117. Marascio J, Spratt DE, Zhang JB, et al. Prospective study to define the clinical utility and benefit of Decipher testing in men following prostatectomy. *Prostate Cancer Prostatic Dis*. 2020;23:295–302.
118. Offersen BV, Alsner J, Nielsen HM, et al. Hypofractionated versus standard fractionated radiotherapy in patients with early breast cancer or ductal carcinoma in situ in a randomized phase III trial: the DBCG HYPO trial. *J Clin Oncol*. 2020;38:3615.
119. Wang SL, Fang H, Hu C, et al. Hypofractionated versus conventional fractionated radiotherapy after breast-conserving surgery in the modern treatment era: a multicenter, randomized controlled trial from China. *J Clin Oncol*. 2020;38:3604–3614.
120. Zapatero A, Guerrero A, Maldonado X, et al. High-dose radiotherapy with short-term or long-term androgen deprivation in localised prostate cancer (DART01/05 GICOR): a randomised, controlled, phase 3 trial. *Lancet Oncol*. 2015;16:320–327.
121. Incrocci L, Wortel RC, Alemayehu WG, et al. Hypofractionated versus conventionally fractionated radiotherapy for patients with localised prostate cancer (HYPRO): final efficacy results from a randomised, multicentre, open-label, phase 3 trial. *Lancet Oncol*. 2016;17:1061–1069.
122. Nichols AC, Theurer J, Prisman E, et al. Radiotherapy versus transoral robotic surgery and neck dissection for oropharyngeal squamous cell carcinoma (ORATOR): an open-label, phase 2, randomised trial. *Lancet Oncol*. 2019;20:1349–1359.
123. Kim TH, Koh YH, Kim BH, et al. Proton beam radiotherapy vs. radiofrequency ablation for recurrent hepatocellular carcinoma: a randomized phase III trial. *J Hepatol*. 2021;74:603–612.
124. Timmerman R, Paulus R, Galvin J, et al. Stereotactic body radiation therapy for inoperable early stage lung cancer. *JAMA*. 2010;303:1070–1076.
125. Brady JL, Binkley MS, Hajj C. Definitive radiotherapy for localized follicular lymphoma staged by F-18-FDG PET-CT: a collaborative study by ILROG. *Blood*. 2019;133(3):237–245 [erratum]. *Blood*. 2019;134:331.
126. Palma DA, Olson R, Harrow S, et al. Stereotactic ablative radiotherapy versus standard of care palliative treatment in patients with oligometastatic cancers (SABR-COMET): a randomised, phase 2, open-label trial. *Lancet*. 2019;393:2051–2058.
127. Garin E, Lenoir L, Rolland Y, et al. Dosimetry based on Tc-99m-macroaggregated albumin SPECT/CT accurately predicts tumor response and survival in hepatocellular carcinoma patients treated with Y-90-loaded glass microspheres: preliminary results. *J Nucl Med*. 2012;53:255–263.
128. Garin E, Lenoir L, Edeline J, et al. Boosted selective internal radiation therapy with Y-90-loaded glass microspheres (B-SIRT) for hepatocellular carcinoma patients: a new personalized promising concept. *Eur J Nucl Med Mol Imaging*. 2013;40:1057–1068.
129. Mazzaferro V, Sposito C, Bhoori S, et al. Yttrium-90 radioembolization for intermediate-advanced hepatocellular carcinoma: a phase 2 study. *Hepatology*. 2013;57:1826–1837.
130. Chiesa C, Mira M, Maccauro M, et al. Radioembolization of hepatocarcinoma with ⁹⁰Y glass microspheres: development of an individualized treatment planning strategy based on dosimetry and radiobiology. *Eur J Nucl Med Mol Imaging*. 2015;42:1718–1738.
131. Chan KT, Alessio AM, Johnson GE, et al. Hepatotoxic dose thresholds by positron-emission tomography after yttrium-90 radioembolization of liver tumors: a prospective single-arm observational study. *Cardiovasc Intervent Radiol*. 2018;41:1363–1372.
132. Ho CL, Chen SR, Cheung SK, et al. Radioembolization with Y-90 glass microspheres for hepatocellular carcinoma: significance of pretreatment C-11-acetate and F-18-FDG PET/CT and posttreatment Y-90 PET/CT in individualized dose prescription. *Eur J Nucl Med Mol Imaging*. 2018;45:2110–2121.
133. Lau WY, Leung WT, Ho S, et al. Treatment of inoperable hepatocellular carcinoma with intrahepatic arterial Y-90 microspheres: a phase-I and phase-II study. *Br J Cancer*. 1994;70:994–999.
134. Strigari L, Sciuto R, Rea S, et al. Efficacy and toxicity related to treatment of hepatocellular carcinoma with Y-90-SIR spheres: radiobiologic considerations. *J Nucl Med*. 2010;51:1377–1385.
135. Flamen P, Vanderlinden B, Delatte P, et al. Multimodality imaging can predict the metabolic response of unresectable colorectal liver metastases to radioembolization therapy with yttrium-90 labeled resin microspheres. *Phys Med Biol*. 2008;53:6591–6603.
136. Song YS, Paeng JC, Kim HC, et al. PET/CT-based dosimetry in Y-90-microsphere selective internal radiation therapy: single cohort comparison with pretreatment planning on ^{99m}Tc-MAA imaging and correlation with treatment efficacy. *Medicine (Baltimore)*. 2015;94:e945.
137. Allimant C, Kafrouni M, Delicque J, et al. Tumor targeting and three-dimensional voxel-based dosimetry to predict tumor response, toxicity, and survival after yttrium-90 resin microsphere radioembolization in hepatocellular carcinoma. *J Vasc Interv Radiol*. 2018;29:1662–1670.e4.
138. Hermann AL, Dieudonn A, Ronot M, et al. Relationship of tumor radiation-absorbed dose to survival and response in hepatocellular carcinoma treated with transarterial radioembolization with Y-90 in the SARAH study. *Radiology*. 2020;296:673–684.
139. Maxon HR, Thomas SR, Hertzberg VS, et al. Relation between effective radiation dose and outcome of radioiodine therapy for thyroid cancer. *N Engl J Med*. 1983;309:937–941.
140. Wierls R, Brans B, Havekes B, et al. Dose-response relationship in differentiated thyroid cancer patients undergoing radioiodine treatment assessed by means of I-124 PET/CT. *J Nucl Med*. 2016;57:1027–1032.
141. Matthay KK, Panina C, Huberty J, et al. Correlation of tumor and whole-body dosimetry with tumor response and toxicity in refractory neuroblastoma. treated with I-131-MIBG. *J Nucl Med*. 2001;42:1713–1721.

Normal-Tissue Tolerance to Radiopharmaceutical Therapies, the Knowns and the Unknowns

Richard L. Wahl¹, George Sgouros², Amir Iravani¹, Heather Jacene³, Daniel Pryma⁴, Babak Saboury⁵, Jacek Capala⁵, and Stephen A. Graves⁶

¹Mallinckrodt Institute of Radiology, Washington University, St. Louis, Missouri; ²Department of Radiology, Johns Hopkins University, Baltimore, Maryland; ³Dana-Farber Cancer Institute, Boston, Massachusetts; ⁴Penn Medicine, University of Pennsylvania, Philadelphia, Pennsylvania; ⁵National Institutes of Health, Bethesda, Maryland; and ⁶University of Iowa, Iowa City, Iowa

Radiopharmaceutical therapies are gaining increasing prominence as they improve survival in patients with common diseases such as metastatic prostate cancer (1,2). However, whereas sodium iodide (¹³¹I) therapy has been used for over 70 y in treating malignant and benign thyroid diseases, we are still in a learning phase in relation to understanding the toxicity from radiopharmaceutical therapies (RPTs). Much of what is considered “known” regarding radiopharmaceutical dose–toxicity relationships is the result of questionable extrapolation from 100+ years of experience with external-beam radiation therapy (EBRT). Although this may have been a reasonable starting point, there are critical differences between EBRT and RPTs.

With external-beam irradiation, dose–response relationships have been informed by a set of measurements of the predicted and actual absorbed dose delivered to normal tissues and tumors. There have been great advancements in external-beam radiation dose delivery, including intensity modulated radiation therapy, as well as treatments in which tumor doses are intensified in specific areas informed by imaging, so called biologically guided radiation therapy (3,4). These advancements have increased control and accuracy in dosing, leading to better patient outcomes.

Several things are clear regarding EBRT. First, external-beam radiation dosimetry to tissues is well-developed and there have been major efforts to standardize methods for absorbed dose measurement among radiation therapy centers globally. It is thus expected that absorbed dose estimates are likely within <10% of one another among sites performing external-beam irradiation (5). In addition, whereas there can be “dose painting” to specific areas of tumor, it is typically the case that the absorbed dose from external beam is quite uniformly delivered in a given volume of tissue treated in a specific part of the body. It has also been clear since early studies with EBRT that radiation delivery to part of an organ is less likely to cause toxicity than radiation therapy of the entire organ. Early reporting of external-beam radiation toxicity in, for example, the liver or kidneys was influenced by the percentage of the organs irradiated, with partial organ irradiation less toxic than whole organ irradiation (i.e., one third of the liver could be irradiated to a higher dose without toxicity than irradiation of the entire

liver, and a part of the kidney could be irradiated to a higher level than a whole [or both] kidneys without systemic toxicity) (6).

Recently, a new approach using personalized treatment planning accounting for the biologic effect of a given radiation dose has been considered (7,8). This approach calls for characterizing radiation dose not only in physical terms of energy deposition (absorbed dose, Gy) but also in terms of biologic effects on the tumor and normal tissue (9,10). All limitations of the knowledge relevant to external radiation therapy are also of concern in RPT.

However, despite the long experience with EBRTs, there remain unanswered questions regarding the effects of absorbed dose rate (standard fractionation vs. hypofractionation), the use of radiotherapy in pediatric patients versus adults, optimal delivery of brachytherapy, optimal use cases for proton and particle therapy, patient-specific biologic factors increasing or decreasing the risk of toxicity, and potential interactions of external-beam radiation with other cancer therapies that may affect the response to radiation.

Compared with external-beam radiation, assessing radiopharmaceutical toxicity is in its relative infancy, or at most early adolescence. The biologic effect of a radiopharmaceutical agent is fundamentally based on “radiation effect” and “energy deposition in tissue,” similar to external-beam radiation effect. However, there are at least 4 fundamental differences in normal-tissue response to radiation from RPT versus external-beam radiation: 1. Spatial nonuniformity of energy deposition by RPT (spatial domain); 2. Absorbed dose rate (temporal domain); 3. Importance of tissue microenvironment and microscale dosimetry (scale domain); and 4. Time variation and paramount importance of pharmacokinetics (systems domain).

There are some additional considerations for RPT versus EBRT, including the knowledge that RPT is generally a systemic therapy and therefore partial-organ irradiation is not typically performed. Additionally, low-energy β -particle, Auger electrons, or α -particles are associated with considerable nonuniformity of absorbed dose. The nonuniformity in absorbed dose is also tied to the spatial distribution of the RPT. Nonuniformity in the spatial distribution may arise due to expression of the molecular target in normal tissues (e.g., prostate specific membrane antigen [PSMA] expression in the salivary glands) or due to physiologic processing/transport of the agent (e.g., retention of most low molecular weight agents in the kidneys). Also related to these nonuniformities is the fact that current 3-dimensional imaging modalities—SPECT and PET—have the resolution and counting statistics needed to quantify macroscale nonuniformities (e.g., kidney renal cortex vs. overall kidney

Received Aug. 24, 2021; revision accepted Oct. 15, 2021.
For correspondence or reprints, contact Richard L. Wahl (rwahl@wustl.edu).
COPYRIGHT © 2021 by the Society of Nuclear Medicine and Molecular Imaging.
DOI: 10.2967/jnumed.121.262751

volume) but not assess nonuniformities at the microscale (e.g., renal tubule vs. renal glomerulus) level. The latter require model-based activity apportionment and microscale S values (11,12). Thus, continued early studies examining normal organ dose response are likely to depend strongly on the scale at which the agent localizes nonuniformly and on its emission properties.

Elsewhere in this supplement (13), early results are provided from the Society of Nuclear Medicine and Molecular Imaging (SNMMI) Dosimetry Task Force “challenge,” showing that even when analyzing the same imaging data, varying laboratories can have different estimates of radiation-absorbed dose to specific tissues of relevance. These differences likely result from nonunified approaches to curve fitting and volume of interest definition among other factors. Indeed, other variables such as dose calibrator performance/calibration, camera sensitivity and calibration, as well as how attenuation, scatter, resolution, and partial-volume factors are addressed, can cause significant variability in estimates of radiation-absorbed dose to tumor and normal tissues. In general, these effects are more impactful on smaller and deeper-situated structures such as tumors, as the variability in dose estimates appears to be less in larger organs (14). That said, planar estimates of lung absorbed dose are, in the authors’ opinion, highly variable depending on the selection of the precise background region of interest. Assessments of dose/response/toxicity are only as good as the estimation of activity concentration in particular organ volume (15). Similarly, estimates of radiation-absorbed dose to the bone marrow can be more challenging if the bone marrow dosimetry is estimated from planar imaging as opposed to SPECT.

Another consideration in linking radiation-absorbed dose in normal tissues to organ toxicity is whether the dosimetry estimates are obtained from the diagnostic companion to the therapeutic agent (as in the case of some theranostic pairs) (16) or from imaging the biodistribution of the therapeutic radiopharmaceutical itself, such as in the case of posttreatment imaging. In principle, the 2 should be highly correlated with a well-selected theranostic pair, but it is likely that a more “true” absorbed dose estimation may be obtained from post-treatment imaging (“dose validation”). Imaging posttherapy activity distributions can have problems as well, such as dead time issues in some γ -cameras with therapeutics with high photon flux, such as ^{131}I , which may degrade absorbed dose rate estimates from early-time-point data, unless major corrections are implemented. Similarly, septal penetration with high-energy γ -emitters such as ^{131}I can degrade quantitation. With pure β -emitters and α -emitters, imageable photon flux via Bremsstrahlung radiation is limited and difficult to use for dosimetry. In these cases, paired theranostic imaging may yield equivalent or improved organ-specific dose estimates in practice.

Variability in radiation-absorbed dose to normal tissues can occur among patients receiving the same number of radioactive molecules in their therapy. Larger patients will have the radiopharmaceutical diluted into a larger volume, although many larger molecules such as radiolabeled antibodies (and many other radiopharmaceuticals) do not substantially accumulate in fat. Thus, dosing some radiopharmaceuticals based on body weight, or lean body mass, can be an imperfect normalizing process. In addition, there can be variable clearance rates of molecules from tissue to tissue and patient to patient. Thus, consideration must be given to recognize that there are population-based absorbed doses to organs, and there are patient-specific absorbed doses, which can substantially diverge from the population average. Notably, some molecules such as radioantibodies, which cross react with normal tissues, can have considerable variability in their clearance from

patient to patient, and depending on the mass of molecules injected, possibly due to cross-reactivity with normal tissues. Patients receiving murine monoclonal antibodies may have rapid clearance of the radioantibody if there are human antimouse antibodies present or if a low protein mass is given versus an unlabeled antibody predose before the radioactivity. Similarly, patients lacking a spleen may have much slower clearance of radioantibody from the blood, and thus higher organ doses/administered activity than in patients with an intact spleen, this having been seen with anti-CD20 antibodies (16). Thus, one must distinguish between individual dosimetry and average population dosimetry in absorbed dose/response/toxicity estimates. As dosimetry methods are harmonized and clinically implemented, we anticipate greater availability of patient-specific dosimetry data that can be linked to organ toxicity.

These admitted uncertainties in radiopharmaceutical dosimetry estimates lead to some variability in the dose–response relationships that have been demonstrated for RPTs. As an example, estimates of absorbed dose to the salivary glands from ^{131}I therapies are being improved by the availability of PET imaging with ^{124}I as compared with planar imaging. Until recently, it has been difficult to perform treatment escalation studies based on organ-absorbed dose because of the relatively cumbersome process of evaluating dosimetry with a suitable theranostic pair. These studies need to be done in greater numbers and are a major opportunity to better refine our understanding of normal-tissue absorbed-dose response.

MECHANISM OF IRRADIATION FROM RPT

Radiation can damage both normal tissues and tumors in several ways. Classically, radiation-induced damage to tissues occurs when ionizing radiation, either as a direct event or through the generation of oxygen-free radical, damages DNA. Although single-stranded DNA breaks can be repaired effectively, breaks in both strands of DNA can result in irreversible damage. A variety of events can occur due to this including deletions of segments of DNA or repair of DNA with less than perfect fidelity. Such a loss of DNA integrity can lead to failed cell proliferation and cell death. The cell membrane and mitochondria can also be damaged by radiation, and such damage can induce apoptosis (17,18).

The multiple molecular mechanisms for radiation-induced cell death are complex and beyond the scope of this review. In short, they include downstream effects of mitotic catastrophe and mitotic death, apoptosis, necrosis, senescence, autophagy, and possibly other pathways including necroptosis and ferroptosis. It is also increasingly appreciated that not just cell intrinsic factors are involved, but also the microenvironment, including immunogenic cell death enhanced by radiation (19).

Virtually all tissues are made of a variety of components. Blood vessels supply nearly every tissue of relevance. Thus, in some cases, the radiation tolerance of a specific tissue may be related to the radiation tolerance of a component of a tissue. For example, in the brain the astrocytes and glial cells proliferate slowly and may themselves be less sensitive to radiation than the blood vessels or supporting cells for the vessels.

In general, tissues that proliferate very slowly are less radiosensitive and will demonstrate radiation induced damage much later than more rapidly proliferating tissues (20). The rapidly proliferating cell populations within bone marrow, skin, testes, and gut are particularly radiosensitive, but can recover very quickly from radiation. These are sometimes called acute responding tissues. The brain, kidneys, and bone are less immediately sensitive, but are

slow to recover (if ever) from radiation-induced damage. The liver is also slow to respond to radiation damage, but it can recover reasonably quickly. Although it is generally the case that slowly proliferating tissues are not radiosensitive, an exception are small lymphocytes, which proliferate slowly but quickly undergo apoptosis after exposure to relatively low doses of radiation.

Although β - and γ -radiation are viewed as having a relative biologic efficiency (RBE) of 1.0, other emerging RPTs, particularly those that use radionuclides that emit α -particles, carry much a higher RBE (21). α -particles, which are helium nuclei with an atomic mass of 4, carry much more energy per disintegration and deposit it at a relatively short distance and thus are considered a form of high-LET (linear energy transfer) radiation. Consequently, a single α -particle traversal of a cell nucleus can cause multiple double-strand breaks and likely lead to cell death (22). Although DNA damage is not the only way tissues are injured by radiation, it is one of the classical events described in radiobiology literature as a major cause of cell death. It is commonly acknowledged that α -particles have an RBE value 3–7 times higher than that of β -particles. Although most forms of radiation exert DNA effects primarily through intermediary oxygen free radicals, α -particles are more likely to interact directly with the DNA (23).

DOSE RATE, BIOLOGICALLY EFFECTIVE DOSE (BED), AND MICRODISTRIBUTION OF DOSE

In general, the higher the absorbed dose rate, the more substantial the normal tissue (and tumor) toxicity is per dose unit (J/kg, Gy). This is in part because high dose rate radiation exposures do not allow normal tissue or tumor to repair substantially. Conventional standard-fraction external-beam radiotherapy is typically given in 1.8–2.0 Gy/d fractions over 6–5-d weeks (~10 Gy/wk). The VISION trial delivered ^{177}Lu in sequential treatments, depositing β -radiation dose to tumors over a total period of approximately 6 mo (1). Although the dose rate with RPT is usually thought of as lower than that of external-beam radiation, there are some situations, such as with short-lived radioisotopes, where a single administered activity can deliver relatively high time-averaged absorbed doses over a relatively short period of time. For example, ^{90}Y -microspheres can deliver a high absorbed dose in a relatively short period of time (e.g., 10 d) from a single treatment. An additional confounding factor when considering absorbed dose is the issue of DNA repair kinetics relative to the rate of radiation-induced damage. Two therapies with equivalent time-averaged dose delivery may result in differing biologic effects due to differences in instantaneous dose rate (i.e., Gy/min from EBRT vs. cGy/min from RPT).

For therapies using radionuclides emitting particles with longer range, such as high-energy β -emitters or emitters with a significant fraction of γ -radiation, microscale dosimetry may be less relevant. However, with shorter-pathlength β -emitters such as ^{177}Lu or with α - or Auger-particle emitters, the particles travel only a relatively short distance, so their microscale dosimetry in tissue is of much greater importance. As an example, ^{90}Y as a more energetic β -particle emitter when attached to octreotate causes renal toxicity in humans, whereas ^{177}Lu -DOTATATE is much less renal-toxic, likely due to the differential microscale dosimetry in the kidneys, as ^{177}Lu is a lower energy β -emitter (24).

NORMAL-TISSUE DOSE LIMITS

A considerable effort has been undertaken to understand the relationships of EBRT dose and normal-tissue toxicity. A seminal

paper by Emami et al. (6) summarized normal-tissue tolerances to external photon irradiation as they were known in 1991, and these data have been gradually updated and expanded through other initiatives such as Quantitative Analysis of Normal Tissue Effects in the Clinic (QUANTEC) and Hypofractionated Treatment Effects in the Clinic (HyTEC) (25,26). These resources present normal-tissue dose limits in terms of TD5/5 and TD50/5, the total doses associated with a complication rate of 5% and 50% within 5 y, respectively, as introduced by Rubin and Cassaret in 1972 (27). Dose limits recommended within these works were the product of high-quality published data, expert opinion, and model-based extrapolation when deviating from typical dose and fractionation schedules (i.e., 2 Gy per treatment fraction). These documents have helped to shape current radiation therapy clinical practice and as such they may act as a “road map” for establishing appropriate normal-tissue dose limits for RPTs.

Normal-tissue dose limits are a function of absorbed dose rate (or dose fractionation schedule in the case of EBRT), radiation quality (α vs. β ; microdistribution), tissue type, and time between treatments. These concepts are detailed in other articles within this journal supplement (28,29). Despite biologic sensitivity to various factors, it is often practical to present dose limits or dose effects in terms of absorbed dose for a particular radiopharmaceutical and treatment pattern, while acknowledging that accurate comparison between different radiopharmaceuticals or radiation modalities requires careful modeling of radiobiologic effects. As such, in the sections below we discuss normal-tissue toxicity from radiopharmaceuticals in terms of absorbed dose from individual therapies. A summary of normal tissues and associated dose limits is provided in Table 1, including tissues for which dose limits from RPT are not currently known. Normal-tissue dose limits are partly known for a handful of organs in the body for specific radiopharmaceuticals; however, it is clear that less is known regarding RPT normal-tissue dose limits in comparison to EBRT treatment techniques. Careful evaluation of the intermodality differences among organs that have been characterized for both RPT and EBRT may inform methods for extrapolation to RPT limits in organ tissues without published data. It is increasingly clear from clinical experiences with RPT that the external-beam-derived organ dose limits do not consistently predict toxicity from radiopharmaceuticals and so these limits should not be strictly enforced and, instead, radiopharmaceutical-specific dose limits are required. Dose escalation studies driven by modern dosimetry are also important to consider, pursuant to avoiding systematic underdosing of patients.

Bone Marrow

The ability to image and assess the biodistribution of the radiopharmaceutical in patients, before treatment, or after the first fraction of a fractionated treatment regimen, make it possible to identify potential dose-limiting tissues. That salivary gland or renal toxicity may be of concern for PSMA-targeting small molecules but not for PSMA-targeting antibodies is apparent to a nuclear medicine physician by visual inspection of images corresponding to each agent at an appropriately chosen time after administration. Ideally, such imaging information, along with properties of the radionuclide, would be used to estimate the absorbed dose and, at minimum, distinguish between a range of administered activities that will be safe versus a range that will lead to toxicity. Although, there are many confounding factors (the unknowns), this process is at the heart of what gives RPT an advantage over treatment modalities that do not incorporate imaging and dosimetry.

TABLE 1

Summary of Normal-Tissue Dose Limits by Organ Tissue and Toxicity Endpoint for External-Beam Radiotherapy (EBRT) and Radiopharmaceutical Therapy (RPT)

Tissue	Toxicity endpoint	Toxicity rate	EBRT limits*	RPT limits†	References
Brain	Symptomatic Necrosis	5%	D _{max} = 72 Gy	Unknown	(25) †
Optic nerve/chiasm	Optic neuropathy	5%	D _{max} = 55–60 Gy	Unknown	(25)
Brain stem	Permanent cranial neuropathy or necrosis	5%	D _{max} = 54 Gy (small volume)	Unknown	(25)
		5%	D _{max} = 59 Gy (1–10 cc)		
		5%	D _{max} = 64 Gy (<1 cc)		
Spinal cord	Myelopathy	5%	D _{max} = 55–60 Gy	Unknown	(25)
Cochlea	Sensory-neural hearing loss (measured @ 4 kHz)	30%	D _{mean} = 45 Gy	Unknown	(25)
Parotid-salivary glands	Long-term salivary function reduced to < 25% of pre-radiation therapy level	20%	D _{mean} = 25 Gy (bilateral)	9.2–33 Gy as single dose caused 25% incidence of transient xerostomia and 1 case of transient mucositis (4%) 131I-Nal has been reported to cause symptomatic xerostomia at doses as low as 5 Gy.	(25,72,76)
Larynx	Vocal dysfunction	20%	D _{max} = 66 Gy	Unknown	(25)
	Aspiration	30%	D _{mean} = 50 Gy	Unknown	(25)
	Edema	20%	D _{mean} = 44 Gy	Unknown	(25)
Pharynx	Symptomatic dysphagia and aspiration	20%	D _{mean} = 50 Gy	Unknown	(25)
Thyroid	Clinical Hypothyroidism	8%	D _{mean} = 45 Gy	Hypothyroidism common in 131I-MIBG and 131I-tositumomab therapies, but dose delivered unclear	(6)
Lungs	Symptomatic pneumonitis	5%	D _{mean} = 7 Gy	D _{mean} > 30 Gy from single 90Y-microsphere ¹¹ Tx (33% toxicity rate; n = 3); D _{mean} > 50 Gy cumulative from 90Y-microsphere Tx (50% toxicity rate; n = 2) D _{mean} > 27 Gy from 131I-radioimmunotherapy	(25,86,87)
Heart	Pericarditis	15%	D _{mean} = 26 Gy	Unknown	(25)
	Long-term cardiac mortality	< 1%	V ₂₅ < 10%	Unknown	
Esophagus	Grade > = 3 acute esophagitis	5%–20%	D _{mean} = 34 Gy	Unknown	(25)
		< 30%	Various dose volume constraints, ranging up to V ₇₀ < 20%		

(continued)

TABLE 1
Summary of Normal-Tissue Dose Limits by Organ Tissue and Toxicity Endpoint for External-Beam Radiotherapy (EBRT) and Radiopharmaceutical Therapy (RPT) (cont.)

Tissue	Toxicity endpoint	Toxicity rate	EBRT limits*	RPT limits†	References
Liver	Classical RILD	5%	D _{mean} = 30–32 Gy	Data at the 5% toxicity rate level is inconclusive, but perhaps suggestive of D _{mean} = ~35–50 Gy (glass ⁹⁰ Y-microspheres) and D _{mean} = ~20–40 Gy (resin ⁹⁰ Y-microspheres). Package insert allows 80–150 Gy. Microsphere tolerance appears higher than agents targeting hepatocytes, but data limited. ⁹⁰ Y-ibritumomab hepatic MTD > 28.5 Gy MIBG, approx. 30 Gy results in < 10% transient liver toxicity	(25,51–55,112)
Stomach	Ulceration	50%	D _{mean} = 42 Gy	D _{mean} > 70 Gy (glass ⁹⁰ Y-microspheres) D _{mean} = 52 Gy (resin ⁹⁰ Y-microspheres)	(25)
Small bowel	Grade > = 3 acute toxicity	5%–7%	Uniform dose of ~45 Gy	Unknown	(25)
Spleen	Sepsis, Pneumonia	< 10%	V ₁₅ < 120 cc	Unknown	(113)
		—	Data inconclusive, but suggestive of ~20% chance of infection event after mean dose of 40 Gy to spleen	Unknown	(113)
Kidneys	End-stage renal disease	5%	D _{mean} = 18 Gy (~38 Gy BED)	23–26 Gy (~36 Gy BED)	(7,25)
		50%	D _{mean} = 28 Gy (~44 Gy BED)	34–38 Gy (~44 Gy BED)	(7,25)
Bladder	Grade > = 3 late toxicity (RTOG grading)	< 6%	D _{max} < 65 Gy	Unknown	(25)
Penile bulb	Severe erectile dysfunction	35%	D _{mean} = 50 Gy	Unknown	(25)
Rectum	Grade 2+ late rectal toxicity	< 15%	Various dose volume constraints ranging from V ₅₀ < 50% up to V ₇₅ < 15%	Unknown	(25)
Bone marrow	Moderate to severe hematopoietic syndrome	—	Acute WB exposure 2–5 Gy	D _{mean} > 2–3 Gy (¹³¹ I-Nal, radioimmunotherapy, ⁹⁰ Y-DOTATOC, ¹³¹ I-MIBG)	(36,85,88,114,115)
	Hematopoietic syndrome w/ anemia from GI syndrome	—	Acute WB exposure 6–7 Gy (LD50/60 with antibiotic and transfusion support)	—	(46)
	Pretransplant myeloablation	—	12.0–13.5 Gy in ~1.5 Gy WB exposures over 4–4.5 d (See “Bone Marrow”)	D _{mean} = ~15 Gy (4.6–32.0 Gy; ¹³¹ I-lomab-B)	(89)
Whole body	Moderate to severe hematopoietic syndrome	—	(See “Bone Marrow”)	MTD of ¹³¹ I-Tositumomab determined to be 75 cGy the MTD for pretreated patients. MTD for patients who had HSC transplants = 65 cGy. MTD for patients with no prior therapy = 85 cGy	(92,93)

*EBRT limits are for conventional fractionation unless otherwise stated.

†RPT limits are specified for β-emitting agents (i.e., ¹⁷⁷Lu, ⁹⁰Y, ¹³¹I).

‡Reference is provided for the QUANTEC summary article, for further details readers are referred to the tissue-specific QUANTEC documents.

¶Although ⁹⁰Y-microspheres are typically treated as medical devices rather than radiopharmaceuticals under regulatory purview, they are included herein for completeness.

RPT agents are usually administered systemically (intrathecal, intracavitary, and hepatic artery injections are some of the exceptions); the potential for hematologic toxicity will therefore depend on a combination of inherent marrow radiosensitivity, prior patient exposure to hematotoxic agents, and the absorbed dose to the marrow. A thorough, but now dated, review of marrow dosimetry focused on radiolabeled antibodies was published in 2000 (30). Best practice guidelines for assessing hematologic toxicity in RPT have also been published (31).

Because the marrow is a distributed organ, direct image-based quantification of the time-integrated activity (TIA) (28) in the marrow is certainly possible; it would require delineation of all marrow-containing regions to identify all of the marrow-containing voxels on PET/CT or SPECT/CT imaging. These could be used to calculate the TIA and from this absorbed dose to the entire marrow. In practice, this is not done—rather, “marrow-rich, low background” regions (e.g., lumbar vertebrae L3 to L5) are segmented and used to extract a TIA concentration that is then used to estimate red marrow absorbed dose (32–34). Although a blood-based approach has been described (35) and used to show that red marrow absorbed dose better predicts hematologic toxicity for antibody-based RPT (36), the imaging-based approach is preferred because it does not assume a red marrow-to-blood activity concentration ratio that is constant over time (33,37) and that applies only to antibodies (38). More significantly, image-based red marrow dosimetry may also be applied when the RPT binds to marrow, bone, or blood components or in situations where there is the possibility of cancer cell infiltration of the marrow. This scenario is common for many RPTs agents, and perhaps most prominently for prostate cancer (39,40), where metastatic dissemination is coincident with the marrow. In fact, the paper by Violet et al. illustrates a technique by which dosimetry for a distributed tissue—tumor metastases in this case—is achieved (39).

Compartamental modeling may also be used to estimate red marrow absorbed dose (41–43). Whole-body absorbed dose has also been used as a surrogate for marrow toxicity (44). For ^{131}I -anti-CD20 antibodies, a whole-body absorbed dose of 75 cGy was established as the maximum-tolerated dose (MTD) in patients with non-Hodgkin lymphoma who had been heavily pretreated with chemotherapy (16).

Red marrow dosimetry for α -particle emitter RPT (α RPT) requires consideration of the microscale distribution of the TIA. This is because the short, 50–80 μm range of α -particles can lead to a highly nonuniform dose distribution to the degree that the average absorbed dose over the marrow volume may not predict biologic effects. Average marrow absorbed dose from antibody, peptide, or small molecule-based α RPT is likely to predict hematologic toxicity whereas bone targeting agents such as $^{223}\text{RaCl}_2$ will overestimate the potential biologic impact of a calculated average marrow absorbed dose (45). Red marrow dosimetry for α RPT agents also must account for the biodistribution of free daughters (46). The special considerations associated with α RPT dosimetry have been previously reviewed (21,47).

With marrow absorbed dose estimates, it is relevant to consider that the marrow is quickly damaged by radiation but can, within limits, regenerate and be able to be treated again. This approach has been taken with chemotherapy for many years, with multiple cycles and intervening times without treatment for the marrow to reconstitute. As an example, ^{131}I -tositumomab therapy was successfully repeated at a 75 cGy total body dose level at months to years after initial treatment, with no evidence of additive toxicity (48). This

differs from what we expect to be the case for slower regenerating tissues such as the liver or kidneys, where we view absorbed dose levels as cumulative and additive toward an upper limit.

Although 2–3 Gy is considered the maximum-tolerated radiation-absorbed dose to the marrow, based on perhaps limited dosimetric data, these limits are those present when the marrow is expected to reconstitute on its own. When stem cell transplant is considered and there is or is not tumor involvement in the marrow, the dosimetric limit is much higher, likely reflecting the tolerance of stem cells to re-engage in the marrow, which has been ablated by radiation. In studies using ^{131}I -anti-CD45 antibodies, a possible marrow dose of up to 48 Gy has been considered acceptable. Early analyses of the clinical data from 49 patients who received ^{131}I -apamistimab show the absorbed dose delivered to marrow (median, 14.7 Gy; range, 4.6–32 Gy) allowed for marrow re-engraftment, thus suggesting the MTD to marrow (with reconstitution) exceeds 32 Gy and supports the protocol-defined 48 Gy MTD (49).

Liver

Therapies resulting in significant liver absorbed dose include ^{90}Y -microspheres (although ^{90}Y -microspheres are typically treated as medical devices rather than radiopharmaceuticals under regulatory purview, they are included herein for completeness), for transarterial radioembolization, radioimmunotherapeutics using a radiometal label, somatostatin analogs, and ^{131}I -MIBG. Radiation-induced liver toxicity typically presents within 4–8 wk of irradiation; however, cases have been reported as early as 2 wk after irradiation and as late as 7 mo after irradiation (50). Classic presentation of radiation-induced liver disease (RILD) includes fatigue, abdominal pain, hepatomegaly, and ascites, in conjunction with jaundice and a rise in the level of alkaline phosphatase. These clinical symptoms are thought to be the result of hepatic “veno-occlusive disease,” whereby vascular congestion results in decreased oxygen delivery to the liver. Nonclassical presentations of radiation-induced liver disease are seen in patients with chronic hepatic diseases, such as cirrhosis and viral hepatitis.

MTD to liver from radioimmunotherapy exceeds 28.5 Gy in a single dose with ^{90}Y -anti-CD20 antibodies given systemically (51). ^{131}I -MIBG dosing has been, in part, driven by dosimetry. Mild transient hepatic function abnormalities have been seen in patients treated with MIBG. These data are complex, but doses up to 30 Gy to the liver have resulted in less than 10% incidence of transient reversible hepatotoxicity (52,53). Clinical protocols have limited dose escalation to 30 Gy to the liver, so liver MTD may be higher than 30 Gy for systemic radiopharmaceuticals. It is believed that radioantibodies and MIBG distribute uniformly through the hepatic parenchyma, resulting in a relatively uniform absorbed dose.

Being the primary target and site of accumulation, clinical use of ^{90}Y -microspheres (both resin and glass) often results in whole liver mean doses more than 30–32 Gy, which is thought to be the TD5/5 in external-beam radiotherapy. Whole liver doses of more than 42 Gy (EBRT TD50/5) are often encountered as well, although somewhat less frequently with resin ^{90}Y -microspheres. Among bilobar treatments, liver toxicity modeling has indicated a 15% complication rate for mean liver doses of 35–70 Gy from glass microspheres (54). Whole liver mean doses in excess of 70 Gy from glass microspheres are known to result in >50% chance of radiation-induced liver toxicity (54). Data from resin microspheres indicate an approximately 50% rate of toxicity for whole liver mean doses of 44–61 Gy (55). Of note is that the product insert for ^{90}Y glass microspheres (Theraspheres; Boston

Scientific Corp.) describes delivering doses of in excess of 80 Gy to the targeted lobe, with recommended doses of up to 150 Gy to the treated lobe. Whole liver mean doses given during a single lobe or segmental infusion may not be comparable to bilobar treatments, which are more commonly seen with resin ^{90}Y -microspheres. Relevant data to this point are presented in the DOSISPHERE-01 study, which compared personalized dosimetry to escalate tumor doses (mean normal liver dose of 119.7 Gy, with 1 patient receiving 150.3 Gy) with a nondosimetry group (mean liver dose of 79.2 Gy) (56). Although liver function alterations occurred, they were viewed as manageable and there was only 1 case of hepatic failure in the dosimetry group (1/28, 3.6%). The reason why tolerable liver absorbed doses appear to be higher for microspheres in comparison to external beam or other β -emitting therapies (MIBG; radioimmunotherapies) is likely because of the microscale dosing of ^{90}Y -microspheres, which tends to be nonuniformly distributed throughout the hepatic arterial system/liver. This results in many areas that receive lower absorbed doses (57). This is particularly true for ^{90}Y -microsphere segmentectomies, in which 10%–30% of the liver often receives a mean dose in excess of 200–400 Gy. To better characterize these effects, dose–response relationships for tumors and normal liver are being refined by use of multicenter data and harmonized software/dosimetry methods among sites (58).

Kidneys

Generally, renal toxicity is defined as an increase in the serum creatinine levels, loss of creatinine clearance, or decrease in glomerular filtration rate (GFR), commonly based on the National Cancer Institute's iterations of Common Terminology Criteria for Adverse Events (CTCAE). The kidneys may be the limiting factor for the maximum cumulative activity of hydrophilic systemic RPT such as radiolabeled peptides, small molecules, or antibody fragments. The kidney tolerance of 23 Gy, originally derived for external-beam radiotherapy, has been suggested for renal excreted radiopharmaceuticals. However, fundamental radiobiologic differences of RPTs and the derived biologic effective dose need to be considered, which may significantly vary depending on multiple factors including the half-life of the radionuclide (59). The renal dosimetry threshold has been used by studies to optimize treatment schedules by modifying the administered activity per cycle or number of cycles of ^{177}Lu -DOTATATE (60,61). These studies have demonstrated wide interpatient variability of renal absorbed dose by a factor of 10, underscoring the importance of dosimetry. The individualized dosimetry-based methodologies have led to enhancing tumor absorbed dose with potential improvement in the patient outcome while maintaining the acceptable safety profile of the RPT.

Notably, to capture the true incidence of renal impairment after RPT a sufficient follow-up time of at minimum 6–12 mo is required (62). Therefore, the incidence and degree of renal impairment after RPT need to be considered in the context of the life expectancy of the patients. For instance, the relatively limited median overall survival of patients with advanced metastatic castrate-resistant prostate cancer (mCRPC) of 13–16 mo may not allow the occurrence of the full spectrum of renal impairment after PSMA RPT. However, the possibility of the development of renal impairment after PSMA RPT could be of more importance in earlier stages of prostate cancer (1,63). Similarly, in the context of neuroendocrine neoplasms (NENs), the implication of renal toxicity may need to be considered in the context of tumor grade, especially

as patients with grade 1 NENs may live a decade or longer compared with much shorter survival of patients with grade 3 NENs.

The enhanced understanding of the mechanisms of renal accumulation of radiolabeled peptides, small molecules, and antibody fragments cannot be overemphasized as this would allow devising the strategies to reduce renal toxicity. Hydrophilic radiolabeled peptides such as ^{177}Lu -DOTATATE are mainly filtered by the glomeruli and partly reabsorbed by the proximal tubular cells (62). Insight into the mechanisms of renal handling of DOTA peptides led to the development of multiple strategies to reduce the renal absorbed dose (62), of which competitive inhibition of proximal tubular reabsorption by pretreatment with positively charged amino acids (arginine and lysine) has achieved a renal dose reduction of approximately 50% and is widely adopted in clinical practice (64,65). In fact, with the adoption of amino acid pretreatment, the incidence of serious toxicity has been low, $\leq 1.5\%$ grade III or IV CTCAE, regardless of the treatment schedule, the number of cycles and administered activity per cycle or cumulatively (65,66).

Specific binding to PSMA of the proximal tubules appears to be the most relevant mechanism of renal retention in PSMA RLT. Using potential differential internalization rate of PSMA isoforms in the renal tubules compared with prostate cancer cells, it has been shown that small-molecule PSMA inhibitors such as 2-(phosphonomethyl) pentanedioic acid (PMPA) can displace noninternalized PSMA ligand 16 h after PSMA RLT in preclinical models (67). Although this appears to improve the therapeutic index of the treatment without significant reduction in the tumor absorbed dose, the translation of these findings in humans remains to be determined. Nonetheless, currently, PSMA RLT is mainly used in the advanced stage of mCRPC and the incidence of grade 3 or 4 renal toxicity remains low (1%–3.5%) (1,63). In a phase 2 study of 28 patients who underwent ^{51}Cr -EDTA GFR measurement before and 3 mo after completion of 4 cycles of ^{177}Lu -PSMA, a very modest decline of approximately 12 mL/min in GFR was noted (39,68,69). The renal toxicity profile of PSMA RLT may be of more clinical importance in the earlier stage of prostate cancer disease continuum, higher administered activity per cycle, higher cumulative activity or use of α -isotopes and requires further investigation. Therapeutic radioisotopes, particularly many α -emitters, may have complicated decay schemes with daughter isotopes that can accumulate in the kidneys. This needs to be carefully considered in evaluating the therapeutic ratios of RPTs.

We believe the 23 Gy tolerance guidance limit from external-beam radiation may be lower than the true tolerance of the kidneys, given the modest renal toxicity seen with modern radiolabeled peptide therapies. We believe absorbed dose escalation studies are essential and should be strongly considered to determine whether 23 Gy represents the true limit for renal radiation-absorbed dose. Adhering to the limit derived from EBRT may result in underdosing of tumors in patients receiving RPT, compromising efficacy.

Salivary Glands

The salivary glands have long been an organ of interest related to RPT toxicity due to their being organs of accumulation and excretion of ^{131}I , which is used to treat both hyperthyroidism and thyroid cancer. Salivary glands are highly radiosensitive, and radiation sialadenitis and xerostomia have become the most frequent complication of high-activity ^{131}I therapies for thyroid cancer, occurring in over 50% of cases (70). Typical thyroid therapy administered activities are in the range of 3.7–7.4 GBq, although cumulative activities of >20 GBq are sometimes used (71). Planar dosimetry has shown

differences in radiation-absorbed doses between the parotid and submandibular glands, with median absorbed dose per administered activity of each single parotid and submandibular gland to be about 0.15 Gy/GBq (range, 0.1–0.3 Gy/GBq) and 0.48 Gy/GBq (range, 0.2–1.2 Gy/GBq) (72). The dosimetry of salivary glands has been investigated more intensively with the availability of ^{124}I PET imaging, which has shown a radiation-absorbed dose of 0.23 Gy/GBq in patients who do not have thyroid stimulation with lemon drops (72). Absorbed dose was noted to be increased by 28% with stimulation of salivary flow. A 7.4 GBq administration of ^{131}I would therefore deliver 1.7 Gy, and 20 GBq would deliver 4.6 Gy. These absorbed doses are lower than the 26 Gy “safe” absorbed dose to the salivary glands for external-beam radiotherapy (73). Although there is variability in methods and results for dosimetry by planar scintigraphy and PET methods, these data suggest a difference between RPT and external beam in this setting, possibly due to microdosimetry differences for ^{131}I , which we do not yet fully understand (71).

The dosimetry studies of small molecules targeting PSMA such as $^{124}\text{I}/^{131}\text{I}$ -MIP-1095, or ^{177}Lu -PSMA-617 or ^{177}Lu -PSMA I&T have shown salivary glands commonly receive the highest radiation-absorbed dose among normal organs (69,74). The underlying mechanism of tracer accumulation is likely related to the extensive expression of PSMA within the salivary glands, although there can be both specific and nonspecific binding in the salivary glands (75). Dosimetry using ^{124}I -MIP-1095 PET/CT to predict ^{131}I -MIP-1095 dosimetry have shown predicted absorbed doses of 9.2–33.3 Gy from a single therapy administration (76). With ^{131}I -MIP-1095 therapy given as a single treatment, 7 of 28 patients treated had mild and transient (3–4 wk duration) xerostomia and 1 patient had transient mucositis. In the multicenter ^{177}Lu -PSMA-617 VISION trial, symptoms of dry mouth occurred in 38.8% of patients, but no grade 3 or greater dry mouth was observed in the 529 patients receiving a mean 37.5 GBq over 6.9 mo (median 5 cycles of 7.4 GBq/cycle). Dosimetry estimates for salivary gland radiation-absorbed dose from ^{177}Lu -PSMA PET posttherapy imaging have been limited and have typically used planar imaging. Delker et al. estimated a mean of 1.4 Gy/GBq to the salivary glands from ^{177}Lu -PSMA-617 therapies (77). This extrapolates to 52.5 Gy to the salivary glands (by extrapolation from the VISION trial), resulting in very low toxicity, but caution may be in order due to the uncertainties of planar imaging-derived dosimetry of small structures (77). Peters et al. performed ^{177}Lu -SPECT/CT dosimetry, including the salivary glands, with PSMA-617 and estimated a mean absorbed dose of 0.38 Gy/GBq (78). This dose extrapolated prescribing within the VISION trial would indicate an average salivary gland absorbed dose of ~14.3 Gy. Despite variability in the rate of xerostomia among studies, observations have typically been of low severity, usually grade 1 CTCAE (1,63). Some of the most direct evidence of the importance of radiation-absorbed dose and RBE have been in the context of α -emitting isotope-labeled small molecules targeting PSMA. Although the antitumor effects of these agents are impressive, the incidence and severity of xerostomia appears higher and, in some instances, the main reason for toxicity-related treatment discontinuation, with over 25% of patients requesting therapy be stopped due to salivary gland toxicities (79). Of note, however, these patients had previously received ^{177}Lu -PSMA targeted therapy, so the effects would need to be viewed as cumulative radiation toxicity. However, when larger molecules targeting PSMA such as antibodies are labeled to α -isotopes, xerostomia appears to

be of less concern due to low salivary gland uptake (80). Various approaches have been attempted to mitigate salivary gland toxicity including sialagogues, local cooling, local injections of botulinum toxin, oral administration of monosodium glutamate, or PSMA inhibitors such as PMPA, with generally limited success and the unclear impact on tumoral uptake that require further investigation (81,82). Because of the current limitations in α -particle dosimetry, it is not possible to speculate on dose–response relationships, and these will need to be developed empirically, most likely with dosimetry obtained from diagnostic surrogates. Whole organ dose estimates from diagnostic surrogates may also then need to be informed by models of microscale α -dosimetry.

Lungs

The most extensive studies of radiation-absorbed dose to the lungs from RPT have been undertaken in thyroid cancer. For several decades, an “80 mCi” rule has been in place to guide high-dose ^{131}I therapies of thyroid cancer. If the whole body has 80 mCi (2.96 GBq) or less, predicted to be present at 48 h after therapy, pulmonary toxicity can be avoided if patients have lung metastases from thyroid cancer. The complexity with these estimates is that when one examines the 80 mCi rule, the predicted radiation-absorbed dose to normal lungs ranged from 57 to 112 Gy; the photon-only portion, which better reflects the dose to normal lung parenchyma, ranged from 4.9 to 55 Gy. Thus, with ^{131}I the heterogeneity of dose means much of the β -dose substantially irradiates the tumor while the γ -dose irradiates more normal lung. In addition, the size of the lungs make a large difference (83). This area of investigation is unsettled but it does illustrate that nonuniform dose delivery can confound estimates of safe doses to organs. ^{124}I PET imaging has been used to further inform lung radiation dosimetry (84). These data suggest that in tumor-involved lungs, higher activities might be given more safely than the activities predicted by the seminal Benua and Leeper method (85).

A dose escalation study using ^{131}I -anti-CD20 antibodies and stem cell support showed that although normal lung absorbed doses under 23.75 Gy were well tolerated (other than intended myeloablative hematopoietic effects), in 2 patients who received 27.5 and 30.75 Gy to lungs—as estimated by planar imaging—significant and severe, but reversible cardiopulmonary toxicity occurred (86). These are among the few dose escalation studies reaching an MTD with RPTs.

Limited data exist regarding lung dose–toxicity relationships for ^{90}Y -microsphere shunting to lungs; however, it is generally accepted that delivering over 30 Gy in a single treatment or over 50 Gy in sequential treatments is undesirable. These generally accepted criteria are based on very few patients, and with somewhat outdated dosimetry methods (87).

Whole-Body Radiation

A single whole-body photon exposure of 3–5 Gy produces an acute gastrointestinal syndrome and hematopoietic toxicity, which can be fatal without major medical intervention (88). Acute whole-body absorbed doses of 6–7 Gy are considered the human $\text{LD}_{50/60}$, that is, the lethal dose for 50% of the population in 60 d, even with supportive treatment (typically antibiotic and transfusion support) (89). Survivable whole-body doses in excess of 7–8 Gy can be reached by reducing the dose rate, or by administering the radiation in smaller fractions over several days. Before hematopoietic stem cell transplant in patients being treated for hematologic malignancies, common dose fractionation for myeloablation

is 1.5 Gy to the whole body, twice per day, up to a total dose of 12.0–13.5 Gy (90). Whole-body dose from radiopharmaceuticals is not often an endpoint of interest due to the nonuniform nature of uptake and energy deposition; however, whole-body absorbed dose has been used effectively as a surrogate for marrow dosimetry in pediatric patients receiving ^{131}I -MIBG (often 3–4 Gy over 2 treatments) (91) and in patients receiving ^{131}I -tositumomab (MTD = 75 cGy, single administration in heavily pretreated patients without major marrow involvement with tumor) (92,93).

SECONDARY MALIGNANCIES AND SIDE EFFECTS

It is known that children are more susceptible to radiation effects than are adults. Indeed, the use of external-beam radiation in children has been declining over the years as a greater understanding of second malignancies and late effects on growth and development are identified along with increased efficacy of alternative cancer treatments. The use of PET imaging has allowed for elimination of external-beam radiation in many cases of Hodgkin disease, thus limiting toxicity (94) by more appropriately limiting external-beam radiation to those with residual tumor by PET. At present the main uses of RPTs in children include ^{131}I for thyroid cancer and ^{131}I -MIBG for neuroblastoma. More recently, somatostatin receptor–targeting agents are being applied for RPTs of neuroblastoma. There has been use of bone-targeting agents in osteosarcoma and radiolabeled monoclonal antibodies, as well (15,95).

A systematic review of the toxicities of ^{131}I therapy in patients with thyroid cancer (96) evaluated 37 articles including adults and children. Relatively early effects after treatment can include alterations in salivary and lacrimal gland function. In this review, post- ^{131}I therapy patients experienced significantly more salivary gland dysfunction (prevalence range: 16%–54%), lacrimal gland dysfunction (prevalence: 11%), transient male gonadal dysfunction (prevalence: 35%–100%, high-level evidence), transient female gonadal dysfunction (prevalence: 28%, low-level evidence), and second primary malignancies (prevalence: 2.7%–8.7%, moderate-level evidence) than unexposed patients. Breast and digestive tract cancer were the most common reported secondary malignancies. Except for the study performed by Lang et al. (97), all studies reported an increased risk of the occurrence of both solid tumors and leukemia after treatment with ^{131}I . ^{131}I therapy seems to have no deleterious effects on female reproductive outcomes (very-low level evidence). The prevalence and severity of adverse effects were correlated to increasing cumulative ^{131}I activity. Gonadal radiation may cause transient or longer-duration azoospermia. As RPTs are used more in younger patients, sperm banking has been considered in patients receiving cumulative administrations in excess of 14 GBq of ^{131}I (98).

In a retrospective review of the Surveillance, Epidemiology, and End Results Program (SEER) registry ($n = 148,215$), the risk for hematologic malignancies after postsurgery radioiodine treatment of well-differentiated thyroid cancer appears to be significantly higher than patients managed with surgery alone (hazard ratio, 1.43; 95% CI, 1.20 to 1.69; $P < 0.001$) (99); however, the absolute risk appears quite low, approximately 0.54% within 10 y of surgery plus radioiodine therapy. In this review, no data regarding administered activities or dosimetry were available.

MIBG is increasingly a routine part of neuroblastoma therapy in the United States and some European countries. In a review of 644 neuroblastoma patients treated with ^{131}I -MIBG (in addition to

other cytotoxic therapies), the cumulative incidence of secondary malignant neoplasm (SMN) was 7.6% and 14.3% at 5 and 10 y from first ^{131}I -MIBG, respectively. No increase in SMN risk was found with increased number of ^{131}I -MIBG treatments or higher cumulative activity per kilogram of ^{131}I -MIBG received ($P = 0.72$ and $P = 0.84$, respectively). Thirteen of the 19 reported SMN were hematologic. These authors concluded the cumulative risk of SMN after ^{131}I -MIBG therapy for patients with relapsed or refractory neuroblastoma was similar to the greatest published incidence for high-risk neuroblastoma after myeloablative therapy, with no dose-dependent increase. However, there was no clear measurement of marrow absorbed dose in this study. External-beam irradiation of over 10 Gy can cause ovarian failure, which is also a toxicity that has been identified in some female patients receiving MIBG treatment (100).

A reasonably large dataset exists for prospective ^{131}I -tositumomab therapy of non-Hodgkin lymphoma (101). SWOG S0016 was a phase III randomized study that compared the safety and efficacy of R-CHOP (rituximab plus cyclophosphamide, doxorubicin, vincristine, and prednisone) with CHOP-RIT (CHOP followed by consolidation with ^{131}I -tositumomab radioimmunotherapy) for previously untreated patients with follicular lymphoma. Five hundred thirty-one previously untreated patients with follicular lymphoma were randomly assigned to receive either 6 cycles of R-CHOP or 6 cycles of CHOP-RIT. Patients in the CHOP-RIT arm had significantly better 10-y progression-free survival than patients in the R-CHOP arm (56% vs. 42%; $P = 0.01$), but 10-y overall survival was not different between the 2 arms (75% vs. 81%; $P = 0.13$). There was no significant difference between the CHOP-RIT and R-CHOP arms in regard to incidence of second malignancies (15.1% vs. 16.1%; $P = 0.81$) or myelodysplastic syndrome or acute myeloid leukemia (4.9% vs. 1.8%; $P = 0.058$). The estimated 10-y cumulative incidences of death resulting from second malignancies were not different (7.1% vs. 3.2%; $P = 0.16$), but cumulative incidence of death resulting from myelodysplastic syndrome or acute myeloid leukemia was higher in the CHOP-RIT arm than in the R-CHOP arm (4% vs. 0.9%; $P = 0.02$) (101). These data support a small but measurable increased incidence of death from acute myeloid leukemia (AML) or myelodysplastic syndrome in the patients who received ^{131}I -tositumomab versus those who did not.

Myelodysplastic syndromes (MDS) and AML can also occur after peptide receptor radionuclide therapy for neuroendocrine tumors. Thirty cases of 1,631 patients treated over a 2 decade period were reported (102). Bodei reported a 2.35% frequency of MDS (103). Other studies have suggested a higher frequency of MDS/AML in patients who have had more extensive chemotherapy (104). It appears that the longer a patient population is observed after RPT, the greater the chance of developing MDS, possibly explaining differences among studies in the frequency of MDS/AML. Overall, the rate of MDS/acute leukemia appears to be similar to that seen from other cytotoxic systemic therapies. Further understanding of risk factors, timelines, and additive or synergistic risk from other treatments is necessary.

CONFOUNDING CLINICAL FACTORS

As RPT becomes more widely applied, there will be more clinical questions to determine how to safely combine external-beam radiation–absorbed doses with absorbed doses delivered by radiopharmaceuticals. Although this is an evolving area and thorough

discussion is beyond the scope of the current review, concerns can include tolerances in patients who have had spinal cord or brain irradiation. Fortunately, it is rare for radiopharmaceuticals to localize substantially to the normal brain or spinal cord. However, lesions close to normal brain may present areas of risk. Similarly, there are concerns with patients who have had a large area of marrow irradiated. Such patients may have a lower marrow reserve, and increased toxicity, with external RPTs. Indeed, limitations of bone marrow irradiation have been included as eligibility criteria for Food and Drug Administration–approved radiopharmaceuticals such as ibritumomab tiuxetan, where key clinical trials excluded patients who had radiation of any type before radioimmunotherapy. Examples of efforts to combine dose planning for RPT of bone metastases with external beam radiation have been described for ^{153}Sm -EDTMP as an example (105). Similar challenges will likely arise with brachytherapy, especially given the importance of this modality in prostate cancer therapy. It remains unclear how much additional absorbed dose can be given depending on the time interval after external beam radiation or RPT.

Tumor burden can also impact radiation tolerances. The clinical trials leading to the approval of anti-CD20 radioimmunotherapies intentionally excluded patients with bone marrow involvement with tumor of >25% (92). This was arbitrary, and some trials have allowed larger amounts of tumor involvement. The admixture of tumor and normal tissue in the marrow, and elsewhere (such as the lung) can make estimations of radiation-absorbed dose to tumor and marrow challenging.

Prior and concurrent therapies can also impact radiation tolerances. Chemotherapy, especially recent, can increase the sensitivity of normal bone marrow to radiation-induced toxicities. In patients with lymphoma receiving a relatively standard bone marrow radiation-absorbed dose from radioimmunotherapy, the duration of time postchemotherapy was the most strongly correlated factor with the severity of myelosuppression (106). Although single-agent RPTs can be effective in diseases such as non-Hodgkin lymphoma, they are unlikely to provide durable disease remissions in a range of cancers. Thus, combination therapies will increasingly be tested and those studies will inform the interplay and optimal timing of RPT and other therapies including cytotoxic treatments.

As we increasingly understand DNA damage and repair, there is a growing appreciation for DNA damage from radiation. There is little specific data regarding RPT and DNA repair mechanisms. More is known regarding external-beam radiation, but at present, some of the known inherited syndromes, such as ataxia telangiectasia, ataxia-telangiectasia-like disorder, radiosensitive severe combined immunodeficiency, Nijmegen breakage syndrome, and *LIG4* deficiency are associated with increased radiosensitivity (96,107). This is an area where additional research is necessary.

SUMMARY AND FUTURE DIRECTIONS

The Latin phrase “*Primum non nocere*” means “First, do no harm.” This approach is often applied to RPTs by regulators and by practitioners. It can be interpreted as “do not exceed dose limits established by external-beam radiation treatments, as harm could be done to an individual patient.” However, like in chemotherapy, sometimes some reversible or addressable harm may be acceptable if there is a reasonable probability of a long-term benefit exceeding the harm. It is very interesting that in radioembolization studies of hepatic malignancies, much higher radiation-absorbed doses can be tolerated than expected from established external-beam

radiation thresholds. This points to the need for dose escalation studies to better understand organ tolerance for RPTs. Underdosing patients is possible if an organ MTD is higher than expected from external-beam data. Similarly, an average dose of a therapeutic radiopharmaceutical that is safe for a population may result in systematic underdosing of a significant fraction of the population, denying individual patients an opportunity for benefit—a clear harm. We must as a field move to individualized radiopharmaceutical dosimetry-based dosing to provide better outcomes for populations who may be systematically underdosed.

Gaps in Our Current Understanding

Most currently available radiation biology data are empiric and there are extensive gaps in knowledge of the effects of radiation at the subcellular, cellular, and microenvironmental levels. The deficiencies start with limited understanding of track structure patterns of ionization and excitation resulting from various radiation types and the secondary charged particles in complex biologic media, particularly at the end of their range, where the energy transfer is most pronounced (108). It is not clear how the low and high linear energy transfer (LET) radiation affects specific subcellular targets. The most investigated is the radiation-induced damage to DNA and the repair mechanisms, including cell cycle control. However, the signals that initiate the checkpoint response, the need for cell cycle progression checkpoints for effective DNA repair, and variations in radiosensitivity throughout the cell cycle are not well characterized. Much less is known about how radiation damage to cell membranes and cellular organelles leads to radiation cytotoxicity. For instance, radiation effects on membranes may cause modifications of cell signaling pathways controlling cell response to stress, including pro- and antiapoptotic signals (109). Only recently, the effect of absorbed dose on gene expression has been investigated (110). It remains to be studied how other radiation characteristics, such as LET and dose rate, would affect signaling pathways and gene expression. This kind of research might also provide means to identify genetic factors determining individual radiation sensitivity, which are currently unknown.

An innate characteristic of RPT is heterogeneity of dose distribution. Therefore, to understand the effect of RPT on tissues, we need to learn more about intracellular signaling and interactions between the microenvironment and bystander effects and their role in response to radiation. There is a growing interest in immunomodulatory effects of local radiotherapy on the tumor microenvironment (111). There are only limited data on the possible combination of RPT with immunotherapy. This is also the case for the combination of RPT with other therapeutic modalities, including external radiation therapy. Considering the number of unknowns listed above for any type of radiation individually, the major problem for combinations is the difficulty with assessment of the effects of combinations of different types of radiation. The same problem hinders combinations of different types of radionuclides, for example, α - and β -emitters, to optimize RPT.

KEY RECOMMENDATIONS

The following are key recommendations:

1. Clinical adoption of dosimetry in instances in which there is considerable patient-to-patient variation in absorbed dose to organs for a given administered activity.
2. Clinical adoption of dosimetry in instances of limited organ reserve.

3. Standardization and validation of radiopharmaceutical dosimetry approaches for organs and tumors with a goal of achieving not over 10% variability among sites—similar to what has been achieved with external-beam radiotherapy.
4. Establishment of a more nuanced balance assessment between potential benefits and toxicities (i.e., some toxicity may be necessary to achieve optimal therapeutic effect and improve patient outcome). These decisions will best be made by considering factors such as aggressiveness of underlying malignancy, life expectancy of patients, and the potential impact of toxicity on the quality of life of the patients.
5. High-quality dose escalation studies based on absorbed dose to better inform the MTD, including MTD of nonhematological organs; these data will help ensure that we do not systematically undertreat patients, thus failing to optimize antitumor effects.
6. Establishment of a registry of short- and long-term toxicities of organs related to known absorbed dose.
7. Examination of toxicities versus dose rate and radiation type (i.e., α -emitters).
8. More thoroughly linked radiation-induced toxicities versus molecular profiles of tissues.
9. Enhanced understanding of the mechanistic normal-tissue toxicity pertinent to each RPT to devise strategies to optimize absorbed dose and rationally minimize toxicities.
10. Establishment of a systematic effort, akin to the QUANTEC or HyTEC external-beam initiatives, to better understand and catalog the dose response relationships for RPTs.

DISCLOSURE

The opinions expressed in this publication are the author(s)' own and do not reflect the view of the National Institutes of Health, the Department of Health and Human Services, or the United States government. No other potential conflict of interest relevant to this article was reported.

REFERENCES

1. Sartor O, de Bono J, Chi KN, et al. Lutetium-177-PSMA-617 for metastatic castration-resistant prostate cancer. *N Engl J Med*. 2021;385:1091–1103.
2. Parker C, Nilsson S, Heinrich D, et al. Alpha emitter radium-223 and survival in metastatic prostate cancer. *N Engl J Med*. 2013;369:213–223.
3. Bentzen SM. Theragnostic imaging for radiation oncology: dose-painting by numbers. *Lancet Oncol*. 2005;6:112–117.
4. Shirvani SM, Huntzinger CJ, Melcher T, et al. Biology-guided radiotherapy: redefining the role of radiotherapy in metastatic cancer. *Br J Radiol*. 2021;94:20200873.
5. Musolino SV. Absorbed dose determination in external beam radiotherapy: an international code of practice for dosimetry based on standards of absorbed dose to water. Technical reports series no. 398. International Atomic Energy Agency (IAEA); 2000. IAEA website. https://www-pub.iaea.org/MTCD/Publications/PDF/TRS398_scr.pdf. Accessed October 31, 2021.
6. Emami B, Lyman J, Brown A, et al. Tolerance of normal tissue to therapeutic irradiation. *Int J Radiat Oncol Biol Phys*. 1991;21:109–122.
7. Wessels BW, Konijnenberg MW, Dale RG, et al. MIRD pamphlet no. 20: the effect of model assumptions on kidney dosimetry and response—implications for radionuclide therapy. *J Nucl Med*. 2008;49:1884–1899.
8. Pouget J-P, Constanzo J. Revisiting the radiobiology of targeted alpha therapy. *Front Med (Lausanne)*. 2021;8:692436.
9. Rich JN. Cancer stem cells in radiation resistance. *Cancer Res*. 2007;67:8980–8984.
10. Hobbs RF, Howell RW, Song H, Baechler S, Sgouros G. Redefining relative biological effectiveness in the context of the EQDX formalism: implications for alpha-particle emitter therapy. *Radiat Res*. 2014;181:90–98.
11. Hobbs RF, Song H, Huso DL, Sundel MH, Sgouros G. A nephron-based model of the kidneys for macro-to-micro α -particle dosimetry. *Phys Med Biol*. 2012;57:4403.
12. Bolch WE, Eckerman KF, Sgouros G, Thomas SR. MIRD pamphlet no. 21: a generalized schema for radiopharmaceutical dosimetry—standardization of nomenclature. *J Nucl Med*. 2009;50:477–484.
13. Uribe C, Peterson A, Van B, et al. An international study of factors affecting variability of dosimetry calculations, part 1: design and early results of the SNMMI dosimetry challenge. *J Nucl Med*. 2021;62(suppl. 3):36S–47S.
14. He B, Wahl RL, Du Y, et al. Comparison of residence time estimation methods for radioimmunotherapy dosimetry and treatment planning—Monte Carlo simulation studies. *IEEE Trans Med Imaging*. 2008;27:521–530.
15. Plyku D, Loeb DM, Prideaux AR, et al. Strengths and weaknesses of a planar whole-body method of ^{153}Sm dosimetry for patients with metastatic osteosarcoma and comparison with three-dimensional dosimetry. *Cancer Biother Radiopharm*. 2015;30:369–379.
16. Wahl RL. The clinical importance of dosimetry in radioimmunotherapy with tositumomab and iodine I 131 tositumomab. *Semin Oncol*. 2003;30(suppl 4):31–38.
17. Kam WW-Y, Banati RB. Effects of ionizing radiation on mitochondria. *Free Radic Biol Med*. 2013;65:607–619.
18. Jonathan EC, Bernhard EJ, McKenna WG. How does radiation kill cells? *Curr Opin Chem Biol*. 1999;3:77–83.
19. Sia J, Szmyd R, Hau E, Gee HE. Molecular mechanisms of radiation-induced cancer cell death: a primer. *Front Cell Dev Biol*. 2020;8:41.
20. McBride WH, Schae D. Radiation-induced tissue damage and response. *J Pathol*. 2020;250:647–655.
21. Sgouros G, Roeske JC, McDevitt MR, et al. MIRD pamphlet no. 22 (abridged): radiobiology and dosimetry of alpha-particle emitters for targeted radionuclide therapy. *J Nucl Med*. 2010;51:311–328.
22. Pugliese MD, Grossi GF, Monforti F, et al. Inactivation of individual mammalian cells by single alpha-particles. *Int J Radiat Biol*. 1997;72:397–407.
23. Sgouros G. Dosimetry, radiobiology and synthetic lethality: radiopharmaceutical therapy (RPT) with alpha-particle-emitters. *Semin Nucl Med*. 2020;50:124–132.
24. Cremonesi M, Botta F, Di Dia A, et al. Dosimetry for treatment with radiolabelled somatostatin analogues: a review. *Q J Nucl Med Mol Imaging*. 2010;54:37.
25. Marks LB, Yorke ED, Jackson A, et al. Use of normal tissue complication probability models in the clinic. *Int J Radiat Oncol Biol Phys*. 2010;76:S10–S19.
26. Grimm J, Marks LB, Jackson A, Kavanagh BD, Xue J, Yorke E. High Dose per Fraction, Hypofractionated Treatment Effects in the Clinic (HyTEC): an overview. *Int J Radiat Oncol Biol Phys*. 2021;110:1–10.
27. Rubin P, Casarett G. Direction for clinical radiation pathology: the tolerance dose. *Front Radiat Ther Oncol*. 1972;6:1–16.
28. Capala J, Graves S, Scott A, et al. Dosimetry for radiopharmaceutical therapy: current practices and commercial resources. *J Nucl Med*. 2021;62(suppl 3):3S–11S.
29. Sgouros G, Dewaraja YK, Escorcía F, et al. Tumor response to radiopharmaceutical therapies: the knowns and the unknowns. *J Nucl Med*. 2021;62(suppl 3):12S–22S.
30. Sgouros G, Stabin M, Erdi Y, et al. Red marrow dosimetry for radiolabeled antibodies that bind to marrow, bone, or blood components. *Med Phys*. 2000;27:2150–2164.
31. Hindorf C, Glatting G, Chiesa C, Linden O, Flux G. EANM Dosimetry Committee guidelines for bone marrow and whole-body dosimetry. *Eur J Nucl Med Mol Imaging*. 2010;37:1238–1250.
32. Sgouros G, Jureidini IM, Scott AM, Graham MC, Larson SM, Scheinberg DA. Bone marrow dosimetry: regional variability of marrow-localizing antibody. *J Nucl Med*. 1996;37:695–698.
33. Schwartz J, Humm JL, Divgi CR, Larson SM, O'Donoghue JA. Bone marrow dosimetry using ^{124}I -PET. *J Nucl Med*. 2012;53:615–621.
34. Hindorf C, Lind Å, Önn O, Tennvall J, Wingårdh K, Strand S-E. Evaluation of methods for red marrow dosimetry based on patients undergoing radioimmunotherapy. *Acta Oncol*. 2005;44:579–588.
35. Sgouros G. Bone marrow dosimetry for radioimmunotherapy: theoretical considerations. *J Nucl Med*. 1993;34:689–694.
36. O'Donoghue JA, Baidoo N, Deland D, Welt S, Divgi CR, Sgouros G. Hematologic toxicity in radioimmunotherapy: dose-response relationships for I-131 labeled antibody therapy. *Cancer Biother Radiopharm*. 2002;17:435–443.
37. Hindorf C, Linden O, Tennvall J, Wingårdh K, Strand SE. Time dependence of the activity concentration ratio of red marrow to blood and implications for red marrow dosimetry. *Cancer*. 2002;94(4, Suppl):1235–1239.
38. Cremonesi M, Ferrari M, Di Dia A, et al. Recent issues on dosimetry and radiobiology for peptide receptor radionuclide therapy. *Q J Nucl Med Mol Imaging*. 2011;55:155–167.

39. Violet J, Jackson P, Ferdinandus J, et al. Dosimetry of Lu-177-PSMA-617 in metastatic castration-resistant prostate cancer: correlations between pretherapeutic imaging and whole-body tumor dosimetry with treatment outcomes. *J Nucl Med*. 2019;60:517–523.
40. Lawal I, Vorster M, Boshomane T, Oloade K, Ebenhan T, Sathegke M. Metastatic prostate carcinoma presenting as a superscan on Ga-68-PSMA PET/CT. *Clin Nucl Med*. 2015;40:755–756.
41. Sgouros G, Graham MC, Divgi CR, Larson SM, Scheinberg DA. Modeling and dosimetry of monoclonal antibody M195 (anti-CD33) in acute myelogenous leukemia. *J Nucl Med*. 1993;34:422–430.
42. Glatting G, Bardies M, Lassmann M. Treatment planning in molecular radiotherapy. *Z Med Phys*. 2013;23:262–269.
43. Frey E, He B, Sgouros G, Flinn I, Wahl R. Estimation of post-therapy marrow dose rate in myeloablative Y-90 ibritumomab tiuxetan therapy. *J Nucl Med*. 2006;47(suppl 1):156P.
44. Wahl RL, Zasadny KR, MacFarlane D, et al. Iodine-131 anti-B1 antibody for B-cell lymphoma: an update on the Michigan Phase I experience. *J Nucl Med*. 1998;39(8, Suppl):21S–27S.
45. Hobbs RF, Song H, Watchman CJ, et al. A bone marrow toxicity model for ²²³Ra alpha-emitter radiopharmaceutical therapy. *Phys Med Biol*. 2012;57:3207–3222.
46. Grant D, Bjerke R, Wittke K, et al. Pharmacokinetics and dosimetry of BAY 1862864, an alpha-emitting targeted thorium conjugate (CD22-TTC) in the Cynomolgus monkey. *Eur J Nucl Med Mol Imaging*. 2018;45:S124.
47. Sgouros G, Allen BJ, Back T, et al. *MIRD Monograph: Radiobiology and Dosimetry for Radiopharmaceutical Therapy with Alpha-Particle Emitters*. Sgouros G, ed. Reston VA: Society of Nuclear Medicine and Molecular Imaging; 2015.
48. Kaminski MS, Radford JA, Gregory SA, et al. Re-treatment with I-131 tositumomab in patients with non-Hodgkin's lymphoma who had previously responded to I-131 tositumomab. *J Clin Oncol*. 2005;23:7985–7993.
49. Passalacqua S, Natwa M, Chen M-K, et al. Relationship of marrow radiation dose and timing of engraftment for targeted radioimmunotherapy with anti-CD45 iodine (¹³¹I) apamistamb [Iomab-B] in patients with active relapsed or refractory acute myeloid leukemia. *J Nucl Med*. 2021;62(suppl 1):82.
50. Kim J, Jung Y. Radiation-induced liver disease: current understanding and future perspectives. *Exp Mol Med*. 2017;49:e359.
51. Wahl RL, Frey EC, Jacene HA, et al. Prospective SPECT-CT organ dosimetry-driven radiation-absorbed dose escalation using the in-111 (111In)/yttrium 90 (90Y) ibritumomab tiuxetan (Zevalin®) theranostic pair in patients with lymphoma at myeloablative dose levels. *Cancers (Basel)*. 2021;13:2828.
52. Quach A, Ji L, Mishra V, et al. Thyroid and hepatic function after high-dose 131I-metaiodobenzylguanidine (131I-MIBG) therapy for neuroblastoma. *Pediatr Blood Cancer*. 2011;56:191–201.
53. Matthay KK, Weiss B, Villablanca JG, et al. Dose escalation study of no-carrier-added 131I-metaiodobenzylguanidine for relapsed or refractory neuroblastoma: new approaches to neuroblastoma therapy consortium trial. *J Nucl Med*. 2012;53:1155–1163.
54. Chiesa C, Mira M, Maccauro M, et al. A dosimetric treatment planning strategy in radioembolization of hepatocarcinoma with 90Y glass microspheres. *Q J Nucl Med Mol Imaging*. 2012;56:503–508.
55. Strigari L, Sciuto R, Rea S, et al. Efficacy and toxicity related to treatment of hepatocellular carcinoma with 90Y-SIR spheres: radiobiologic considerations. *J Nucl Med*. 2010;51:1377–1385.
56. Garin E, Tzelikas L, Guuu B, et al. Major impact of personalized dosimetry using ⁹⁰Y loaded glass microspheres SIRT in HCC: Final overall survival analysis of a multicenter randomized phase II study (DOSISPHERE-01). *J Clin Oncol*. 2020;38(4, suppl):516.
57. Walrand S, Hesse M, Chiesa C, Lhommel R, Jamar F. The low hepatic toxicity per Gray of ⁹⁰Y glass microspheres is linked to their transport in the arterial tree favoring a nonuniform trapping as observed in posttherapy PET imaging. *J Nucl Med*. 2014;55:135–140.
58. Lam M, Salem R, Garin E. Abstract No. LB02 A global study of advanced dosimetry in the treatment of hepatocellular carcinoma with Yttrium-90 glass microspheres: analyses from the TARGET study. *J Vasc Interv Radiol*. 2021;32:S42.
59. Oehme L, Dorr W, Wust P, Kotzerke J. [Influence of time-dose-relationships in therapeutic nuclear medicine applications on biological effectiveness of irradiation: consequences for dosimetry]. *Nucl Med (Stuttg)*. 2008;47:205–209.
60. Garske-Román U, Sandström M, Fröss Baron K, et al. Prospective observational study of (177)Lu-DOTA-octreotate therapy in 200 patients with advanced metastasized neuroendocrine tumours (NETs): feasibility and impact of a dosimetry-guided study protocol on outcome and toxicity. *Eur J Nucl Med Mol Imaging*. 2018;45:970–988.
61. Del Prete M, Buteau F-A, Arsenaault F, et al. Personalized ¹⁷⁷Lu-octreotate peptide receptor radionuclide therapy of neuroendocrine tumours: initial results from the P-PRRT trial. *Eur J Nucl Med Mol Imaging*. 2019;46:728–742.
62. Vegt E, de Jong M, Wetzels JF, et al. Renal toxicity of radiolabeled peptides and antibody fragments: mechanisms, impact on radionuclide therapy, and strategies for prevention. *J Nucl Med*. 2010;51:1049–1058.
63. Hofman MS, Emmett L, Sandhu S, et al. [¹⁷⁷Lu]Lu-PSMA-617 versus cabazitaxel in patients with metastatic castration-resistant prostate cancer (TheraP): a randomised, open-label, phase 2 trial. *Lancet*. 2021;397:797–804.
64. Rolleman EJ, Valkema R, de Jong M, Kooij PP, Krenning EP. Safe and effective inhibition of renal uptake of radiolabelled octreotide by a combination of lysine and arginine. *Eur J Nucl Med Mol Imaging*. 2003;30:9–15.
65. Strosberg J, El-Haddad G, Wolin E, et al. Phase 3 Trial of (177)Lu-Dotatate for Midgut Neuroendocrine Tumors. *N Engl J Med*. 2017;376:125–135.
66. Kwekkeboom DJ, Teunissen JJ, Bakker WH, et al. Radiolabeled somatostatin analog [¹⁷⁷Lu-DOTA0,Tyr3]octreotate in patients with endocrine gastroenteropancreatic tumors. *J Clin Oncol*. 2005;23:2754–2762.
67. Kratochwil C, Giesel FL, Leotta K, et al. PMPA for nephroprotection in PSMA-targeted radionuclide therapy of prostate cancer. *J Nucl Med*. 2015;56:293–298.
68. Violet J, Sandhu S, Irvani A, et al. Long term follow-up and outcomes of re-treatment in an expanded 50 patient single-center phase II prospective trial of ¹⁷⁷Lu-PSMA-617 theranostics in metastatic castrate-resistant prostate cancer. *J Nucl Med*. 2020;61:857–865.
69. Violet J, Jackson P, Ferdinandus J, et al. Dosimetry of (177)Lu-PSMA-617 in metastatic castration-resistant prostate cancer: correlations between pretherapeutic imaging and whole-body tumor dosimetry with treatment outcomes. *J Nucl Med*. 2019;60:517–523.
70. Nakada K, Ishibashi T, Takei T, et al. Does lemon candy decrease salivary gland damage after radioiodine therapy for thyroid cancer? *J Nucl Med*. 2005;46:261–266.
71. Jentzen W, Schneider E, Freudenberg L, et al. Relationship between cumulative radiation dose and salivary gland uptake associated with radioiodine therapy of thyroid cancer. *Nucl Med Commun*. 2006;27:669–676.
72. Jentzen W, Balschweid T, Schmitz J, et al. The influence of saliva flow stimulation on the absorbed radiation dose to the salivary glands during radioiodine therapy of thyroid cancer using 124 I PET (CT) imaging. *Eur J Nucl Med Mol Imaging*. 2010;37:2298–2306.
73. Eisbruch A, Ten Haken RK, Kim HM, Marsh LH, Ship JA. Dose, volume, and function relationships in parotid salivary glands following conformal and intensity-modulated irradiation of head and neck cancer. *Int J Radiat Oncol Biol Phys*. 1999;45:577–587.
74. Okamoto S, Thieme A, Allmann J, et al. Radiation dosimetry for (177)Lu-PSMA I&T in metastatic castration-resistant prostate cancer: absorbed dose in normal organs and tumor lesions. *J Nucl Med*. 2017;58:445–450.
75. Rupp NJ, Umbricht CA, Pizzuto DA, et al. First clinicopathologic evidence of a non-psma-related uptake mechanism for (68)Ga-PSMA-11 in salivary glands. *J Nucl Med*. 2019;60:1270–1276.
76. Zechmann CM, Afshar-Oromieh A, Armor T, et al. Radiation dosimetry and first therapy results with a 124 I/131 I-labeled small molecule (MIP-1095) targeting PSMA for prostate cancer therapy. *Eur J Nucl Med Mol Imaging*. 2014;41:1280–1292.
77. Delker A, Fendler WP, Kratochwil C, et al. Dosimetry for 177 Lu-DKFZ-PSMA-617: a new radiopharmaceutical for the treatment of metastatic prostate cancer. *Eur J Nucl Med Mol Imaging*. 2016;43:42–51.
78. Peters SM, Privé BM, de Bakker M, et al. Intra-therapeutic dosimetry of [¹⁷⁷Lu] Lu-PSMA-617 in low-volume hormone-sensitive metastatic prostate cancer patients and correlation with treatment outcome. *Eur J Nucl Med Mol Imaging*. July 4, 2021 [Epub ahead of print].
79. Feurecker B, Tauber R, Knorr K, et al. Activity and adverse events of actinium-225-PSMA-617 in advanced metastatic castration-resistant prostate cancer after failure of lutetium-177-PSMA. *Eur Urol*. 2021;79:343–350.
80. Tagawa ST, Osborne J, Fernandez E, et al. Phase I dose-escalation study of PSMA-targeted alpha emitter ²²⁵Ac-1591 in men with metastatic castration-resistant prostate cancer (mCRPC). *J Clin Oncol*. 2020;38(15, suppl):5560.
81. Irvani A, Violet J, Azad A, Hofman MS. Lutetium-177 prostate-specific membrane antigen (PSMA) theranostics: practical nuances and intricacies. *Prostate Cancer Prostatic Dis*. 2020;23:38–52.
82. Harsini S, Saprunoff H, Alden T, Mohammadi B, Wilson D, Benard F. The effects of monosodium glutamate on PSMA radiotracer uptake in men with recurrent prostate cancer: a prospective, randomized, double-blind, placebo-controlled intraindividual imaging study. *J Nucl Med*. 2021;62:81–87.
83. Sgouros G, Song H, Ladenson PW, Wahl RL. Lung toxicity in radioiodine therapy of thyroid carcinoma: development of a dose-rate method and dosimetric implications of the 80-mCi rule. *J Nucl Med*. 2006;47:1977–1984.
84. Hobbs RF, Wahl RL, Lodge MA, et al. ¹²⁴I PET-based 3D-RD dosimetry for a pediatric thyroid cancer patient: real-time treatment planning and methodologic comparison. *J Nucl Med*. 2009;50:1844–1847.

85. Benua RS, Cicale NR, Sonenberg M, Rawson R. The relation of radioiodine dosimetry to results and complications in the treatment of metastatic thyroid cancer. *Am J Roentgenol Radium Ther Nucl Med.* 1962;87:171–182.
86. Press OW, Eary JF, Appelbaum FR, et al. Radiolabeled-antibody therapy of B-cell lymphoma with autologous bone marrow support. *N Engl J Med.* 1993;329:1219–1224.
87. Ho S, Lau W, Leung T, Chan M, Johnson P, Li A. Clinical evaluation of the partition model for estimating radiation doses from yttrium-90 microspheres in the treatment of hepatic cancer. *Eur J Nucl Med.* 1997;24:293–298.
88. Waselenko JK, MacVittie TJ, Blakely WF, et al. Medical management of the acute radiation syndrome: recommendations of the Strategic National Stockpile Radiation Working Group. *Ann Intern Med.* 2004;140:1037–1051.
89. Anno GH, Young R, Bloom R, Mercier J. Dose response relationships for acute ionizing-radiation lethality. *Health Phys.* 2003;84:565–575.
90. Wong JY, Filippi AR, Dabaja BS, Yahalom J, Specht L. Total body irradiation: guidelines from the international lymphoma radiation oncology group (ILROG). *Int J Radiat Oncol Biol Phys.* 2018;101:521–529.
91. Pandit-Taskar N, Zanzonico P, Hilden P, Ostrovnyaya I, Carrasquillo JA, Modak S. Assessment of organ dosimetry for planning repeat treatments of high-dose ¹³¹I-MIBG therapy: ¹²³I-MIBG vs. post-therapy ¹³¹I-MIBG imaging. *Clin Nucl Med.* 2017;42:741.
92. Kaminski MS, Zasadny KR, Francis IR, et al. Iodine-131-anti-B1 radioimmunotherapy for B-cell lymphoma. *J Clin Oncol.* 1996;14:1974–1981.
93. Kaminski MS, Estes J, Zasadny KR, et al. Radioimmunotherapy with iodine 131I tositumomab for relapsed or refractory B-cell non-Hodgkin lymphoma: updated results and long-term follow-up of the University of Michigan experience. *Blood.* 2000;96:1259–1266.
94. Jairam V, Roberts KB, James BY. Historical trends in the use of radiation therapy for pediatric cancers: 1973–2008. *Int J Radiat Oncol Biol Phys.* 2013;85(3):e151–e155.
95. Jacene H, Crandall J, Kasamon YL, et al. Initial experience with tositumomab and I-131-labeled tositumomab for treatment of relapsed/refractory Hodgkin lymphoma. *Mol Imaging Biol.* 2017;19:429–436.
96. Clement SC, Peeters R, Ronckers C, et al. Intermediate and long-term adverse effects of radioiodine therapy for differentiated thyroid carcinoma—a systematic review. *Cancer Treat Rev.* 2015;41:925–934.
97. Lang BH, Wong IO, Wong KP, Cowling BJ, Wan KY. Risk of second primary malignancy in differentiated thyroid carcinoma treated with radioactive iodine therapy. *Surgery.* 2012;151:844–850.
98. Krassas GE, Pontikides N. Gonadal effect of radiation from ¹³¹I in male patients with thyroid carcinoma. *Arch Androl.* 2005;51:171–175.
99. Molenaar RJ, Sidana S, Radivoyevitch T, et al. Risk of hematologic malignancies after radioiodine treatment of well-differentiated thyroid cancer. *J Clin Oncol.* 2018;36:1831–1839.
100. Clement SC, Kraal K, van Eck-Smit B, et al. Primary ovarian insufficiency in children after treatment with ¹³¹I-metaiodobenzylguanidine for neuroblastoma: report of the first two cases. *J Clin Endocrinol Metab.* 2014;99:E112–E116.
101. Shadman M, Li H, Rimsza L, et al. Continued excellent outcomes in previously untreated patients with follicular lymphoma after treatment with CHOP plus rituximab or CHOP plus ¹³¹I-tositumomab: long-term follow-up of phase III randomized study SWOG-S0016. *J Clin Oncol.* 2018;36:697.
102. Chantadisai M, Kulkarni H, Baum R. Therapy-related myeloid neoplasm after peptide receptor radionuclide therapy (PRRT) in 1631 patients from our 20 years of experiences: Prognostic parameters and overall survival. *Eur J Nucl Med Mol Imaging.* 2021;48:1390–1398.
103. Bodei L, Kidd M, Paganelli G, et al. Long-term tolerability of PRRT in 807 patients with neuroendocrine tumours: the value and limitations of clinical factors. *Eur J Nucl Med Mol Imaging.* 2015;42:5–19.
104. Brieau B, Hentic O, Lebtahi R, et al. High risk of myelodysplastic syndrome and acute myeloid leukemia after ¹⁷⁷Lu-octreotate PRRT in NET patients heavily pretreated with alkylating chemotherapy. *Endocr Relat Cancer.* 2016;23:L17–L23.
105. Hobbs RF, McNutt T, Baechler S, et al. A treatment planning method for sequentially combining radiopharmaceutical therapy and external radiation therapy. *Int J Radiat Oncol Biol Phys.* 2011;80:1256–1262.
106. Baechler S, Hobbs RF, Jacene HA, Bochud FO, Wahl RL, Sgouros G. Predicting hematologic toxicity in patients undergoing radioimmunotherapy with ⁹⁰Y-ibritumomab tiuxetan or ¹³¹I-tositumomab. *J Nucl Med.* 2010;51:1878–1884.
107. Seibold P, Auvinen A, Averbek D, et al. Clinical and epidemiological observations on individual radiation sensitivity and susceptibility. *Int J Radiat Biol.* 2020;96:324–339.
108. Ahmed MM, Coleman CN, Mendonca M, et al. Workshop report for cancer research: Defining the shades of Gy: Utilizing the biological consequences of radiotherapy in the development of new treatment approaches—meeting viewpoint. *Cancer Res.* 2018;78:2166–2170.
109. Eichholtz-Wirth H, Sagan D. Altered signaling of TNFalpha-TNFR1 and SODD/BAG4 is responsible for radioresistance in human HT-R15 cells. *Anticancer Res.* 2002;22(1A):235–240.
110. John-Aryankalayil M, Palayoor ST, Makinde AY, et al. Fractionated radiation alters oncomir and tumor suppressor miRNAs in human prostate cancer cells. *Radiat Res.* 2012;178:105–117.
111. Buchwald ZS, Wynne J, Nasti TH, et al. Radiation, immune checkpoint blockade and the abscopal effect: a critical review on timing, dose and fractionation. *Front Oncol.* 2018;8:612.
112. Sangro B, Gil-Alzugaray B, Rodriguez J, et al. Liver disease induced by radioembolization of liver tumors: description and possible risk factors. *Cancer.* 2008;112:1538–1546.
113. Trip AK, Sikorska K, van Sandick JW, et al. Radiation-induced dose-dependent changes of the spleen following postoperative chemoradiotherapy for gastric cancer. *Radiother Oncol.* 2015;116:239–244.
114. Verburg FA, Stokkel MP, Düren C, et al. No survival difference after successful ¹³¹I ablation between patients with initially low-risk and high-risk differentiated thyroid cancer. *Eur J Nucl Med Mol Imaging.* 2010;37:276–283.
115. Hartung-Knemeyer V, Nagarajah J, Jentzen W, et al. Pre-therapeutic blood dosimetry in patients with differentiated thyroid carcinoma using ¹²⁴I-iodine: predicted blood doses correlate with changes in blood cell counts after radioiodine therapy and depend on modes of TSH stimulation and number of preceding radioiodine therapies. *Ann Nucl Med.* 2012;26:723–729.

An International Study of Factors Affecting Variability of Dosimetry Calculations, Part 1: Design and Early Results of the SNMMI Dosimetry Challenge

Carlos Uribe^{1,2}, Avery Peterson³, Benjamin Van³, Roberto Fedrigo⁴, Jake Carlson⁵, John Sunderland⁶, Eric Frey^{*7,8}, and Yuni K. Dewaraja^{*3}

¹Functional Imaging, BC Cancer, Vancouver, British Columbia, Canada; ²Department of Radiology, University of British Columbia, Vancouver, British Columbia, Canada; ³Department of Radiology, University of Michigan Medical School, Ann Arbor, Michigan; ⁴Department of Integrative Oncology, BC Cancer Research Institute, Vancouver, British Columbia, Canada; ⁵U-M Library, University of Michigan, Ann Arbor, Michigan; ⁶Department of Radiology, University of Iowa, Iowa City, Iowa; ⁷Radiological Physics Division, Johns Hopkins University, Baltimore, Maryland; and ⁸Rapid, LLC, Baltimore, Maryland

In this work, we present details and initial results from a ¹⁷⁷Lu dosimetry challenge that has been designed to collect data from the global nuclear medicine community aiming at identifying, understanding, and quantitatively characterizing the consequences of the various sources of variability in dosimetry. **Methods:** The challenge covers different approaches to performing dosimetry: planar, hybrid, and pure SPECT. It consists of 5 different and independent tasks to measure the variability of each step in the dosimetry workflow. Each task involves the calculation of absorbed doses to organs and tumors and was meant to be performed in sequential order. The order of the tasks is such that results from a previous one would not affect subsequent ones. Different sources of variability are removed as the participants advance through the challenge by giving them the data required to begin the calculations at different steps of the dosimetry workflow. Data from 2 patients after a therapeutic administration of ¹⁷⁷Lu-DOTATATE were used for this study. The data are hosted in Deep Blue Data, a data repository service run by the University of Michigan. Participants submit results in standardized spreadsheets and with a short description summarizing their methods. **Results:** In total, 178 participants have signed up for the challenge, and 119 submissions have been received. Sixty percent of submissions have used voxelized dose methods, with 47% of those using commercial software. In initial analysis, the volume of organs showed a variability of up to 49.8% whereas for lesions this was up to 176%. Variability in time-integrated activity was up to 192%. Mean absorbed doses varied up to 57.7%. Segmentation is the step that required the longest time to complete, with a median of 43 min. The median total time to perform the full calculation was 89 min. **Conclusion:** To advance dosimetry and encourage its routine use in radiopharmaceutical therapy applications, it is critical that dosimetry results be reproducible across centers. Our initial results provide insights into the variability associated with performing dose calculations. It is expected that this dataset, including results from future stages, will result in efforts to standardize and harmonize methods and procedures.

Key Words: dosimetry; radiopharmaceutical therapies; variability; ¹⁷⁷Lu; SPECT/CT; neuroendocrine tumors

J Nucl Med 2021; 62:36S–47S
DOI: 10.2967/jnumed.121.262748

Radiopharmaceutical therapies (RPTs) have demonstrated clinical utility in the treatment of disease such as thyroid, liver, neuroblastoma, neuroendocrine, lymphatic, and prostate cancers (1). Also, a new wave of theranostic radiopharmaceuticals (i.e., therapeutic and diagnostic) with highly specific molecular targeting for these and other cancers is entering clinical trials (2,3). This relatively new paradigm for treatment of widely metastatic cancer using radiopharmaceuticals has some advantages compared with other systemic therapies. The theranostics approach permits imaging of the biodistribution of the radiopharmaceutical, thus allowing physicians to treat what they see and see what they treat. Quantitative imaging has the potential to assess whether the binding of the radiopharmaceutical to a target of interest (e.g., a protein in the membrane of a cancer cell or a molecule involved in biochemical or metabolic cellular pathways) warrants targeted RPT. Imaging during or after treatment allows us to quantitatively assess the response to the therapy (e.g., by measuring decreasing uptake of responding tumors). Nuclear medicine imaging modalities, such as PET and SPECT, can provide quantitative 3-dimensional images representing the biodistribution, which is needed for dose estimation.

Quantitative 3-dimensional imaging is the basis of dosimetry calculations that estimate the amount of radiation dose (energy per unit mass) delivered to different tissues. Personalized dose assessments potentially facilitate optimizing treatment response by delivering the maximum possible dose to tumors while simultaneously monitoring the radiation dose to healthy organs and keeping them below toxic thresholds.

Despite this potential, RPT in clinical practice is most commonly administered using a simpler, nonpersonalized approach that ignores the potential for dose optimization based on imaging. Typically, and according to the U.S. Food and Drug Administration package inserts for most therapeutic radiopharmaceuticals, patients are administered the same activity on each therapy cycle; this approach does not account for individual differences in metabolic clearance or uptake of the radiopharmaceutical or anatomy. Moreover, dosimetry is also not routinely performed because it is

Received Jun. 23, 2021; revision accepted Sep. 30, 2021.
For correspondence or reprints, contact Carlos Uribe (curibe@bccrc.ca).
*Contributed equally to this work.
COPYRIGHT © 2021 by the Society of Nuclear Medicine and Molecular Imaging.

believed to be difficult and time-consuming, requires expertise or staff that is not always available, and is not reimbursed.

The Committee on MIRD of the Society of Nuclear Medicine and Molecular Imaging (SNMMI) has developed a general framework for absorbed dose calculation at the organ, suborgan, voxel, and cellular levels (4). Guidelines for dose estimation using planar imaging, hybrid (SPECT plus planar), and multi-SPECT imaging workflows have also been published (5,6). The latest in this series, guidelines for image quantification of ^{177}Lu using SPECT/CT (7), was published in 2016 as a collaboration between the MIRD committee and the dosimetry committee of the European Association of Nuclear Medicine.

The MIRD schema is straightforward, and the European Association of Nuclear Medicine has published guidelines for systematic ways to account for the impact of factors that affect bias and variability (precision) in dose calculations (8). There remains, however, a scarcity of data on variability, and this scarcity has complicated the goal of incorporating uncertainty estimation into dosimetry practice. Variability of absorbed dose results between different centers, practitioners, and patients is a key concern for dose-based treatment planning. This lack of knowledge of uncertainty has made it difficult to draw rigorous inferences about the robustness of dose–response relationships and to compare and combine data from different institutions and agents. Lack of these data has inhibited routine clinical implementation and complicated initiatives targeting reimbursement for dosimetry and dosimetry-based treatment planning.

The dosimetry workflow includes 5 general steps. In the first—data acquisition—quantitative SPECT images, planar images, or a combination of planar and SPECT images are acquired at multiple time points after the administration of the radiopharmaceutical. In the second—segmentation and registration—tissues of interest (e.g., tumors and organs at risk) are delineated (segmented) to define volumes of interest (VOIs) used in the analysis. Various methods are available to perform this segmentation and to register images acquired at multiple time points.

In the third step—data preparation—standard phantom dosimetry applies S values calculated using reference computational phantoms (9,10) that represent the average population anatomy. In this method, activities for tissues of interest (e.g., organs or tumors) are extracted from images. One approach to patient-specific, organ-level dosimetry is to calculate dose at the voxel level using activity and tissue maps based on imaging calculations from exact, individualized patient anatomy based on imaging (e.g., CT); dose rate maps (3-dimensional images of the dose deposited per unit time) are calculated from the activity images. In these approaches, organ-level dose rates can be calculated by averaging over tissues of interest.

The fourth step is integration. In standard-phantom dosimetry, the activities are integrated over time to obtain time-integrated activity (TIA) values. In some approaches to patient-specific dosimetry, activity images are integrated at the voxel level to form TIA images; in other approaches, dose rate images are integrated over time to calculate absorbed dose maps (3-dimensional images of the absorbed dose). The integration often involves the use of curve fitting.

The fifth step is dose calculation. In standard phantom dosimetry, S factors are combined with TIA values to calculate tissue-specific absorbed doses. In some patient-specific approaches, dose maps are calculated from TIA images using either Monte Carlo simulations or convolution with a precalculated dose kernel. Dose maps provide an estimate of absorbed dose in each voxel of the

image (i.e., a voxelized approach). Regions of interest within the dose map can be used to provide different statistical values for absorbed dose within the tissue (e.g., the mean absorbed dose to the organ or tumor).

Variation in methods or application in any of these steps can result in variation in dose estimates for the same patient. Variability in the nuclear medicine images (from calibration, imaging, and reconstruction protocol, including compensations for image-degrading factors, or quantum noise) directly affects the variability of dose estimates. Variability in defining tissue VOIs leads to variability in both activity and mass estimates. Variation in methods for integrating the time–activity or time–dose-rate curves also contribute to variability in dose estimates. Variation in the dose calculation method or code, such as the S factors used, can also result in variations in dose estimates.

This is the first installment of multiple planned publications reporting on the ^{177}Lu SNMMI Dosimetry Challenge. Here, we present details of the methodology used to conduct the challenge, including the design, the data used, the hosting of the data, and the variables collected. The challenge has gathered data from the global nuclear medicine community and aimed at identifying, understanding, and quantitatively characterizing the consequences of the multiple sources of variability in the dosimetry calculation pipeline. The challenge covers planar, hybrid, and pure SPECT dosimetry workflows using 5 different and independent tasks. For each participant and task, the study collects, among other variables, information about the methods used to perform the various steps of the dosimetry workflow, the software used, and the time required to perform the calculations. Having data on the magnitude of the various sources of variability is essential in developing harmonized and standardized dosimetry workflows that reduce variability. Reduced variability would allow for more precise, predictable, and repeatable therapeutic regimens and outcomes. The major goal of this study is to acquire such data.

Besides detailing the experimental methodology, this first publication summarizes the demographics of participants, categorizes and tabulates the general dosimetry approaches, and reports on the types of software used. Additionally, descriptive statistics associated with the uncurated absorbed dose calculation results from task 1 as submitted by the participants are reported. These data highlight the problem of variability in absorbed doses and other measured quantities in the dosimetry workflow. Further analysis of the correlations between different variables in the dosimetry workflow, a quantitative analysis as sources of variability are removed as the challenge progresses through tasks 2–5, and a detailed comparison of results calculated with different dosimetry approaches (i.e., planar vs. multiple SPECT/CT vs. hybrid approaches) will follow in the subsequent publications.

This dosimetry challenge focused on dosimetry for ^{177}Lu -labeled therapy for neuroendocrine tumors, but the methodology developed could be applied in subsequent studies involving dosimetry calculations for RPTs using different radionuclides or targeting different diseases.

MATERIALS AND METHODS

Study Design

This study has been designed to measure the variability contributed by each step in the dosimetry workflow. However, variability in data acquisition is limited to comparison of pure SPECT, hybrid SPECT–planar, and planar-only acquisition protocols. Variability due

to other aspects of data acquisition is important but is beyond the scope of what could be achieved in the time frame or with the resources available. The study was designed to accommodate a standard phantom and patient-specific dosimetry workflows at both the tissue and the voxel levels. Five discrete and independent tasks, each involving calculation of organ- and tumor-absorbed doses but starting at different points in the dosimetry workflow, were created for the study. Figure 1 shows schematically the tasks and the parts of the different workflow variability that is targeted by each task. The tasks were meant to be performed in sequential order and are summarized in Table 1. Pretherapy diagnostic image sets (CT or MRI) were provided to aid in delineation of organs and tumors. The order of the tasks and the provision of data were designed so that results from an earlier task would not affect the results of a subsequent one. Also, different sources of variability were removed as the participants advanced through the challenge (Fig. 1). We intentionally did not specify the methods or software to be used by participants.

Tasks 1, 4, and 5 each used 4 sequential ^{177}Lu -DOTATATE SPECT/CT datasets acquired after therapeutic injection. The reconstructed SPECT images had voxel values in units of activity concentration (Bq/mL). Thus, the results of these 3 challenge tasks focus exclusively on the absorbed dose calculation workflow and purposely exclude variability and bias due to SPECT acquisition protocols, calibration, reconstruction, or quantification. This variability outside the absorbed dose calculation workflow can affect the results in 2 ways. First, variability in input data for differences in these factors would directly increase variability in the output dose values. Second, there could also be indirect effects. For example, image quantification, resolution, contrast, and noise properties are dependent on the scanner hardware and on the image acquisition and reconstruction protocols. Variability in these properties could result in, for example, variability between operators in defining VOIs and the resulting absorbed dose calculations.

In tasks 1–3, participants were asked to perform the entire dosimetry workflow, from segmenting images to absorbed dose calculations. Participants were asked to identify their VOI delineation method. We did not require partial-volume correction (PVC), for several reasons. A main reason is that there is currently no single, well-accepted method for PVC at the organ or especially the voxel level. A practical,

widely used approach for organ- or tumor-level PVC is to apply volume-dependent recovery coefficients determined from phantom measurements. However, there are well-known limitations to using this approach, as recovery coefficients depend not only on volume but on other factors such as activity distribution and shape. For the purpose of this study, we thus treated PVC as part of the image acquisition, reconstruction, and quantification aspects of dosimetry, which are not addressed in this challenge. Neglecting PVC can cause large errors in dose estimates for small objects such as tumors. However, the interest here was in variability. It was emphasized in the instructions that applying PVC was not required but that if PVC was included, a description of the procedure should be added to the summary of the participant's methods. We collected the volume of the region used to quantify the activity in the image and the volume of the region used to estimate the mass.

In task 4, we removed the variability associated with segmentation by providing participants with VOIs in the form of DICOM-RT structures or mask images that were to be applied to the SPECT/CT data to calculate organ and tumor activities and subsequently the corresponding absorbed doses. However, specific time-activity curve generation, fitting and integration, and dose calculation methods were left to the discretion of the participant. The tumor segmentations provided were defined manually by a radiologist; organ segmentations were based on deep-learning tools with fine adjustment by experts. Since we were testing primarily variability, the accuracy of the segmentations is not a limiting factor.

The difference in results from tasks 1 and 4 allows isolation of the impact of VOI segmentation on the variability of absorbed dose estimates. In task 5, a time-integrated-activity image in units of Bq/mL-s was provided. Participants were instructed to use this in combination with the segmentations from task 4. For each participant, the difference in calculated absorbed dose between task 5 and task 4 isolates the impact of differences in curve fitting and integration on the absorbed dose estimate. Results for task 5 provide data about variability due to the dose calculation method or software.

Sequential planar acquisitions are sometimes used to estimate absorbed dose. Methods for quantifying organ and tumor activities in these images have not been well standardized and require several cascaded corrections with poorly understood variabilities and biases. To

mitigate some of these complexities, hybrid SPECT/planar methods use a single SPECT/CT scan at a time point coincident with one of a series of planar acquisitions to act as a quantitative calibration standard for the sequential planar data. Planar and hybrid methods are somewhat commonly used in clinical trials to reduce both acquisition time and, thus, cost and patient discomfort. Tasks 2 and 3 are designed to interrogate variability in absorbed dose estimates from these methods in comparison to pure SPECT-based methods.

Task 2 provided participants with a series of 4 ^{177}Lu -DOTATATE planar images (in units of counts) acquired after therapeutic injections (same patients and time points as for all other tasks). A sensitivity calibration factor was provided to convert in-air planar counts to activity. Participants were informed that the sensitivity data for the planar images were intentionally adjusted by a scaling factor (we used a factor of 2, which was unknown to participants) so that the results from task 1 (SPECT/CT) would not bias the results from

RGB

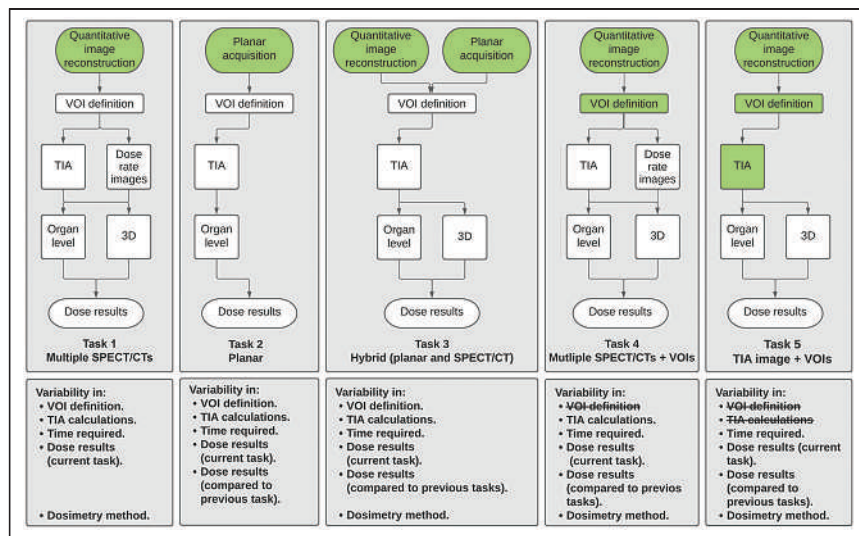


FIGURE 1. Overview of dosimetry challenge showing each task. Green boxes show data provided to participants in each task. In addition to these data, participants were provided with pretherapy diagnostic images (CT and MRI) to aid in organ and tumor delineation.

TABLE 1
Description of Different Tasks Compromising ¹⁷⁷Lu Dosimetry Challenge Including Data Provided and Measurable Quantities with Collected Data

Stage	Task	Data provided	What is being measured?
1	1	Quantitative SPECT/CT images at 4 time points after therapeutic injection	Variability in segmentation; variability in TIA; variability in dosimetry methods used (e.g., organ level vs. 3-dimensional dosimetry); time required to complete procedure; overall variability in dose results
2	2	Planar acquisitions at 4 points after therapeutic injection; all data available in task 1; calibration factor to convert counts to activity values	Variability in segmentation; variability in TIA; time required to complete procedure; variability in dose results from planar studies; variability in dose results compared with SPECT/CT from task 1
	3	Four planar acquisitions from task 2; single-time-point SPECT scan provided in task 1 (participants may use VOIs delineated in tasks 1 and 2)	Variability in segmentation; variability in TIA; variability in dosimetry methods used (e.g., organ level vs. 3-dimensional dosimetry); time required to complete procedure; variability in dose results from hybrid planar/SPECT/CT; variability in dose results compared with planar (task 2) and SPECT/CT (task 1)
3	4	All data from task 1; predefined VOIs for tumors and organs at risk	Variability in TIA; variability in dosimetry methods used (e.g., organ level vs. 3-dimensional dosimetry); time required to complete procedure; variability in dose results (no variability in segmentation); variability in dose results compared with task 1
4	5	All data from task 4; TIA image from task 1 SPECT images	Time required to complete procedure; variability in dose results; no variability in segmentation or TIA calculation

In addition to nuclear medicine image data provided for each task described in this table, pretherapy diagnostic images (i.e., diagnostic CT and MRI) were provided to facilitate delineation of tumors and organs.

task 2 (planar). It was incumbent on participants to select methods and perform corrections for scatter, attenuation, and other factors based on other data supplied (e.g., CT scans to estimate transmission factors). From task 2 entries, we anticipate not only understanding the variability in planar absorbed dose calculations but also having the ability to draw conclusions about differences in, and variability between, dose estimates as compared with dose estimates from the multiple SPECT/CT protocol from task 1.

Task 3 uses the 4 sequential planar scans from task 2 and a quantitative SPECT/CT dataset acquired at 24 h after injection. Differences in absorbed dose estimates between tasks 2 and 3 provide a measure of the difference in bias and variability associated with having the single SPECT/CT scan as a calibration standard for the planar images.

Datasets

All images were provided in DICOM format. Data from 2 patients (labeled A and B) who underwent a therapeutic administration of ¹⁷⁷Lu-DOTATATE were used for this study (11–15). The same data were provided to all participants.

For each patient, 4 quantitative SPECT/CT images were acquired on a Intevo system (Siemens Healthineers) as part of an internal review board–approved research study at the University of Michigan. The acquisition of 360 frames was performed using 3 energy windows (120 projection views per window over 360°), a main window (186–227 keV), and scatter windows (165–186 keV and 227–248 keV). Images were reconstructed using xSPECT Quant software (48 iterations, 1 subset, without a postreconstruction filter; Siemens), which includes compensation for attenuation, scatter, and the collimator detector response. A sensitivity factor from a National Institute of Standards and Technology–traceable ⁷⁵Se calibration source was applied by the scanner’s software to generate quantitative images (in units of Bq/mL) (16).

Details about the anonymized identifiers, therapeutic injection, acquired SPECT/CT and planar scans, and baseline and diagnostic scans are summarized in Table 2. These details were given to participants in the instructions and are also available in the DICOM headers of the shared images. No additional registration of the SPECT and CT images at each time point or between any image at different time points was performed. Participants were asked to estimate absorbed doses to each kidney, if possible, or to the kidneys as a whole, the spleen, healthy liver (i.e., the region of the liver without tumors), and specified tumors. Tumor locations were indicated on a fused SPECT/CT image provided in the instructions (Fig. 2). Patient B was splenectomized; no values are reported for this organ in this patient.

The planar images were acquired as part of the posttherapy imaging at the same time points as the SPECT scans. Transmission scans were not acquired, and the patient may have voided before the first scan. The provided diagnostic CT scan could be used to estimate the body thickness required for geometric mean attenuation compensation. The planar images were acquired with energy windows suitable for triple-energy-window scatter compensation.

Data Distribution

We looked for a centralized data library that could provide participants with access to the dataset, including images and metadata; allow the release of data needed for different stages at appropriate times during the study; and generate a digital object identifier and host the dataset beyond the end of the study, to allow use as a standard for future benchmarking methods and as a way to cite the data.

On the basis of these requirements, we selected Deep Blue Data (<https://deepblue.lib.umich.edu/data>), a data repository service run by the University of Michigan Library, to host the study data. Datasets, along with the associated documentation and metadata needed to discover, understand, and use the data, are deposited into Deep

TABLE 2

Summary of Anonymized Patient Identifiers, Injected Activity, Information About Date and Time of Injection, and Acquired Scans for Each of 2 Patient Datasets Used for Dosimetry Challenge

Patient	Anonymized patient identifier	Injected activity (GBq)	Date and time of injection	SPECT/CT and planar scans performed	Diagnostic scans performed
A	ANON54121	7.21	Nov 15, 2018, 9:22 AM	Day of treatment and days 1, 4, and 5 after treatment	Baseline MRI with contrast; ⁶⁸ Ga PET 185 d before baseline CT and 468 d before first SPECT/CT
B	ANON60350	7.31	May 15, 2019, 9:55 AM	Day of treatment and days 1, 4, and 8 after treatment	Baseline CT with contrast; ⁶⁸ Ga PET 36 d after baseline CT and 69 d before first SPECT/CT

Blue Data. The challenge data were released in 4 stages as indicated in Table 1.

Participants had access to data from all previous stages and were specifically asked not to let results from a previous task influence results for a subsequent one.

Data Collection

The challenge was initiated by the SNMMI Dosimetry Task Force. An invitation to participate was issued through e-mail announcements to membership, through the SNMMI website, and through informal communications with other relevant international organizations. Each participant in the challenge self-identified themselves, their profession, and their respective institution, with the understanding that results would be presented only in aggregate form.

To aid in the identification and diagnosis of problems and distinct sources of variability in absorbed dose calculations, participants were asked to provide intermediate results for each stage of the dosimetry workflow. Table 3 summarizes the data and variables collected. A protected spreadsheet having unprotected cells available for reporting results and for pasting screenshots of VOI definitions and curve-fit plots, as well as having pull-down menus for items with a discrete number of answers, was created for each challenge task and provided

to participants. In addition, to further understand possible outlier results, participants were asked to submit a page summarizing their methods and highlighting details of their procedures that might not have been covered in the collected variables.

Data Analysis

In this document, we are reporting only the demographics associated with the submission and early results from task 1, uninformed by subsequent tasks results. To show the variability in absorbed doses and other parameters of the dosimetry workflow, we calculated various descriptive statistics and generated various plots using data reported for task 1. All the results are presented in aggregated form. These data serve as a baseline for comparison of data from other tasks and include all sources of variability from all steps of the dosimetry workflow studied.

To understand the expertise of the submitters and the methods used, histograms of the self-reported professions of the submitters, the dosimetry method used (i.e., voxelized vs. organ level methods), the source of S factors, and the type of software used are shown.

To highlight the distribution and variability of the submitted results for task 1, violin plots of the volume of segmented regions, the reported TIA values, and the mean absorbed doses are shown. These plots are presented separately by patient and organ or tumor. Descriptive statistics including the minimum, mean, SD, and maximum, as well as the 25%, median, and 75% quartiles, were also calculated for the different distributions.

Because of limited resolution, activity in an organ can cover a larger region in the image than its physical size. A common method to compensate for this is to use a larger VOI to measure object activity and a smaller (more physically correct) region to estimate object volume or mass. Thus, we generated volume violin plots showing the distribution of volumes of the segmented VOIs used for activity and mass. Moreover, we generated bar plots that indicate whether the volumes used to measure the activity of an organ or tumor were identical to, smaller than, or bigger than those used to estimate the mass. In addition, some participants reported using a 4-mL sphere located inside an organ or tumor for which the absorbed dose was calculated; we account for this method separately within the bar plots.

Bar plots showing the functional forms used to fit the time-activity curve are shown for each organ and tumor.

Lastly, box plots with corresponding descriptive statistics are shown for the self-reported times required to perform the different steps of the dosimetry workflow.

The next publication resulting from the dosimetry challenge will include a more quantitative and comprehensive analysis of the variability of the absorbed dose using data from the different tasks of the challenge. Variance-component analysis based on mixed-effect models

RGB

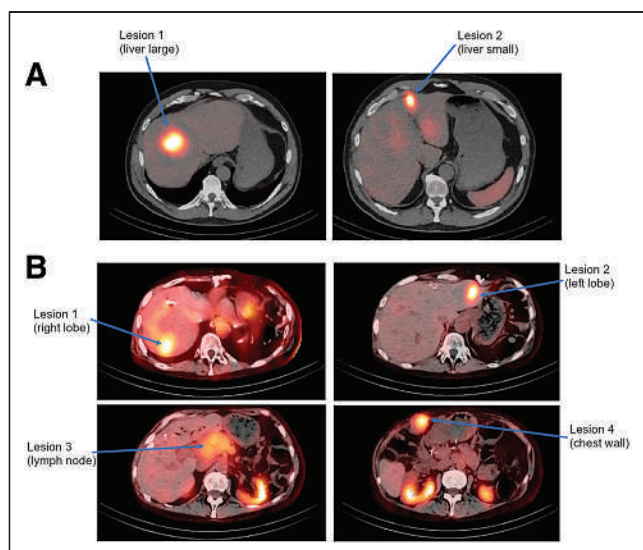


FIGURE 2. Specified tumor locations for patient A (A) and patient B (B), for whom participants were asked to calculate dose.

TABLE 3

Variables Collected in Submission Process, with Research Questions Expected to Be Answered with Those Variables

Category	Variables collected	Research questions asked
Expertise	Submitter title	Is procedure being performed by technologist, physicist, physician, or other?
Software and dosimetry type	Software used; type of dosimetry calculations performed; Monte Carlo code used (if applicable); S-factor source	Is voxelized or tissue-level dosimetry being performed? Is commercial software being used, or is in-house software being used? How are voxelized calculations performed, and what code is used for voxelized S-factor kernels?
VOI delineation	Image or images used for delineation; delineation method; threshold value (if fixed-threshold methods used); method for mass and activity determination; time needed; screenshots of generated VOIs	Are VOIs drawn using diagnostic pretherapy images, or only on SPECT, or only on therapeutic CT? Are manual, fixed thresholding, or AI methods used for segmentation? How were masses and activities of organ/tumor estimated? How much time does segmentation process take?
TIA generation	Method of integration; fit function; number of fit parameters; time needed; screenshots of time–activity curves	Are fits being performed using exponential, biexponential, or other types of functions? What is variability in TIA? How much time is required to perform this step of procedure?
Dose results	Volume of organ/tumor; mass of organ/tumor; total measured activity at each scan time-point; values of fit parameters; units of fit parameters; mean dose rates of each organ at each scan time-point; dose results; radiobiology results if applicable	What is variability in fit parameters? What is variability in mass and activity values measured in organs/tumors? What is variability in dose values and dose rates (if applicable)? How common is it to see radiobiology metrics reported? How do they vary?

will be used to assess the relative contribution of each factor—such as software, VOI delineation method, and TIA generation method—to the variability in the absorbed dose calculation. Regression analysis will be performed to study the impact of these factors on dose results. We expect to provide guidance to the community about the areas on which efforts should be focused for standardization.

RESULTS

Here, we show preliminary results for task 1 and summarize the data as reported by the participants. We have performed initial vetting of the data to make sure that items were reported in the correct cells of the spreadsheet and that obvious unit errors were not present. When these were identified, we confirmed the results with the participant and have reported the updated values. More complete vetting of the data and detailed statistical analysis that identifies and characterizes more fully the magnitude of sources of variability will be published in part 2 of this study after data from all 5 tasks are collected and analyzed.

At the time of writing of this article, a total of 178 individuals had registered. We had received 119 submissions corresponding to 61 and 58 spreadsheets for patients A and B, respectively. A submission represents a received spreadsheet filled out by a participant. Each spreadsheet contains fillable cells for all the variables presented in Table 3. However, the numbers of the results presented for a particular item do not necessarily add to 119 as some participants did not report all the variables. Submitters, including their country and institution, can be found in the Acknowledgments section of this document. Several participants registered independently but submissions were made as part of a group.

Figure 3A shows the expertise of the participants who submitted data. The values in the graph do not add up to the number of

submissions received for each patient as some of the participants submitted results using more than one dosimetry method.

Figure 3B shows the distribution of dosimetry methods used. Sixty percent of submissions used a voxelized approach. Organ-level approaches using precalculated S factors from a standard phantom accounted for 32% of submissions. Two submissions performed an organ-level approach but used a patient-specific mesh in combination with a Monte Carlo simulation. Four submissions reported calculating the dose to a 4-mL sphere placed inside the organ or tumor (i.e., did not segment the entire organ). Lastly, 4 submissions did not include information that would allow us to classify the method as organ- or voxel-based.

Figure 3C shows the distribution of S-factor sources based on submissions that reported using organ-level approaches. From these, 69% used OLINDA (17), and 60% of those used version 1 (including versions 1.0 and 1.1), 24% used version 2 (Hermes Medical Solutions, Sweden) (including versions 2.0, 2.1, and 2.2), 8% used only the OLINDA spheres models, and the remaining 8% used OLINDA in combination with other S-factor sources. The IDAC software (18), which follows International Commission on Radiological Protection publication 133 (19), accounted for 19% of submissions. Two submissions used OpenDose (20) in combination with factors published by Olguin et al. (21) for the tumors. Two submissions reported using local energy deposition instead of S factors. Lastly, 6 submissions are not included in Figure 3C as they reported also using local-energy-deposition–estimated doses using 4-mL spheres drawn within the organ or tumor.

Figure 3D shows the type of software used in voxelized dosimetry approaches. The commercial category includes submissions that performed their dosimetry calculation using commercially

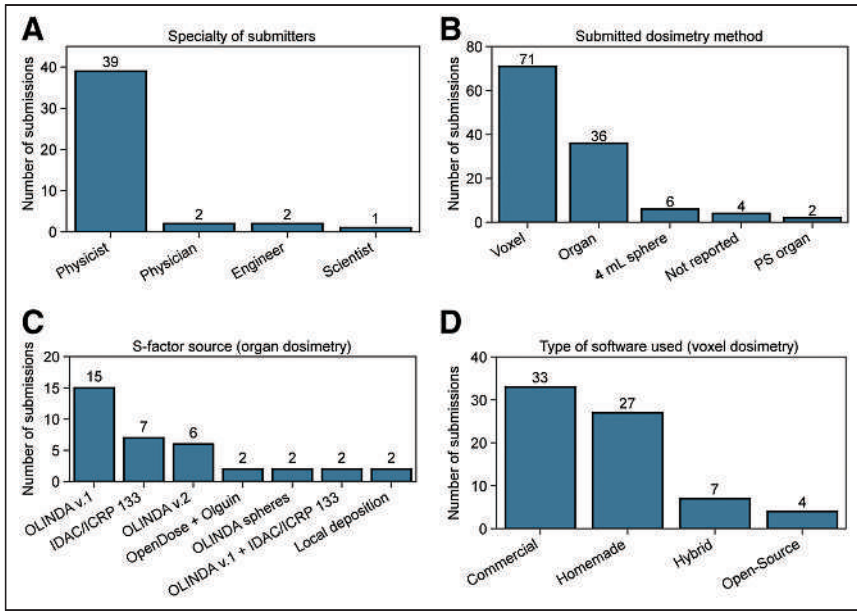


FIGURE 3. Number of submissions received, categorized by specialty of submitter (A), type of dosimetry method (B), source of S-factor calculations in cases of organ dosimetry (C), and type of software used for voxelized dosimetry (D). OpenDose + Olguin = 2 submissions that used OpenDose (20) in combination with factors published by Olguin et al. (21) for the tumors; PS = patient-specific; scientist = nonphysicist.

available software. Submissions that indicated that the software used was developed in-house were classified as homemade; 47% and 38% of the voxelized approaches were performed with commercial and homemade software, respectively. Hybrid submissions were those that used commercial software but for which a significant part of the calculation relied on in-house software, such as custom Monte Carlo simulation code. The hybrid submissions accounted for 10% of the voxelized approaches.

The indicated software in commercial and hybrid submissions included MIM (MIM Software), Hermes (Hermes Medical Solutions), Voximetry (Voximetry Inc.), and Varian (Siemens Healthineers), with 22, 10, 4, and 4 submissions, respectively. The 4 submissions categorized as open-source used OpenDose3D (20).

Figure 4 summarizes the method used to determine the volume and mass of the organ or tumor. Most participants used identical VOIs for these tasks. There were, however, cases in which the activity region was smaller, with participants drawing small spheres inside the organ to estimate the activity concentration, and some used larger VOIs to possibly account for partial-volume effects. The number of submissions that used each of the described methods is shown in Supplemental Table 1 (supplemental materials are available at <http://jnm.snmjournals.org>).

Figures 5A and 6A show the VOIs used for activity determination and for mass. Dosimetry calculations require an accurate measurement of both quantities. Larger

VOIs are often used to compensate for partial-volume effects. If the mass of the VOI is estimated from this larger VOI, it can result in an underestimation of the absorbed dose. Detailed statistics (i.e., mean, SD, coefficient of variation, quartiles, and number of points) are presented in Supplemental Tables 2 and 3. For organs, the volume of the left kidney in patient B had the highest coefficient of variation: $102.4 \text{ mL} \pm 48.2\%$ and $98.7 \text{ mL} \pm 49.8\%$ for the activity and mass VOIs, respectively. Tumor 2 of patient B showed the highest variability for the activity VOI, at $14.1 \text{ mL} \pm 74.5\%$, and also for the mass VOI, at $12.5 \text{ mL} \pm 76.0\%$. Large variations in activity and mass do not necessarily result in large variations in absorbed doses, since dose is related to the ratio of these 2 quantities.

Figures 5B and 6B show the distribution of the calculated TIAs. For the organs, the highest variability in this parameter was observed for the left kidney of patient A, for whom reported values ranged from 182.3 to $1.57 \times 10^5 \text{ MBq} \cdot \text{h}$ with a coefficient of variation of 191.8%. For the lesions, tumor 2 of patient B showed the highest variability, with reported values ranging from 407.3 to $4.14 \times 10^4 \text{ MBq} \cdot \text{h}$ and a coefficient of variation of 172.2%. Detailed statistics on the TIA plots are shown in Supplemental Table 4. The reported TIAs from 3 submissions were excluded from the analysis because the reported values were almost certainly given in different units. Large variations in the TIA do not necessarily translate into large variations in absorbed dose. Some centers used a small sphere placed inside an organ to estimate its absorbed dose. The lower values of the ranges of the TIA correspond to the number of disintegrations in those smaller spheres. For these spheres, the TIA

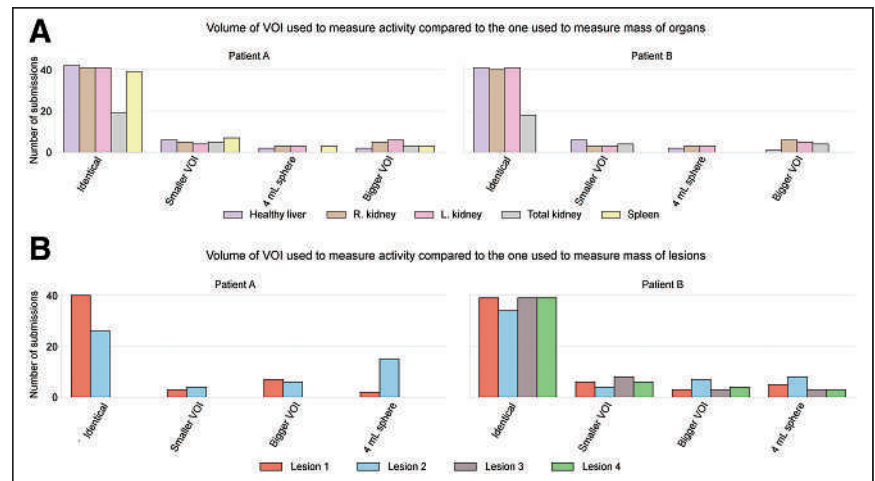


FIGURE 4. Comparison between size of VOI to measure activity and mass of organs (A) and tumors (B). Identical refers to same VOI used for both. VOI to measure activity is used as reference (e.g., bigger VOI means that bigger region was used to measure activity, compared with VOI used to measure mass); 4-mL sphere is method that used small sphere to estimate activity in that region and uses that volume for mass.

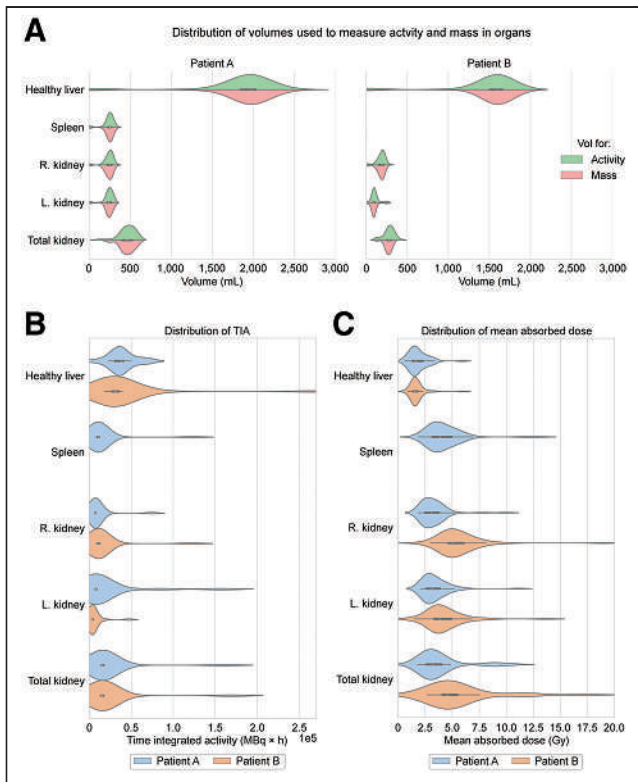


FIGURE 5. Distributions of volumes used for activity and mass (A), TIA (B), and mean absorbed doses (C) for healthy organs.

is small but the dose, because of the smaller mass, is much closer to that estimated from the entire organ.

Figures 5C and 6C show the distribution of the mean absorbed doses reported. The absorbed doses for the total kidneys of both patients showed the highest variability (reported as average value \pm coefficient of variation calculated as SD divided by the mean), with values of 3.83 Gy \pm 54.6% (range, 1.78–10.52 Gy) and 5.60 Gy \pm 57.7% (range, 1.47–17.33 Gy) for patients A and B, respectively. Lesion 1 of patient B had the highest reported variability overall, at 4.21 Gy \pm 98.1% (range, 0.72–33.32 Gy). Descriptive statistics for the absorbed doses are provided in Supplemental Table 5. Figures 7A and 7B show the type of function used to model the biodistribution of the organs and tumors, respectively. The reported functions included mono- and biexponential decays, an exponential uptake followed by a washout phase, and other types of functions. We did not specify the form of the washout function in the uptake-and-washout option although we were expecting a combination of exponential functions for the washout phase. We asked the participants for the different fit parameters, and we will report further on the functions used in the subsequent publications. Other types of functions included trapezoidal fits, trapezoids combined with monoexponential fits, 3-phase exponential fits, and semi- or fully automated methods that relied on combinations of mono- and biexponential fits. Detailed numbers are provided in Supplemental Table 6. The submissions indicated that monoexponential functions were the most widely used for the time–activity curve fitting of the organ biodistribution, but the exponential uptake followed by a washout phase was more common for the tumors. Comparisons of the other types of methods will be studied more carefully once the challenge concludes.

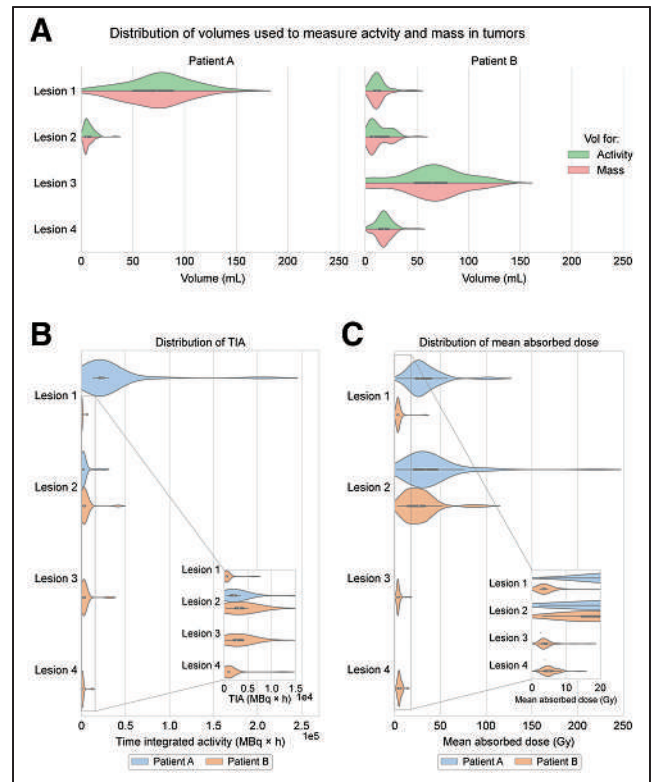


FIGURE 6. Distributions of volumes used for activity and mass (A), TIA (B), and mean absorbed doses (C) for tumors.

Figure 7C summarizes the time spent performing each task of the dosimetry workflow, as reported by the participants. Segmentation is the step that takes the longest time, with a median of 43 min to complete all requested VOIs and a range of 6–600 min. The median duration of the last step of the dose calculation (i.e., after generating the time–activity curve and calculating the TIA) was 33 min, but the maximum was 4,790 min. This maximum included computational time to run a Monte Carlo simulation and was not purely time invested by the participant. The median total time required to complete the dosimetry workflow was 89 min. Detailed times are presented in Supplemental Table 7.

Lastly, Supplemental Figure 1 shows 2 qualitative word clouds that summarize methods used by the participants to segment organs and tumors. The reporting of these methods has not been done in a standard way, but rather, participants entered a short description of their procedure. However, participants tended to use manual segmentation for the organs but semiautomatic gradient-based or thresholding methods for the tumors.

DISCUSSION

Few studies have tried to systematically evaluate the variability in dosimetry calculations performed using different protocols or methods.

Mora-Ramirez et al. (22) compared 5 commercially available dose programs on a cohort of patients treated with ¹⁷⁷Lu-DOTA-TATE. Organ masses, TIA, and absorbed doses were estimated using software from the different vendors, and the resulting values were compared. They concluded that absorbed doses estimated with the different applications were of the same order of

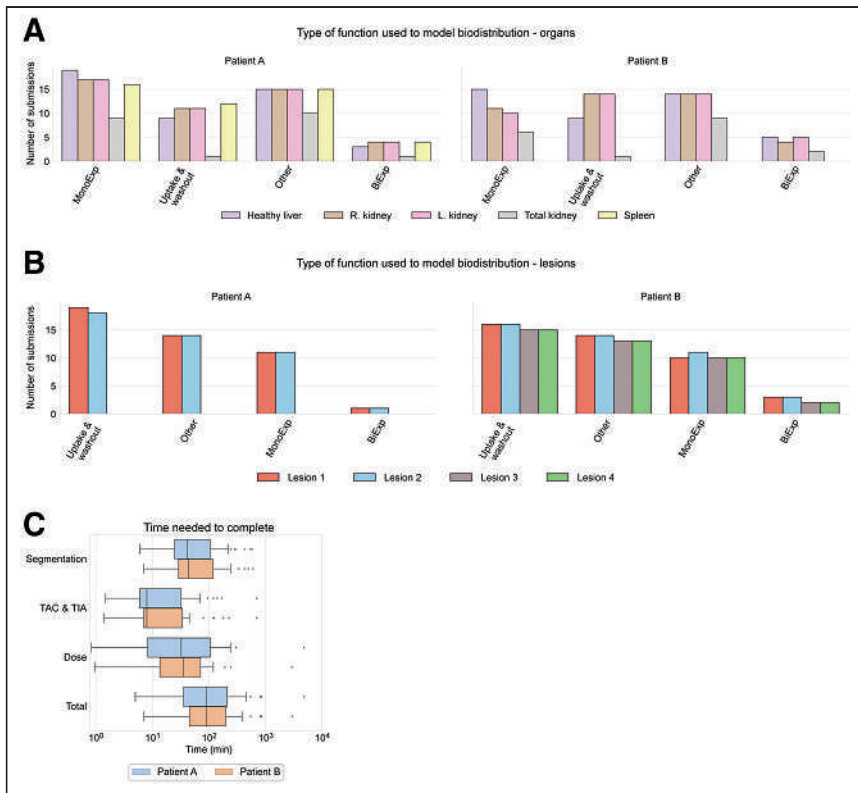


FIGURE 7. Bar plots showing the type of function used to fit the time–activity curve for the organs (A) and the tumors (B). Box plots showing time to complete each task (volume delineation, TAC generation, remainder of dose calculation) (C). BiExp = biexponential decay; MonoExp = monoexponential decay; TAC = time–activity curve; Uptake & Washout = exponential uptake followed by a washout phase.

magnitude but that not all of them addressed the same part of the dosimetry workflow (i.e., some applications follow the whole dosimetry workflow whereas some others start or end at particular steps).

Multiple publications by He et al. investigated the contribution to variability from different steps of the imaging and dosimetry process: image quantification, quantum noise, VOI definition, and patient variability (23–26).

Gustafsson et al. also looked at the uncertainties in the absorbed doses to kidneys by introducing variabilities in different steps of the dosimetry workflow, including the γ -camera calibration (27).

Peters et al. (28) used phantoms to evaluate the quantification accuracy of images in multicenter and multivendor cameras and concluded that standardization of protocols and accuracy is feasible. A study by the International Atomic Energy Agency included 9 different centers to look at the accuracy and precision in the activity quantification for planar and SPECT using ¹³³Ba as a surrogate for ¹³¹I (29).

Finocchiaro et al. (30) recently applied the European Association of Nuclear Medicine guidelines for uncertainty analysis in dose calculations for RPT (8) to a cohort of clinical cases. They aimed to show the uncertainties that can be expected in internal dosimetry and to identify which parameters have the greatest effect on those uncertainties. The results of the dosimetry challenge are expected to expand on that study because it includes the use of different segmentation methods (Figs. 5A and 6A) and because, in task 4, it isolates the effects of VOI definition.

Despite these previous efforts, there are still many unknowns, and more multicenter data are required. This study is unique because, to the best of our knowledge, it is the first study to invite the whole nuclear medicine community to perform dosimetry calculations on a standardized dataset without restrictions on, or prescription of, methods to be used. We think that this is a good representation of the current procedures implemented in nuclear medicine departments all around the world. However, we do recognize a limitation in that the current challenge does not address the variability in image acquisition parameters, reconstruction protocols, equipment calibration methods, and PVC. Moreover, the challenge does not address the accuracy of the results as it focuses only on identifying the sources of variability. This precludes use of the dataset for absolute benchmarking of the accuracy of dosimetry tools. We are working on addressing these limitations in a future study using simulated datasets for which the truth is fully known and allowing participants to select reconstruction and PVC methods and protocols.

The preliminary results presented in this work are only for task 1 of the challenge and do not yet allow comparison of acquisition approaches (i.e., planar vs. hybrid vs. SPECT). Also, sources of variability have not yet been systematically eliminated (they will be in task 4). These initial find-

ings act as the baseline against which further tasks will be compared. The results already show substantial variability in many of the methods and calculations. We believe that this is an invaluable dataset and that results from subsequent tasks will provide data on the most critical sources of variability and help guide standardization and harmonization efforts in areas that have the most impact.

Medical physicists were, by a large margin, the professionals most frequently performing dosimetry calculations in this study, perhaps reflecting that this is a research project (Fig. 3). However, there are multiple disciplines involved in clinical RPT procedures, including technologists for image acquisition and physicians to interpret the images and make therapeutic decisions, among others. To optimize and reduce variability in dose assessments, it is important that all involved disciplines have knowledge of the dosimetry procedure. For example, technologists with knowledge of dosimetry procedures will better understand the need to record appropriate parameters and patient positioning. In addition, as with other procedures, technologists may be involved in the segmentation process or other aspects of the dosimetry workflow, though not in this study. The dosimetry challenge has created a standard dataset that might be used as an educational resource for training of various professionals in dosimetry procedures. We have received internal communications from participants who are using the data to educate their trainees.

Commercial software accounted for most of the submissions. However, when homemade and hybrid tools are combined, they account for most submissions, which means that there are still many noncommercial tools used. Although Mora-Ramirez et al.

(22) compared 5 commercial software packages, we hypothesize that as the challenge evolves, the data will shed light on variability differences between in-house and commercial tools. This, in combination with the dataset made available through the challenge, can potentially be used to reduce the variability between the multiple tools used because it can act as a common benchmark for testing and development. Trainees, manufacturers, and developers can compare their results with the ones found in this and future articles of the challenge.

The first step that submitters had to perform for this challenge was the segmentation. Typically, segmentation was performed directly by the medical physicists. This was the most time-consuming task, and it is expected to be the largest source of variability in the absorbed dose results. As an example, a submission in which the kidney segmentation included only the renal cortex and medulla reported a 20.4% lower kidney-absorbed dose than one using the whole kidney (Supplemental Fig. 2), despite using the same software and methodology. To avoid these differences, it will be important to ensure and standardize the areas of organs that are segmented through input from physicians. Procedures in external-beam radiation therapy are initiated when technologists (dosimetrists) perform the segmentation. This is a model that RPT could potentially adopt, with appropriate training and standardization. Alternatively, use of simpler methods, such as using a small sphere inside a normal organ as a surrogate for the entire organ, could be recommended after validation to determine the resulting accuracy and precision. A small sphere is placed inside the kidneys to extrapolate the absorbed dose to the whole organ.

Variability in the TIA can be caused by variation in the activity values on the time-activity curve, which are impacted by the segmentation, and by variation in the fit function used to model the biodistribution. We will not be able to completely quantify the effect of the segmentation on variability in absorbed dose estimates without the results of task 4. However, we observed that the fit function varied widely among the submissions. Because monoexponential fits do not account for tracer uptake at early time points, monoexponential fits may, depending on the length of the uptake phase, result in absorbed dose estimates substantially different from fits obtained through the use of functions that model uptake and washout. However, a larger number of fitting parameters can reduce the precision of the fit. Other methods to address this issue included the use of a numeric integration (e.g., using a trapezoid) at the early time points. Differences between the fitting functions at late time points, such as when using mono- versus biexponential washout, can have a larger effect on the TIA and thus the absorbed dose. Guidelines to recommend fitting models for different situations could reduce this variability.

The variability in the different steps is reflected in the variability of the absorbed dose. However, the absorbed dose is also affected by differences in dose calculation methodology, such as the source of the S factors or Monte Carlo code used. In the submitted results, the reported absorbed doses differed by up to 100 times (tumor 2 of patient A in Fig. 6). On the last task of the challenge, we measure the variability due explicitly to this factor, and we thus expect to better understand the differences due to dose calculation method.

Lastly, although the median time spent to complete segmentation was the largest, the time spent for the final step of the dose calculation showed the highest variation. This is explained by the different dosimetry method. Applying an S factor to the TIA can be fast if that factor comes from a precalculated table or predefined phantom anatomy. However, when Monte Carlo simulations are used, the duration was up to orders of magnitude longer. Understanding of

the time needed to perform the various parts of the calculation may provide important insights for reimbursement purposes.

Overall, this study aims to raise questions on best practices to reduce variability in dosimetry measurements. However, for the purposes of dosimetry standardization, it is essential that the accuracy of each dosimetry approach also be considered. Questions related to dosimetric accuracy are best answered using simulated data, which provide knowledge of ground truth. In this study, we used patient images and focused on investigating variability.

The initial results of the challenge presented here provide evidence of the importance of understanding the sources of variability in absorbed dose estimates. The dataset that has been, and will continue to be, collected has already generated important questions for future study. Some of these questions may be addressed in future stages of the challenge, and others may point to additional studies needed to harmonize and standardize dosimetry calculations once the challenge ends.

CONCLUSION

To advance dosimetry and encourage its routine use in therapeutic applications of RPT, it is critical that dosimetry results be reproducible across centers. There is currently a lack of comprehensive data on the sources of variability. The ^{177}Lu dosimetry challenge presented in this study aims at collecting data from the international nuclear medicine community that can provide information needed for future standardization and harmonization procedures. The methodology and initial results of the first task were presented. Those results provide insights into the variability in expertise, software, segmentation, TIA calculations, absorbed dose results, and time required to perform the procedure. It is expected that this dataset, including results from future stages, will result in efforts to standardize and harmonize methods and procedures. This is deemed a critical step to justify and motivate reimbursement for dose assessments and clinical adoption of dosimetry-guided treatment in RPT, with the ultimate goal of improving patient outcomes.

DISCLOSURE

Yuni Dewaraja acknowledges support from NCI grant R01CA240706, under which the patient imaging studies were performed. Eric Frey acknowledges support from NCI SBIR grant R44 CA213782. Carlos Uribe acknowledges support from Natural Sciences and Engineering Research Council of Canada (NSERC) grant RGPIN-2021-02965. Yuni Dewaraja is a consultant with MIM (MIM Software) and receives research funding from Varian (Siemens Healthineers) and software support from Siemens (Siemens Healthineers) and MIM (MIM Software). Eric Frey is a cofounder and chief financial officer at Radiopharmaceutical Imaging and Dosimetry, LLC. Avery Peterson started a paid internship with MIM (MIM Software) after completing the analysis of the data in this article but before completing the submission. No other potential conflict of interest relevant to this article was reported.

ACKNOWLEDGMENTS

We acknowledge Bonnie Clarke, the director of research and discovery at the SNMMI, for all her help with the implementation, communication, and data collection of the challenge. We also gratefully acknowledge—by submitter, institution, and country—all the participants who submitted the results listed here: Adam Kesner, MSKCC,

United States; Albert Bartrés, Onkologikoa Fundazioa, Spain; Alesia Milano, Italy; Andrew Prideaux, Hermes Medical Solutions, United States; Anne-Laurène Wenger, University Hospital of Zürich, Switzerland; Arda Könik, PhD, DABSNM, Dana Farber Cancer Institute, United States; Ashok Tiwari, University of Iowa, United States; Avery Peterson, University of Michigan, United States; Azadeh Akhavan, Geneva University Hospital, Switzerland; Benjamin Van, University of Michigan, United States; Carlos Montes Fuentes, Hospital Universitario de Salamanca, Spain; Chae Moon Hong, Kyungpook National University Hospital, South Korea; Daniel McGowan, Oxford University Hospitals NHS FT, England; Daniele Pistone, University of Messina, Italy; David Adam, University of Wisconsin–Madison, United States; Diana McCrumb, BAMF Health, United States; Domenico Finocchiaro, Azienda USL di Reggio Emilia, Italy; Edoardo D’Andrea, Italy; Eric Brunner, BAMF Health, United States; Erin McKay, St. George Hospital, Australia; George Andl, Varian Medical Systems, United States; Greta Mok, University of Macau, China; Heying Duan, Stanford University, United States; Hina J. Shah, MD, DNB, BWH and DFCI, United States; Ivan Yeung, TECHNIA Institute, University Health Network, Canada; Jacob Hesterman, Invicro, United States; Joe Grudzinski, Voximetry Inc., United States; Johan Blakkisrud, Oslo University Hospital, Norway; Joshua Scheuermann, University of Pennsylvania, United States; Juan Camilo Ocampo Ramos, MSKCC, United States; Julia Brosch-Lenz, University Hospital LMU Munich, Germany; Keon Min Kim, Seoul National University, South Korea; Lara Bonney, Oxford University Hospitals NHS FT, England; Lorena Sandoval, Instituto Nacional de Cancerología, Colombia; Lukas Carter, MSKCC, United States; Natalie M. Cole, MIM Software, United States; Nathaly Barbosa, Instituto Nacional de Cancerología, Colombia; Nuria Carrasco Vela, Hospital Dr. Peset, Spain; Paulo Ferreira, Champalimaud Centre for the Unknown, Portugal; Price Jackson, Peter MacCallum Cancer Centre, Australia; Raquel Barquero, Hospital Clínico Universitario, Valladolid, Spain; Rachele Danieli, Italy; Richard Laforest, Washington University, United States; Sean McGurk, Sheffield Teaching Hospitals NHS Foundation Trust, England; Shalini Subramanian, Rapid, LLC, United States; Stephen A. Graves, PhD, University of Iowa, United States; Su Bin Kim, Seoul National University, South Korea; Tay Young Soon, Singapore General Hospital, Singapore; Teresa Pérez, Hospital Universitario de Gran Canaria Dr. Negrín, Spain; Valentina Ferri, Stanford University, United States; Vikram Adhikarla, City of Hope, United States; William Erwin, UT M.D. Anderson Cancer Center, United States; Ying Xiao, University of Pennsylvania and IROC Philadelphia RT, United States; and Yazdan Salimi, Geneva University Hospital, Switzerland.

KEY POINTS

QUESTION: Within the dosimetry workflow, what is the impact of the various sources of variability in dose results?

PERTINENT FINDINGS: Reported volumes varied by up to 142%; TIA, by up to 179%; organ doses, by up to 58%; and tumor doses, by up to 98%.

IMPLICATIONS FOR PATIENT CARE: Standardization and harmonization of methods and procedures in dosimetry are deemed a critical step in justifying and motivating reimbursement for dose assessments and clinical adoption of dosimetry-guided treatment in RPT, with the ultimate goal of improving patient outcomes.

REFERENCES

1. St. James S, Bednarz B, Benedict S, et al. Current status of radiopharmaceutical therapy. *Int J Radiat Oncol Biol Phys.* 2021;109:891–901.
2. Malcolm J, Falzone N, Lee BQ, Vallis KA. Targeted radionuclide therapy: new advances for improvement of patient management and response. *Cancers (Basel).* 1999;40:375–61S.
3. Sgouros G, Bodei L, McDevitt MR, Nedrow JR. Radiopharmaceutical therapy in cancer: clinical advances and challenges. *Nat Rev Drug Discov.* 2020;19:589–608.
4. Bolch WE, Eckerman KF, Sgouros G, Thomas SR. MIRD pamphlet no. 21: a generalized schema for radiopharmaceutical dosimetry—standardization of nomenclature. *J Nucl Med.* 2009;50:477–484.
5. Siegel JA, Thomas SR, Stubbs JB, et al. MIRD pamphlet no. 16: techniques for quantitative radiopharmaceutical biodistribution data acquisition and analysis for use in human radiation dose estimates. *J Nucl Med.* 1999;40(suppl):37S–61S.
6. Dewaraja YK, Frey EC, Sgouros G, et al. MIRD pamphlet no. 23: quantitative SPECT for patient-specific 3-dimensional dosimetry in internal radionuclide therapy. *J Nucl Med.* 2012;53:1310–1325.
7. Ljungberg M, Celler A, Konijnenberg MW, et al. MIRD pamphlet no. 26: joint EANM/MIRD guidelines for quantitative ¹⁷⁷Lu SPECT applied for dosimetry of radiopharmaceutical therapy. *J Nucl Med.* 2016;57:151–162.
8. Gear JJ, Cox MG, Gustafsson J, et al. EANM practical guidance on uncertainty analysis for molecular radiotherapy absorbed dose calculations. *Eur J Nucl Med Mol Imaging.* 2018;45:2456–2474.
9. Menzel HG, Clement C, DeLuca P. ICRP publication 110: realistic reference phantoms—an ICRP/ICRU joint effort. A report of adult reference computational phantoms. *Ann ICRP.* 2009;39:3–5.
10. Stabin MG, Xu XG, Emmons MA, Segars WP, Shi C, Fernald MJ. RADAR reference adult, pediatric, and pregnant female phantom series for internal and external dosimetry. *J Nucl Med.* 2012;53:1807–1813.
11. Dewaraja YK, Van BJ. Lu-177 DOTATATE anonymized patient datasets: multi-time point Lu-177 SPECT/CT scans. Deep Blue Data website. <https://doi.org/10.7302/0n8e-rz46>. Published February 10, 2021. Modified May 19, 2021. Accessed October 12, 2021.
12. Dewaraja YK, Van BJ. Lu-177 DOTATATE anonymized patient datasets: multi-time point Lu-177 planar whole body scans. Deep Blue Data website. <https://doi.org/10.7302/y4xd-s758>. Published February 10, 2021. Modified May 19, 2021. Accessed October 12, 2021.
13. Dewaraja YK, Van BJ. Lu-177 DOTATATE anonymized patient datasets: pre-therapy diagnostic images. Deep Blue Data website. <https://doi.org/10.7302/vqmy-g059>. Published February 10, 2021. Modified May 19, 2021. Accessed October 12, 2021.
14. Dewaraja YK, Van BJ. Lu-177 DOTATATE anonymized patient datasets: lesion and organ volumes of interest. Deep Blue Data website. <https://doi.org/10.7302/vhrh-qg23>. Published May 19, 2021. Accessed October 12, 2021.
15. Dewaraja YK, Van BJ. Lu-177 DOTATATE anonymized patient datasets: Lu-177 SPECT time integrated activity maps. Deep Blue Data website. <https://doi.org/10.7302/9nct-bk44>. Published August 23, 2021. Accessed October 12, 2021.
16. Ghosh P. *Clinical Impact of Absolute SPECT/CT Quantification in Theranostics and Dosimetry.* Siemens; 2020:1–41.
17. Stabin MG, Sparks RB, Crowe E. OLINDA/EXM: the second-generation personal computer software for internal dose assessment in nuclear medicine. *J Nucl Med.* 2005;46:1023–1027.
18. Andersson M, Johansson L, Eckerman K, Mattsson S. IDAC-Dose 2.1, an internal dosimetry program for diagnostic nuclear medicine based on the ICRP adult reference voxel phantoms. *EJNMMI Res.* 2017;7:88.
19. Bolch WE, Jokisch D, Zankl M, et al. ICRP publication 133: the ICRP computational framework for internal dose assessment for reference adults: specific absorbed fractions. *Ann ICRP.* 2016;45:5–73.
20. Gil AV, Amato E, Auditore L, et al. OpenDose3D: a free, collaborative 3D Slicer module for patient-specific dosimetry. *Eur J Nucl Med Mol Imaging.* 2020;47(suppl):S314–S315.
21. Olguin E, President B, Ghaly M, Frey E, Sgouros G, Bolch WE. Specific absorbed fractions and radionuclide S-values for tumors of varying size and composition. *Phys Med Biol.* 2020;65:235015.
22. Mora-Ramirez E, Santoro L, Cassol E, et al. Comparison of commercial dosimetric software platforms in patients treated with ¹⁷⁷Lu-DOTATATE for peptide receptor radionuclide therapy. *Med Phys.* 2020;47:4602–4615.
23. He B, Frey EC. The impact of 3D volume of interest definition on accuracy and precision of activity estimation in quantitative SPECT and planar processing methods. *Phys Med Biol.* 2010;55:3535–3544.
24. He B, Frey EC. Effects of shortened acquisition time on accuracy and precision of quantitative estimates of organ activity. *Med Phys.* 2010;37:1807–1815.

25. He B, Wahl RL, Sgouros G, et al. Comparison of organ residence time estimation methods for radioimmunotherapy dosimetry and treatment planning-patient studies. *Med Phys*. 2009;36:1595–1601.
26. He B, Du Y, Segars WP, et al. Evaluation of quantitative imaging methods for organ activity and residence time estimation using a population of phantoms having realistic variations in anatomy and uptake. *Med Phys*. 2009;36:612–619.
27. Gustafsson J, Brodin G, Cox M, Ljungberg M, Johansson L, Gleisner KS. Uncertainty propagation for SPECT/CT-based renal dosimetry in ^{177}Lu peptide receptor radionuclide therapy. *Phys Med Biol*. 2015;60:8329–8346.
28. Peters SMB, van der Werf NR, Segbers M, et al. Towards standardization of absolute SPECT/CT quantification: a multi-center and multi-vendor phantom study. *EJNMMI Phys*. 2019;6:29.
29. Zimmerman BE, Grošev D, Buvat I, et al. Multi-centre evaluation of accuracy and reproducibility of planar and SPECT image quantification: an IAEA phantom study. *Z Med Phys*. 2017;27:98–112.
30. Finocchiaro D, Gear JI, Fioroni F, et al. Uncertainty analysis of tumour absorbed dose calculations in molecular radiotherapy. *EJNMMI Phys*. 2020; 7:63.

Reimbursement Approaches for Radiopharmaceutical Dosimetry: Current Status and Future Opportunities

Stephen A. Graves¹, Alexandru Bageac², James R. Crowley³, and Denise A.M. Merlino⁴

¹Department of Radiology, University of Iowa, Iowa City, Iowa; ²Radiology Associates of North Texas, Fort Worth, Texas; ³Diagnostic Radiology, Carilion Clinic, Roanoke, Virginia; and ⁴Merlino Healthcare Consulting Corp., Magnolia, Massachusetts

Interest in performing dosimetry for clinical radiopharmaceutical therapy procedures has grown in recent years. Several approved therapies include dosimetry in the Food and Drug Administration–approved label instructions, and other therapies are best used under a patient-tailored paradigm. This paper, which is a product of the Society of Nuclear Medicine and Molecular Imaging Dosimetry Task Force, presents motivations and general workflows for radiopharmaceutical therapy dosimetry, as well as existing strategies for obtaining reimbursement for clinical activities related to dosimetry. Several specific patient examples are provided, including suggested codes for reimbursement. In addition to current reimbursement approaches, key dosimetry services that are not supported under the current coding structure are presented and suggested as areas of focus in the coming years.

Key Words: RPT; dosimetry; SPECT/CT; PET/CT

J Nucl Med 2021; 62:48S–59S

DOI: 10.2967/jnumed.121.262752

Radiopharmaceutical therapy (RPT) is a rapidly growing oncologic intervention whereby electron- or α -emitting radionuclides, formulated for accumulation within or near cancer cells, are administered by intravenous, intraarterial, or interstitial injection. The mechanism for accumulation within or near cancer cells can be physical in nature, such as ⁹⁰Y-labeled microspheres that become trapped in the arterioles of hypervascular lesions, or biochemical in nature, such as the binding of a radiolabeled peptide or antibody to a biologic receptor.

In most cases, the mass of radiolabeled compound administered for therapy is below any threshold for pharmacologic effects, and it is primarily the energy imparted into tissue by radioactive decay that effects a therapeutic response. The interactions between radiation and human biology—including biologic effects—have been extensively investigated over the last approximately 125 y (1,2). The primary endpoints of radiation therapy are so-called deterministic effects in target and nontarget tissue. (Stochastic effects, such as secondary hematologic malignancies, have also been shown to result from radiation exposure and chemotherapy. Current models suggest that these effects are not associated with a dose threshold, but rather the effect risk is thought to increase with increasing cumulative treatment. Rather than individualized dosimetry for

toxicity avoidance, stochastic effects are better informed by population-level dosimetry data for risk modeling.) Examples of a deterministic effects include radiation-induced nephropathy (kidney damage) and radiation-induced tumor shrinkage. Deterministic effects, which are the product of cell killing, are associated with a dose threshold, below which no effect is observed. Beyond the radiation dose threshold, the severity or magnitude of a deterministic effect is expected to increase with increasing dose. These dose-dependent effects for various biologic endpoints, tissue types, radiation types, and dose rates have been described in literature.

Radiation dose from RPT is therefore a measure that is expected to correlate with tumor control probability and normal-tissue complication probability. Indeed, there is a growing body of evidence showing that dose–response relationships are observed in RPT (3–10). Although not covered in this paper, the current state of knowledge regarding normal-tissue toxicity relationships and dose–response relationships within the context of RPT is thoroughly described in 2 other papers within this dosimetry supplement. Dose to tumors and normal tissues can vary widely among patients for a given administered activity level due to differences in tissue mass, pharmacokinetics, tissue geometries, and tumor phenotype (11–13). It is therefore critical to monitor patient-specific radiation-absorbed dose by established dosimetry techniques, whereby appropriate changes in management may be made. As with other types of radiation therapy, applying these therapies under a dosimetry-guided paradigm allows clinicians to minimize the risk of long-term toxic side effects, as well as assess for potential benefit in a particular patient.

DOSIMETRY FOR RPT

The process of obtaining patient-specific dosimetry for RPT involves characterizing the time-ordered distribution of radiopharmaceutical in the body, especially those tissues that are receiving the greatest radiation dose, or those that are naturally most sensitive to radiation. Techniques currently available for obtaining data regarding the distribution of radiopharmaceutical in a patient include the following: whole-body (WB) emission counting (1-dimensional projection of γ -emitting activity in a patient); planar γ -imaging (2-dimensional projection of γ -emitting activity in a patient); SPECT imaging (3-dimensional [3D] reconstruction of γ -emitting activity in a patient); PET imaging (3D reconstruction of β^+ -emitting activity in a patient); and blood or urine sampling (average activity concentration in compartment).

Generally, it is not optimal to rely on the use of only one of these technologies independently for patient-specific dosimetry, as each has weaknesses. With that said, the dosimetric accuracy and precision that can be obtained by use of only one of these data-collection techniques may be appropriate depending on the

Received Jun. 22, 2021; revision accepted Sep. 22, 2021.
For correspondence or reprints, contact Stephen A. Graves (stephen-a-graves@uiowa.edu).
COPYRIGHT © 2021 by the Society of Nuclear Medicine and Molecular Imaging.

particular RPT and specific patient management needs. Additionally, the number of data-collection time points can influence the accuracy of dosimetric calculations, with increased data collection being associated with improved dosimetric precision (11,14–19). Considerations needed when developing a dosimetry plan for a given RPT and patient should include: tissues of interest for dosimetry, potential impact of dosimetry on patient management (thus necessitating a certain level of accuracy and precision), and the ability of a patient to undergo dosimetric data collection. Even within a particular RPT, these factors vary on a per-patient basis, thus necessitating flexibility in dosimetry methods and associated reimbursement mechanisms.

Normal organs receiving the highest levels of absorbed dose in the body tend to be organs that are involved in concentrating and excreting the radiopharmaceutical, such as the liver, kidneys, bladder, and gastrointestinal tract. Significant radiation dose is also commonly observed in the spleen and secretory tissues (salivary glands, adrenal glands, pituitary gland). Although not typically receiving the highest absorbed dose, the bone marrow is a particularly radiosensitive tissue, and one that is of importance in RPT dosimetry. For a given RPT, usually only 1 or 2 of these organs will limit the quantity of radiopharmaceutical that can be administered without exceeding toxicity thresholds. A summary of approved and late-stage investigational agents, and their most commonly limiting normal organ tissues (20–29), is listed in Table 1.

In addition to consideration of dose-limiting normal organs, tumor dosimetry provides valuable information regarding potential patient benefit or the need for modifications to administered activity to reach a certain probability of benefit. Although an extensive review of tumor and normal organ dose–response relationships is beyond the scope of this document, typically solid tumor doses (from low–linear energy transfer sources) in excess of 100 Gy are needed to achieve high rates of response, whereas doses of less than approximately 50 Gy often do not provide therapeutic benefit from RPTs (7,9,10,30–33). In some cases, potential patient benefit may be minimal, thereby leading to a decision to not proceed with therapy. In this situation, unnecessary radiation exposure to the patient and public can be avoided, as well as an overall reduction in health-care costs. On the other hand, if a patient’s organ dosimetry is favorable, and tumor targets could benefit from dose escalation, it likely makes sense to administer additional radioactivity to achieve optimal therapeutic outcomes.

PRIMARY STAKEHOLDERS

Like any medical service and procedure, dosimetry for RPT needs to meet the requirements and expectations of an array of health-care stakeholders that span the entire billing process. Stakeholder interests should be contextualized in terms of the marginal increase in the cost of care, which overall tends to be dominated by the radiopharmaceutical cost in these procedures. Indeed, Centers for Medicare and Medicaid Services (CMS) reimbursement for ¹⁷⁷Lu-DOTATATE or ¹³¹I-metaiodobenzylguanidine (¹³¹I-MIBG) often exceeds \$200,000 for a course of therapy. By comparison, CMS reimbursement for services relating to dosimetry and treatment planning is unlikely to exceed \$10,000–\$15,000 for a course of therapy, depending on the workflow (see “Specific Coding Examples” for details). This represents, at most, a 5%–7% increase in the total cost of care. With this as context, stakeholder interests relating to dosimetry are described below.

- The most important group of stakeholders, *patients*, benefits from improved quality of care. In a given patient, dosimetry-guided RPT has significant potential for toxicity prevention, tumor control improvement, or total avoidance of futile medical intervention.
- Despite the expense of performing dosimetry, medical payers are expected to see a reduction in long-term costs due to avoidance of unnecessary (and typically vastly expensive) cancer therapies in a subset of patients, as well as potential for improved patient outcomes, which further reduces expense liabilities.
- Clinicians stand to benefit from cost-recovery on existing dosimetry practices, reduced liability from adoption of dosimetric guidance (avoiding over-, under-, and futile administration of RPT), and by remaining competitive in offering the highest level of care possible for patients.
- Radiopharmaceutical development and manufacturing entities can benefit from increases in administered activity to patients who stand to benefit most from doing so, and potentially from improved therapeutic windows in late-stage trials (thus reducing the number of patients needed to conduct trials).
- Technical providers of imaging services stand to benefit from increased use of imaging services, in particular existing γ -camera imaging infrastructure.
- The general public stands to benefit from improved control over the release of radioactive patients, which results in

TABLE 1
List of Common and Emerging Radiopharmaceutical Therapeutics, Their Clinical Indications, and Typical Dose-Limiting Tissues

Radiopharmaceutical	Indication	Dose-limiting tissues
¹³¹ I-NaI	Thyroid cancers	Marrow, lungs (20,21)
⁹⁰ Y-microspheres	Intrahepatic tumors, including primary and metastatic disease	Liver, lungs, stomach (22)
¹⁷⁷ Lu-DOTATATE	Low-grade neuroendocrine tumors	Marrow, kidneys (23)
¹³¹ I-MIBG	Paraganglioma, pheochromocytoma	Marrow, kidneys, liver (24,25)
²²³ RaCl ₂	Metastatic castration-resistant prostate cancer (mCRPC)	Marrow, gastrointestinal (26)
¹⁷⁷ Lu-PSMA-617 (investigational)	Metastatic castration-resistant prostate cancer (mCRPC)	Marrow, salivary glands, kidneys (27)
¹⁷⁷ Lu-DOTATOC (investigational)	Low-grade neuroendocrine tumors	Marrow, kidneys (28)
¹³¹ I-Iomab-B (investigational)	Acute myeloid leukemia (AML)	Liver (29)

approximately 720 person-Sieverts of radiation exposure per year in the United States (34).

DOSIMETRY TECHNIQUES

General Workflows

As mentioned in the section “Dosimetry for RPT,” multiple data-collection methods are available for dosimetry. Additionally, different radiopharmaceuticals have workflows that are conducive to their typical administration schedule. For example, high-specific-activity ^{131}I -MIBG (Azedra; Progenics Pharmaceuticals Inc.) is nominally administered as 2 treatments separated by at least 90 d, whereas ^{177}Lu -DOTATATE (Lutathera; Novartis) is administered over 4 therapeutic administrations, each separated by approximately 60 d. Given the goals of using dosimetry to enhance the safety and efficacy of RPT, it is important to have dosimetry results at a time or times in which treatment decisions can be made. In the case of fractionated therapies (e.g., ^{177}Lu -DOTATATE [Lutathera]), acquiring dosimetry data after the administration of each therapy can allow for adaptation in subsequent administrations to meet specific treatment planning goals. In the case of high-specific-activity ^{131}I -MIBG (Azedra), however, this may or may not be possible, due to potentially reaching or exceeding normal-tissue limits in the first treatment. Likewise, ^{90}Y -microsphere therapies are often administered with a single intraarterial infusion, in which case dosimetry and treatment planning are needed before the first therapeutic administration. Therefore, the 2 main dosimetry/treatment planning workflows are as follows:

- Administration of a small amount of the therapeutic, or a predictive surrogate, for purposes of dosimetry and treatment planning before administration of the primary RPT. This workflow is typically used for ^{90}Y -microspheres, ^{131}I -MIBG, and ^{131}I -NaI.
- Administration of a full RPT administration, followed by dosimetry for modification of subsequent treatments. This workflow is commonly used for ^{177}Lu -DOTATATE and could be used for various agents currently under investigation.

Dosimetric Sampling

Within a given workflow, a dosimetry schedule should be created based on the needs of a particular RPT and patient. The goal of this schedule should be the accurate determination of dose to relevant tissues (dose-limiting organs or tumors); however, the exact imaging and data-collection sequence will vary with situation. Several specific schedule examples are presented in the section “Specific Coding Examples,” however, the following general statements can be made regarding the dosimetry of each agent and tissue type.

^{131}I -NaI. Thyroid uptake should be confirmed and quantified with pretreatment imaging. SPECT/CT and planar γ -imaging are appropriate for this when using ^{123}I -NaI or ^{131}I -NaI, and PET/CT is appropriate when using ^{124}I -NaI. Generally, a single imaging time point is adequate for determination of initial tumor uptake fraction; however, quantification of dose to tumor requires anatomic imaging, for example, PET/CT or SPECT/CT, and multiple imaging time points. Quantification of dose to lungs, relevant in cases in which significant lung metastatic disease exists, requires multiple imaging time points and at least 1 anatomic reference scan (e.g., SPECT/CT or PET/CT). Accurate quantification or prediction of marrow dosimetry requires blood sampling at multiple time points and WB planar or SPECT/CT imaging at multiple time points. In

summary, a complete and optimal dosimetry workup requires serial blood sampling, serial WB planar imaging, and at least one SPECT/CT that is concordant with one of the planar imaging time points. Some practices have developed population-based biologic clearance models, which may allow for a reduction in the needed data (omission of one or more planar or blood sampling time points); however, these approximations may reduce dosimetric accuracy somewhat (35–37).

^{131}I -MIBG and ^{177}Lu -DOTATATE. For both agents, marrow and kidney dosimetry are normal organs of interest. Optimal renal dosimetric sampling can be achieved by multiple SPECT/CT imaging time points over the first approximately 7 d after administration of the therapeutic or a surrogate. Bone marrow dosimetry for these agents can be performed by addition of WB planar imaging and blood sampling at multiple time points. The blood contribution to total marrow dose is less for ^{131}I -MIBG than for ^{177}Lu -DOTATATE, and therefore fewer collections may be needed. Tumor dosimetry, similar to kidney dosimetry, is best performed with serial SPECT/CT imaging. Some investigators have proposed ^{177}Lu -DOTATATE imaging time-point reduction strategies for kidneys and tumors (11,18,19); however, these approximations may reduce dosimetric accuracy somewhat (14). Similarly, rather than WB imaging to determine marrow dose from ^{131}I -MIBG, some recommendations include the use of WB counting (rather than imaging) in pediatric patients who would otherwise require general anesthesia for imaging (38,39).

$^{223}\text{RaCl}_2$. Because of the low administered activity and photon emission abundance, the retention and distribution of ^{223}Ra in a patient is typically assessed by planar imaging only; however, quantitative SPECT/CT has been investigated (40–43).

^{90}Y -Microspheres. ^{90}Y -microspheres are unique among RPTs, due to their nature of maintaining a fixed irradiation geometry after administration. Because of this, only a single imaging time point is needed for dose assessment. For treatment planning purposes, typically $^{99\text{m}}\text{Tc}$ -macroaggregated albumin ($^{99\text{m}}\text{Tc}$ -MAA) is administered in a way that is consistent with the desired ^{90}Y -microsphere administration method (same catheter position in the hepatic arterial tree, same infusion rate). Dose to tumor, liver, and potentially lung and stomach are of interest after this MAA administration. Liver and tumor dosimetric predictions, as well as evaluation for gastric shunting, are made by way of a single SPECT/CT image after administration of MAA. The axial field of view of a single SPECT/CT acquisition is often not adequate for inclusion of the entire lungs, thus lung shunting should be evaluated by collection of an additional SPECT/CT scan, or by conjugate-view planar imaging. In general, lung shunting has been reported to be overestimated by planar imaging, and therefore SPECT/CT may be preferred (44–46). After administration of ^{90}Y -microspheres, additional 3D imaging at a single time point (SPECT/CT or PET/CT) is needed to confirm microsphere distribution and associated dosimetry. Some discordance is expected when comparing $^{99\text{m}}\text{Tc}$ -MAA predicted dosimetry and ^{90}Y -SPECT/CT estimated dosimetry due to the difference in image quality; however, comparison of these measurements can confirm general treatment distribution and potential eligibility for subsequent ^{90}Y -microsphere administrations in the case of progression or undercoverage.

Simplified Dosimetry Methods

As mentioned above, simplified dosimetry methods for ^{131}I -NaI, ^{177}Lu -DOTATATE, and ^{131}I -MIBG have been proposed (18,19,35,

36,47). These techniques have the potential to reduce the number of imaging sessions or data acquisition requirements, but at the cost of increased dosimetric uncertainty.

In the context of ^{131}I -NaI dosimetry, work by Hänscheid et al. demonstrated that a single measurement time point 1–2 d after administration maximized the accuracy of marrow dosimetry, with an average residual error of approximately 13% (35). That said, significant under- and overestimation was observed in some cases, with the estimated/true dose ratio ranging from 0.69 to 1.24 at 24 h. Similar results are described by Jentzen et al., wherein approximately 85% of patients had residual error of less than 20%, and absolute estimated/true maximum tolerated activity ratios ranged from 0.54 to 1.30 (36). Work by Jentzen et al. was largely confirmed by Atkins et al. (37). These findings suggest that use of a “simplified” ^{131}I dosimetry strategy may require an additional 20%–30% safety margin compared with standard dosimetric sampling.

For ^{177}Lu -DOTATATE, data by Sandström et al. indicate that single-time-point renal dosimetry (with an assumption of monoexponential clearance) results in a residual error of less than 20% in most cases; however, the ratio of estimated to true dose ranges from approximately 0.5 to approximately 1.3 (14). Assumption of biexponential clearance, such as what was originally described by Madsen et al. (48), may improve results somewhat; however, this was not examined by Sandström et al. in their cohort of 777 patients (14). Single-time-point dosimetry has been proposed for other tissues (liver, marrow, tumors) (47); however, further validation is needed.

To date, only 1 publication addresses simplified dosimetry for ^{131}I -MIBG (15). The authors concluded that reasonably accurate tumor dosimetry could be achieved using 2 imaging time points; however, further study is needed to evaluate the applicability of single-time-point methods.

Dosimetry Calculations

Two main methods exist for assessing patient-specific dosimetry, regardless of RPT type: absorbed fraction (e.g., MIRD schema) calculations, and 3D voxelwise dosimetry. These 2 methods are not mutually exclusive, meaning that in a single patient dose to 1 tissue (e.g., bone marrow) may be best assessed by an absorbed fraction calculation, whereas dose to another tissue may be best assessed by a 3D voxelwise dose calculation (e.g., liver). Precise methods and considerations regarding these 2 calculations methods are well described elsewhere (49–52) and thus beyond the scope of this document; however, a general diagram of dosimetry calculation steps, including final treatment plan generation, is shown in Figure 1. As described in the previous section, the exact combination of input data required for dosimetry depends on RPT- and patient-specific factors.

Similarly, the radiation dosimetry and treatment planning workflow will vary depending on specific information required by the physician provider for treatment planning purposes. The primary difference between these 2 dose calculation strategies is that absorbed fraction calculations typically result in mean dose to whole organs, whereas voxelwise calculations can provide a 3D dose map within the patient anatomy, including isodose lines and dose volume histograms. This distinction is relevant when considering the appropriateness of existing treatment planning current procedural terminology (CPT; a registered trademark of the American Medical Association) codes.

CPT CODE DESCRIPTIONS

Depending on the specific clinical workflow, personnel effort, documentation, and medical necessity, several existing CPT codes may be applicable to activities relating to radiopharmaceutical dosimetry and treatment planning. A list of existing and potentially pertinent codes and associated relative value units ([RVUs], data obtained from CMS.gov (53)) is provided in Table 2. Detailed

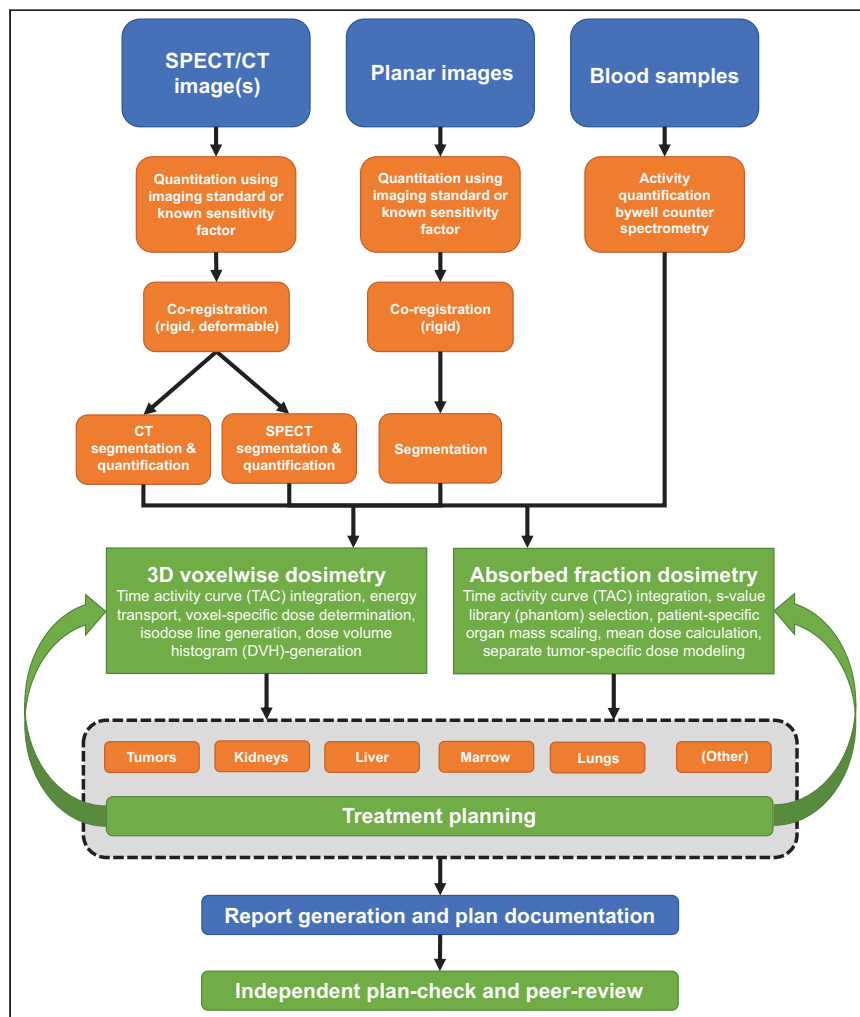


FIGURE 1. Overview of typical RPT dosimetry and treatment planning workflow. Specific input data, dose calculation method, and tissues of interest will depend on the specific radiopharmaceutical and clinical need. Members of the multidisciplinary team responsible for executing the steps of this workflow should be qualified to perform radiopharmaceutical therapy dosimetry, able to interpret dosimetric findings, and able to perform the final treatment plan as documented and reviewed.

TABLE 2

CPT Codes That May Be Considered Applicable to Radiopharmaceutical Dosimetry and Treatment Planning or Related Activities

CPT	Short description	Long description	Physician time (min)	Physician RVU	Physicist/technologist time (min)	Non-facility RVU	Facility RVU
78800	Single area planar	Radiopharmaceutical localization of tumor, inflammatory process or distribution of radiopharmaceutical agent(s) (includes vascular flow and blood-pool imaging, when performed); planar, single area (e.g., head, neck, chest, pelvis), single day imaging	27	0.64	88	7.53	2.06
78801	Multiple area planar	Radiopharmaceutical localization of tumor, inflammatory process or distribution of radiopharmaceutical agent(s) (includes vascular flow and blood-pool imaging, when performed); planar, 2 or more areas (e.g., abdomen and pelvis, head and chest), 1 or more days imaging or single area imaging over 2 or more days	30	0.73	99	8.31	3.13
78802	WB single day	Radiopharmaceutical localization of tumor, inflammatory process or distribution of radiopharmaceutical agent(s) (includes vascular flow and blood-pool imaging, when performed); planar, WB, single day imaging	30	0.80	109	9.21	4.87
78804	WB 2 or more days	Radiopharmaceutical localization of tumor, inflammatory process or distribution of radiopharmaceutical agent(s) (includes vascular flow and blood-pool imaging, when performed); planar, WB, requiring 2 or more days imaging	40	1.01	216	19.42	–
78803	SPECT single area/single day	Radiopharmaceutical localization of tumor, inflammatory process or distribution of radiopharmaceutical agent(s) (includes vascular flow and blood-pool imaging, when performed); tomographic (SPECT), single area (e.g., head, neck, chest, pelvis), single day imaging	42	1.09	130	11.38	–
78830	SPECT/CT single area/single day	Radiopharmaceutical localization of tumor, inflammatory process or distribution of radiopharmaceutical agent(s) (includes vascular flow and blood-pool imaging, when performed); tomographic (SPECT) with concurrently acquired CT transmission scan for anatomic review, localization and determination/detection of pathology, single area (e.g., head, neck, chest, pelvis), single day imaging	45	1.49	141	14.46	–

(continued)

TABLE 2

CPT Codes That May Be Considered Applicable to Radiopharmaceutical Dosimetry and Treatment Planning or Related Activities (cont.)

CPT	Short description	Long description	Physician time (min)	Physician RVU	Physicist/technologist time (min)	Non-facility RVU	Facility RVU
78831	SPECT minimum of 2 areas in 1 d or single are over 2 or more days	Radiopharmaceutical localization of tumor, inflammatory process or distribution of radiopharmaceutical agent(s) (includes vascular flow and blood-pool imaging, when performed); tomographic (SPECT), minimum 2 areas (e.g., pelvis and knees, abdomen and pelvis), single day imaging, or single area imaging over 2 or more days	55	1.82	224	20.87	–
78832	SPECT/CT minimum of 2 areas in 1 d or single are over 2 or more days	Radiopharmaceutical localization of tumor, inflammatory process or distribution of radiopharmaceutical agent(s) (includes vascular flow and blood pool imaging, when performed); tomographic (SPECT) with concurrently acquired CT transmission scan for anatomic review, localization and determination/detection of pathology, minimum 2 areas (e.g., pelvis and knees, abdomen and pelvis), single day imaging, or single area imaging over 2 or more days	60	2.12	264	27.19	–
78835	Quantification for SPECT/CT (use with 78830 or 78832) *report multiple units	Radiopharmaceutical quantification measurement(s) single area (list separately in addition to code for primary procedure)	17	0.47	23	3.00	–
78814	Limited PET/CT	PET with concurrently acquired CT for attenuation correction and anatomic localization imaging; limited area (e.g., chest, head/neck)	60	2.20	Carrier-priced	0.00	–
78580	–	Pulmonary perfusion imaging (e.g., particulate)	20	0.74	93	6.96	–
77300	Basic radiation dosimetry calculation	Basic radiation dosimetry calculation, central axis depth dose calculation, time-dose factor, nominal standard dose, gap calculation, off axis factor, tissue inhomogeneity factors, calculation of nonionizing radiation surface and depth dose, as required during course of treatment, only when prescribed by the treating physician	15	0.62	14	1.93	–
77370 ³	–	Special medical radiation physics consultation	0	0.00	65	3.75	–
77261	–	Treatment planning: (simple, intermediate, complex)	36	1.30	–	2.06	2.06
77262	–		54	2.00	–	3.13	3.13
77263	–		82	3.14	–	4.87	4.87

(continued)

TABLE 2
CPT Codes That May Be Considered Applicable to Radiopharmaceutical Dosimetry and Treatment Planning or Related Activities (cont.)

CPT	Short description	Long description	Physician time (min)	Physician RVU	Physicist/technologist time (min)	Non-facility RVU	Facility RVU
77295	—	3-dimensional radiation treatment plan, including dose-volume histograms	112	4.29	165	14.07	—

Stochastic effects, such as secondary hematologic malignancies, have also been shown to result from radiation exposure and chemotherapy. Current models suggest that these effects are not associated with a dose threshold, but rather the effect risk is thought to increase with increasing cumulative treatment. Rather than individualized dosimetry for toxicity avoidance, stochastic effects are better informed by population-level dosimetry data for risk modeling.

examples of these codes are included in the section “Specific Coding Examples”; however, the codes can generally be divided into those for γ -imaging (78800, 78801, 78802, 78803, 78804, 78830, 78831, 78832, 78580), PET imaging (78814), dosimetry and treatment planning (77300, 77261, 77262, 77263, 77295), and ancillary services (77370, 78835). Notable exclusions from the table below include more general PET imaging codes (i.e., 78811, 78812, 78813, 78815, 78816), which might be applicable in the case where PET or PET/CT is used for pretreatment dosimetry. Codes relating to brachytherapy dosimetry and treatment planning (i.e., 77316, 77317, 77318) may also be considered applicable in some situations.

SPECIFIC CODING EXAMPLES

Below is a series of clinical workflows that may be encountered, including reimbursement coding that is relevant to imaging, dosimetry, and treatment planning. We have intentionally omitted descriptions and codes related to radiopharmaceuticals, radiopharmaceutical administrations, patient consultation, and follow-up. Coding for these related activities are left for other documents.

Example 1. ⁹⁰Y-Radioembolization (with Pretreatment ^{99m}Tc-MAA Mapping)

A patient was determined to be a candidate for ⁹⁰Y radioembolization. Dosimetric planning for treatment began by preparation of a calibrated quantity of ^{99m}Tc-MAA. An interventional radiologist localized a catheter to a satisfactory location within the arterial supply of a liver for infusion of the ^{99m}Tc-MAA. Catheter tip placement was optimized based on tumor location and the perfused volume indicated by iodine-enhanced digital subtraction fluoroscopy or cone beam CT imaging in the interventional suite. After infusion of the ^{99m}Tc-MAA, the patient was relocated to a SPECT/CT scanner for imaging. Acquired were SPECT/CT images centered on the liver (78830) and conjugate planar images covering the extent of lungs and liver (bundled with 78830).

After acquisition, it was confirmed by the authorized user and treating physician that the perfused volume within the liver was appropriate for therapy. A decision was made regarding sphere type (glass vs. resin) based on desired sphere specific activity and specific gravity.

Lung shunt fraction (LSF) was calculated by manually drawing regions of interest (ROIs) on conjugate planar views—lungs, liver, and corresponding background ROIs. Counts quantified in each region were corrected for background, a geometric mean was

calculated for the lungs and liver separately, and the fraction of total activity in the lungs was calculated (78835 for each ROI). On the basis of institutional policy, this LSF was considered sufficiently low that a more accurate 3D evaluation was not needed. This LSF was transcribed in the patient medical record.

Dosimetry proceeded by use of 510(k)-cleared medical device software for 3D microsphere dosimetry. A physicist, physician, or another qualified individual segmented the whole liver, the perfused portion of the liver, the tumor, and the tumor plus a planning margin to account for breathing motion and potential microinvasion. A 3D dose plan normalized to a nominal administered activity was reviewed by the authorized user, and it was determined that an administered activity of 3.52 GBq was appropriate to maximize tumor dose, without exceeding dose limits to normal liver parenchyma. Three-dimensional dosimetry statistics for this final treatment plan were generated, and a treatment plan report was generated and signed by the physicist and authorized user (77295). An independent qualified individual reviewed this plan for appropriateness and accuracy, including performing a simplified dose calculation via the partition model. This secondary dose verification was documented in the medical record (77300).

Approximately 2 wk after the initial mapping procedure, the patient returned for treatment. The interventional radiologist placed the catheter tip at the same location within the liver arterial vasculature, and ⁹⁰Y-microspheres were infused according to manufacturer-recommended methods. Because stasis was reached during administration, only 3.24 GBq were administered. The patient was transferred for posttreatment Bremsstrahlung SPECT/CT imaging, whereby a single SPECT/CT view, centered on the liver (78830), and a conjugate planar image including the extent of lungs and liver (bundled with 78830) were acquired. On the basis of these images, dosimetry was performed to assess the delivered dose (77300).

The following is a summary of the procedure and corresponding CPT codes:

- MAA mapping SPECT/CT and planar, 78830;
- Lung shunt quantification, 78835 (2 units);
- 3D radiation treatment planning, 77295;
- Plan check/simple dosimetry, 77300;
- ⁹⁰Y SPECT/CT and planar, 78830; and
- Treatment verification (simple dosimetry), 77300.

Comments. If posttreatment ⁹⁰Y PET/CT imaging covering the liver and lungs is performed rather than posttreatment SPECT/CT

and planar, 78814 (limited area PET/CT) would take the place of the posttreatment imaging code 78830. If pretreatment MAA mapping is not performed, the pretreatment imaging, LSF assessment, treatment planning codes, and treatment plan verification codes (78830, 78835, 77295, 77300) would not be applicable. If treatment planning is performed using methods other than a full-3D voxelwise calculation (e.g., partition method or whole liver mean dose determination), simple, intermediate, or complex treatment planning codes (77261, 77262, or 77263) should be used in place of 77295. If SPECT/CT is not acquired after ^{99m}Tc -MAA administration, 78800 or 78801 for the planar imaging would be billed in lieu of 78830. Assuming lung shunt quantification is performed from the planar images, 78580 could be used in lieu of 78835 units. Additionally, 77295 would no longer be applicable (see the earlier text).

Example 2. ^{177}Lu -DOTATATE (with Tumor, Marrow, and Kidney Dosimetry)

After clinical evaluation and results from diagnostic ^{68}Ga -DOTATOC PET/CT imaging, a patient was deemed to be eligible for treatment with ^{177}Lu -DOTATATE RPT. No pretreatment dosimetry was performed; however, eligibility for subsequent ^{177}Lu -DOTATATE administrations (every 8 wk) would be determined on the basis of prior and cumulative radiation doses from treatment.

The patient presented for the first therapeutic administration. The patient had a peripheral intravenous catheter placed, and an infusion of nephroprotective amino acids was started. After approximately 30 min had elapsed (~200 cc of fluid infused), it was confirmed by a nuclear medicine technologist that no signs of extravasation were present. The RPT (7.4 GBq of ^{177}Lu -DOTATATE) was administered through the same intravenous catheter by standard institutional practice, and the amino acid infusion proceeded until completion, approximately 4 h after the start of infusion.

After completion of RPT administration, a blood sample was collected for dosimetric purposes. The patient was monitored and released. In the following days, at 24 h after injection, 72 h after injection, and 120 h after injection, the patient returned for dosimetric sampling. Each dosimetric sampling consisted of blood collection, WB planar imaging (78804), and abdominal SPECT/CT (78832). On the basis of the 24-h SPECT/CT acquisition, it was determined that extravasation of ^{177}Lu had not occurred.

Dosimetry proceeded by use of 510(k)-cleared medical device software for generalized 3D RPT dosimetry. A physicist, physician, or another qualified individual segmented organs of interest (whole liver, spleen, kidneys) as well as the 3 largest tumor lesions. Marrow dosimetry was performed by absorbed-fraction (MIRD) methods based on WB, blood, and normal organ time-integrated-activity quantification. A 3D dose plan normalized to a nominal administered activity was reviewed by the authorized user, and it was determined that a cumulative administered activity of 25.5 GBq was appropriate to maximize tumor dose, without exceeding dose limits to normal tissues (kidneys, liver, marrows) and within the limits of radiopharmaceutical availability. Three-dimensional dosimetry statistics for this final treatment plan were generated, and a treatment plan report was generated and signed by the physicist and authorized user (77295). An independent qualified individual reviewed this plan for appropriateness and accuracy, including performing a simple dose calculation via established absorbed-fraction (MIRD) methods. This

secondary dose verification was documented in the medical record (77300).

After 8 wk, the patient returned for the second (Tx 2). On the basis of the target cumulative administered activity of 25.5 GBq, the patient was deemed eligible for an additional full administration of 7.4 GBq. The treatment was administered, and the patient underwent the same dosimetric sampling regimen as described above. Posttreatment dosimetry was performed to evaluate for deviation from expected tumor and normal organ doses. On the basis of compliance with the original treatment plan, treatment 3 (Tx 3) proceeded in the same manner with a 7.4 GBq administration and posttreatment dosimetry. The final treatment (Tx 4) was delivered in compliance with the initial treatment plan, with an administered activity of 3.3 GBq (cumulative 25.5 GBq). After the terminal treatment, dosimetric sampling was repeated. On the basis of these data, dosimetry was performed and combined with results from all 4 treatments (77300). A final patient-specific dose report was generated and documented in the medical record.

The following is a summary of the procedure and corresponding CPT codes:

- Tx 1 ^{177}Lu WB planar imaging (3 d), 78804;
- Tx 1 ^{177}Lu abdominal SPECT/CT (3 d), 78832;
- 3D radiation treatment planning, 77295;
- Plan check/simple dosimetry, 77300;
- Tx 2 ^{177}Lu WB planar imaging (3 d), 78804;
- Tx 2 ^{177}Lu abdominal SPECT/CT (3 d), 78832;
- Dosimetry assessment, 77300;
- Tx 3 ^{177}Lu WB planar imaging (3 d), 78804;
- Tx 3 ^{177}Lu abdominal SPECT/CT (3 d), 78832;
- Dosimetry assessment, 77300;
- Tx 4 ^{177}Lu WB planar imaging (3 d), 78804;
- Tx 4 ^{177}Lu abdominal SPECT/CT (3 d), 78832; and
- Dosimetry assessment, 77300

Comments. If tumors are not included within the abdominal SPECT/CT field of view, and tumor dosimetry is needed, additional SPECT fields of view would be required. This would not change the coding unless only a single posttreatment SPECT/CT were planned, in which case 78832 would be submitted in lieu of 78830. If marrow dosimetry is not performed, WB planar imaging (78804) and blood sampling should be omitted unless otherwise deemed medically necessary.

Example 3. ^{177}Lu -DOTATATE (Dialysis Patient, Marrow Dosimetry)

After clinical evaluation and results from diagnostic ^{68}Ga -DOTATOC PET/CT imaging, a patient was deemed to be eligible for treatment with ^{177}Lu -DOTATATE RPT. In addition to having advanced neuroendocrine tumors, this patient had poor kidney function due to obstruction and was therefore receiving hemodialysis 3 d per week. Because of the compromised kidney function, blood clearance of any therapeutic radiopharmaceutical was expected to be significantly inhibited compared with the typical patient presentation. For this reason, the decision was made to initially administer 3.7 GBq of ^{177}Lu -DOTATATE (rather than the standard 7.4 GBq), followed by bone marrow dosimetry to develop a treatment plan for subsequent administrations. For this patient, treatment was deemed to be palliative, and therefore kidney, liver, and tumor dosimetry were considered to be secondarily important to the most likely normal-tissue toxicity (bone marrow).

RPT was administered (methods consistent with what was described in Example 6.2), and the following dosimetric sampling was performed:

- Blood sampling at 4 h after administration (end of AA infusion);
- Hemodialysis performed from 4.5 to 7 h after administration;
- Blood sampling at 7.5 h after administration;
- Blood sampling and WB conjugate planar imaging at 24 h after administration;
- Blood sampling and WB conjugate planar imaging at 46 h after administration;
- Hemodialysis performed from 47 to 49 h after administration;
- Blood sampling performed at 49 h after administration; and
- Blood sampling and WB conjugate planar imaging at 96 h after administration.

After completion of dosimetric sampling, a special medical physics consult (77370) was ordered by the treating physician. The consult request was made to evaluate the effect of hemodialysis and blood retention of ^{177}Lu -DOTATATE and associated marrow dosimetric effects. Dosimetry calculations were performed by a qualified medical physicist in addition to evaluating the impact of dialysis, and a consultation report was generated and documented. It was determined that minimal blood clearance occurred between dialysis sessions. Absorbed-fraction (MIRD)-based marrow dosimetry indicated significant elevation of population average dose values (more than 4 times the approved label average value). On the basis of this analysis performed by the qualified medical physicist, it was determined that addition of a hemodialysis session at 24 h after administration would be beneficial for marrow dosimetry due to increased peptide removal after the initial tumor uptake phase. A treatment plan was developed (77262) that included this modification while targeting a total administered activity of 14.8 GBq, with the remaining activity (11.1 GBq) to be split between treatments 2 and 3. An independent qualified individual reviewed this plan for appropriateness and accuracy, including performing a simple dose calculation via established absorbed-fraction (MIRD) methods. This secondary dose verification was documented in the medical record (77300).

Treatments 2 and 3 were completed according to the treatment plan, with postadministration dosimetry performed as described above. Bone marrow dosimetry (77300) was performed after each treatment, with dose reports (fraction and cumulative) being documented in the patient medical record.

The following is a summary of the procedure and corresponding CPT codes:

- Tx 1 ^{177}Lu WB planar imaging (3 d), 78804;
- Med physics special consult: dialysis pharmacokinetics, 77370;
- Treatment planning (intermediate), 77262;
- Tx 1 marrow dosimetry, 77262;
- Tx 2 ^{177}Lu WB planar imaging (3 d), 78804;
- Tx 2 marrow dosimetry, 77300;
- Tx 3 ^{177}Lu WB planar imaging (3 d), 78804; and
- Tx 3 marrow dosimetry, 77300.

Comments. The choice of 77262 (intermediate) rather than 77261 (simple) or 77263 (complex) in this example is based on the time-sensitive nature of radiation dose delivery, including appropriate timing of dialysis; however, this treatment plan did not consider many specific treatment areas or organs at risk,

and therefore 77263 would likely not be appropriate. A reduction in administered activity in this example led to elimination of 1 treatment administration compared with standard administration workflows – this led to substantial and immediate payer cost savings, and reduced risk of severe toxicity experienced by the patient.

Example 4. ^{131}I -MIBG (with Tumor, Marrow, and Kidney Dosimetry)

After clinical evaluation and results from diagnostic ^{123}I -MIBG SPECT/CT imaging, a patient was deemed to be eligible for treatment with ^{131}I -MIBG RPT. Per the Food and Drug Administration–approved label for this RPT, pretreatment dosimetry was performed using a small quantity of the therapeutic radiopharmaceutical.

Radiopharmaceutical was administered (185 MBq) in a manner consistent with manufacturer recommendations and institutional policy. After administration, dosimetric sampling was collected. Dosimetric sampling consisted of blood sample collection at 4, 24, 48, and 96 h after administration and imaging (WB conjugate planar + SPECT/CT of the abdomen) at 24, 48, and 96 h after administration.

Dosimetry proceeded by use of 510(k)-cleared medical device software for generalized 3D RPT dosimetry. A physicist, physician, or another qualified individual segmented organs of interest (whole liver, spleen, kidneys) as well as the 3 largest tumor lesions. Marrow dosimetry was performed by absorbed-fraction (MIRD) methods based on WB, blood, and normal organ time-integrated-activity quantification. A 3D dose plan normalized to a nominal administered activity was reviewed by the authorized user, and it was determined that a cumulative administered activity of 26 GBq was appropriate to maximize tumor dose, without exceeding dose limits to normal tissues (in this case bone marrow). ^{131}I -MIBG is typically administered over 2 treatments, and therefore a plan of administering 13 GBq in each treatment, separated by at least 90 d. Three-dimensional dosimetry statistics for this final treatment plan were generated, and a treatment plan report was generated and signed by the physicist and authorized user (77295). An independent qualified individual reviewed this plan for appropriateness and accuracy, including performing a simple dose calculation via established absorbed-fraction (MIRD) methods. This secondary dose verification was documented in the medical record (77300).

The patient returned for initial treatment. In accordance with the treatment plan, 13 GBq of ^{131}I -MIBG was administered. The patient underwent posttreatment dosimetric sampling with the same blood collection and imaging time points as described above. Dosimetry was performed (77300) over the 96 h after administration, and a posttreatment dose report was documented and reviewed by the treating physician (77300). On the basis of exposure rate measurements, the patient was retained with “in-patient” status until the end of day 2, at which time the patient met Nuclear Regulatory Commission and state release criteria. Before and after release, the patient was monitored for treatment-related adverse events.

After 90 d had elapsed, the patient returned for an additional treatment of 13 GBq (26 GBq cumulative) in accordance with the treatment plan. Dosimetry was again performed (77300), with a final cumulative dose report being generated, documented, and reviewed by the treating physician.

The following is a summary of the procedure and corresponding CPT codes:

- Pre-Tx 131I WB planar imaging (3 d), 78804;
- Pre-Tx 131I abdominal SPECT/CT (3 d), 78832;
- 3D radiation treatment planning, 77295;
- Plan check/simple dosimetry, 77300;
- Tx 1 131I WB planar imaging (3 d), 78804;
- Tx 1 131I abdominal SPECT/CT (3 d), 78832;
- Dosimetry assessment, 77300;
- Tx 2 131I WB planar imaging (3 d), 78804;
- Tx 2 131I abdominal SPECT/CT (3 d), 78832; and
- Dosimetry assessment, 77300

Comments. Many patients who can benefit from ¹³¹I-MIBG therapy are quite young (below the age of 4), and therefore require general anesthesia for dosimetric imaging. In these cases the treating physician, in collaboration with the multidisciplinary team, may choose to forgo dosimetry after Tx 1 and Tx 2, or develop a nonstandard pretreatment dosimetry workflow in consultation with a qualified medical physicist (77370). An example of a modified dosimetric sampling would be standard blood collections; WB planar imaging at 24 h; and WB counting (nonanesthetized) at 4, 24, 48, and 96 h after administration. In general, these modifications preclude tumor dosimetry; however, dose to the primary limiting organ (bone marrow) can be assessed with reduced precision. Additional details regarding abbreviated dosimetry methods can be found in the EANM procedure guidelines for ¹³¹I-MIBG therapy (39).

CURRENT DEFICIENCIES AND FUTURE NEEDS

Although the coding strategies described herein are appropriate to meet the immediate need for baseline support of dosimetry and treatment planning for RPT, the existing CPT code set does not contain a sufficient spectrum of codes to describe the current and anticipated process of care for RPT procedures. Some services fit within the scope of existing codes; however, many services remain unsupported or undersupported by existing codes. New and dedicated codes for theranostics should be developed, with collaboration between relevant stakeholders (Society of Nuclear Medicine and Molecular Imaging [SNMMI], American Society for Radiation Oncology [ASTRO], American College of Radiology [ACR], Society of Interventional Radiology [SIR], American Association of Physicists in Medicine [AAPM], and others). What follows are several notable deficiencies among the current coding structure; however, this list is neither intended to be comprehensive nor authoritative.

Partition and Volume-Based ⁹⁰Y-Microsphere Treatment Planning

Although 77295 may be appropriate when the clinical case rises to a level of complexity requiring generation and review of 3D isodose volumes relative to normal tissue and tumor targets, a common method of calculation in somewhat simpler cases (e.g., single lesion, well-defined uptake, limited volume of perfusion) involves an approximation of uniform activity distribution in the target tumor and normal liver. Under this approximation, one must determine the volume of treated liver + tumor, the total liver volume, the tumor-to-liver concentration ratio, and the fraction of activity shunting to lungs and other normal tissues. On the basis of these data, calculations can be performed to provide a range of potential treatment plans, from which the authorized user can select the most appropriate. The effort for these activities may

exceed what is included in 77261–77263, and thus new codes may need to be developed based on plan complexity.

WB Counting

In some cases, particularly pediatric patients, it may be more appropriate to use serial WB counting in lieu of serial WB planar imaging for the purposes of bone marrow dose assessment. WB counting may involve use of a scintillation spectrometer (i.e., shielded NaI thyroid uptake probe) or use of an ion chamber survey meter. The WB counting procedures, which can allow for data acquisition without general anesthesia in pediatric patients, is not currently supported by any existing code.

More Than 2 SPECT/CT or WB Planar Scans

As indicated by examples provided in the section “Specific Coding Examples” in this paper, it is sometimes necessary to obtain more than 2 imaging fields of view (areas) or imaging time points to adequately characterize the spatial and temporal distribution of radiopharmaceutical in organs and tumors of interest. 78804 and 78832 provide reimbursement for only 2 WB planar images and SPECT/CT areas or imaging timepoints, respectively. Revision of these code, or creation of a modifier to account for additional timepoints, should be undertaken.

RPT “Simulation”

Although not commonly performed (with the exception of ¹³¹I-MIBG), administration of a small quantity of the therapeutic radiopharmaceutical or an appropriate surrogate followed by dosimetric sampling may emerge as a useful technique for treatment planning. This process may or may not include supportive compounds, such as infusion of renal-protective amino acids, as these compounds are known to alter the pharmacokinetics of the therapeutic radiopharmaceutical. Dedicated codes for this workflow and associated radiopharmaceutical costs may be needed.

Blood Collection and Counting

Analysis of biologic samples is needed for determination of bone marrow dose in most cases. Analysis may include whole-blood spectroscopic counting, plasma spectroscopic counting, and determination of the patient’s hematocrit. These procedures, typically performed by a nuclear medicine technologist, appear unsupported by the current code set.

Sequential PET/CT for RPT

Interest is growing in the use of positron-emitting surrogates for RPTs, such as ⁶⁴Cu-DOTATATE as a surrogate for ¹⁷⁷Lu-DOTATATE. Currently there are no codes for multiple-time-point PET/CT imaging, such as what is available for SPECT/CT.

Consensus Regarding “Simplified” Dosimetry

As discussed in the section “Primary Stakeholders,” there are some emerging data suggesting that adequate dosimetry can be performed from a limited number of imaging time points based on population pharmacokinetic data. These emerging techniques should be examined by experts in the field, to develop consensus recommendations regarding which clinical scenarios are well-suited to simplification or time-point reduction.

DISCLAIMER

The opinions provided in this paper are those of members of the SNMMI Dosimetry Task Force based on their coding experience. Always check with your local insurance carriers, as policies vary

by region. The billing strategies described in this paper are unlikely to be accepted universally, and so the final decision for coding for any procedure must be made by the physician, considering regulations of insurance carriers and any local, state or federal laws that apply to the physician's practice. Neither SNMMI nor any of its officers, directors, agents, employees, committee members, or other representatives shall have any liability for any claim, whether founded or unfounded, of any kind whatsoever, including but not limited to any claim for costs and legal fees, arising from the use of these opinions.

DISCLOSURE

Denise A.M. Merlino is a consultant of the SNMMI. No other potential conflict of interest relevant to this article was reported.

ACKNOWLEDGMENTS

We are grateful for input from ASTRO and ACR representatives, as well as support and input from the SNMMI Dosimetry Task Force.

KEY POINTS

QUESTION: Is it possible to obtain reimbursement for radiopharmaceutical dosimetry?

PERTINENT FINDINGS: Existing reimbursement codes are applicable to several RPT dosimetry procedures, provided the code description matches the activity being performed. Some activities are not well supported by existing codes, and efforts should be made to address this need.

IMPLICATIONS FOR PATIENT CARE: Cost recovery for radiopharmaceutical dosimetry will allow for widespread adoption, thus leading to improved clinical management of patients.

REFERENCES

- Becquerel H, Curie P. Action physiologique des rayons du radium. *Compt Rend Acad Sci.* 1901;132:1289–1291.
- Daniel J. The x-rays. *Science.* 1896;3:562–563.
- Strigari L, Konijnenberg M, Chiesa C, et al. The evidence base for the use of internal dosimetry in the clinical practice of molecular radiotherapy. *Eur J Nucl Med Mol Imaging.* 2014;41:1976–1988.
- Wessels BW, Konijnenberg MW, Dale RG, et al. MIRD pamphlet no. 20: the effect of model assumptions on kidney dosimetry and response: implications for radionuclide therapy. *J Nucl Med.* 2008;49:1884–1899.
- Chiesa C, Mira M, Bhoori S, et al. Radioembolization of hepatocarcinoma with 90 Y glass microspheres: treatment optimization using the dose-toxicity relationship. *Eur J Nucl Med Mol Imaging.* 2020;47:3018–3032.
- Violet J, Jackson P, Ferdinandus J, et al. Dosimetry of ¹⁷⁷Lu-PSMA-617 in metastatic castration-resistant prostate cancer: correlations between pretherapeutic imaging and whole-body tumor dosimetry with treatment outcomes. *J Nucl Med.* 2019;60:517–523.
- Garin E, Tselikas L, Guiu B, et al. Personalised versus standard dosimetry approach of selective internal radiation therapy in patients with locally advanced hepatocellular carcinoma (DOSISPHERE-01): a randomised, multicentre, open-label phase 2 trial. *Lancet Gastroenterol Hepatol.* 2021;6:17–29.
- Ilhan E, Sandström M, Wassberg C, et al. Dose response of pancreatic neuroendocrine tumors treated with peptide receptor radionuclide therapy using ¹⁷⁷Lu-DOTATATE. *J Nucl Med.* 2015;56:177–182.
- Pauwels S, Barone R, Walrand S, Borson-Chazot F. Practical dosimetry of peptide receptor radionuclide therapy with ⁹⁰Y-labeled somatostatin analogs. *J Nucl Med.* 2005;46:925.
- Chansanti O, Jahangiri Y, Matsui Y, et al. Tumor dose response in Yttrium-90 resin microsphere embolization for neuroendocrine liver metastases: a tumor-specific analysis with dose estimation using SPECT-CT. *J Vasc Interv Radiol.* 2017;28:1528–1535.
- Hou X, Brosch J, Uribe C, et al. Feasibility of single-time-point dosimetry for radiopharmaceutical therapies. *J Nucl Med.* 2021;62:1006–1011.
- Menda Y, Madsen MT, O'Dorisio TM, et al. ⁹⁰Y-DOTATOC dosimetry-based personalized peptide receptor radionuclide therapy. *J Nucl Med.* 2018;59:1692–1698.
- Fendler WP, Reinhardt S, Ilhan H, et al. Preliminary experience with dosimetry, response and patient reported outcome after ¹⁷⁷Lu-PSMA-617 therapy for metastatic castration-resistant prostate cancer. *Oncotarget.* 2017;8:3581.
- Sandström M, Freedman N, Fröss-Baron K, Kahn T, Sundin A. Kidney dosimetry in 777 patients during ¹⁷⁷Lu-DOTATATE therapy: aspects on extrapolations and measurement time points. *EJNMMI Phys.* 2020;7:73.
- Seo Y, Huh Y, Huang S-Y, et al. Simplified and practical pretherapy tumor dosimetry: a feasibility study for ¹³¹I-MIBG therapy of neuroblastoma using ¹²⁴I-MIBG PET/CT. *Med Phys.* 2019;46:2477–2486.
- Zhao W, Esquinas PL, Frezza A, Hou X, Beauregard J-M, Celler A. Accuracy of kidney dosimetry performed using simplified time activity curve modelling methods: a ¹⁷⁷Lu-DOTATATE patient study. *Phys Med Biol.* 2019;64:175006.
- Jackson PA, Hofman MS, Hicks RJ, Scalzo M, Violet J. Radiation dosimetry in ¹⁷⁷Lu-PSMA-617 therapy using a single posttreatment SPECT/CT scan: a novel methodology to generate time-and tissue-specific dose factors. *J Nucl Med.* 2020;61:1030–1036.
- Hänscheid H, Lapa C, Buck AK, Lassmann M, Werner RA. Dose mapping after endoradiotherapy with ¹⁷⁷Lu-DOTATATE/DOTATOC by a single measurement after 4 days. *J Nucl Med.* 2018;59:75–81.
- Madsen MT, Menda Y, O'Dorisio TM, O'Dorisio MS. Single time point dose estimate for exponential clearance. *Med Phys.* 2018;45:2318–2324.
- Benua RS, Cicale NR, Sonnenberg M, Rawson R. The relation of radioiodine dosimetry to results and complications in the treatment of metastatic thyroid cancer. *Am J Roentgenol Radium Ther Nucl Med.* 1962;87:171–182.
- Sgouros G, Song H, Ladenson PW, Wahl RL. Lung toxicity in radioiodine therapy of thyroid carcinoma: development of a dose-rate method and dosimetric implications of the 80-mCi rule. *J Nucl Med.* 2006;47:1977–1984.
- Kennedy A, Coldwell D, Sangro B, Wasan H, Salem R. Radioembolization for the treatment of liver tumors: general principles. *Am J Clin Oncol.* 2012;35:91–99.
- Strosberg J, El-Haddad G, Wolin E, et al. Phase 3 trial of ¹⁷⁷Lu-Dotatate for midgut neuroendocrine tumors. *N Engl J Med.* 2017;376:125–135.
- Prima DA, Chin BB, Noto RB, et al. Efficacy and safety of high-specific-activity ¹³¹I-MIBG therapy in patients with advanced pheochromocytoma or paraganglioma. *J Nucl Med.* 2019;60:623–630.
- Quach A, Ji L, Mishra V, et al. Thyroid and hepatic function after high-dose ¹³¹I-metaiodobenzylguanidine (¹³¹I-MIBG) therapy for neuroblastoma. *Pediatr Blood Cancer.* 2011;56:191–201.
- Hoskin P, Sartor O, O'Sullivan JM, et al. Efficacy and safety of radium-223 dichloride in patients with castration-resistant prostate cancer and symptomatic bone metastases, with or without previous docetaxel use: a prespecified subgroup analysis from the randomised, double-blind, phase 3 ALSYMPCA trial. *Lancet Oncol.* 2014;15:1397–1406.
- Sartor O, de Bono J, Chi KN, et al. Lutetium-177-PSMA-617 for metastatic castration-resistant prostate cancer. *N Engl J Med.* 2021;385:1091–1103.
- Forrer F, Uusijärvi H, Storch D, Maecke HR, Mueller-Brand J. Treatment with ¹⁷⁷Lu-DOTATOC of patients with relapse of neuroendocrine tumors after treatment with ⁹⁰Y-DOTATOC. *J Nucl Med.* 2005;46:1310–1316.
- Natwa M, Passalacqua S, Chen M-K, et al. Low incidence rates of mucositis, febrile neutropenia or sepsis in the prospective, randomized phase 3 sierra trial for patients with relapsed or refractory acute myeloid leukemia with targeted delivery of anti-CD45 iodine (¹³¹I) apamistamab [Iomab-B] [abstract]. *J Nucl Med.* 2021;62(suppl 1):1694.
- Garin E, Rolland Y, Pracht M, et al. High impact of macroaggregated albumin-based tumour dose on response and overall survival in hepatocellular carcinoma patients treated with ⁹⁰Y-loaded glass microsphere radioembolization. *Liver Int.* 2017;37:101–110.
- Kappadath SC, Mikell J, Balagopal A, Baladandayuthapani V, Kaseb A, Mahvash A. Hepatocellular carcinoma tumor dose response after ⁹⁰Y-radioembolization with glass microspheres using ⁹⁰Y-SPECT/CT-based voxel dosimetry. *Int J Radiat Oncol Biol Phys.* 2018;102:451–461.
- Maxon HR, Thomas SR, Hertzberg VS, et al. Relation between effective radiation dose and outcome of radioiodine therapy for thyroid cancer. *N Engl J Med.* 1983;309:937–941.
- Flux GD, Haq M, Chittenden SJ, et al. A dose-effect correlation for radioiodine ablation in differentiated thyroid cancer. *Eur J Nucl Med Mol Imaging.* 2010;37:270–275.

34. Strom DJ, Thomadsen BR, Suleiman OH, Quinn DM, Miller KL. *NCRP Report No. 160, Ionizing Radiation Exposure of the Population of the United States*. National Council on Radiation Protection and Measurements (NCRP); 2009.
35. Hänscheid H, Lassmann M, Luster M, Kloos RT, Reiners C. Blood dosimetry from a single measurement of the whole body radioiodine retention in patients with differentiated thyroid carcinoma. *Endocr Relat Cancer*. 2009;16:1283–1289.
36. Jentzen W, Bockisch A, Ruhlmann M. Assessment of simplified blood dose protocols for the estimation of the maximum tolerable activity in thyroid cancer patients undergoing radioiodine therapy using ^{124}I . *J Nucl Med*. 2015;56:832–838.
37. Atkins F, Van Nostrand D, Moreau S, Burman K, Wartofsky L. Validation of a simple thyroid cancer dosimetry model based on the fractional whole-body retention at 48 hours post-administration of ^{131}I . *Thyroid*. 2015;25:1347–1350.
38. Chittenden SJ, Pratt BE, Pomeroy K, et al. Optimization of equipment and methodology for whole body activity retention measurements in children undergoing targeted radionuclide therapy. *Cancer Biother Radiopharm*. 2007;22:243–249.
39. Giammarile F, Chiti A, Lassmann M, Brans B, Flux G. EANM procedure guidelines for ^{131}I -meta-iodobenzylguanidine (^{131}I -mIBG) therapy. *Eur J Nucl Med Mol Imaging*. 2008;35:1039–1047.
40. Gustafsson J, Rodeño E, Mínguez P. Feasibility and limitations of quantitative SPECT for ^{223}Ra . *Phys Med Biol*. 2020;65:085012.
41. Ghaly M, Sgouros G, Frey E. Quantitative dual isotope SPECT imaging of the alpha-emitters Th-227 and Ra-223 [abstract]. *J Nucl Med*. 2019;60(suppl 1):41.
42. Pacilio M, Ventroni G, De Vincentis G, et al. Dosimetry of bone metastases in targeted radionuclide therapy with alpha-emitting ^{223}Ra -dichloride. *Eur J Nucl Med Mol Imaging*. 2016;43:21–33.
43. Takahashi A, Miwa K, Sasaki M, Baba S. A Monte Carlo study on ^{223}Ra imaging for unsealed radionuclide therapy. *Med Phys*. 2016;43:2965–2974.
44. Elschot M, Nijssen JF, Lam MG, et al. $^{99\text{m}}\text{Tc}$ -MAA overestimates the absorbed dose to the lungs in radioembolization: a quantitative evaluation in patients treated with ^{166}Ho -microspheres. *Eur J Nucl Med Mol Imaging*. 2014;41:1965–1975.
45. Dittmann H, Kopp D, Kupferschlaeger J, et al. A prospective study of quantitative SPECT/CT for evaluation of lung shunt fraction before SIRT of liver tumors. *J Nucl Med*. 2018;59:1366–1372.
46. Lopez B, Mahvash A, Lam MG, Kappadath SC. Calculation of lung mean dose and quantification of error for ^{90}Y -microsphere radioembolization using $^{99\text{m}}\text{Tc}$ -MAA SPECT/CT and diagnostic chest CT. *Med Phys*. 2019;46:3929–3940.
47. Hou X, Brosch J, Uribe C, et al. Feasibility of single-time-point dosimetry for radiopharmaceutical therapies. *J Nucl Med*. 2021;62:1006–1011.
48. Madsen M. Single time point dose estimate for bi-exponential clearance. *Soc Nuclear Med*; 2017.
49. Bolch WE, Eckerman KF, Sgouros G, Thomas SR. MIRD pamphlet no. 21: a generalized schema for radiopharmaceutical dosimetry—standardization of nomenclature. *J Nucl Med*. 2009;50:477–484.
50. Dewaraja YK, Frey EC, Sgouros G, et al. MIRD pamphlet no. 23: quantitative SPECT for patient-specific 3-dimensional dosimetry in internal radionuclide therapy. *J Nucl Med*. 2012;53:1310–1325.
51. Bolch WE, Bouchet LG, Robertson JS, et al. MIRD pamphlet no. 17: the dosimetry of nonuniform activity distributions—radionuclide S values at the voxel level. *J Nucl Med*. 1999;40:11S–36S.
52. Siegel JA, Thomas SR, Stubbs JB, et al. MIRD pamphlet no. 16: techniques for quantitative radiopharmaceutical biodistribution data acquisition and analysis for use in human radiation dose estimates. *J Nucl Med*. 1999;40:37S–61S.
53. Physician Fee Schedule: July 2021 release. <https://www.cms.gov/medicare/medicare-fee-service-payment/physicianfeesched/pfs-relative-value-files/rvu21c>. Accessed November 1, 2021.

Dosimetry in Clinical Radiopharmaceutical Therapy of Cancer: Practicality Versus Perfection in Current Practice

Neeta Pandit-Taskar¹, Amir Iravani², Dan Lee³, Heather Jacene⁴, Dan Pryma⁵, Thomas Hope⁶, Babak Saboury⁷, Jacek Capala⁷, and Richard L. Wahl²

¹Memorial Sloan Kettering Cancer Center, New York, New York; ²Washington University School of Medicine, St. Louis, Missouri; ³Ochsner Medical Center, New Orleans, Louisiana; ⁴Dana-Farber Cancer Institute, Boston, Massachusetts; ⁵Penn Medicine, University of Pennsylvania, Philadelphia, Pennsylvania; ⁶University of San Francisco, San Francisco, California; and ⁷National Institutes of Health, Bethesda, Maryland

The use of radiopharmaceutical therapies (RPTs) in the treatment of cancers is growing rapidly, with more agents becoming available for clinical use in last few years and many new RPTs being in development. Dosimetry assessment is critical for personalized RPT, insofar as administered activity should be assessed and optimized in order to maximize tumor-absorbed dose while keeping normal organs within defined safe dosages. However, many current clinical RPTs do not require patient-specific dosimetry based on current Food and Drug Administration-labeled approvals, and overall, dosimetry for RPT in clinical practice and trials is highly varied and underutilized. Several factors impede rigorous use of dosimetry, as compared with the more convenient and less resource-intensive practice of empiric dosing. We review various approaches to applying dosimetry for the assessment of activity in RPT and key clinical trials, the extent of dosimetry use, the relative pros and cons of dosimetry-based versus fixed activity, and practical limiting factors pertaining to current clinical practice.

Key Words: dosimetry; theranostics; radiopharmaceutical therapy; RPT; radionuclide

J Nucl Med 2021; 62:60S–72S
DOI: 10.2967/jnumed.121.262977

Radiopharmaceutical therapies (RPTs) have been used in the treatment of cancers for many decades. Recent advances in theranostics have led to Food and Drug Administration (FDA) approval of new RPTs and a surge in the development of several novel radiotargeted small molecules or antibodies for therapy. Dosimetry assessment is important to maximizing absorbed radiation dose to tumor in order to optimize tumor response and minimize normal-organ absorbed dose and toxicity. Personalized dosimetry can help adjust for interpersonal variation in biodistribution and tolerance to RPT, as well as intrapersonal heterogeneity of tumor uptake, and can be used to maximize administered activity when repeat dosing might be precluded by the development of tumor resistance or antibodies, such as after radioimmunotherapy.

Despite the recognized need for, and advantages of, dosimetry for personalized RPT (1), the use of dosimetry in clinical care varies widely across different RPTs (2). It is notable that,

currently, dosimetry has not been mandated for all FDA-approved RPTs. Furthermore, dosimetry is incorporated inconsistently in the development of novel agents; for example, the recently completed VISION trial with ¹⁷⁷Lu-prostate-specific membrane antigen (PSMA) included a fixed activity in prespecified cycles. Dosimetry in routine clinical practice is limited by variations in methodologies for establishing administered activity in published studies and trials, and by the lack of large prospective studies showing superior outcomes and survival benefit for dosimetry-based treatments as compared with empiric dosing. Although guidelines have been developed for optimizing various RPTs with dosimetry (3,4), application of these for dosimetry remains inconsistent.

Integrating dosimetry into routine clinical care poses technical, logistical, and practical challenges. Key drawbacks include differences in methodology, need for elaborate scanning procedures and blood or urine sampling, suitability of paired diagnostic radiopharmaceuticals, and available processing software. The ease of using a fixed activity allows for uniform and universal use, leading to the predominance of this method for administering activity in clinical RPT.

We present an overview of administered activity in various RPTs, extent of use, and integration of dosimetry for activity in routine clinical care. We compare and contrast methodologies for determining administered activity and use of dosimetry in published studies and key trials for FDA-approved RPT. We enumerate logistic challenges and present our perspective for balanced use of dosimetry in clinical practice and trials. This review is limited to RPT in malignancies and is not meant to be a comprehensive review of the literature on all RPT, dosimetry methodologies or biology, which are discussed in other articles of this supplement to *The Journal of Nuclear Medicine*.

CLINICAL EVIDENCE AND PRACTICE: VARIATION IN DOSIMETRY ASSESSMENT AND SELECTION OF ADMINISTERED ACTIVITY FOR RPT

In current practice, RPT is administered differently for different agents. Several approaches have been used to determine activity for treatment, ranging from fixed activity dosing to that based on pre- or posttreatment dosimetry with or without posttreatment validation. Some agents include dosimetry in the package label, such as FDA-approved ¹³¹I-tositumomab and ¹³¹I-iodobenguane (5), whereas others such as ²²³RaCl₂ and ¹⁷⁷Lu-DOTATATE (Lutathera; Advanced Accelerator Applications) do not (Table 1).

Received Oct. 14, 2021; revision accepted Oct. 22, 2021.
For correspondence or reprints, contact Neeta Pandit-Taskar (pandit-n@mskcc.org).
COPYRIGHT © 2021 by the Society of Nuclear Medicine and Molecular Imaging.

TABLE 1
RPT Administration for Different Agents

Agent	Indication	Cycles and intervals	Administered activity per cycle	Dosimetry required?	Organ constraints
¹³¹ I-sodium iodide	Differentiated thyroid cancer, remnant ablation, adjuvant, treatment of metastatic disease; benign thyroid disease such as goiter	1	Empiric variable activity based on indication or dosimetry guided to 2 Gy to blood or 2,960 MBq (80 mCi) retained in WB at 48 h if diffuse lung metastases	No	2 Gy to blood
¹⁵³ Sm-lexidronam	Symptomatic osteoblastic metastases	1	Fixed-weight-based activity, 37 MBq/kg	No	NA
⁸⁹ SrCl	Symptomatic osteoblastic metastases	1	Fixed activity, 148 MBq	No	NA
²²³ Ra-dichloride	Prostate cancer, metastatic disease to bone	6 at 4-wk intervals	Fixed-weight-based activity, 55 kBq/kg	No	NA
¹⁷⁷ Lu-DOTATATE	Neuroendocrine tumor with somatostatin receptor expression	4 at 8-wk intervals	Fixed activity, 7.4 GBq	No	NA
¹⁷⁷ Lu-PSMA-617	Prostate cancer, metastatic disease	4-6 cycles at 6-wk intervals	Fixed activity, 7.4 GBq	No	NA
¹³¹ I-MIBG/HSA- ¹³¹ I-iodobenguane*	Pheochromocytoma or paraganglioma	2 at 12-wk intervals	Fixed activity, for weight >62.5 kg, 17.5 GBq; for weight <62.5 kg, 296 MBq/kg	Yes, WB planar days 0, 1-2, 2-5	*12 Gy to red marrow, 16.5 Gy to lung, 18 Gy to kidney, and 31 Gy to liver
⁹⁰ Y-ibritumomab tiuxetan	Follicular or low-grade NHL	1	14.8 MBq/kg if platelets >150,000; 11.1 MBq/kg if platelets >100,000 and <150,000	No	NA
¹³¹ I-tositumomab†	Relapsed or refractory NHL	1	Based on dosimetry: 75 cGy to WB if platelets >150,000; 65 cGy to WB if platelets >100,000 and <150,000	Yes, WB planar days 0, 2-4, 6-7	75 or 65 cGy to WB
⁹⁰ Y-TheraSphere	Unresectable hepatocellular carcinoma	1 (whole-liver treatment often split over separate treatments)	80-150 Gy to liver	Yes, tomographic perfused liver volume and planar lung shunt	80-150 Gy to liver, <30 Gy to lung per treatment and <50 Gy cumulative
⁹⁰ Y-SIR-Spheres	Unresectable liver metastases from colorectal cancer	1 (whole-liver treatment often split over separate treatments)	Calculation based on body surface area, liver volume, involved tumor volume, and lung shunt	Yes, tomographic perfused liver volume and planar lung shunt	<30 Gy to lung

*The limits in the last column pertain to ¹³¹I-iodobenguane only.

†No longer commercially available.

NA = not applicable; HSA = high specific activity; NHL = non-Hodgkin Lymphoma.

Radioactive Iodine (RAI) Therapy for Differentiated Thyroid Cancer

One of the earliest reports of use of RAI dosimetry was described in 1962 by Benua et al. (6). Dosimetry has been found to be useful for planning RAI treatment of differentiated thyroid cancer, especially for treatment of metastatic disease using high activity. Dosimetry estimates are aimed primarily at limiting absorbed dose to critical organs such as blood (bone marrow) (2 Gy) and lung (2.96 GBq [80-mCi whole-body (WB) retention at 48 h]) (6,7).

Dosing schemes for the treatment of thyroid cancer have been based on an empiric fixed activity, upper-limit-of-blood and body/lung dosimetry, and quantitative tumor or lesion dosimetry. Clinicians commonly use a fixed activity based on American Thyroid Association guidelines, which recommend a risk-adapted approach to choosing the empiric activity of RAI while acknowledging that dosimetry methods may be best reserved for patients with distant metastases, especially those involving bones (which generally require larger activity), to avoid marrow and pulmonary toxicity (7). Generally, the flat activity ranges from 1.1 to 5.55 GBq (30–150 mCi) in postsurgical ablation settings and up to 11.1 GBq (300 mCi) for treatments of metastatic disease (8). American Thyroid Association guidelines (7) recommend 1.1 GBq (30 mCi) of activity for low-risk thyroid remnant ablation (low-volume central neck nodal metastasis with no other known gross residual disease or other adverse features), whereas a higher activity may be administered to patients with less than total or near-total thyroidectomy and in whom a larger remnant is suspected or for whom adjuvant therapy is intended. When RAI is intended for initial adjuvant therapy aimed at suspected microscopic residual disease, an activity of 3.7–5.5 GBq (100–150 mCi) is generally used. For administration of RAI in metastatic settings, a higher fixed activity of up to 7.4–9.25 GBq (200–250 mCi) may be used. American Thyroid Association guidelines have no firm recommendation for blood- or body-based dosimetry for RAI treatment for locoregional or distant metastatic disease.

Recent guidelines recommend greater individualization and deintensification, though there is general clinical ambivalence regarding RAI therapy, recognizing that a large number of patients have an excellent overall prognosis (7). Prospective blinded and randomized studies on deescalation of activity are limited, especially in low- or intermediate-risk patients; some include a small number of patients for remnant ablation (9,10). RAI dosimetry approaches vary but primarily assess the maximum tolerated absorbed radiation dose (MTD) to the bone marrow or the lesion or lung absorbed-dose limit; lesion-absorbed dose is rarely used clinically for establishing administered activity. (11–13). Bone marrow MTD is based on a surrogate threshold blood-absorbed dose of 2 Gy (6,14–19) and is generally performed before treatment, allowing for appropriate adjustment of activity. In a retrospective study (8), whereas an activity within 5.18 GBq (140 mCi) rarely exposed blood to more than 2 Gy, activity of 9.25 GBq (250 mCi) frequently exceeded the bone marrow threshold (in 22%–50% of patients), with the investigators noting that elder subjects were at higher risk for exceeding limits. Dosimetry is also preferred for those presenting with recurrent disease after receiving fixed-activity treatments, for maximizing treatment in high-risk patients to improve efficacy (11), and for those receiving RAI therapy using recombinant thyroid-stimulating hormone because of a more rapid clearance. Target-based dosimetry methods have generally used an absorbed dose of 300 Gy to the thyroid remnant and 80 Gy to metastatic lesions (20); however, technical

limitations in the assessment of remnant or lesion size may lead to inaccuracies in the calculated absorbed dose (21).

There are very limited data on the activity and the absorbed radiation dose–response relationship and outcomes in metastatic disease, as wide variation in lesion-absorbed dose has been noted (12,22,23). Dosimetry generally comprises $^{131}\text{I-NaI}$ scans at multiple time points combined with blood sampling. The poor imaging characteristics of $^{131}\text{I-NaI}$, the quantification heterogeneity of interlesional and intralesional uptake, and the inaccuracies in the measurement of lesion mass make establishing dose–response relationships all the more challenging.

Some of these challenges may be overcome using $^{124}\text{I-NaI}$ PET imaging for lesion dosimetry and planning of treatments, especially in those who require a high-activity treatment (11,24). $^{124}\text{I-NaI}$ PET/CT dosimetry imaging may simplify blood-absorbed dose assessment by requiring fewer blood samples (25) and improving remnant and individual-lesion dosimetry (26–28). Although $^{124}\text{I-NaI}$ PET–based dosimetry typically requires multiple sessions of serial PET/CT imaging, recent data suggest that a simplified approach, with imaging only at 24 and 96 h, may suffice for dosimetry (29). Additional data are emerging, but ^{124}I is not yet FDA-approved and is limited in availability for wide use.

Bone-Targeted Therapy

^{153}Sm -lexidronam, used for pain palliation, is administered in a fixed activity based on body weight—37 MBq/kg—as determined in phase I and II studies. RPT escalation studies used an empiric, non-dosimetry-based activity with clinical endpoints, though dosimetry was assessed for marrow and critical organs (30). A phase II study showed efficacy and pain control in 74% of patients. Similarly, $^{89}\text{SrCl}_2$ is administered at a fixed activity of 148 MBq (4 mCi). Although ^{89}Sr -chloride and ^{153}Sm -ethylenediamine tetra (methylene phosphonic acid) yielded significant and durable pain relief, there are scant data on impact on patient survival.

α -emitting $^{223}\text{RaCl}_2$ marked a paradigm shift in the use of RPT, expanding it from palliation alone to the treatment of bone metastases. The ALSYMPCA trial noted pain relief, improved overall survival, and a delay in symptomatic skeletal events in patients with metastatic castration-resistant prostate cancer treated with $^{223}\text{RaCl}_2$ (31, 32). $^{223}\text{RaCl}_2$ (Xofigo; Bayer) is administered in 6 cycles of 55 kBq/kg each, does not require dosimetry assessment, and is based on phase I and II studies that used fixed-weight–based activity escalation with clinical endpoints to determine maximum tolerated activity. The phase I trial gave single administrations of up to 250 kBq/kg, which was later escalated to multiple infusions of 55 kBq/kg every 4 wk (33). A phase II trial used 6 infusions of 55 kBq/kg or 88 kBq/kg and an extended regimen of 12 infusions of 55 kBq/kg, with no improvement in outcomes at higher activity, though higher rates of complications were noted (34). Recent phase I/II study data on retreatment used an additional 6 infusions of 55 kBq/kg (35) without any dosimetry estimates and reported good tolerance and low toxicity, allowing for additional treatment beyond the standard regimen at the same fixed-activity regimen.

That the hematologic toxicities associated with the current standard regimen are relatively minor suggests that some patients may be eligible for more infusions or higher administered activities. Prior treatments, extent of bone marrow involvement, and combination treatments may lead to higher toxicities, limiting benefit (36). It could be argued that dosimetry would help optimize treatments in such situations. However, quantitative imaging to inform

activity selection is difficult because of lack of a validated companion diagnostic for dosimetry and scant, polychromatic photon emissions from ^{223}Ra that require prolonged image acquisition times (37). Bone tracers such as $^{99\text{m}}\text{Tc}$ -based bone scans or Na^{18}F PET may be used for lesion-based dosimetry (37,38) but are not ideal theranostic pairs, given differences in biodistribution and lack of bowel excretion, similar to $^{223}\text{RaCl}_2$ (39).

Peptide Receptor Radionuclide Therapy (PRRT) with ^{177}Lu -DOTATATE

PRRT with ^{177}Lu -DOTATATE was approved by the FDA in 2018 after the multicenter, randomized 2-arm NETTER1 study. ^{177}Lu -DOTATATE is administered in a fixed activity of 7.4 GBq/cycle over 4 cycles, each approximately 8 wk apart (40,41), without requiring any dosimetry for establishing treatment activity or number of cycles, similar to the schema in the NETTER1 study. Currently, most centers use fixed-activity-based dosing schedules without performing any dosimetry for kidney-, marrow-, or lesion-absorbed dose; modifications of the activity or the number of administrations is based primarily on clinical risk factors or toxicity (mainly hematologic). Activity is modified primarily by lowering the fixed activity rather than by dosimetry. Initial studies assessed a total activity threshold averaging 26.4 GBq for ^{177}Lu -octreotate treatments. These studies were based on planar dosimetry data from only 5 patients and on a kidney-absorbed dose limit of 23 Gy adapted from radiation oncology-derived limits and not established from prospective dosimetry of actual kidney-absorbed dose (42). Overall, wide variation in the estimated kidney-absorbed dose across studies performed using varying methodologies (43) suggests undertreatment of most patients (relative to the allowable maximum kidney-absorbed dose) and possible overtreatment of a subset of patients with fixed activity.

^{68}Ga - or ^{64}Cu -DOTATATE imaging establishes somatostatin receptor-expressing lesions and is used primarily for patient selection. Although dosimetry is more feasible with ^{64}Cu -DOTATATE imaging, given the longer half-life of ^{64}Cu , its accuracy is not yet established and use for dosimetry with clinical PRRT remains to be validated. Evaluation of kidney-absorbed dose can be based on the posttreatment ^{177}Lu -DOTATATE imaging and is recommended in those with preexisting renal conditions or at higher risk for renal toxicity (44,45) but is not routinely assessed in all patients. Repeat treatments are ideally most optimally planned using dosimetry, which remains underperformed.

Data, primarily retrospective, have emerged on suboptimal absorbed doses with fixed activity and cycles. At least 2 dosimetry-based treatment schemes have been investigated, both using a presumed 23 Gy as MTD and potentially as a surrogate for tumor-absorbed dose. In one approach, variable activity is given over a fixed number of cycles. In the first cycle, activity is personalized to glomerular filtration rate and the patient's body surface area, whereas in subsequent cycles activity is based on the absorbed dose after the first cycle (Gy/GBq to the kidney) in order to achieve a total prescribed 23 Gy to the kidney over 4 cycles (44). On the basis of the severity of baseline hematologic or renal impairment, the prescribed 23 Gy can be reduced by 25%–50%. Using this schema, Del Prete et al. (44) reported a median 1.3-fold increase (range, 0.5- to 2.1-fold) in the cumulative maximum tumor-absorbed dose in 85% of patients who underwent all 4 cycles of treatment, compared with the simulated fixed-activity regimen. Although kidney-absorbed dose per activity unit was highly variable, ranging from 0.2 to 4.2 Gy/GBq, and although it

is true that renal toxicity can develop slowly, no patient experienced severe renal toxicity within a 9-mo follow-up period and short-term grade 3 or 4 toxicity occurred in less than 10% of patients.

Another method is to administer a fixed activity over a variable number of cycles based on dosimetry, with the total activity limited to the kidney-absorbed dose threshold of 23 Gy (45). In 200 patients prospectively treated using this schema, Garske-Román et al. (45) performed organ and tumor dosimetry using SPECT imaging and blood-based dosimetry for the bone marrow-absorbed dose. They noted that only 25% of patients had to be restricted to treatment with exactly 4 cycles, per the commonly accepted treatment protocol, whereas almost half the patients received more than 4 (range, 5–10) cycles of treatment. In 61% of patients, the predefined absorbed dose threshold of 23 Gy was reached. Although the 2-Gy bone marrow-absorbed dose was not reached in any patient, 22% of therapies were stopped because of hematologic toxicity before reaching 23 Gy to the kidneys. Transient grade 3 or 4 hematologic toxicity of any kind was seen in 15% of patients, and therapy generally was continued after the nadir had passed. Interestingly, the difference between dosimetry-based and fixed activity can be seen in the fact that median progression-free survival (PFS) and overall survival were longer in patients in whom the absorbed dose to the kidneys reached 23 Gy than in those who did not reach this threshold; this discrepancy remained statistically significant even after excluding those who stopped treatment because of progression during treatment. This finding highlights differences from the standard approach of fixed dosing.

Overall, the wide variation in estimated kidney-absorbed dose across studies performed using varying methodologies (43) suggests undertreatment of most patients (relative to the allowable maximum kidney-absorbed dose) and possible overtreatment of a subset of patients with fixed activity. Moreover, the kidney-absorbed dose thresholds are not established through formal activity escalation studies but are radiation oncology-derived thresholds.

PSMA-Targeted Therapy for Prostate Cancer

PSMA-targeted therapy for prostate cancer is not currently FDA-approved at the time of preparation of this article but has shown evidence of efficacy in 2 prospective randomized trials of patients with metastatic prostate cancer (46,47). The first phase III registration study of a ^{177}Lu -PSMA-directed therapy (VISION trial) showed improvements in radiologic PFS and overall survival compared with the standard of care (46), and a randomized phase II trial (TheraP trial) showed improvement in PFS and prostate-specific antigen response compared with second-line chemotherapy (47). In the VISION trial, ^{177}Lu -PSMA-617 was given at the fixed activity of 7.4 GBq for each of the 4 cycles at 6-wk intervals; additional cycles based on patient response, tolerance, and presence of residual disease were also administered as a fixed activity with no interim dosimetry. In published studies, including the VISION trial, pretreatment assessment was limited to ^{68}Ga -PSMA PET imaging, primarily used for establishing targetable PSMA-expressing lesions; dosimetry was not included in either pre- or posttreatment imaging when deciding to continue, discontinue, or repeat treatment (48–50). Similarly, a phase II study of randomized patients used a fixed activity of 6.0 GBq ($n = 14$) or 7.4 GBq (51).

Given the possibility of salivary gland and marrow toxicity, dosimetry has been focused mostly on absorbed dose to salivary glands and marrow, whereas few data are on absorbed dose to tumors; variations in methodology are notable across studies.

Using posttreatment dosimetry, for 2 treatments averaging 6–7.4 GBq/cycle, salivary gland- and kidney-absorbed dose was found to be 1.2–2.8 Gy/GBq and 0.5–0.7 Gy/GBq, respectively. Reported lesion-absorbed dose estimates are extremely variable, ranging from 1.2 to 47.5 Gy/GBq (52–54).

The relationship between reported dose (activity or absorbed dose) and response is variable; in 40 patients treated with activity ranging from 4 to 9 GBq, no correlation was noted between activity and toxicity or response, though a trend toward an increasing response was noted at the highest level of treatment activity (55). The clinical parameters for assessing response vary; objective response by imaging and biochemical (prostate-specific antigen) response are commonly used instead of survival data. A recent report on voxel-based dosimetry also showed large variations in absorbed dose and no significant dose–effect relationship (56). However, several of these studies were underpowered and did not provide adequate counter evidence to studies in which such relationships were demonstrated (57). A significant correlation has been noted between WB tumor-absorbed dose and prostate-specific antigen response such that patients receiving less than 10 Gy were less likely to achieve at least a 50% decrease in prostate-specific antigen (57) than those who received a higher dose. The inconsistent patient response across studies may be explained by the large variations in lesion-absorbed dose observed (58), small sample size, differences in selection of patients, and variable dosimetry methods.

The data on outcomes from the VISION trial are encouraging, showing a significantly prolonged PFS (median, 8.7 vs. 3.4 mo.) and overall survival (median, 15.3 vs. 11.3 mo.) for those treated with ^{177}Lu -PSMA-617 plus standard care, versus the standard of care (46). However, outcome data in prior studies have been variable. In a phase II study, 43 patients with metastatic castration-resistant prostate cancer were randomized to receive either 6.0 GBq ($n = 14$) or 7.4 GBq ($n = 29$) of ^{177}Lu -PSMA; the median overall survival was 14 mo; however, no significant differences were noted between the 2 activity arms (51).

Single-time-point posttreatment imaging with SPECT/CT-based dosimetry was described recently (59) but is not yet widely applied. Other techniques, such as based on modeling using pharmacokinetic data, are being explored (59). Data from smaller cohorts for activity computation from a single posttreatment scan that can be applied to a much broader patient population showed the best estimate of tumor activity at 72 h after injection of the treatment (59).

Several groups outside the United States have published data on the use of ^{225}Ac -PSMA, primarily using a fixed-activity schema. Again, the amount of activity and number of cycles (60,61) vary widely, and none of the groups used individual dosimetry to plan overall activity or number of treatments, relying mainly on clinical parameters for tumor burden and toxicity (62,63). For ^{225}Ac -PSMA agents, a higher toxicity profile has limited patient treatments, highlighting the need for dosimetry. However, dosimetry for ^{225}Ac -PSMA treatments is more complex, and although limited, published studies have generally used scan and clearance data to project from ^{177}Lu -PSMA-617 studies (64). However, dosimetry data are limited to a few normal organs, and no tumor-absorbed dose data are available.

^{131}I -Metaiodobenzylguanidine (MIBG) Therapy

^{131}I -MIBG therapy is well established for the treatment of metastatic neuroblastoma, as well as metastatic paragangliomas and pheochromocytoma. Although ^{131}I -MIBG has been extensively used over the past 2 decades, distinct variations in approach are

evident. For treatment of paragangliomas and pheochromocytoma with conventional non–high specific activity ^{131}I -Iobenguane (high specific activity) administration of an empiric activity or an activity fixed by body weight has been the predominant approach (65). However, the FDA-approved (July 2018) agent for paragangliomas and pheochromocytoma, high-specific-activity ^{131}I -MIBG, or ^{131}I -iobenguane (Azedra; Progenics Pharmaceuticals), incorporates upfront dosimetry estimates in treatment planning for unresectable, locally advanced, or metastatic pheochromocytoma or paragangliomas (66); RPT activity for ^{131}I -iobenguane is determined after dosimetry using 3 WB scans over 3–5 d. Although a standard treatment regimen consists of 2 treatments given at least 90 d apart, each with an activity of 18.5 GBq (500 mCi), or 296 MBq/kg (8 mCi/kg) for a body weight of less than 62.5 kg, the activity is reduced on the basis of a dosimetry assessment for absorbed dose to normal organs, including lung, kidney, liver, and marrow (66). An activity–response relationship was noted, with more responses after 2 treatment cycles than after 1 cycle in phase I or II studies (67). Toxicity was mainly hematologic, and 25% of heavily pretreated patients required supportive care, with recovery noted in most. Dosimetry is key for such subgroups of patients for whom individual optimization and assessment of appropriate, probably lower, bone marrow–absorbed dose thresholds would need to be done.

For neuroblastoma, a predominantly pediatric disease, ^{131}I -MIBG activity is weight-based, including multiple infusions of either low-activity (37–148 MBq/kg, or 1–4 mCi/kg) or high-activity (296–666 MBq/kg, or 8–18 mCi/kg) ^{131}I -MIBG therapy (68). Dose-escalation studies used an activity range of 296–666 MBq/kg (8–18 mCi/kg), as generally used in clinical RPT (69). Myelosuppression is the most common adverse event that limits maximum activity; high-activity treatments often require supportive treatment such as platelet or stem cell transfusions, highlighting the critical role of marrow dosimetry (4). Those who respond to high-activity ^{131}I -MIBG treatments may benefit from additional treatment based on red marrow activity and guided by a dosimetry index (70). Pretreatment ^{131}I -MIBG imaging–derived absorbed dose estimates appear to be reproducible but can underestimate therapeutic activity and exhibit large interpatient variations in WB- and tumor-absorbed dose (71–73). Repeat treatments raise additional concerns about the indirectness and potential inaccuracy of methods for measuring absorbed dose to normal organs (besides marrow, WB, and red marrow). Large inpatient variations in WB-absorbed dose were shown via WB counting without use of imaging for absorbed dose estimates and a maximum 4-Gy total absorbed dose for 2 treatments (74). Technical differences distinguish ^{123}I -MIBG and ^{131}I -MIBG when used for dosimetry, given the shorter half-life of the ^{123}I isotope. However, integrating dosimetry into routine ^{123}I -MIBG diagnostic assessments remains attractive because of its feasibility and lower absorbed dose. The ability of ^{123}I -MIBG to predict WB-absorbed dose (75) and serial ^{123}I -MIBG WB scans for normal-organ–absorbed dose for planning tandem high-activity treatments in neuroblastoma has been shown and routinely used in some institutions (76). ^{124}I -MIBG (not FDA-approved) provides the advantages of multiple-time-point imaging, PET quantitation for dosimetry calculations, and superior lesion detection and scoring. However, limited availability and cost have restricted its utilization (77,78).

Radioimmunotherapy

Two radioimmunotherapy agents— ^{90}Y -ibritumomab tiuxetan and ^{131}I -tositumomab—have been approved by the FDA for treating

non-Hodgkin lymphoma. Pretreatment imaging assessment with ^{111}In -ibritumomab tiuxetan was previously required before treatment with ^{90}Y -ibritumomab tiuxetan. However, that requirement was meant mainly to ensure optimal biodistribution before therapy and was subsequently eliminated as a prerequisite to treatment. The FDA-approved treatment regimen for patients who had less than 25% bone marrow involvement includes a single treatment with activity based on body weight (14.8 or 11.1 MBq/kg [0.4 mCi or 0.3 mCi/kg] for patients with normal platelet counts or between 110,000 and 150,000, respectively; maximum activity limited to 1.18 GBq [32 mCi]).

Initial ^{90}Y -ibritumomab tiuxetan studies did not demonstrate a definitive correlation between hematologic toxicity and planar imaging-derived estimates of absorbed dose to the red marrow and WB (79). A report from 4 clinical trials that included 179 patients with relapsed or refractory non-Hodgkin lymphoma also noted a lack of correlation between hematologic toxicity and absorbed dose to the red marrow or WB or between hematologic toxicity and effective half-life in blood (80). Similarly, dosimetry failed to predict hematologic toxicity in 50 patients with advanced follicular non-Hodgkin lymphoma receiving ^{90}Y -ibritumomab tiuxetan in the front-line consolidation setting (81). Organ dosimetry estimates using WB dosimetry and SPECT/CT have shown over a 3-fold interpersonal variability in administered activity/Mbq and allowed for activity escalation to the myeloablative range (82), highlighting challenges to integrating routine dosimetry into treatment.

In contrast, activity for ^{131}I -tositumomab (Bexxar; GlaxoSmithKline) was based on individual pretreatment dosimetry with maximum WB-absorbed dose limiting the total activity to patients, performed both with ^{131}I -tositumomab as the theranostic pair and with ^{131}I -tositumomab as a single treatment with no repeat cycles or repeat treatment recommendations, given the antibody's murine origin. The maximum activity for individuals was determined from a prospective dosimetry-driven dose-escalation approach that showed a response relationship for WB-absorbed dose and hematologic toxicity. Because of the high variability (up to 4-fold) of ^{131}I excretion and clearance, the ^{131}I -tositumomab regimen used a simplified method to determine activity based on patient-specific kinetics to deliver a 0.65- or 0.75-Gy WB-absorbed dose.

A correlation between body-surface-area-corrected bone marrow-absorbed dose and hematologic toxicity using ^{131}I -rituximab has been noted. Using dosimetry based on WB SPECT/CT for marrow, Boucek et al. (83) noted a strong correlation between WB effective half-life and marrow effective half-life of antibody, as well as finding that the bone marrow activity concentration was proportional to activity per unit weight, height, or body surface area; however, Sgouros et al., using 3-dimensional SPECT-based dosimetry, found no correlation between WB tumor burden and hematologic toxicity (84). Less severe declines in platelet counts with ^{131}I -tositumomab than with ^{90}Y -ibritumomab tiuxetan (85) suggest that dosimetry could be beneficial in predicting toxicity profiles. Other studies of ^{131}I -tositumomab dosimetry observed trends toward increased tumor regression with higher tumor-absorbed dose (86–89). Tumor dose uniformity and tumor size are important factors (84,88,90), and correlations were observed between higher tumor-absorbed dose and longer PFS (86,89). Additionally, heavily pretreated patients may have higher marrow toxicity, and dosimetry estimates based on WB may not be predictive of toxicity.

The activity of ^{131}I -tositumomab, based on a 75-cGy WB-absorbed dose, showed less toxicity in patients who had not had

prior therapies than in those who had previously received a mean of 4 different chemotherapies. A higher ^{131}I -tositumomab activity was feasible in patients who had not had prior stem cell transplants, unlike those who had received a transplant (91).

In the myeloablative setting, the radioimmunotherapy activity depends on the non-bone-marrow critical-organ threshold. Studies in this setting report on treatment efficacy (92–94), but direct comparisons of dosimetry and nondosimetry approaches in this setting were not feasible.

^{90}Y -Microsphere Therapies

^{90}Y -microsphere therapies are directed into a single organ or compartment, limiting RPT uptake to that organ or compartment. Since activity is localized to the organ of delivery and systemic absorption is low, dosimetry is meant primarily to maximize the absorbed dose to the lesions and limit the dose absorbed by the remainder of the healthy organ where the lesion is located (such as liver). Currently, 2 FDA-approved RPT ^{90}Y -microspheres (SIR-Spheres [SIRTeX] or TheraSphere [Boston Scientific]) are clinically used for selective internal radiation therapy of liver metastasis. Calculation of the activity is based on liver and lesion volume derived from CT measurements. Pretreatment imaging with $^{99\text{m}}\text{Tc}$ -macroaggregated albumin is used to assess biodistribution, exclude extrahepatic perfusion, and measure pulmonary activity. Estimation of the radiation dose to the lung can affect activity. The calculations are easy to perform using designated methodology and worksheets or software (95–97). Although several groups have shown the feasibility of dosimetry using planar or SPECT imaging, such approaches remain limited to the groups' institutions (98). $^{99\text{m}}\text{Tc}$ -macroaggregated albumin is not an ideal surrogate for ^{90}Y -microspheres but is a reasonable predictor of normal liver-absorbed dose; data from small studies suggest a good correlation with posttreatment dosimetry for tumor and normal liver using SPECT/CT (98,99) or PET/CT (100).

Data on the use of dosimetry in improving outcomes are emerging (101); a recent prospective multicenter study called DOSISPHERE randomly assigned locally advanced hepatocellular carcinoma patients (1:1) to receive either standard dosimetry (120 ± 20 Gy) targeted to the perfused lobe or personalized dosimetry based on at least 205 Gy targeted to the index lesion. Personalized dosimetry treatments improved objective response rates (71%) over standardized dosimetry treatments (36%) (102). Although small in size, the study supports the use of personalized dosimetry. Large phase II or III systematic studies using dosimetry to establish dosing regimens, efficacy, and outcomes are limited.

UNMET NEEDS

Activity and Radiation Dose–Response and Outcome-Based Data

Although studies have shown the value of dosimetry in RPT, supporting data are heterogeneous and there are limited outcome-based data demonstrating the superiority of dosimetry-based over standardized or non-dosimetry-based approaches across all RPTs.

For thyroid cancer treatment, the optimal activity level and the use of dosimetry remain highly controversial (103). Given the high variation in activity and dosimetry methods for determining activity and tumor-absorbed dose across studies, comparison of outcomes based on published data is difficult. Small studies show efficacy to be related to mean lesion-absorbed dose, though again with large variations in disease stage and extent, differentiation, and lesion size (104). Use of dosimetry instead of empiric activity

may allow for lower hematologic toxicity. The current limit of 2 Gy (200 rads) to the blood may be exceeded in about 1%–22% of patients using empiric treatment with 3.7–11.1 GBq (100–300 mCi) of activity as compared with dosimetry-based activity (105); this difference is higher for patients 70 y or older (22%–38%) than in those younger than 70 y (8%–15%) or when 9.25 GBq (250 mCi) of empiric activity is used (50%) (8). Additionally, small studies observed a higher likelihood of response using dosimetry-based activity in patients with locoregional disease (104) and in those who experienced recurrence after treatment with an empiric dosage (106). The activity and absorbed dose–response relationship remains unclear, with some studies supporting a correlation (20) and others showing a lack of correlation (107). Prospective randomized studies are lacking, given that survival studies require long follow-up periods because of good survival in this population.

The activity and absorbed dose–response relationship for hematotoxicity with PRRT also remains unclear. In a study of 200 patients with neuroendocrine tumors, no dose–response correlation was seen using blood-based bone marrow dosimetry (108). Attempts to limit hematologic toxicity remain challenged by the inherent difficulties of image-based bone marrow dosimetry and the absence of validation studies and prior treatments in the patients studied (109–112). (Dosimetry methodology for bone marrow estimates poses several issues, which are discussed elsewhere in this supplement to *The Journal of Nuclear Medicine*.) Overall, whereas more recent data have emerged on dosimetry, the specific clinical situations in which to perform dosimetry—and how—remain controversial, as does dosimetry’s impact on outcomes. A large variation in lesion AD has also been noted from ¹⁷⁷Lu-PSMA studies and may explain variable response rates and toxicities in patients. Use of individualized dosimetry may be leveraged to improve response and decrease toxicity (58). Variations in the lesion-absorbed dose from current published data lead to questions about the need for activity based on lesion-absorbed dose. On the other hand, given the multitude of published studies that use a fixed empiric activity, without dosimetry, and nevertheless showed clinical utility and better responses with increasing cycles of treatment, empiric dosing is the predominant method in providing clinically relevant RPT. However, whether dosimetry-based activity in these patients would have provided significantly superior responses can be known only from randomized trials, which are lacking.

Assessing Optimal Administration Activity: Lesion Versus Normal-Tissue Limits

Individualized dosimetry studies for PRRT have focused on renal and marrow dosimetry (113–115). Dosimetry of 200 patients with WB and blood showed that for a renal threshold of 23 Gy and a blood threshold of 2 Gy, 50% of patients could be treated with more than 4 cycles of 7.4 GBq of ¹⁷⁷Lu-octreotate and 20% of patients could be treated with fewer than 4 cycles (113). Renal toxicity can be mitigated with amino acids, the overall incidence of grade 3–4 renal toxicities appears low, and long-term hematotoxicity appeared in about 11% of patients (41,116). However, current clinical activity is limited by the 23- to 28-Gy absorbed dose to the kidneys, based on prior retrospective or prospective dosimetry studies (45,117,118). The 23- to 28-Gy threshold is highly debated, as it is extrapolated from the results of external-beam radiotherapy (EBRT) (119) and may not be ideal for RPT. Some have noted that the renal threshold may be as high as 40 Gy

for those without preexisting conditions (120). Additionally, such renal-based thresholding prevents maximizing the dose absorbed by the tumor, and current fixed-activity schemata frequently fall short of in vivo saturation of somatostatin receptors in tumor lesions (121).

Thresholds for all RPTs and for all normal organs are based on the EBRT data (119), which is in turn based on organ volume and assumption of uniform distribution of radiation in organs. Large ranges are applicable to EBRT on the basis of organ exposure: for example, 23–50 Gy can be applied for the whole kidney, or one third of the kidney volume exposed for a 5/5 tolerance dose (the radiation dose that would result in 5% risk of severe complications within 5 y after irradiation) (119). The systemic distribution for RPT leads to the assumption that the entire organ is exposed, likely producing conservative estimates for total activity. In addition, the relative biologic effectiveness of RPT differs significantly from that of EBRT because of a more prolonged but slower radiation dose rate that also depends on the isotope and linear energy transfer. Establishing appropriate RPT thresholds is especially relevant in treatments given the likelihood of delivering a lower absorbed dose with fixed activity/cycles to lesions. Treating to the maximum limits is important, and those limits may differ according to radiopharmaceutical kinetics and the radionuclide used. Fixed dosing may not reach maximum organ limits or maximize the lesion-absorbed dose in many patients.

It is also important to delineate what parameters should be regarded as MTD. Generally, a 2-Gy limit to the marrow or blood is used to limit hematologic toxicity, a common occurrence with RPT. However even with this threshold, hematologic toxicity remains extremely unpredictable across different RPTs. Moreover, universal application of this threshold has limitations in patients for whom marrow disease is the predominant presentation, such as those with neuroblastoma or hematologic toxicities, and different parameters for MTD are required. The impact of prior chemotherapy or radiation therapy creates unpredictable adverse-event profiles that require a better understanding of how combination therapies, including radiosensitizing chemotherapy, may contribute to short- and long-term hematologic complications. Such knowledge can be gained via well-designed trials and further prospective or randomized investigations (122,123).

As such, endpoint parameters for dosimetry should include assessments of the absorbed dose to tumor and normal organs in order to optimize the tumor-to-background ratio for RPT delivery. Although fixed-activity regimens are easy to administer, it is likely that a subgroup of the population will be under- or overtreated. These subpopulations—for instance, patients with a higher disease burden, preexisting conditions affecting key organs, heavily pretreated, or receiving combination therapies—should be identified and their treatment based on individual dosimetry. Dosimetry imaging should be integrated early in the process of establishing MTD, and activity should be recommended upfront so that it can be further tailored on the basis of clinical response, side effects, and lab findings.

Considerations for Combination Therapies

Therapies combining RPT with radiation or chemotherapy are gaining interest and, although aimed at improving outcomes, risk increased toxicities. Although dosimetry may not entirely predict the biologic variances and toxicities of a coadministered biologic agent, dosimetry may be useful in assessing the biodistribution of combination treatments and normal-organ dosimetry. Incorporation

of dosimetry has, however, been limited thus far. The combination of ^{153}Sm -lexidronam and $^{223}\text{RaCl}_2$ with docetaxel (124) guided treatments using a flat activity escalation schema based on the clinical MTD for single-agent use of $^{153}\text{Sm}/^{223}\text{RaCl}_2$ and docetaxel and on the clinical dose-limiting toxicity, without dosimetry (125). Incorporation of dosimetry in clinical trials with ^{177}Lu -DOTA-TATE or ^{177}Lu PSMA-617 (<https://www.clinicaltrials.gov/>) has been limited. Similarly, trials of ^{131}I -MIBG combined with chemotherapy or sensitizing agents used a fixed weight-based activity; varying toxicity profiles and response rates have been seen (126).

Limitations to Current Dosimetry Methodologies

In general, dosimetry methods are based on assessing average absorbed dose in organs (127) using MIRD age-dependent hermaphrodite phantoms (Oak Ridge National Laboratory), Monte Carlo simulations for organ-absorbed cross-radiation doses, or simplified calculations of self-absorbed radiation doses to organs. Safe limits or tolerance limits for normal organs are based on data derived from external-beam therapies, complicating analysis insofar as the biologic effects of radiation for EBRT differ from those for RPT, affecting apoptosis, structural and physiologic changes in the cell, and DNA damage.

Intrapersonal variation adds complexity as well. RPT is associated with individual biologic variation in distribution and tissue absorption related to WB, to blood and organ clearance, and to microdistribution, complicating assessment. Biologic and pharmacokinetic differences, as well as the effect of the RPT ligand/molecule or biologic agent, contribute further to individual variation due to difference in penetration causing heterogeneous distribution, affecting uniformity of absorbed-dose rate within normal and tumor tissue. Additional complications include the complex geometric configuration of the target tissue, self-dosing, and cross-tissue dose assessment.

Dosimetry Challenges with α -Emitters

Dosimetry for α -emitters is limited by insufficient γ -emissions and the likelihood of daughter radionuclide on-target migration decay versus off-target migration decay. Imaging is possible if the decay consists of γ -emissions, such as in ^{223}Ra or ^{227}Th decay (128). This approach is limited in practice, however, as most of the γ -emissions are in low quantities, requiring longer imaging times for optimal assessment of targeting and uptake in organs.

Using preclinical data for dosimetry is not ideal. Such data are often inaccurate when translated into human beings, probably because of different kinetics and affinity profiles, greater in vivo heterogeneity, and nonuniformity of RPT within lesions based on size, location, and tumor microenvironment. For instance, quantitation of ^{223}Ra -chloride using phantoms has been shown to be feasible, but significant challenges remain, including validation and reproducibility (129).

Microdosimetry and modeling methods enhance assessments of local effects (130,131) but are difficult to perform and require expertise. A more suitable option would be to use an isotope with a short-lived daughter isotope to restrict all subsequent radiation to the target tumor and clear rapidly, avoiding off-target toxic effects—unless the daughter is excreted rapidly or is relatively nontoxic by virtue of its biodistribution. The general assumption uses a relative biologic effectiveness of 5 and instant decay of unstable daughter nuclides (64). Given the complexity of dosimetry, several phase I or II clinical studies have used activity based on body weight, such as the use of ^{213}Bi -HuM195/ 225

Ac-lintuzumab in leukemia patients (132,133). Ongoing studies (NCT02998047, NCT0257596, NCT03441048, and NCT03746431) are treating with a weight-based activity schema (134). Although some phase I studies such as ^{227}Th -BAY 2315497 in prostate cancer (NCT03724747) and ^{225}Ac -FPI-1434 (NCT03746431) include either posttreatment dosimetry assessment or pretreatment ^{111}In -dosimetry, the activity dose escalation is fixed, based on body weight.

Technical Aspects of Imaging

Use of planar and SPECT imaging versus PET imaging poses technical challenges for dosimetry. SPECT imaging is superior to planar imaging, but attenuation and scatter effects require complex corrections (135). SPECT imaging also includes key technical factors that are important for accurate dosimetry but are not universally available, such as dead times, conversion factors, and calibration of the sources and cameras. For ^{177}Lu -SPECT quantitation, for example, dead times may impact dose estimates by up to about 22%, requiring corrections (136,137).

Multiple-time-point SPECT imaging is ideal but time-intensive. The use of pre- versus posttherapy assessment and the ideal single time point for WB and SPECT imaging must be examined in larger multicenter studies. As data are emerging on the use of single-time-point imaging (138–140), validation of such methods across various RPTs is critical. Although PET enables easier and more accurate dosimetry than does SPECT imaging, some RPTs do not offer companion PET imaging suitable for dosimetry. An example is ^{68}Ga -DOTATATE/PSMA, for which a short half-life limits multiple-time-point imaging.

Reconstruction parameters and dosimetry calculation methods using commercially available software also vary widely across centers. Although software packages have grown more available through vendors in recent years, the methodology used by each vendor is different; details of the exact methodologies and comparative assessments are unavailable as well. Additionally, specific research groups or centers may perform detailed dosimetry according to internally developed methods. Efforts at harmonization are ongoing (141,142), but no formal accreditation program for quantitative SPECT/CT exists for multicenter trials.

Resources and Expertise

Many centers lack the necessary trained personnel, such as medical physicists or certified, dosimetry-trained technicians who can calculate activity. To address this challenge, a simplified schema or worksheet to calculate activity, such as that developed for SIR-Spheres or ^{131}I -tositumomab, should be developed for each RPT. Many steps of the dosimetry calculation could feasibly be automated, particularly as more data emerge supporting the clinical utility of tumor dose–response relationships, such as the data from the DOSISPHERE study. A template developed by the International Atomic Energy Agency allows for biodistribution assessments that can be leveraged for organ-level dosimetry, based on the assumption of a uniform distribution of activity (143).

Another challenge of dosimetry is that patients must visit centers multiple times to satisfy the requirements of multiple-time-point imaging. With technologic advances and evolving strategies, it is important to develop simplified approaches that can easily be applied to common RPTs across clinical settings. A more practical alternative may be found in single-time-point imaging. For example, whereas ^{131}I -NaI dosimetry requires multiple-time-point imaging, quantitation with planar and SPECT imaging may

be overcome by novel techniques using $^{124}\text{I-NaI}$ (23,29,144–146). Simplified methods with single or no blood sampling and single WB ^{131}I imaging have been described but are not widely used (147–151).

Studies have demonstrated the feasibility of using $^{124}\text{I-PET}$ for dosimetry to predict absorbed dose in the treatment of thyroid cancer (152). However, parameters must be thoroughly optimized to compensate for several factors liable to impair accurate quantification, including a low positron ratio of 23%, a complex decay schema, and coincidence and annihilation photon emissions (153). Similar simplified approaches have been investigated for PRRT (115,139,154–157). Single-time-point PET imaging after treatment showed a high correlation with conventional posttreatment 3-time-point SPECT/CT imaging for $^{90}\text{Y-DOTATOC}$ (139). Others have used multiple-time-point imaging at cycle 1 to derive an effective half-life for individual patients that is then integrated into subsequent cycles at 24-h imaging (154). Single-time-point imaging at 24 or 96 h after treatment for all cycles has shown feasibility and acceptable levels of uncertainty (115,156).

Tradeoffs: Access, Cost, Use

Use of dosimetry is limited by its complexity and practical difficulty, as well as time constraints. Ideally, individualized activity, informed by dosimetry and data, would be administered to all patients undergoing any type of RPT; in practice, however, widespread, routine application of radiation dosimetry will depend on the availability of resources such as equipment, personnel, expertise, and funding.

Administration of RPTs such as PRRT, radioimmunotherapy, and radioembolization is time-intensive for clinical and supportive staff; dosimetry adds further burdens of time and energy to an already intensive process. Centers may prefer empiric dosing methods that do not require time-intensive procedures and detailed calculations, such as the several FDA-approved RPT agents that feature fixed treatment schemata and are easily integrated into clinical practice. Centers lacking inpatient treatment facilities may steer patients toward lower-dose empiric treatments rather than the higher activity that dosimetry may determine to be necessary; without the requirements of imaging and dose calculations, administration of empiric or fixed activity without dosimetry is simple, fast, and convenient.

Lack of financial reimbursement represents an additional challenge to dosimetry-based treatment planning in RPT, as poor reimbursement rates compound the already high costs associated with multiple imaging procedures, specialized personnel, and other necessary resources. Although reimbursement for SPECT imaging for dosimetry is available, it has yet to be universally adopted and approved across all RPTs. (Reimbursement codes for medical physicist and dosimetry calculations of RPT are discussed elsewhere in this supplement to *The Journal of Nuclear Medicine*.)

Costs associated with inpatient therapies may limit their use, especially in the United States. Certain RPTs are administered in an inpatient setting because of considerations regarding activity and radiation exposure to the public and caregivers and require special hospital rooms, layouts, or structures, which add to the cost.

Challenges with Clinical Trials

Overall, the use of RPT in clinical practice should be informed by clinical trials. It is beyond the scope of this publication to discuss design details for trials testing RPT, but it can be said that current use of dosimetry in RPT is variable and suboptimal. The clinical trials that led to recent approvals of RPTs did not

incorporate dosimetry and provided little or no absorbed dose data for tumor and normal tissues. This one-size-fits-all approach also results in under- or overtreatment, delivering absorbed radiation doses and activity that differ by orders of magnitude between individuals (158) and resulting in incomplete remissions or cures. Fixed activity, as used in PRRT, falls short of the recommended 23-Gy kidney-absorbed dose, and about 73% of patients could receive more cycles of therapy (115). The lack of optimizing to presumed MTD jeopardizes efficacy. Moving forward, these issues will grow only more consequential with the growth of combined therapies and other therapeutic modalities.

For clinical trials and the evaluation of novel therapeutics, dosimetry should form an integral part of phase I assessment as pretherapeutic treatment planning to establish organ-absorbed dose, to assess MTD and maximum tolerated activity, and to recommend a phase II dose. Dosimetry of normal-organ and WB exposure must be established for safety. If dose escalation is planned, these assessments should be performed at each dose level and correlated with lab data on safety. Additional benefit would be derived from posttreatment dosimetry in phase I to assess the actual dose delivered. For phase II studies, dosimetry may be used to establish the dose–response relationship and efficacy. Limited dosimetry to assess actual activity and to plan repeat cycles and establish relevant dose–response relationships may be important.

A methodologic balance should be struck to encourage practicality and broaden the use of RPT with dosimetry. Methodologies should aim to obtain dosimetry in critical normal organs and lesions while keeping future clinical translation in perspective. For example, whereas multiple imaging examinations before and after each treatment cycle provide the most comprehensive estimates, the demanding schedules lower patient enrollment and compliance, delay treatments, and cause anxiety in patients otherwise eager to initiate treatment. For certain RPTs, multiple sessions of scanning and blood sampling that last up to several days or even weeks can lead to patient fatigue. Such issues impede timelines and increase cost in studies sponsored by the drug development industry, as well as those initiated by investigators. Detailed dosimetry data from the developmental phase may be used to develop simpler methodologies for clinical practice. It should be recognized that dosimetry for clinical trials with α -emitters can be even more challenging, and given the issues discussed here, a less onerous posttreatment approach to dosimetry is desirable.

For multicenter trials, the establishment of standardized procedures across multiple centers represents a further challenge. Intense effort is required to ensure a shared, uniform methodology and the cross-calibration of systems at all centers. In such situations, it is vital that appropriate phantoms and traceable calibration be made available, ensuring comparability of image processing, reconstruction, volume delineation, and volumetric assessment. Maximizing use thus requires simpler dosimetry procedures that provide reasonable assessments for clinical administration at low resource costs. Cross-collaborations between facilities that have dosimetry capabilities and those that do not may be possible. Efforts to promote such collaboration are under way (159).

Engaging with and understanding the needs of industry are important as well: industry can champion the growth of RPT by supporting the development of novel RPTs in pursuit of commercial interests. Establishing easily adaptable and balanced methodologies should be a priority for all.

CONCLUSION

Although dosimetry assessment is recognized as important for personalized RPT and as critical in certain settings, its use remains low overall and uneven across RPTs and institutions. As clinical experience with RPT has widened, the shortcomings and logistics preventing routine application of dosimetry in clinical RPT have become more apparent, whereas fixed-activity regimens' convenience and ease of integration into clinical practice have enabled their wide use. As such, identifying clinical situations in which dosimetry can complement and enhance the therapeutic effect of empiric dosing can be advantageous. Critical further steps to expand the use of dosimetry include standardization of dosimetry use in management decisions on RPT activity, automation of key processes, and well-conducted multicenter prospective trials of dosimetry-driven versus empiric therapy that provide evidence of better outcomes for dosimetry-based treatments. However, balanced optimization is essential so that dosimetry methodology is not so rigorous as to undercut the benefit that can otherwise be achieved with an empiric-activity approach.

DISCLOSURE

The opinions expressed in this publication are the author(s)' own and do not reflect the view of the National Institutes of Health, the Department of Health and Human Services, or the United States government. No other potential conflict of interest relevant to this article was reported.

REFERENCES

1. Lassmann M, Eberlein U. The relevance of dosimetry in precision medicine. *J Nucl Med*. 2018;59:1494–1499.
2. Sjögreen Gleisner K, Spezi E, Solny P, et al. Variations in the practice of molecular radiotherapy and implementation of dosimetry: results from a European survey. *EJNMMI Phys*. 2017;4:28.
3. Hindorf C, Glatting G, Chiesa C, Linden O, Flux G; EANM Dosimetry Committee. EANM Dosimetry Committee guidelines for bone marrow and whole-body dosimetry. *Eur J Nucl Med Mol Imaging*. 2010;37:1238–1250.
4. Gear J, Chiesa C, Lassmann M, et al. EANM Dosimetry Committee series on standard operational procedures for internal dosimetry for ¹³¹I mIBG treatment of neuroendocrine tumours. *EJNMMI Phys*. 2020;7:15.
5. AZEDRA® (iobenguane I 131) injection, for intravenous use: full prescribing information. Azedra website. <https://www.azedra.com/content/pdf/full-prescribing-information.pdf>. Revised March 2021. Accessed October 28, 2021.
6. Benua RS, Cicale NR, Sonenberg M, Rawson RW. The relation of radioiodine dosimetry to results and complications in the treatment of metastatic thyroid cancer. *AJR*. 1962;87:171–182.
7. Haugen BR, Alexander EK, Bible KC, et al. 2015 American Thyroid Association management guidelines for adult patients with thyroid nodules and differentiated thyroid cancer: the American Thyroid Association guidelines task force on thyroid nodules and differentiated thyroid cancer. *Thyroid*. 2016;26:1–133.
8. Tuttle RM, Leboeuf R, Robbins RJ, et al. Empiric radioactive iodine dosing regimens frequently exceed maximum tolerated activity levels in elderly patients with thyroid cancer. *J Nucl Med*. 2006;47:1587–1591.
9. Mallick U, Harmer C, Yap B, et al. Ablation with low-dose radioiodine and thyrotropin alfa in thyroid cancer. *N Engl J Med*. 2012;366:1674–1685.
10. Schlumberger M, Leboulloux S, Catargi B, et al. Outcome after ablation in patients with low-risk thyroid cancer (ESTIMABL1): 5-year follow-up results of a randomised, phase 3, equivalence trial. *Lancet Diabetes Endocrinol*. 2018;6: 618–626.
11. Lassmann M, Reiners C, Luster M. Dosimetry and thyroid cancer: the individual dosage of radioiodine. *Endocr Relat Cancer*. 2010;17:R161–R172.
12. Van Nostrand D, Atkins F, Yeganeh F, Acio E, Bursaw R, Wartofsky L. Dosimetrically determined doses of radioiodine for the treatment of metastatic thyroid carcinoma. *Thyroid*. 2002;12:121–134.
13. Chiesa C, Castellani MR, Vellani C, et al. Individualized dosimetry in the management of metastatic differentiated thyroid cancer. *Q J Nucl Med Mol Imaging*. 2009;53:546–561.

14. Lassmann M, Hanscheid H, Chiesa C, et al. EANM Dosimetry Committee series on standard operational procedures for pre-therapeutic dosimetry I: blood and bone marrow dosimetry in differentiated thyroid cancer therapy. *Eur J Nucl Med Mol Imaging*. 2008;35:1405–1412.
15. Van Nostrand D, Atkins F, Moreau S, et al. Utility of the radioiodine whole-body retention at 48 hours for modifying empiric activity of ¹³¹I-iodine for the treatment of metastatic well-differentiated thyroid carcinoma. *Thyroid*. 2009;19: 1093–1098.
16. Dorn R, Kopp J, Vogt H, Heidenreich P, Carroll RG, Gulec SA. Dosimetry-guided radioactive iodine treatment in patients with metastatic differentiated thyroid cancer: largest safe dose using a risk-adapted approach. *J Nucl Med*. 2003; 44:451–456.
17. Driedger AA, Quirk S, McDonald TJ, et al. A pragmatic protocol for I-131 rhTSH-stimulated ablation therapy in patients with renal failure. *Clin Nucl Med*. 2006;31:454–457.
18. Verburg FA, Biko J, Diessl S, et al. I-131 activities as high as safely administrable (AHASA) for the treatment of children and adolescents with advanced differentiated thyroid cancer. *J Clin Endocrinol Metab*. 2011;96:E1268–E1271.
19. Ma C, Xie J, Liu W, et al. Recombinant human thyrotropin (rhTSH) aided radioiodine treatment for residual or metastatic differentiated thyroid cancer. *Cochrane Database Syst Rev*. 2010;2010:CD008302.
20. Maxon HR, Thomas SR, Hertzberg VS, et al. Relation between effective radiation dose and outcome of radioiodine therapy for thyroid cancer. *N Engl J Med*. 1983; 309:937–941.
21. Hanscheid H, Lassmann M, Luster M, et al. Iodine biokinetics and dosimetry in radioiodine therapy of thyroid cancer: procedures and results of a prospective international controlled study of ablation after rhTSH or hormone withdrawal. *J Nucl Med*. 2006;47:648–654.
22. de Keizer B, Brans B, Hoekstra A, et al. Tumour dosimetry and response in patients with metastatic differentiated thyroid cancer using recombinant human thyrotropin before radioiodine therapy. *Eur J Nucl Med Mol Imaging*. 2003;30: 367–373.
23. Sgouros G, Kolbert KS, Sheikh A, et al. Patient-specific dosimetry for ¹³¹I thyroid cancer therapy using ¹²⁴I PET and 3-dimensional-internal dosimetry (3D-ID) software. *J Nucl Med*. 2004;45:1366–1372.
24. Plyku D, Hobbs RF, Huang K, et al. Recombinant human thyroid-stimulating hormone versus thyroid hormone withdrawal in ¹²⁴I PET/CT-based dosimetry for ¹³¹I therapy of metastatic differentiated thyroid cancer. *J Nucl Med*. 2017;58:1146–1154.
25. Jentzen W, Bockisch A, Ruhlmann M. Assessment of simplified blood dose protocols for the estimation of the maximum tolerable activity in thyroid cancer patients undergoing radioiodine therapy using ¹²⁴I. *J Nucl Med*. 2015;56:832–838.
26. Freudenberg LS, Jentzen W, Stahl A, Bockisch A, Rosenbaum-Krumme SJ. Clinical applications of ¹²⁴I-PET/CT in patients with differentiated thyroid cancer. *Eur J Nucl Med Mol Imaging*. 2011;38(suppl 1):S48–S56.
27. Wierts R, Brans B, Havekes B, et al. Dose-response relationship in differentiated thyroid cancer patients undergoing radioiodine treatment assessed by means of ¹²⁴I PET/CT. *J Nucl Med*. 2016;57:1027–1032.
28. Pettinato C, Spezi E, Nanni C, et al. Pretherapeutic dosimetry in patients affected by metastatic thyroid cancer using ¹²⁴I PET/CT sequential scans for ¹³¹I treatment planning. *Clin Nucl Med*. 2014;39:e367–e374.
29. Jentzen W, Freudenberg L, Eising EG, Sonnenschein W, Knust J, Bockisch A. Optimized ¹²⁴I PET dosimetry protocol for radioiodine therapy of differentiated thyroid cancer. *J Nucl Med*. 2008;49:1017–1023.
30. Eary JF, Collins C, Stabin M, et al. Samarium-153-EDTMP biodistribution and dosimetry estimation. *J Nucl Med*. 1993;34:1031–1036.
31. Parker C, Sartor O. Radium-223 in prostate cancer. *N Engl J Med*. 2013;369: 1659–1660.
32. Parker C, Lewington V, Shore N, et al.; Targeted Alpha Therapy Working Group. Targeted alpha therapy, an emerging class of cancer agents: a review. *JAMA Oncol*. 2018;4:1765–1772.
33. Parker CC, Coleman RE, Sartor O, et al. Three-year safety of radium-223 dichloride in patients with castration-resistant prostate cancer and symptomatic bone metastases from phase 3 randomized Alpharadin in symptomatic prostate cancer trial. *Eur Urol*. 2018;73:427–435.
34. Sternberg CN, Saad F, Graff JN, et al. A randomised phase II trial of three dosing regimens of radium-223 in patients with bone metastatic castration-resistant prostate cancer. *Ann Oncol*. 2020;31:257–265.
35. Sartor O, Heinrich D, Mariados N, et al. Re-treatment with radium-223: 2-year follow-up from an international, open-label, phase 1/2 study in patients with castration-resistant prostate cancer and bone metastases. *Prostate*. 2019;79: 1683–1691.
36. Zhao H, Howard LE, De Hoedt AM, et al. Safety of concomitant therapy with radium-223 and abiraterone or enzalutamide in a real-world population. *Prostate*. 2021;81:390–397.

37. Pacilio M, Ventroni G, De Vincentis G, et al. Dosimetry of bone metastases in targeted radionuclide therapy with alpha-emitting ²²³Ra-dichloride. *Eur J Nucl Med Mol Imaging*. 2016;43:21–33.
38. Murray I, Chittenden SJ, Denis-Bacelar AM, et al. The potential of ²²³Ra and ¹⁸F-fluoride imaging to predict bone lesion response to treatment with ²²³Ra-dichloride in castration-resistant prostate cancer. *Eur J Nucl Med Mol Imaging*. 2017;44:1832–1844.
39. Keizman D, Fosboel MO, Reichegger H, et al. Imaging response during therapy with radium-223 for castration-resistant prostate cancer with bone metastases: analysis of an international multicenter database. *Prostate Cancer Prostatic Dis*. 2017;20:289–293.
40. Strosberg J, El-Haddad G, Wolin E, et al. Phase 3 trial of ¹⁷⁷Lu-dotatate for mid-gut neuroendocrine tumors. *N Engl J Med*. 2017;376:125–135.
41. Kwekkeboom DJ, de Herder WW, Kam BL, et al. Treatment with the radiolabeled somatostatin analog [¹⁷⁷Lu-DOTA⁰,Tyr³]octreotate: toxicity, efficacy, and survival. *J Clin Oncol*. 2008;26:2124–2130.
42. Kwekkeboom DJ, Bakker WH, Kooij PP, et al. [¹⁷⁷Lu-DOTAOTyr³]octreotate: comparison with [¹¹¹In-DTPA]octreotide in patients. *Eur J Nucl Med*. 2001;28:1319–1325.
43. Lassmann M, Eberlein U. Radiation dosimetry aspects of ¹⁷⁷Lu. *Curr Radiopharm*. 2015;8:139–144.
44. Del Prete M, Buteau FA, Arsenault F, et al. Personalized ¹⁷⁷Lu-octreotate peptide receptor radionuclide therapy of neuroendocrine tumours: initial results from the P-PRRT trial. *Eur J Nucl Med Mol Imaging*. 2019;46:728–742.
45. Garske-Román U, Sandstrom M, Fross Baron K, et al. Prospective observational study of ¹⁷⁷Lu-DOTA-octreotate therapy in 200 patients with advanced metastasized neuroendocrine tumours (NETs): feasibility and impact of a dosimetry-guided study protocol on outcome and toxicity. *Eur J Nucl Med Mol Imaging*. 2018;45:970–988.
46. Sartor O, de Bono J, Chi KN, et al. Lutetium-177-PSMA-617 for metastatic castration-resistant prostate cancer. *N Engl J Med*. 2021;385:1091–1103.
47. Hofman MS, Emmett L, Sandhu S, et al. [¹⁷⁷Lu]Lu-PSMA-617 versus cabazitaxel in patients with metastatic castration-resistant prostate cancer (TheraP): a randomised, open-label, phase 2 trial. *Lancet*. 2021;397:797–804.
48. Hofman MS, Violet J, Hicks RJ, et al. [¹⁷⁷Lu]-PSMA-617 radionuclide treatment in patients with metastatic castration-resistant prostate cancer (LuPSMA trial): a single-centre, single-arm, phase 2 study. *Lancet Oncol*. 2018;19:825–833.
49. Heck MM, Tauber R, Schwaiger S, et al. Treatment outcome, toxicity, and predictive factors for radioligand therapy with ¹⁷⁷Lu-PSMA-I&T in metastatic castration-resistant prostate cancer. *Eur Urol*. 2019;75:920–926.
50. Rahbar K, Ahmadzadehfah H, Kratochwil C, et al. German multicenter study investigating ¹⁷⁷Lu-PSMA-617 radioligand therapy in advanced prostate cancer patients. *J Nucl Med*. 2017;58:85–90.
51. Calais J, Gafita A, Eiber M, et al. Prospective phase 2 trial of PSMA-targeted molecular radiotherapy with ¹⁷⁷Lu-PSMA-617 for metastatic castration-resistant prostate cancer (RESIST-PC): efficacy results of the UCLA cohort. *J Nucl Med*. 2021;62:1440–1446.
52. Okamoto S, Thieme A, Allmann J, et al. Radiation dosimetry for ¹⁷⁷Lu-PSMA I&T in metastatic castration-resistant prostate cancer: absorbed dose in normal organs and tumor lesions. *J Nucl Med*. 2017;58:445–450.
53. Fendler WP, Reinhardt S, Ilhan H, et al. Preliminary experience with dosimetry, response and patient reported outcome after ¹⁷⁷Lu-PSMA-617 therapy for metastatic castration-resistant prostate cancer. *Oncotarget*. 2017;8:3581–3590.
54. Kamaldeep, Wanage G, Sahu SK, et al. Examining absorbed doses of indigenously developed ¹⁷⁷Lu-PSMA-617 in metastatic castration-resistant prostate cancer patients at baseline and during course of peptide receptor radioligand therapy. *Cancer Biother Radiopharm*. 2021;36:292–304.
55. Rathke H, Giesel FL, Flechsig P, et al. Repeated ¹⁷⁷Lu-labeled PSMA-617 radioligand therapy using treatment activities of up to 9.3 GBq. *J Nucl Med*. 2018;59:459–465.
56. Barna S, Haug AR, Hartenbach M, et al. Dose calculations and dose-effect relationships in ¹⁷⁷Lu-PSMA I&T radionuclide therapy for metastatic castration-resistant prostate cancer. *Clin Nucl Med*. 2020;45:661–667.
57. Violet J, Jackson P, Ferdinandus J, et al. Dosimetry of ¹⁷⁷Lu-PSMA-617 in metastatic castration-resistant prostate cancer: correlations between pretherapeutic imaging and whole-body tumor dosimetry with treatment outcomes. *J Nucl Med*. 2019;60:517–523.
58. Kratochwil C, Giesel FL, Stefanova M, et al. PSMA-targeted radionuclide therapy of metastatic castration-resistant prostate cancer with ¹⁷⁷Lu-labeled PSMA-617. *J Nucl Med*. 2016;57:1170–1176.
59. Jackson PA, Hofman MS, Hicks RJ, Scalzo M, Violet J. Radiation dosimetry in ¹⁷⁷Lu-PSMA-617 therapy using a single posttreatment SPECT/CT scan: a novel methodology to generate time- and tissue-specific dose factors. *J Nucl Med*. 2020;61:1030–1036.
60. Satapathy S, Sood A, Das CK, Mittal BR. Evolving role of ²²⁵Ac-PSMA radioligand therapy in metastatic castration-resistant prostate cancer: a systematic review and meta-analysis. *Prostate Cancer Prostatic Dis*. 2021;24:880–890.
61. Yadav MP, Ballal S, Bal C, et al. Efficacy and safety of ¹⁷⁷Lu-PSMA-617 radioligand therapy in metastatic castration-resistant prostate cancer patients. *Clin Nucl Med*. 2020;45:19–31.
62. Violet J, Sandhu S, Irvani A, et al. Long-term follow-up and outcomes of retreatment in an expanded 50-patient single-center phase II prospective trial of ¹⁷⁷Lu-PSMA-617 theranostics in metastatic castration-resistant prostate cancer. *J Nucl Med*. 2020;61:857–865.
63. Sun M, Niaz MO, Nelson A, Skafida M, Niaz MJ. Review of ¹⁷⁷Lu-PSMA-617 in patients with metastatic castration-resistant prostate cancer. *Cureus*. 2020;12:e8921.
64. Kratochwil C, Bruchertseifer F, Rathke H, et al. Targeted alpha-therapy of metastatic castration-resistant prostate cancer with ²²⁵Ac-PSMA-617: dosimetry estimate and empiric dose finding. *J Nucl Med*. 2017;58:1624–1631.
65. Carrasquillo JA, Pandit-Taskar N, Chen CC. I-131 metaiodobenzylguanidine therapy of pheochromocytoma and paraganglioma. *Semin Nucl Med*. 2016;46:203–214.
66. Highlights of prescribing information. Azedra website. <https://www.azedra.com/content/pdf/full-prescribing-information.pdf>. Published June 2021. Accessed November 9, 2021.
67. Pryma DA, Chin BB, Noto RB, et al. Efficacy and safety of high-specific-activity ¹³¹I-MIBG therapy in patients with advanced pheochromocytoma or paraganglioma. *J Nucl Med*. 2019;60:623–630.
68. Wilson JS, Gains JE, Moroz V, Wheatley K, Gaze MN. A systematic review of ¹³¹I-meta iodobenzylguanidine molecular radiotherapy for neuroblastoma. *Eur J Cancer*. 2014;50:801–815.
69. Matthay KK, Tan JC, Villablanca JG, et al. Phase I dose escalation of iodine-131-metaiodobenzylguanidine with myeloablative chemotherapy and autologous stem-cell transplantation in refractory neuroblastoma: a new approaches to Neuroblastoma Therapy Consortium Study. *J Clin Oncol*. 2006;24:500–506.
70. Matthay KK, Quach A, Huberty J, et al. Iodine-131–metaiodobenzylguanidine double infusion with autologous stem-cell rescue for neuroblastoma: a new approaches to neuroblastoma therapy phase I study. *J Clin Oncol*. 2009;27:1020–1025.
71. Fielding SL, Flower MA, Ackery D, Kemshead JT, Lashford LS, Lewis I. Dosimetry of iodine 131 metaiodobenzylguanidine for treatment of resistant neuroblastoma: results of a UK study. *Eur J Nucl Med*. 1991;18:308–316.
72. Lashford LS, Lewis IJ, Fielding SL, et al. Phase I/II study of iodine 131 metaiodobenzylguanidine in chemoresistant neuroblastoma: a United Kingdom Children's Cancer Study Group investigation. *J Clin Oncol*. 1992;10:1889–1896.
73. Matthay KK, Panina C, Huberty J, et al. Correlation of tumor and whole-body dosimetry with tumor response and toxicity in refractory neuroblastoma treated with ¹³¹I-MIBG. *J Nucl Med*. 2001;42:1713–1721.
74. Buckley SE, Saran FH, Gaze MN, et al. Dosimetry for fractionated ¹³¹I-mIBG therapies in patients with primary resistant high-risk neuroblastoma: preliminary results. *Cancer Biother Radiopharm*. 2007;22:105–112.
75. Monsieurs M, Brans B, Bacher K, Dierckx R, Thierens H. Patient dosimetry for ¹³¹I-MIBG therapy for neuroendocrine tumours based on ¹²³I-MIBG scans. *Eur J Nucl Med Mol Imaging*. 2002;29:1581–1587.
76. Pandit-Taskar N, Zanzonico P, Hilden P, Ostrovnyaya I, Carrasquillo JA, Modak S. Assessment of organ dosimetry for planning repeat treatments of high-dose ¹³¹I-MIBG therapy: ¹²³I-MIBG versus posttherapy ¹³¹I-MIBG imaging. *Clin Nucl Med*. 2017;42:741–748.
77. Huang SY, Bolch WE, Lee C, et al. Patient-specific dosimetry using pretherapy [¹²⁴I]m-iodobenzylguanidine ([¹³¹I]mIBG) dynamic PET/CT imaging before [¹³¹I]mIBG targeted radionuclide therapy for neuroblastoma. *Mol Imaging Biol*. 2015;17:284–294.
78. Seo Y, Huh Y, Huang SY, et al. Technical note: simplified and practical pretherapy tumor dosimetry—a feasibility study for ¹³¹I-MIBG therapy of neuroblastoma using ¹²⁴I-MIBG PET/CT. *Med Phys*. 2019;46:2477–2486.
79. Wiseman GA, Leigh B, Erwin WD, et al. Radiation dosimetry results for Zevalin radioimmunotherapy of rituximab-refractory non-Hodgkin lymphoma. *Cancer*. 2002;94:1349–1357.
80. Wiseman GA, Korrmehl E, Leigh B, et al. Radiation dosimetry results and safety correlations from ⁹⁰Y-ibritumomab tiuxetan radioimmunotherapy for relapsed or refractory non-Hodgkin's lymphoma: combined data from 4 clinical trials. *J Nucl Med*. 2003;44:465–474.
81. Delaloye AB, Antonescu C, Louton T, Kuhlmann J, Hagenbeek A. Dosimetry of ⁹⁰Y-ibritumomab tiuxetan as consolidation of first remission in advanced-stage follicular lymphoma: results from the international phase 3 first-line indolent trial. *J Nucl Med*. 2009;50:1837–1843.
82. Wahl RL, Frey EC, Jacene HA, et al. Prospective SPECT-CT organ dosimetry-driven radiation-absorbed dose escalation using the In-111 (¹¹¹In)/yttrium 90

- (⁹⁰Y) ibritumomab tiuxetan (Zevalin®) theranostic pair in patients with lymphoma at myeloablative dose levels. *Cancers (Basel)*. 2021;13:2828.
83. Boucek JA, Turner JH. Validation of prospective whole-body bone marrow dosimetry by SPECT/CT multimodality imaging in ¹³¹I-anti-CD20 rituximab radioimmunotherapy of non-Hodgkin's lymphoma. *Eur J Nucl Med Mol Imaging*. 2005;32:458–469.
 84. Sgouros G, Squeri S, Ballangrud AM, et al. Patient-specific, 3-dimensional dosimetry in non-Hodgkin's lymphoma patients treated with ¹³¹I-anti-B1 antibody: assessment of tumor dose-response. *J Nucl Med*. 2003;44:260–268.
 85. Jacene HA, Filice R, Kasecamp W, Wahl RL. Comparison of ⁹⁰Y-ibritumomab tiuxetan and ¹³¹I-tositumomab in clinical practice. *J Nucl Med*. 2007;48:1767–1776.
 86. Dewaraja YK, Schipper MJ, Shen J, et al. Tumor-absorbed dose predicts progression-free survival following ¹³¹I-tositumomab radioimmunotherapy. *J Nucl Med*. 2014;55:1047–1053.
 87. Kaminski MS, Estes J, Zasadny KR, et al. Radioimmunotherapy with iodine ¹³¹I tositumomab for relapsed or refractory B-cell non-Hodgkin lymphoma: updated results and long-term follow-up of the University of Michigan experience. *Blood*. 2000;96:1259–1266.
 88. Koral KF, Dewaraja Y, Li J, et al. Update on hybrid conjugate-view SPECT tumor dosimetry and response in ¹³¹I-tositumomab therapy of previously untreated lymphoma patients. *J Nucl Med*. 2003;44:457–464.
 89. Roberson PL, Smith LB, Morgan MA, et al. Beyond dose: using pretherapy biomarkers to improve dose prediction of outcomes for radioimmunotherapy of non-Hodgkin lymphoma. *Cancer Biother Radiopharm*. 2017;32:309–319.
 90. Hartmann Siantar CL, DeNardo GL, DeNardo SJ. Impact of nodal regression on radiation dose for lymphoma patients after radioimmunotherapy. *J Nucl Med*. 2003;44:1322–1329.
 91. Jacene H, Crandall J, Kasamon YL, et al. Initial experience with tositumomab and I-131-labeled tositumomab for treatment of relapsed/refractory Hodgkin lymphoma. *Mol Imaging Biol*. 2017;19:429–436.
 92. Chiesa C, Botta F, Coliva A, et al. Absorbed dose and biologically effective dose in patients with high-risk non-Hodgkin's lymphoma treated with high-activity myeloablative ⁹⁰Y-ibritumomab tiuxetan (Zevalin). *Eur J Nucl Med Mol Imaging*. 2009;36:1745–1757.
 93. Gopal AK, Rajendran JG, Gooley TA, et al. High-dose [¹³¹I]tositumomab (anti-CD20) radioimmunotherapy and autologous hematopoietic stem-cell transplantation for adults > or = 60 years old with relapsed or refractory B-cell lymphoma. *J Clin Oncol*. 2007;25:1396–1402.
 94. Winter JN, Inwards DJ, Spies S, et al. Yttrium-90 ibritumomab tiuxetan doses calculated to deliver up to 15 Gy to critical organs may be safely combined with high-dose BEAM and autologous transplantation in relapsed or refractory B-cell non-Hodgkin's lymphoma. *J Clin Oncol*. 2009;27:1653–1659.
 95. TheraSphere™: Y-90 glass microspheres. Boston Scientific website. <https://www.bostonscientific.com/en-US/products/cancer-therapies/therasphere-y90-glass-microspheres.html>. Accessed October 28, 2021.
 96. Simplicit90Y™: personalized dosimetry software. Boston Scientific website. <https://www.bostonscientific.com/en-US/products/cancer-therapies/simplicit90y-personalized-dosimetry-software.html>. Accessed October 28, 2021.
 97. About SIR-Spheres microspheres. SIRTeX website. <https://www.sirtex.com/us/clinicians/about-sir-spheres-microspheres/>. Accessed October 28, 2021.
 98. Son MH, Ha LN, Bang MH, et al. Diagnostic and prognostic value of ^{99m}Tc-MAA SPECT/CT for treatment planning of ⁹⁰Y-resin microsphere radioembolization for hepatocellular carcinoma: comparison with planar image. *Sci Rep*. 2021;11:3207.
 99. Kafrouni M, Allimant C, Fourcade M, et al. Analysis of differences between ^{99m}Tc-MAA SPECT- and ⁹⁰Y-microsphere PET-based dosimetry for hepatocellular carcinoma selective internal radiation therapy. *EJNMMI Res*. 2019;9:62.
 100. Richetta E, Pasquino M, Poli M, et al. PET-CT post therapy dosimetry in radioembolization with resin ⁹⁰Y microspheres: comparison with pre-treatment SPECT-CT ^{99m}Tc-MAA results. *Phys Med*. 2019;64:16–23.
 101. Garin E, Rolland Y, Edeline J, et al. Personalized dosimetry with intensification using ⁹⁰Y-loaded glass microsphere radioembolization induces prolonged overall survival in hepatocellular carcinoma patients with portal vein thrombosis. *J Nucl Med*. 2015;56:339–346.
 102. Garin E, Tselikas L, Guiu B, et al. Personalised versus standard dosimetry approach of selective internal radiation therapy in patients with locally advanced hepatocellular carcinoma (DOSISPHERE-01): a randomised, multicentre, open-label phase 2 trial. *Lancet Gastroenterol Hepatol*. 2021;6:17–29.
 103. Van Nostrand D, Wartofsky L. Radioiodine in the treatment of thyroid cancer. *Endocrinol Metab Clin North Am*. 2007;36:807–822.
 104. Klubo-Gwiezdzińska J, Van Nostrand D, Atkins F, et al. Efficacy of dosimetric versus empiric prescribed activity of ¹³¹I for therapy of differentiated thyroid cancer. *J Clin Endocrinol Metab*. 2011;96:3217–3225.
 105. Kulkarni K, Van Nostrand D, Atkins F, Aiken M, Burman K, Wartofsky L. The relative frequency in which empiric dosages of radioiodine would potentially overtreat or undertreat patients who have metastatic well-differentiated thyroid cancer. *Thyroid*. 2006;16:1019–1023.
 106. Lee JJ, Chung JK, Kim SE, et al. Maximal safe dose of I-131 after failure of standard fixed dose therapy in patients with differentiated thyroid carcinoma. *Ann Nucl Med*. 2008;22:727–734.
 107. Samuel AM, Rajashekharrao B, Shah DH. Pulmonary metastases in children and adolescents with well-differentiated thyroid cancer. *J Nucl Med*. 1998;39:1531–1536.
 108. Brabander T, van der Zwan WA, Teunissen JJM, et al. Long-term efficacy, survival, and safety of [¹⁷⁷Lu-DOTA⁰,Tyr³]octreotate in patients with gastroenteropancreatic and bronchial neuroendocrine tumors. *Clin Cancer Res*. 2017;23:4617–4624.
 109. Kipnis ST, Hung M, Kumar S, et al. Laboratory, clinical, and survival outcomes associated with peptide receptor radionuclide therapy in patients with gastroenteropancreatic neuroendocrine tumors. *JAMA Netw Open*. 2021;4:e212274.
 110. Salas-Ramirez M, Tran-Gia J, Kesenheimer C, et al. Quantification of fat fraction in lumbar vertebrae: correlation with age and implications for bone marrow dosimetry in molecular radiotherapy. *Phys Med Biol*. 2018;63:025029.
 111. Cremonesi M, Ferrari M, Zoboli S, et al. Biokinetics and dosimetry in patients administered with ¹¹¹In-DOTA-Tyr³-octreotide: implications for internal radiotherapy with ⁹⁰Y-DOTATOC. *Eur J Nucl Med*. 1999;26:877–886.
 112. Baum T, Rohmeier A, Syvარი I, et al. Anatomical variation of age-related changes in vertebral bone marrow composition using chemical shift encoding-based water-fat magnetic resonance imaging. *Front Endocrinol (Lausanne)*. 2018;9:141.
 113. Sandström M, Garske-Roman U, Granberg D, et al. Individualized dosimetry of kidney and bone marrow in patients undergoing ¹⁷⁷Lu-DOTA-octreotate treatment. *J Nucl Med*. 2013;54:33–41.
 114. Bergsma H, Konijnenberg MW, van der Zwan WA, et al. Nephrotoxicity after PRRT with ¹⁷⁷Lu-DOTA-octreotate. *Eur J Nucl Med Mol Imaging*. 2016;43:1802–1811.
 115. Sundlöf A, Sjogreen-Gleisner K, Svensson J, et al. Individualised ¹⁷⁷Lu-DOTA-TATE treatment of neuroendocrine tumours based on kidney dosimetry. *Eur J Nucl Med Mol Imaging*. 2017;44:1480–1489.
 116. Sabet A, Ezziddin K, Pape UF, et al. Long-term hematotoxicity after peptide receptor radionuclide therapy with ¹⁷⁷Lu-octreotate. *J Nucl Med*. 2013;54:1857–1861.
 117. Del Prete M, Buteau F-A, Arsenault F, et al. Personalized ¹⁷⁷Lu-octreotate peptide receptor radionuclide therapy of neuroendocrine tumours: initial results from the P-PRRT trial. *Eur J Nucl Med Mol Imaging*. 2019;46:728–742.
 118. Sandström M, Garske-Roman U, Johansson S, Granberg D, Sundin A, Freedman N. Kidney dosimetry during ¹⁷⁷Lu-DOTATATE therapy in patients with neuroendocrine tumors: aspects on calculation and tolerance. *Acta Oncol*. 2018;57:516–521.
 119. Emami B, Lyman J, Brown A, et al. Tolerance of normal tissue to therapeutic irradiation. *Int J Radiat Oncol Biol Phys*. 1991;21:109–122.
 120. Bodei L, Cremonesi M, Ferrari M, et al. Long-term evaluation of renal toxicity after peptide receptor radionuclide therapy with ⁹⁰Y-DOTATOC and ¹⁷⁷Lu-DOTATATE: the role of associated risk factors. *Eur J Nucl Med Mol Imaging*. 2008;35:1847–1856.
 121. Sabet A, Nagarajah J, Dogan AS, et al. Does PRRT with standard activities of ¹⁷⁷Lu-octreotate really achieve relevant somatostatin receptor saturation in target tumor lesions? Insights from intra-therapeutic receptor imaging in patients with metastatic gastroenteropancreatic neuroendocrine tumors. *EJNMMI Res*. 2013;3:82.
 122. Goncalves I, Burbury K, Michael M, et al. Characteristics and outcomes of therapy-related myeloid neoplasms after peptide receptor radionuclide/chemoradiotherapy (PRRT/PRCRT) for metastatic neuroendocrine neoplasia: a single-institution series. *Eur J Nucl Med Mol Imaging*. 2019;46:1902–1910.
 123. Kesavan M, Claringbold PG, Turner JH. Hematological toxicity of combined ¹⁷⁷Lu-octreotate radiopeptide chemotherapy of gastroenteropancreatic neuroendocrine tumors in long-term follow-up. *Neuroendocrinology*. 2014;99:108–117.
 124. Morris MJ, Pandit-Taskar N, Stephenson RD, et al. Phase I/II study of docetaxel and Sm-153 for castrate metastatic prostate cancer (CMPC): summary of dose-escalation cohorts and first report on the expansion cohort [abstract]. *J Clin Oncol*. 2009;27(suppl):5057.
 125. Morris MJ, Loriot Y, Sweeney CJ, et al. Radium-223 in combination with docetaxel in patients with castration-resistant prostate cancer and bone metastases: a phase 1 dose escalation/randomised phase 2a trial. *Eur J Cancer*. 2019;114:107–116.
 126. DuBois SG, Granger MM, Groshen S, et al. Randomized phase II trial of MIBG versus MIBG, vincristine, and irinotecan versus MIBG and vorinostat for

- patients with relapsed or refractory neuroblastoma: a report from NANT consortium. *J Clin Oncol*. 2021;39:3506–3514.
127. Bolch WE, Eckerman KF, Sgouros G, Thomas SR. MIRD pamphlet no. 21: a generalized schema for radiopharmaceutical dosimetry—standardization of nomenclature. *J Nucl Med*. 2009;50:477–484.
 128. Staudacher AH, Bezak E, Borysenko A, Brown MP. Targeted alpha-therapy using ^{227}Th -APOMAB and cross-fire antitumour effects: preliminary in-vivo evaluation. *Nucl Med Commun*. 2014;35:1284–1290.
 129. Gustafsson J, Rodeno E, Minguez P. Feasibility and limitations of quantitative SPECT for ^{223}Ra . *Phys Med Biol*. 2020;65:085012.
 130. Sgouros G. Alpha-particles for targeted therapy. *Adv Drug Deliv Rev*. 2008;60:1402–1406.
 131. Huang CY, Guatelli S, Oborn BM, Allen BJ. Microdosimetry for targeted alpha therapy of cancer. *Comput Math Methods Med*. 2012;2012:153212.
 132. Rosenblat TL, McDevitt MR, Mulford DA, et al. Sequential cytarabine and alpha-particle immunotherapy with bismuth-213-lintuzumab (HuM195) for acute myeloid leukemia. *Clin Cancer Res*. 2010;16:5303–5311.
 133. Jurcic JG, Rosenblat TL. Targeted alpha-particle immunotherapy for acute myeloid leukemia. *Am Soc Clin Oncol Educ Book*. 2014:e126–e131.
 134. Pandit-Taskar N, O'Donoghue JA, Durack JC, et al. A phase I/II study for analytic validation of ^{89}Zr -J591 immunopET as a molecular imaging agent for metastatic prostate cancer. *Clin Cancer Res*. 2015;21:5277–5285.
 135. He B, Wahl RL, Sgouros G, et al. Comparison of organ residence time estimation methods for radioimmunotherapy dosimetry and treatment planning: patient studies. *Med Phys*. 2009;36:1595–1601.
 136. Desy A, Bouvet GF, Frezza A, Despres P, Beauregard JM. Impact of dead time on quantitative ^{177}Lu -SPECT (QSPECT) and kidney dosimetry during PRRT. *EJNMMI Phys*. 2020;7:32.
 137. Frezza A, Desport C, Uribe C, et al. Comprehensive SPECT/CT system characterization and calibration for ^{177}Lu quantitative SPECT (QSPECT) with dead-time correction. *EJNMMI Phys*. 2020;7:10.
 138. Del Prete M, Arsenault F, Saighi N, et al. Accuracy and reproducibility of simplified QSPECT dosimetry for personalized ^{177}Lu -octreotate PRRT. *EJNMMI Phys*. 2018;5:25.
 139. Madsen MT, Menda Y, O'Dorisio TM, O'Dorisio MS. Technical note: single time point dose estimate for exponential clearance. *Med Phys*. 2018;45:2318–2324.
 140. Gosewisch A, Schleske M, Gildehaus FJ, et al. Image-based dosimetry for ^{225}Ac -PSMA-I&T therapy using quantitative SPECT. *Eur J Nucl Med Mol Imaging*. 2021;48:1260–1261.
 141. Tran-Gia J, Denis-Bacelar AM, Ferreira KM, et al. A multicentre and multi-national evaluation of the accuracy of quantitative Lu-177 SPECT/CT imaging performed within the MRTDosimetry project. *EJNMMI Phys*. 2021;8:55.
 142. Lassmann M, Eberlein U, Tran-Gia J. Multicentre trials on standardised quantitative imaging and dosimetry for radionuclide therapies. *Clin Oncol (R Coll Radiol)*. 2021;33:125–130.
 143. Kesner AL, Poli GL, Beykan S, Lassmann M. The IAEA radiotracer biodistribution template: a community resource for supporting the standardization and reporting of radionuclide pre-dosimetry data. *Phys Med*. 2017;44:83–85.
 144. Freudenberg LS, Jentzen W, Gorges R, et al. ^{124}I -PET dosimetry in advanced differentiated thyroid cancer: therapeutic impact. *Nuklearmedizin*. 2007;46:121–128.
 145. Freudenberg LS, Jentzen W, Muller SP, Bockisch A. Disseminated iodine-avid lung metastases in differentiated thyroid cancer: a challenge to ^{124}I PET. *Eur J Nucl Med Mol Imaging*. 2008;35:502–508.
 146. Kolbert KS, Pentlow KS, Pearson JR, et al. Prediction of absorbed dose to normal organs in thyroid cancer patients treated with ^{131}I by use of ^{124}I PET and 3-dimensional internal dosimetry software. *J Nucl Med*. 2007;48:143–149.
 147. Hänscheid H, Lassmann M, Luster M, Kloos RT, Reiners C. Blood dosimetry from a single measurement of the whole body radioiodine retention in patients with differentiated thyroid carcinoma. *Endocr Relat Cancer*. 2009;16:1283–1289.
 148. Atkins F, Van Nostrand D, Moreau S, Burman K, Wartofsky L. Validation of a simple thyroid cancer dosimetry model based on the fractional whole-body retention at 48 hours post-administration of ^{131}I . *Thyroid*. 2015;25:1347–1350.
 149. Sisson J. Practical dosimetry of I-131 in patients with thyroid carcinoma. *Cancer Biother Radiopharm*. 2002;17:101–105.
 150. Thomas S, Samarantunga R, Sperling M, Maxon H. Predictive estimate of blood dose from external counting data preceding radioiodine therapy for thyroid cancer. *Nucl Med Biol*. 1993;20:157–162.
 151. Jentzen W, Bockisch A, Ruhlmann M. Assessment of simplified blood dose protocols for the estimation of the maximum tolerable activity in thyroid cancer patients undergoing radioiodine therapy using Iodine-124. *J Nucl Med*. 2015;56:832–838.
 152. Ho AL, Grewal RK, Leboeuf R, et al. Selumetinib-enhanced radioiodine uptake in advanced thyroid cancer. *N Engl J Med*. 2013;368:623–632.
 153. Jentzen W, Freudenberg L, Bockisch A. Quantitative imaging of ^{124}I with PET/CT in pretherapy lesion dosimetry: effects impairing image quantification and their corrections. *Q J Nucl Med Mol Imaging*. 2011;55:21–43.
 154. Garske U, Sandstrom M, Johansson S, et al. Minor changes in effective half-life during fractionated ^{177}Lu -octreotate therapy. *Acta Oncol*. 2012;51:86–96.
 155. Jackson PA, Beauregard JM, Hofman MS, Kron T, Hogg A, Hicks RJ. An automated voxelized dosimetry tool for radionuclide therapy based on serial quantitative SPECT/CT imaging. *Med Phys*. 2013;40:112503.
 156. Hänscheid H, Lapa C, Buck AK, Lassmann M, Werner RA. Dose mapping after endoradiotherapy with ^{177}Lu -DOTATATE/DOTATOC by a single measurement after 4 days. *J Nucl Med*. 2018;59:75–81.
 157. Willowson KP, Eslick E, Ryu H, Poon A, Bernard EJ, Bailey DL. Feasibility and accuracy of single time point imaging for renal dosimetry following ^{177}Lu -DOTATATE ('Lutate') therapy. *EJNMMI Phys*. 2018;5:33.
 158. Eberlein U, Cremonesi M, Lassmann M. Individualized dosimetry for theranostics: necessary, nice to have, or counterproductive? *J Nucl Med*. 2017;58(suppl):97S–103S.
 159. Dosimetry for I-131 therapy. Society of Nuclear Medicine and Molecular Imaging website. <https://www.snmni.org/ClinicalPractice/content.aspx?PreviewContentItem=XbWi2IWw&RDtoken=25722&userID=&navItemNumber=33445>. Accessed October 28, 2021.

Dosimetry for Radiopharmaceutical Therapy: The European Perspective

Michael Lassmann¹, Uta Eberlein¹, Jonathan Gear², Mark Konijnenberg³, and Jolanta Kunikowska⁴

¹Department of Nuclear Medicine, University of Würzburg, Würzburg, Germany; ²Joint Department of Physics, Royal Marsden NHS Foundation Trust and Institute of Cancer Research, London, United Kingdom; ³Department of Radiology and Nuclear Medicine, Erasmus MC, Rotterdam, The Netherlands; and ⁴Nuclear Medicine Department, Medical University of Warsaw, Warsaw, Poland

This review presents efforts in Europe over the last few years with respect to standardization of quantitative imaging and dosimetry and comprises the results of several European research projects on practices regarding radiopharmaceutical therapies (RPTs). Because the European Union has regulatory requirements concerning dosimetry in RPTs, the European Association of Nuclear Medicine released a position paper in 2021 on the use of dosimetry under these requirements. The importance of radiobiology for RPTs is elucidated in another position paper by the European Association of Nuclear Medicine. Furthermore, how dosimetry interacts with clinical requirements is described, with several clinical examples. In the future, more efforts need to be undertaken to increase teaching and standardization efforts and to incorporate radiobiology for further individualizing patient treatment, with the aim of improving the outcome and safety of RPTs.

Key Words: quantitative imaging; dosimetry; radiobiology

J Nucl Med 2021; 62:73S–79S

DOI: 10.2967/jnumed.121.262754

The number of radiopharmaceutical therapies (RPTs) that have obtained marketing authorization in Europe has increased in recent years (²²³RaCl₂ [Xofigo; Bayer] (1), ¹⁷⁷Lu-oxodotreotide [Lutathera; Advanced Accelerator Applications] (2)), and several others are presently in late stages of clinical trials (¹⁷⁷Lu-PSMA-617 (3), ¹⁷⁷Lu-lilotomab (4)).

Dose-effect relationships after RPTs have been derived mostly from retrospective studies, the results of which have been nicely summarized in a review by Strigari et al. (5). For RPTs, prospective evidence with therapy prescription based on patient-specific dosimetry still needs to be obtained (6). Evidence demonstrating the superiority of dosimetry-guided prescription was provided in the DOSISPHERE trial on ⁹⁰Y-microsphere therapy of liver cancer (7). This class of therapies is considered as treatment with a medical device and is therefore not considered further in this review of RPTs.

Quantitative imaging plays a major role in individualized treatment planning and posttherapeutic dose verification in RPTs. Sequential quantitative SPECT/CT measurements of therapeutically used radiopharmaceuticals permits determination of the

spatial and temporal activity distribution in patients' organs or tissues (8).

Several projects funded by the European Union's Horizon 2020 program provided additional input to the multistep approach needed for dosimetry in nuclear medicine (www.mrtdosimetry-empir.eu, www.medirad-project.eu) (9,10). Driven by the increasing number of therapeutic procedures, the European Association of Nuclear Medicine (EANM) dosimetry committee developed a guidance document for assessing uncertainties in absorbed dose calculations (11). As a European Council directive (12) requires pretherapeutic treatment planning and absorbed dose verification for RPTs (12), the EANM released a statement to help centers comply with the directive step by step, allowing for a change from the current practice to a patient-specific treatment (6) for the range of resources currently available across Europe. Because radiobiologic response is gaining increasing influence in clinical applications and in more fundamental research, the EANM also published a position paper on how best to integrate radiobiology in the world of nuclear medicine (13).

Consequently, the aim of this review is to summarize recent efforts in Europe for RPTs, with the aim of improving patient treatment by individualization based on dosimetry. RPTs, for this report, are defined as treatment with radiopharmaceuticals, in contrast to locoregional treatments with medical devices such as selective internal radiation therapy.

MULTICENTER TRIALS INVOLVING STANDARDIZED QUANTITATIVE IMAGING AND DOSIMETRY

In a recent review, Lassmann et al. summarized efforts to standardize quantitative imaging for dosimetry in major multicenter trials, mostly by European sites (14). Table 1 presents the setup and results for the most important SPECT/CT studies since 2018.

Wevrett et al. (15) reported on an intercomparison of quantitative imaging with ¹⁷⁷Lu in European hospitals using a shell sphere consisting of 2 isolated concentric spheres allowing the creation of a core filled with a high activity concentration, surrounded by a less active background shell (15). The authors concluded that reasonable uncertainties were reported by the participants; however, further research into the nature of the uncertainties should be done.

Peters et al. (16) evaluated the quantitative accuracy and inter-system variations for 4 Dutch centers by repeatedly scanning a cylindrical phantom with 6 spheric inserts using standardized acquisition settings. The reconstructions were performed using vendor-specific algorithms and a vendor-neutral quantitative reconstruction for all systems. For each sphere, the authors

Received Jun. 28, 2021; revision accepted Oct. 13, 2021.
For correspondence or reprints, contact Uta Eberlein (eberlein_u@ukw.de).
COPYRIGHT © 2021 by the Society of Nuclear Medicine and Molecular Imaging.

TABLE 1
List of Recent SPECT/CT Studies (Published in 2018 or Later) for Quantitative Imaging and Dosimetry for Therapeutically Used Radionuclides

Label	Phantom used for calibration	Source volume	Traceable activity	Centers or devices (n)	Estimated accuracy	Remarks	Reference
¹⁷⁷ Lu	Two concentric spheres in elliptic phantom with lung and spine inserts		Yes	7 centers	22% spread for inner sphere, 117% for outer shell, 23% for total activity	Site-specific calibrations with locally available phantom and reconstruction	Wevrett (15)
¹⁷⁷ Lu	Cylindric phantom with 6 spheric inserts	0.5–113 mL	No	4 centers	Calibration factors; focus on comparing recovery coefficients	Vendor-specific and -neutral reconstruction	Peters (16)
¹³¹ I	Specific calibration and validation phantom, lesions in abdominal phantom	0.8 – 196 mL	Yes	9 systems	15.7% uncertainty of activity in 65-mL sphere	Dead-time measurement and centralized reconstruction	Gregory (17)
¹⁷⁷ Lu	Petri dish in air		No	2 centers	Not given		Sundlöv (18)
¹⁷⁷ Lu	Calibration: Jaszczak cylinder and NEMA sphere phantom; validation: 2-organ anthropomorphic phantom (2-compartment kidney, spleen)	35 mL (kidney medulla)/75 mL (kidney cortex), 125 mL (spleen)	Yes	8 centers, 9 systems	Ratios: 1.02 ± 0.09 (kidney) and 1.05 ± 0.11 (spleen) between radionuclide calibrator-based and SPECT/CT-based activity	Site-specific reconstruction	Tran-Gia (10)
¹³³ Ba/ ¹³¹ I	Four cylindric phantoms	1.68, 6.72, 26.9, 107.4 mL	Yes	8 systems	5.6% for GE Healthcare systems		Tran-Gia (20)
¹⁷⁷ Lu	Four-organ anthropomorphic phantom (2-compartment kidney, liver, spleen)	According to ICRP 110 (58)	Yes	1 system	Not applicable	Variable time-dependent activities mimicking ¹⁷⁷ Lu-DOTATATE therapy	MRTDosimetry (21)
¹³¹ I	Cylindric phantom	0.5–144 mL	No	4 centers	<5.4%	Site-specific reconstruction	Taprogge (9)

NEMA = National Electrical Manufacturers Association; ICRP = International Commission on Radiological Protection.

calculated mean and maximum recovery coefficients for 3 repeated measurements and defined the intersystem variations as the range of recovery coefficients over all systems. Overall, the authors concluded that eliminating the effects of system hardware and the use of standardized reconstruction algorithms is the key element for multicenter dosimetry and quantitative biomarker studies.

The first multicenter trial to investigate the role of ^{123}I and ^{131}I SPECT/CT-based tumor dosimetry in predicting response to radioiodine therapy was the SEL-I-METRY trial (17), which included a network of centers with consistent methods of radioiodine activity quantification (17). Image quantification was validated by imaging a 3-dimensionally printed phantom mimicking a patient's activity distribution. The errors in the validation of phantom activities were comparable to the measurement uncertainties derived from an uncertainty analysis. For example, the uncertainty for ^{131}I in a 5-cm sphere was at 16% on average (17).

In a two-center Swedish study on the treatment of patients with neuroendocrine tumors, the aim was to determine the feasibility, safety, and efficacy of individualizing treatment with ^{177}Lu -DOTATATE, based on renal dosimetry. The calibration of the systems used was derived from a planar scan or a SPECT/CT scan by using a thin layer of ^{177}Lu in a Petri dish placed in air, with the activity traceable to a standard laboratory (18).

Further efforts to standardize SPECT/CT calibration were undertaken in the joint European Metrology Research Project, MRTDosimetry (<http://mrtdosimetry-empir.eu/>), which terminated in mid-2019. The main goals of the project were to improve accuracy and metrologic traceability in the calculation of absorbed doses from time sequences of quantitative imaging measurements and to determine uncertainties in the relationship to the full dosimetry-related measurement chain from a primary standard to a range of commercial and noncommercial dosimetry calculation platforms. For this review, 3 subprojects are of interest. Regarding the first subproject, a study with ^{177}Lu by Tran-Gia et al. (10), the setup and results of a comparison exercise are reported. This study included 9 SPECT/CT systems with the same setup (system, acquisition, and reconstruction) for calibration, determination of the recovery coefficients for partial-volume correction, and a validation using a 3-dimensionally printed 2-organ phantom. The results were that similar combinations of imaging system and reconstruction led to image calibration factors that agreed within their respective uncertainties, provided the same software was used. Activity recovery still leads to uncertainties of up to 15%. Accurate partial-volume correction still remains a challenge and is an unsolved problem, particularly at the voxel level (19).

The second subproject, an international quantitative SPECT/CT imaging comparison exercise, included 8 SPECT/CT systems and was set up to assess the applicability of ^{133}Ba sources as a surrogate for ^{131}I and to determine a cross-calibration factor (20). Cylinders of 4 different dimensions were fabricated with a 3-dimensional printing system and either were filled with solid ^{133}Ba (produced at 2 metrology institutions) or were left hollow, to be filled with liquid ^{131}I on site. Equivalent camera and reconstruction setups yielded comparable calibration factors. A cross-calibration factor between ^{133}Ba and ^{131}I , which agreed with the ratio of the emission probabilities, was obtained, thus confirming that traceable solid ^{133}Ba sources are useful as surrogates for liquid ^{131}I in SPECT/CT calibrations (20).

In the third subproject, a series of SPECT/CT images was acquired of a 4-organ 3-dimensional phantom (left and right kidneys, liver, and spleen) and filled 6 times with varying ^{177}Lu activities mimicking 6 time points of a representative

^{177}Lu -DOTATATE therapy (21), starting with a medulla-to-cortex ratio of 3:1. The late time point for scanning was 144 h after administration. To control the variability caused by camera and workstation setups, 6 sets of images were prepared (raw and reconstructed) to cover GE Healthcare, Siemens, and Hermes DICOM formats (21). In the near future, these data sets will be made publicly available for the testing and commissioning of dosimetry software.

Another European project, MEDIRAD (<http://www.medirad-project.eu/>), which started in 2017, aims to address the need to better understand and evaluate the health effects of low-dose ionizing radiation exposure from diagnostic and therapeutic imaging. In one of the work packages, necessary tools to establish, in a multicenter setting, the range of absorbed doses delivered to healthy organs of thyroid cancer patients undergoing thyroid ablation will be developed and implemented. The technical part of the project comprises standardization of quantitative imaging, as well as centralized dosimetry reading (9).

The first results of these joint European efforts emphasize the need to define a standardized and reproducible calibration across sites for SPECT/CT quantitative imaging as a prerequisite for dosimetry in multicenter trials. Furthermore, for dosimetry, efforts in Europe include the OpenDose collaboration, which provides an open-access resource platform for available dosimetry data and tools to be used for nuclear medicine dosimetry (22).

RECENT ACCOMPLISHMENTS OF THE EANM DOSIMETRY COMMITTEE

The dosimetry task group, which subsequently became a committee of the EANM, was formed in 2001 (23) in response to an observed knowledge gap within the field. The committee founded the International Symposia on Radionuclide Therapy and Radiopharmaceutical Dosimetry. Four initial symposia were organized, between 2004 and 2011, coordinated jointly by the EANM radionuclide therapy committee in cooperation with the MIRD committee of the Society of Nuclear Medicine and Molecular Imaging (24). The success of these symposia translated into the regular Do.MoRe Track of the annual EANM congress, which continues to be a world-leading meeting attracting participation and attendees from around the globe, including America and Australia. In 2020, the track was reorganized to bring together all disciplines concerned with physics, dosimetry, and radiobiology and is now called the Cutting-Edge Science Track.

Teaching and dissemination of knowledge became a substantial component of the committee's activities, running courses on both basic and advanced dosimetry techniques. After the formation of the European School of Multimodality Imaging and Therapy, these courses were translated into a hands-on practical session covering the essentials for the implementation of dosimetry in nuclear medicine therapy. During the course, attendees are given the opportunity to work alongside dosimetry experts, processing raw scintigraphy data while learning the theory required to calculate an absorbed dose. In addition to the formal courses, committee members deliver numerous European School of Multimodality Imaging and Therapy webinars and lectures throughout Europe for national societies and other organizations. In 2013, a curriculum for education and training of medical physicists in nuclear medicine was developed in collaboration with the European Federation of Organizations in Medical Physics (25). Specific training courses for technologists have not been offered by the EANM; however,

the dosimetry committee has been repeatedly involved in technologist teaching symposia on dosimetry during the annual EANM congresses.

The committee has contributed to several clinical EANM guidelines for both therapy and dosimetry (26–29) and continues to expand its series of standard operational procedures, including dosimetry procedures for ^{131}I -MIBG treatment of neuroendocrine tumors, published in 2020 (30), and dosimetry in liver radioembolization with ^{90}Y microspheres (31). Similarly, a dosimetry guideline for ^{177}Lu -labeled prostate-specific membrane antigen (PSMA)-targeting and somatostatin-receptor-targeting compounds is complete and shortly to be submitted. This document reviews current practice and dosimetry methods, complementing a previous publication (32).

Similar guidance has been produced to match the needs of the community. The guideline on good practices in clinical dosimetry reporting, published in 2011 (33), continues to provide essential advice for scientists who are preparing and submitting publications and reports containing data on internal dosimetry. Guidance describing a framework for modeling the uncertainty in the absorbed dose calculation was also provided to answer concerns over the accuracy and precision of clinical dosimetry (11). All these guidelines are available free of charge on the home page of the EANM (www.eanm.org).

In 2015, an EANM internal dosimetry task force was formed with the mandate of reporting on the current status and potential prospects of treatment planning for RPTs (34). The report evaluated whether dosimetry is feasible for the therapeutic procedures currently used, examined the evidence for absorbed dose-effect correlations, and speculated on how personalized treatment planning may be further developed (34,35). The results of a survey by the task group (including representatives of the committee) describing variations in the practice of RPTs and implementation of dosimetry in Europe were also published (36).

Furthermore, the EANM supported the International Atomic Energy Agency initiative to write a soon-to-be-published handbook on dosimetry for RPTs in collaboration with the Society of Nuclear Medicine and Molecular Imaging, the American Association of Physicists in Medicine, and the European Federation of Organisations for Medical Physics. Members of the EANM dosimetry committee were also involved in writing the upcoming International Commission on Radiation Units and Measurements report 96 (“Dosimetry-Guided Radiopharmaceutical Therapy”).

COMPLIANCE WITH REGULATORY REQUIREMENTS IN EUROPE

Regulatory requirements in the European Union differ slightly from those in the rest of the world. For the European Union, European Community Directive 2013/59/Euratom states in article 56 that “exposures of target volumes in nuclear medicine treatments shall be individually planned and their delivery appropriately verified” (12). Because the implementation of the directive differs in the European Union member states, the EANM considered it necessary to form a multidisciplinary working group to provide guidance on how to interpret article 56 of the directive with regard to RPTs (6). A potential discrepancy might arise with the European pharmaceutical regulations when personalized planning leads to a conflict between the approved prescription posology and the optimization principle of European Community directive 2013/59/Euratom, as was summarized in the corresponding EANM position paper (6).

The paper proposes distinguishing between 3 levels of compliance with the optimization principle of the directive, inspired by the indication of levels in prescribing, recording, and reporting of absorbed doses in analogy to radiotherapy as described by International Commission on Radiation Units and Measurements report 91 (37). As stated in the position paper (6), level 1 is defined by administering the activity within 10% of the intended activity, typically according to the package insert or to the respective EANM guidelines, followed by verification of the therapy delivery, if applicable. Level 2, “Activity-Based Prescription and Patient-Specific Dosimetry,” defines the need for dosimetry for nonstandardized treatments in the developmental phase or for approved radiopharmaceuticals being used off-label with significantly (>25% more than in the label) higher activities. This level implies recording and reporting of the absorbed dose to organs at risk and, optionally, the absorbed dose to treatment regions. Level 3, “Dosimetry-Guided Patient-Specific Prescription and Verification,” is strongly encouraged by the EANM to foster research that eventually leads to treatment planning, whenever possible and relevant.

For many RPTs, the position paper provides examples of the minimum compliance level (6) for optimizing and standardizing patient-specific therapeutic practices in nuclear medicine in Europe. Because evidence of the superiority of therapy prescriptions based on patient-specific dosimetry has not been obtained yet for many therapeutic radiopharmaceuticals with a marketing authorization, the scheme was derived to help advance the field of RPTs. The scheme ensures that new therapies are introduced clinically and cost-effectively and that research for generating further evidence is stimulated. In addition, the authors state that a better understanding of radiobiology is key to the long-term improvement of RPTs (6).

Traditionally, safety and efficacy form the first aim in phase 1 and phase 2 clinical trials. This approach leads to generic knowledge about the therapeutic window for a radiopharmaceutical. Therefore, these trials provide an optimal opportunity to gather sufficient information on dose-response relationships for new RPTs (6).

RADIOBIOLOGY

In 2021, the EANM published a position paper on the role of radiobiology in nuclear medicine (13). For this paper, a group of EANM radiobiology, physics, and dosimetry experts summarized the main issues concerning radiobiology in nuclear medicine.

Extrapolation, to RPTs, of data obtained from the vast experience in radiobiology for external-beam radiation therapy or brachytherapy is complex because of differences in absorbed dose rates and spatial and temporal dose distributions. As a result, irradiated organs and tissues respond differently in RPTs (38–40), and the condition of RPT patients with metastatic disease diverges considerably from external-beam radiation therapy patients with single tumors. DNA damage induction and repair will strongly differ from the external-beam radiation therapy experience because of the comparatively low dose rates varying over time with physical decay and kinetic clearance, such as in patients after prostate cancer RPT (41,42). Repair of sublethal DNA damage proceeds in parallel to the absorbed dose delivery, and this effect has led to a higher threshold in the absorbed dose, inducing late kidney damage after ^{90}Y peptide therapy in comparison to the well-established external-beam radiation therapy threshold dose (43). Consequently,

there is a need to generate and apply more radiobiologic knowledge specific to nuclear medicine diagnostic and therapeutic procedures.

In the EANM position paper, the authors provided an example concerning ^{177}Lu -DOTATATE therapy with advanced, progressive, somatostatin receptor subtype 2-positive midgut neuroendocrine tumors, the patient group that was studied in the NETTER-1 phase 3 trial (44). Further optimization of ^{177}Lu -DOTATATE therapy while keeping toxicity low may include improved personalized dosimetry (45) in conjunction with a deep biologic evaluation of superior radionuclides, improved somatostatin receptor subtype 2 ligands, increased somatostatin receptor subtype 2 levels, the role of tumor microenvironment, and combinations with immunotherapy, targeted therapy, or DNA-modulating agents, as well as predictive markers for improved patient selection and treatment follow-up (46–50).

The position of the EANM is that radiobiology will contribute to the optimization of RPTs to ensure that they are effective and safe for each individual patient (13). It is expected that a better understanding of radiobiologic parameters will enhance the capabilities of new and existing nuclear medicine applications. There is a need to better define the dose-effect relationships of systemic ionizing radiation for tumors and for normal tissue. To achieve this goal, the EANM recommends a strong link between all disciplines involved (radiochemists, radiopharmacists, radiobiologists, medical physicists, and physicians) (13).

DOSIMETRY AND THE INTERACTION WITH CLINICAL REQUIREMENTS

Recent RPTs with marketing authorization, such as $^{223}\text{RaCl}_2$ or ^{177}Lu -DOTATATE therapy, investigated dosimetry during initial phase I and II trials. With other therapies, such as ^{131}I -NaI, 80 y of experience has shown that treatment of patients with fixed activities or based on disease, thyroid uptake, and volume is safe, with limited side effects.

^{131}I -MIBG has been used as an effective salvage therapy over many decades for pheochromocytoma, neuroblastoma, medullary thyroid carcinoma, and selected cases of neuroendocrine. Hemotoxicity may be observed in some patients but can be well tolerated and controlled with stem cell harvest if necessary.

^{177}Lu -DOTATATE therapy for neuroendocrine patients, with 30 y of experience, is based on the Rotterdam protocol with the 4 injections of 7.4 GBq per cycle (29.6 GBq in total) (2,44). For peptide radionuclide therapy, the main side effect is nephrotoxicity, with the kidney as the dose-limiting organ. Using nephroprotection with amino acid infusion, renal toxicity is reduced to occasional cases. A dosimetry-tailored activity escalation study on 200 patients receiving 22.2–74 GBq (51) and a second study on 74 patients receiving 14.8–37.8 GBq (52) showed renal toxicity grades 3–4 in only 1 patient. Salvage treatments administering up to 4 additional peptide radionuclide therapy cycles, and cumulative activities of up to 60.5 GBq for ^{177}Lu -DOTATATE (53) or up to 30.7 GBq for tandem $^{90}\text{Y}/^{177}\text{Lu}$ -DOTATATE (54), did not show any increase in kidney or bone marrow-related side effects.

The latest development in ^{177}Lu -PSMA therapy for prostate cancer patients showed a very good clinical response, with limited side effects. The results of the VISION phase III study found a 4-mo gain in life expectancy and a 5-mo delay in disease progression in the $6 \times 7.4\text{-GBq}$ treatment group, compared with the standard of care (3). Most side effects were mild, of grade 1–2, and comprised bone marrow suppression (47%), dry mouth (39%),

hepatotoxicity (10%), and renal effects (9%) (3). Adverse events of at least grade 3 were higher for ^{177}Lu -PSMA therapy than for the standard of care (52.7% vs. 38%) but did not, however, have an impact on quality of life (3).

From a clinical perspective, the most important issue regarding treatment optimization is always patient safety. However, preservation and improvement of quality of life are no less significant.

Treatment optimization and personalization through individual planning of the absorbed doses delivered to target organs, taking into account the absorbed doses delivered to nontarget organs, is a challenge. When optimizing treatment procedures, we need to consider that the main goal is to help and treat the patient. The object of our research is, in most cases, an oncologic patient with an often-poor clinical condition and progressive disease. Swift and efficient treatment is paramount, and for this reason dosimetry-guided prescriptions should not delay the start of treatment procedures.

Most dosimetry approaches require quantitative imaging, ideally up to 4 or 6 time points. Depending on the imaging modality, these could take up to 30–60 min. For many clinical centers, this may be difficult to achieve. Access to SPECT/CT systems may be limited in busy centers occupied with other daily imaging, and the patients' condition and quality of life should be considered. For patients with a poor performance status, simplified personalized dosimetry regimens could become an important asset. Dosimetry based on single-time-point acquisitions, particularly using only 1 SPECT/CT scan, are now on the rise and could offer a compromise between the accuracy and resources needed for dosimetry (55). Such dosimetry could also be perfectly connected to the development of artificial intelligence methods to improve the dosimetry-guided treatment planning (56,57).

Several areas have been identified in which dosimetry plays an important role and is highly desired: RPT in children, radiopharmaceuticals under clinical development, and off-label use of radiopharmaceuticals with administrations of activity that are significantly higher ($\geq 25\%$) than the recommended activity, including the total activity accumulated over all cycles and treatments (6). In daily clinical practice, dosimetry studies could also be considered in selected patients with risk factors.

As has been discussed in the EANM position papers (6,13), a better understanding of therapy dosimetry, that is, how much and where the energy is delivered, and radiobiology, that is, radiation-related processes in tissues, are keys to the long-term improvement of our treatments.

CONCLUSION

Today, standardization of quantitative imaging and dosimetry between laboratories is feasible. However, care has to be taken to minimize the variability in image acquisition and reconstruction. In the next few years, further individualization of patient treatment will be needed, as well as greater effort to increase teaching and standardization and to incorporate radiobiology — all with an aim of improving the outcome and safety of patients undergoing RPTs.

DISCLOSURE

No potential conflict of interest relevant to this article was reported.

REFERENCES

1. Poeppel TD, Handkiewicz-Junak D, Andreoff M, et al. EANM guideline for radionuclide therapy with radium-223 of metastatic castration-resistant prostate cancer. *Eur J Nucl Med Mol Imaging*. 2018;45:824–845.

2. Bodei L, Mueller-Brand J, Baum RP, et al. The joint IAEA, EANM, and SNMMI practical guidance on peptide receptor radionuclide therapy (PRRT) in neuroendocrine tumours. *Eur J Nucl Med Mol Imaging*. 2013;40:800–816.
3. Sartor O, de Bono J, Chi KN, et al. Lutetium-177-PSMA-617 for metastatic castration-resistant prostate cancer. *N Engl J Med*. 2021;385:1091–1103.
4. Kolstad A, Illidge T, Bolstad N, et al. Phase 1/2a study of ¹⁷⁷Lu-lilotomab satetraxetan in relapsed/refractory indolent non-Hodgkin lymphoma. *Blood Adv*. 2020;4:4091–4101.
5. Strigari L, Konijnenberg M, Chiesa C, et al. The evidence base for the use of internal dosimetry in the clinical practice of molecular radiotherapy. *Eur J Nucl Med Mol Imaging*. 2014;41:1976–1988.
6. Konijnenberg M, Herrmann K, Kobe C, et al. EANM position paper on article 56 of the Council Directive 2013/59/Euratom (basic safety standards) for nuclear medicine therapy. *Eur J Nucl Med Mol Imaging*. 2021;48:67–72.
7. Garin E, Tselikas L, Guiu B, et al. Personalised versus standard dosimetry approach of selective internal radiation therapy in patients with locally advanced hepatocellular carcinoma (DOSISPHERE-01): a randomised, multicentre, open-label phase 2 trial. *Lancet Gastroenterol Hepatol*. 2021;6:17–29.
8. Flux G, Bardies M, Monsieurs M, Savolainen S, Strands SE, Lassmann M. The impact of PET and SPECT on dosimetry for targeted radionuclide therapy. *Z Med Phys*. 2006;16:47–59.
9. Taprogge J, Leek F, Schurrat T, et al. Setting up a quantitative SPECT imaging network for a European multi-centre dosimetry study of radioiodine treatment for thyroid cancer as part of the MEDIRAD project. *EJNMMI Phys*. 2020;7:61.
10. Tran-Gia J, Denis-Bacelar AM, Ferreira KM, et al. A multicentre and multi-national evaluation of the accuracy of quantitative Lu-177 SPECT/CT imaging performed within the MRTDosimetry project. *EJNMMI Phys*. 2021;8:55.
11. Gear JI, Cox MG, Gustafsson J, et al. EANM practical guidance on uncertainty analysis for molecular radiotherapy absorbed dose calculations. *Eur J Nucl Med Mol Imaging*. 2018;45:2456–2474.
12. Council of the European Union. European Council directive 2013/59/Euratom on basic safety standards for protection against the dangers arising from exposure to ionising radiation and repealing directives 89/618/Euratom, 90/641/Euratom, 96/29/Euratom, 97/43/Euratom and 2003/122/Euratom. *Off J Eur Union*. 2014; L13:1–73.
13. Aerts A, Eberlein U, Holm S, et al. EANM position paper on the role of radiobiology in nuclear medicine. *Eur J Nucl Med Mol Imaging*. 2021;48:3365–3377.
14. Lassmann M, Eberlein U, Tran-Gia J. Multicentre trials on standardised quantitative imaging and dosimetry for radionuclide therapies. *Clin Oncol (R Coll Radiol)*. 2021;33:125–130.
15. Wevret J, Fenwick A, Scuffham J, et al. Inter-comparison of quantitative imaging of lutetium-177 (¹⁷⁷Lu) in European hospitals. *EJNMMI Phys*. 2018;5:17.
16. Peters SMB, Meyer Viol SL, van der Werf NR, et al. Variability in lutetium-177 SPECT quantification between different state-of-the-art SPECT/CT systems. *EJNMMI Phys*. 2020;7:9.
17. Gregory RA, Murray I, Gear J, et al. Standardised quantitative radioiodine SPECT/CT imaging for multicentre dosimetry trials in molecular radiotherapy. *Phys Med Biol*. 2019;64:245013.
18. Sundlöv A, Sjogreen-Gleisner K, Svensson J, et al. Individualised ¹⁷⁷Lu-DOTA-TATE treatment of neuroendocrine tumours based on kidney dosimetry. *Eur J Nucl Med Mol Imaging*. 2017;44:1480–1489.
19. Tran-Gia J, Salas-Ramirez M, Lassmann M. What you see is not what you get: on the accuracy of voxel-based dosimetry in molecular radiotherapy. *J Nucl Med*. 2020;61:1178–1186.
20. Tran-Gia J, Robinson AP, Bobin C, et al. An international quantitative SPECT/CT imaging exercise for assessment of Ba-133 as surrogate for I-131 [abstract]. *Eur J Nucl Med Mol Imaging*. 2020;47(suppl):S448–S449.
21. Final publishable report. http://mrtodosimetry-empir.eu/wp-content/uploads/2019/08/15HLT06_Publishable_Report_M36_Final.pdf. MRTDosimetry website. Published June 1, 2016. Accessed October 18, 2021.
22. Chauvin M, Borys D, Botta F, et al. OpenDose: open-access resource for nuclear medicine dosimetry. *J Nucl Med*. 2020;61:1514–1519.
23. Flux GD, Bardies M, Lassmann M. Biting the magic bullet: celebrating a decade of the EANM Dosimetry Committee. *Eur J Nucl Med Mol Imaging*. 2014;41:1–3.
24. Chiesa C, Luster M, Lassmann M. 4th international symposium on targeted radiotherapy and dosimetry (ISTARD): best ranked abstract publication. *Q J Nucl Med Mol Imaging*. 2012;56:485–486.
25. Del Guerra A, Bardies M, Belcari N, et al. Curriculum for education and training of medical physicists in nuclear medicine: recommendations from the EANM Physics Committee, the EANM Dosimetry Committee and EFOMP. *Phys Med*. 2013;29:139–162.
26. Giammarile F, Bodei L, Chiesa C, et al. EANM procedure guideline for the treatment of liver cancer and liver metastases with intra-arterial radioactive compounds. *Eur J Nucl Med Mol Imaging*. 2011;38:1393–1406.
27. Hindorf C, Glatting G, Chiesa C, Linden O, Flux G, Committee ED. EANM Dosimetry Committee guidelines for bone marrow and whole-body dosimetry. *Eur J Nucl Med Mol Imaging*. 2010;37:1238–1250.
28. Kratochwil C, Fendler WP, Eiber M, et al. EANM procedure guidelines for radionuclide therapy with Lu-177-labelled PSMA-ligands (Lu-177-PSMA-RLT). *Eur J Nucl Med Mol Imaging*. 2019;46:2536–2544.
29. Lassmann M, Hänscheid H, Chiesa C, et al. EANM Dosimetry Committee series on standard operational procedures for pre-therapeutic dosimetry I: blood and bone marrow dosimetry in differentiated thyroid cancer therapy. *Eur J Nucl Med Mol Imaging*. 2008;35:1405–1412.
30. Gear J, Chiesa C, Lassmann M, et al. EANM Dosimetry Committee series on standard operational procedures for internal dosimetry for ¹³¹I mIBG treatment of neuroendocrine tumours. *EJNMMI Phys*. 2020;7:15.
31. Chiesa C, Sjogreen-Gleisner K, Walrand S, et al. EANM Dosimetry Committee Series on Standard Operational Procedures: a unified methodology for ^{99m}Tc-MAA pre- and ⁹⁰Y peri-therapy dosimetry in liver embolization with ⁹⁰Y microspheres. *EJNMMI Phys*. In press. <https://doi.org/10.1186/s40658-021-00394-3>.
32. Ljungberg M, Celler A, Konijnenberg MW, et al. MIRD pamphlet no. 26: joint EANM/MIRD guidelines for quantitative ¹⁷⁷Lu SPECT applied for dosimetry of radiopharmaceutical therapy. *J Nucl Med*. 2016;57:151–162.
33. Lassmann M, Chiesa C, Flux G, Bardies M, Committee ED. EANM Dosimetry Committee guidance document: good practice of clinical dosimetry reporting. *Eur J Nucl Med Mol Imaging*. 2011;38:192–200.
34. Stokke C, Gabina PM, Solny P, et al. Dosimetry-based treatment planning for molecular radiotherapy: a summary of the 2017 report from the Internal Dosimetry Task Force. *EJNMMI Phys*. 2017;4:27.
35. Internal dosimetry task force report on: treatment planning for molecular radiotherapy—potential and prospects. European Association of Nuclear Medicine website. https://www.eanm.org/content-eanm/uploads/documents/EANM_2017_iDTF-Report_online.pdf. Accessed October 18, 2021.
36. Sjogreen Gleisner K, Spezi E, Solny P, et al. Variations in the practice of molecular radiotherapy and implementation of dosimetry: results from a European survey. *EJNMMI Phys*. 2017;4:28.
37. Report 91. *JICRU*. 2014;14:1–160.
38. Pouget JP, Lozza C, Deshayes E, Boudousq V, Navarro-Teulon I. Introduction to radiobiology of targeted radionuclide therapy. *Front Med (Lausanne)*. 2015;2:12.
39. Sgouros G, Bodei L, McDevitt MR, Nedrow JR. Radiopharmaceutical therapy in cancer: clinical advances and challenges. *Nat Rev Drug Discov*. 2020;19:589–608.
40. Morris ZS, Wang AZ, Knox SJ. The radiobiology of radiopharmaceuticals. *Semin Radiat Oncol*. 2021;31:20–27.
41. Schumann S, Scherthan H, Lapa C, et al. DNA damage in blood leucocytes of prostate cancer patients during therapy with ¹⁷⁷Lu-PSMA. *Eur J Nucl Med Mol Imaging*. 2019;46:1723–1732.
42. Schumann S, Eberlein U, Lapa C, et al. α -particle-induced DNA damage tracks in peripheral blood mononuclear cells of [²²³Ra]RaCl₂-treated prostate cancer patients. *Eur J Nucl Med Mol Imaging*. 2021;48:2761–2770.
43. Barone R, Borson-Chazot F, Valkema R, et al. Patient-specific dosimetry in predicting renal toxicity with ⁹⁰Y-DOTATOC: relevance of kidney volume and dose rate in finding a dose-effect relationship. *J Nucl Med*. 2005;46(suppl 1):99S–106S.
44. Strosberg J, El-Haddad G, Wolin E, et al. Phase 3 trial of ¹⁷⁷Lu-dotatate for midgut neuroendocrine tumors. *N Engl J Med*. 2017;376:125–135.
45. Sundlöv A, Sjogreen-Gleisner K. Peptide receptor radionuclide therapy: prospects for personalised treatment. *Clin Oncol (R Coll Radiol)*. 2021;33:92–97.
46. Hofving T, Sandblom V, Arvidsson Y, et al. ¹⁷⁷Lu-octreotate therapy for neuroendocrine tumours is enhanced by Hsp90 inhibition. *Endocr Relat Cancer*. 2019;26:437–449.
47. Brabander T, Nonnekens J, Hofland J. The next generation of peptide receptor radionuclide therapy. *Endocr Relat Cancer*. 2019;26:C7–C11.
48. Feijtel D, de Jong M, Nonnekens J. Peptide receptor radionuclide therapy: looking back, looking forward. *Curr Top Med Chem*. 2020;20:2959–2969.
49. Bodei L, Kidd MS, Singh A, et al. PRRT genomic signature in blood for prediction of ¹⁷⁷Lu-octreotate efficacy. *Eur J Nucl Med Mol Imaging*. 2018;45:1155–1169.
50. Bodei L, Kidd MS, Singh A, et al. PRRT neuroendocrine tumor response monitored using circulating transcript analysis: the NETest. *Eur J Nucl Med Mol Imaging*. 2020;47:895–906.
51. Garske-Roman U, Sandstrom M, Fross Baron K, et al. Prospective observational study of ¹⁷⁷Lu-DOTA-octreotate therapy in 200 patients with advanced metastasized neuroendocrine tumours (NETs): feasibility and impact of a dosimetry-guided study protocol on outcome and toxicity. *Eur J Nucl Med Mol Imaging*. 2018;45:970–988.

52. Sabet A, Ezziddin K, Pape UF, et al. Accurate assessment of long-term nephrotoxicity after peptide receptor radionuclide therapy with ^{177}Lu -octreotate. *Eur J Nucl Med Mol Imaging*. 2014;41:505–510.
53. van der Zwan WA, Brabander T, Kam BLR, et al. Salvage peptide receptor radionuclide therapy with [^{177}Lu -DOTA,Tyr 3]octreotate in patients with bronchial and gastroenteropancreatic neuroendocrine tumours. *Eur J Nucl Med Mol Imaging*. 2019;46:704–717.
54. Zemezak A, Gut P, Pawlak D, et al. The safety and efficacy of the repeated PRRT with [^{90}Y]/[^{177}Lu]Lu-DOTATATE in patients with NET. *Int J Endocrinol*. 2021; 2021:6615511.
55. Hänscheid H, Lassmann M. Will SPECT/CT cameras soon be able to display absorbed doses? Dosimetry from single activity concentration measurements. *J Nucl Med*. 2020;61:1028–1029.
56. Götz TI, Schmidkonz C, Chen S, Al-Baddai S, Kuwert T, Lang EW. A deep learning approach to radiation dose estimation. *Phys Med Biol*. 2020;65:035007.
57. Rydén T, Van Essen M, Marin I, Svensson J, Bernhardt P. Deep-learning generation of synthetic intermediate projections improves ^{177}Lu SPECT images reconstructed with sparsely acquired projections. *J Nucl Med*. 2021;62:528–535.
58. Menzel HG, Clement C, DeLuca P. ICRP publication 110: adult reference computational phantoms. *Ann ICRP*. 2009;39:1–164.

REGISTER TODAY!
SNMMI 2022
Therapeutics Conference
March 10-12, 2022
New Orleans, LA

VISIT SNMMI'S

"Radiopharmaceutical Therapy Central"

YOUR SOURCE FOR THE LATEST RADIOPHARMACEUTICAL THERAPY NEWS, EDUCATION, AND RESOURCES FROM SNMMI.

The screenshot shows the SNMMI Radiopharmaceutical Therapy Central website. At the top left is the SNMMI Value Initiative logo (SOCIETY OF NUCLEAR MEDICINE & MOLECULAR IMAGING). To the right are social media icons for LinkedIn, Facebook, Twitter, YouTube, and Instagram, along with a 'Sign In' button and a 'Keyword Search' field. Below this is a navigation menu with 'SNMMI.ORG', 'HOME', 'EDUCATION', 'RESOURCES', and 'ABOUT SNMMI'. The main header features a large banner with the title 'SNMMI Radiopharmaceutical Therapy Central' and four images: two showing PET scans, one showing a laboratory setting with a person in a white coat, and one showing a person in a blue lab coat. Below the banner is a section titled 'Updates and Announcements' with a sub-header 'Get the latest radiopharmaceutical therapy updates from SNMMI and around the world, including recent articles from *The Journal of Nuclear Medicine (JNM)*.' This section contains a list of five articles with links and dates. At the bottom, there are three columns: 'Education' (Explore leading research articles and continuing education for radiopharmaceutical therapies, including recorded content from SNMMI meetings, webinars, and more.), 'Patient Resources' (Take the guesswork out of your next doctor's visit with these helpful therapy related resources, including: Therapy Procedures, Fact Sheets, Videos), and a 'More >>>' button. A small image of two people is visible in the Patient Resources column.

www.snmmi.org/Therapy

PERSONALIZED DOSIMETRY MADE EASY

Hermes Medical Dosimetry Software supports all five tasks of the SNMMI Lu-177 Dosimetry Challenge below and is FDA-cleared.

- 1) Dosimetry from multiple SPECT/CT images
- 2) Dosimetry from a series of whole-body planar images
- 3) Dosimetry from hybrid imaging: a SPECT/CT and series of whole-body planar images
- 4) Dosimetry SPECT/CT images and VOIs
- 5) Dosimetry from time-integrated-activity image and VOIs

Complications such as indistinguishable organs are accounted for.



We provide you with **two possible** approaches to dosimetry where integrated tools and workflow save time and decrease chance of error transferring measurements between tools.



Voxel Dosimetry – taking dosimetry to the next level of personalization in minutes

- Can be performed from a single image timepoint
- Support for ^{68}Ga ; ^{166}Ho ; ^{111}In ; ^{123}I ; ^{131}I ; ^{177}Lu ; ^{223}Ra ; $^{99\text{m}}\text{Tc}$; ^{90}Y ; ^{89}Zr
- Voxel-level absorbed dose calculation using a Monte-Carlo method
- Provides dose maps and tables similar to Radiation Beam Oncology for the referent physicians
- Allows for quick implementation of new research isotope.



Organ Dosimetry with Olinda/EXM – streamlining the gold standard

- Over 1,000 isotopes supported
- Load, normalize, align, segment, curve fit, and generate organ level dose all in the same streamlined program
- Record patient dose results as DICOM, screen capture, and csv files for your records.



The editors of *The Journal of Nuclear Medicine* and SNMMI gratefully acknowledge the following companies for their generous support of this supplement:

■ Title Sponsor



■ Silver Sponsors



■ Bronze Sponsors



